HISTOCHEMICAL CORRELATES OF FIRING CHARACTERISTICS IN THE OCULOMOTOR SYSTEM OF RHESUS MONKEY

Ümit Suat Mayadalı

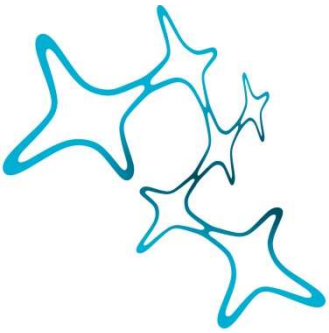

Graduate School of
Systemic Neurosciences
LMU Munich

Dissertation der
Graduate School of Systemic Neurosciences der
Ludwig-Maximilians-Universität München

07 Juli, 2022

Supervisor
Prof. Dr. Anja K.E. Horn-Bochtler
Chair of Vegetative Anatomy
Institute of Anatomy, Faculty of Medicine, LMU, Munich, Germany

First Reviewer: Prof. Dr. Anja K.E. Horn-Bochtler
Second Reviewer: Prof. Dr. Hans Straka

Date of Submission: 07.07.2022
Date of Defense: 28.09.2022

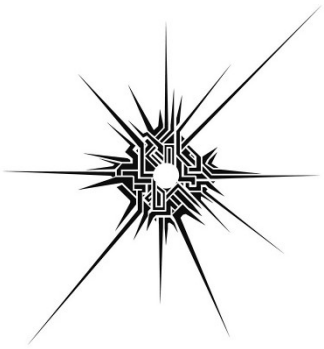

“I tell you what, this has been really fun. And I got to help make something pretty cool, so I’ve got no complaints. I mean, not me, exactly, but close enough. It’s the kind of thing that makes you glad you stopped and smelled the pine trees along the way, you know?”

-Gabbro, from Outer Wilds

Excerpts from “Outer Wilds”, writer Kelsey Beachum;
from the developers Mobius Digital and published by Annapurna Interactive

Abstract

Quick and accurate eye movements are achieved through the precise and well-timed firing of various neurons in the oculomotor circuit, which is determined by their cell characteristics. To date, intrinsic membrane properties of motor and premotor neurons enabling healthy saccade generation have not been studied in the monkey brainstem. This thesis investigates ion channel and transmitter-related profiles of motoneurons in the abducens and trochlear nuclei, and various premotor neuron groups such as burst neurons (BN), omnipause neurons (OPN) and vestibular Y-group neurons in a comparative manner. The overarching aim of this work is therefore to establish the histochemical profiles of oculomotor neurons concerning their fast-firing and bursting capacity. This goal was pursued with the immunolabeling-based examination of all aforementioned neuron populations for voltage-gated potassium channels (Kv), which facilitate the fast-firing capacity of neurons. Next, the expression of low-voltage activated (LVA) cation channels was investigated to assess the bursting characteristics of motoneurons and premotor BNs of the saccadic circuitry. Lastly, the expression of transmitter-related proteins in motoneurons of the abducens and trochlear nuclei was investigated to address anatomical and physiological differences found between their subpopulations.

Motoneurons of extraocular muscles are classified by their innervation of slow contracting, fatigue-resistant multiply-innervated (MIF) or fast-contracting, fatigable singly-innervated (SIF) fibers. A previous concept based on their anatomical segregation suggested that MIF motoneurons mediate slow eye movements or gaze holding, whereas SIF motoneurons generate fast eye movements. However, this view has been challenged recently as electrophysiological recordings in cat revealed that both groups are active for all eye movements with a burst/tonic discharge, albeit with different dynamic properties. Therefore, my first aim was to establish ion channel and transmitter profiles of SIF and MIF motoneurons to investigate their differences and to address the incongruencies between anatomical, histochemical and electrophysiological data. Histochemical analyses revealed significant differences between MIF and SIF motoneurons, as well as abducens internuclear neurons, in terms of Kv and LVA channel and transmitter-related protein immunolabeling. These findings provided strong evidence explaining the physiological differences between these neuronal groups without conflicting established histochemical and anatomical signatures.

My second aim was the investigation of intrinsic membrane properties of premotor BNs, which relay calculated saccadic signals to motoneurons. According to neuromimetic computational models based on clinical findings, BNs supposedly express LVA channels i.e. T-type voltage-activated calcium (Cav3) channels and hyperpolarization-activated cyclic nucleotide-gated (HCN) channels. These channels produce post-inhibitory rebound bursting in neurons that receive a sustained inhibition, and subsequently are disinhibited. Therefore, the model predicts that the bursting of BNs should be in response to the cessation of tonic inhibition they receive from OPNs. Excitatory BNs of the vertical and inhibitory BNs

of the horizontal saccades similarly expressed LVA channels, confirming the prediction of neuromimetic models of eye movements. According to these models, saccadic disorders such as progressive supranuclear palsy can be explained by a dysfunction of LVA channels in BNs. Here, I provide the histochemical substrate for this hypothesis.

My third aim was to establish a module of co-expressed histochemical markers that could delineate distinct firing patterns observed in various neurons of the oculomotor system. The investigation of Kv channels in neurons of the oculomotor system revealed that Kv1.1&Kv3.1 were expressed in all fast-firing neurons of the brainstem saccadic circuitry; including both premotor BN populations, tonic-firing OPNs and dorsal Y-group neurons, burst/tonic firing SIF motoneurons and internuclear neurons, but not in MIF motoneurons. These findings suggest Kv channel function as a prerequisite to the precise and well-timed activity of various neurons in the oculomotor system. However, Kv channel immunolabeling is not sufficient to delineate distinct firing characteristics of these neurons. Furthermore, no pattern of co-expression with LVA channels or transmitter-related proteins was observed to suggest any distinctions between tonic- or burst-firing in neurons of the oculomotor circuitry.

Overall, this research solidified the immunohistochemical method as a valid tool for indirectly assessing the physiological properties of various neurons in the monkey oculomotor system. This methodology was validated firstly in a bottom-up approach, as used in the examination of motoneurons based on anatomical and electrophysiological findings. Then it was validated in a top-down approach, as used in the examination of premotor BNs based on clinical and mathematical hypotheses. Establishing the histochemical profiles of various neurons related to their firing patterns paves the way for the post-mortem evaluation of human clinical cases with saccadic disorders.

Table of Contents

Abbreviations

4-AP: 4-aminopyridine
AD: Alzheimer's disease
ALS: Amyotrophic lateral sclerosis
AP: Action potential
BN: Burst neuron
Cav: Voltage-gated calcium (Ca^{2+}) channel
CB: Calbindin
cMRF: Central mesencephalic reticular formation
CR: Calretinin
DPP10: Dipeptidyl peptidase 10
EBN: Excitatory burst neuron
EPSP: Excitatory postsynaptic potential
FOR: Fastigial oculomotor region
GABA: γ-Aminobutyric acid
GAD: Glutamate decarboxylase
GlyT2: Glycine transporter subtype 2
HCN: Hyperpolarization-activated cyclic nucleotide–gated channel
HD: Huntington's disease
IBN: Inhibitory burst neuron
I_h: H-current, by HCN channels
INC: Interstitial nucleus of Cajal
INT: Internuclear neuron
IPSP: Inhibitory postsynaptic potential
I_T: T-current, by T-type calcium channels
KCC2: K^+-Cl^- co-transporter 2
Kv: Voltage-gated potassium (K^+) channel
MIF: Multiply-innervated fiber
MLF: Medial longitudinal fasciculus
MN: Motoneuron
mRNA: 'Messenger' ribonucleic acid
MVN: Medial vestibular nucleus
Nav: Voltage-gated sodium (Na^+) channel
nIII: Oculomotor nucleus
nIV: Trochlear nucleus

NMDAR1: N-methyl-D-aspartate (NMDA) receptor subunit 1

NPH: Prepositus hypoglossi nucleus

nVI: Abducens nucleus

OPN: Omnipause neuron

PAV: Parvalbumin

PD: Parkinson's disease

PGD: Nucleus paragigantocellularis dorsalis

PIR: Post-inhibitory rebound

PN: Perineuronal net

PPRF: Paramedian pontine reticular formation

PSP: Progressive supranuclear palsy (i.e. Steele- Richardson-Olszewski syndrome)

RIMLF: Rostral interstitial nucleus of medial longitudinal fascicle

RIP: Raphe interpositus nucleus

SC: Superior colliculus

SCA: Spinocerebellar Ataxia

SIF: Singly-innervated fiber

SVN: Superior vestibular nucleus

VOR: Vestibuloocular reflex

Yd: Dorsal Y-group

Introduction

Accurate visual perception of the world around us depends on the ability to generate appropriate eye movements. Obtaining a clear and high-resolution view of an object of interest requires the light emanating from that object to fall onto a relatively small portion of the retina, called the fovea. Foveation of objects moving at high velocities relative to the observer is possible only through quick processing of the visual information and accompanying accurate and fine-tuned motor responses carried out by the eye movement (oculomotor) system. Humans, alongside non-human primates, employ distinct strategies in their nervous systems to tackle the challenges of achieving clear vision by separating self-movement-induced visual field shifts from the movement of targets in the visual field at an evolutionarily basic level. Clear vision of moving targets in the visual field (smooth pursuit), shifting the gaze from one target to another rapidly (saccade) or stabilization of image during own body movements (vestibulo-ocular response) is carried out by several distinct pathways in the brain (Fig. 1). Involvement of voluntary gaze control or generation of simple reflexes differentiate stimulus-response times greatly; however, the final pathway to generate eye movements converge on the motor neurons of the extraocular muscles in all situations. Regardless, clear vision demands quick, accurate and fine-tuned control of eye movements. This is achievable only through healthy, precise and well-timed activity of various neurons of the oculomotor system, without which all variety of eye movement types might be severely impaired.

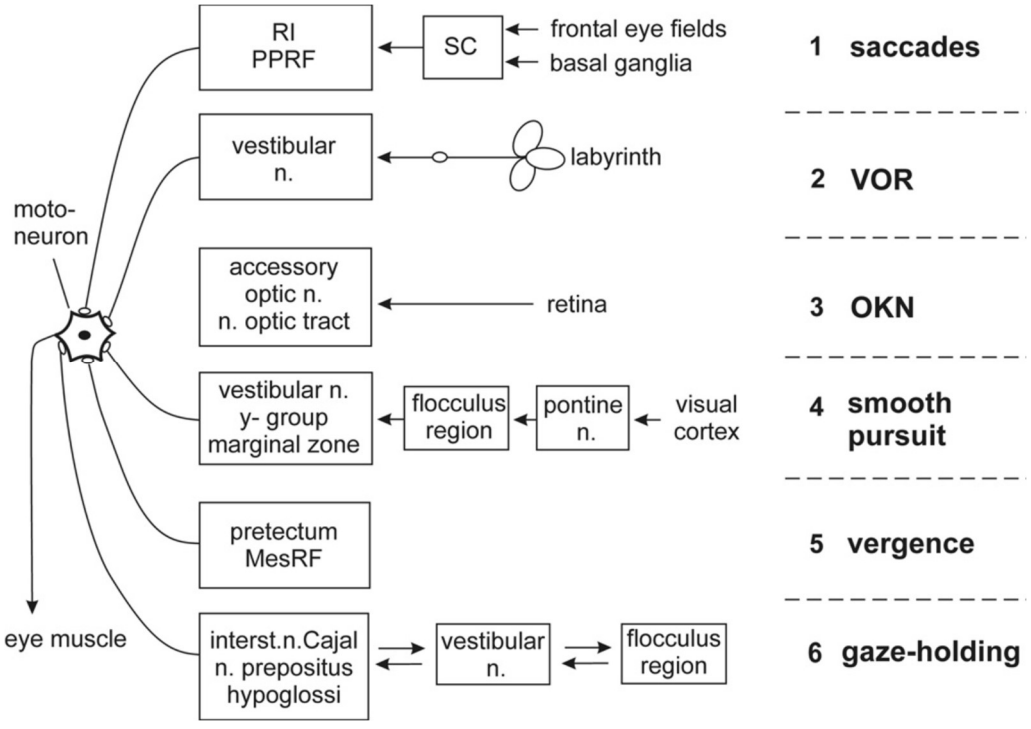

Figure 1: A simplified summary of distinct premotor networks for five eye movement types and gaze-holding. MesRF, mesencephalic reticular formation; n., nucleus; OKN, optokinetic response; PPRF, paramedian pontine reticular formation; RI, rostral interstitial nucleus of the medial longitudinal fascicle; SC, superior colliculus; VOR, vestibulo-ocular reflex. Figure taken with permission from (Horn & Adamcyzk, 2011). Reprinted from "The human

nervous system" (Third Edition), Anja K.E. Horn and Christopher Adamczyk, Chapter 9 - Reticular Formation: Eye Movements, Gaze and Blinks, Pages 328-366., Copyright Elsevier (2011).

1. Basic organization of the oculomotor system (premotor-motor) and anatomical layout

1.1. Extraocular muscles and their motor innervation

Eye movements are achieved through the coordinated action of six extraocular muscles. Lateral and medial rectus muscles mediate horizontal eye movements whereas superior and inferior rectus muscles are responsible for vertical eye movements (Fig. 2a). Lastly, superior and inferior oblique muscles contribute to eye movements around the torsional axis. Different contraction patterns of the extraocular muscles, as commanded by the motor neurons, yield diverse types of eye movements including saccades, smooth pursuit, vestibuloocular and optokinetic reflexes, and also fixation (Leigh & Zee, 2015). The variation in speed and persistence of these eye movements derive from the contraction of distinct muscle fiber types and their endowment with fast or slow myosin heavy chain isoforms, the number of mitochondria in the sarcoplasm, the number and distribution of nerve endings along muscle fibers and the activity of associated motoneurons (Spencer & Porter, 2006; Hoh, 2020; Horn & Straka, 2021). Extraocular muscle fibers are traditionally grouped into one of two main categories according to their innervation patterns. Fast-contracting, fatigable twitch-type muscle fibers are innervated by a single "en plaque" ending near the middle of the muscle belly (singly-innervated muscle fiber – SIF), whereas slow-contracting, non-fatigable non-twitch type muscle fibers are synaptically contacted along the entire length of the fiber by multiple "en grappe" nerve endings (multiply-innervated muscle fiber – MIF) (Fig. 2b). Eye movements result from coordinated contractions of largely synergistic extraocular muscles through the task-specific cooperation of MIFs and SIFs (Spencer & Porter, 2006).

For horizontal eye movements, lateral rectus muscles are activated by the motoneurons in the abducens nucleus (nVI) located in the hindbrain pontine tegmentum; and simultaneously, medial rectus muscles are activated by the motoneurons in the oculomotor nucleus (nIII) located in the mesencephalon. The conjugate eye movements require coordinated activation of the ipsilateral lateral rectus muscle and the contralateral medial rectus muscle in the direction of the eye movement, which involves the interaction of the ipsilateral abducens nucleus and the contralateral oculomotor nucleus (Büttner-Ennever & Akert, 1981; Büttner-Ennever, 2006). The signal required by this coordination between the ipsilateral abducens and contralateral oculomotor nucleus is transmitted by a neuronal subpopulation located within the abducens nucleus, called internuclear neurons (INT), whose axons run in the medial longitudinal fasciculus (MLF) up to the oculomotor nucleus targeting the medial rectus motoneurons contralaterally (Baker & Highstein, 1975; Horn *et al.*, 2018). Vertical and torsional eye movements are achieved through the activity of the motoneurons in the oculomotor and trochlear (nIV) nuclei located in the mesencephalon and rostral hindbrain, respectively (Horn & Straka, 2021).

The extraocular motoneurons are cholinergic and can be delineated anatomically and histochemically in terms of their innervation targets, of MIFs and SIFs, respectively. Early studies in monkey identified the motoneurons of MIFs and SIFs via tracer injection to the relevant extraocular muscle for retrograde labeling. Injected tracer into the muscle belly is picked up by terminals of both MIF and SIF motoneurons, resulting in retrograde labeling of the motoneurons of the respective eye muscle within the motor nuclei (Büttner-Ennever *et al.*, 2001; Ugolini *et al.*, 2006). On the other hand, tracer injections into the distal ends of the extraocular muscles, which spare the en-plaque endings, yield labeling of subpopulations of motoneurons in the periphery of the respective motor nuclei and are considered as motoneurons of MIFs (Fig. 2c) (Büttner-Ennever *et al.*, 2001; Ugolini *et al.*, 2006). These MIF motoneurons of the medial and inferior rectus muscles are localized at the dorsomedial border of nIII within the so-called C-group, those of the superior rectus and inferior oblique muscles lie within the S-group between both nIII. MIF motoneurons of the lateral rectus muscle are more scattered towards the medial periphery of nVI; and MIF motoneurons of the superior oblique muscles are confined to a dorsal cap in nIV (Figure 2c) (Büttner-Ennever *et al.*, 2001; Wasicky *et al.*, 2004; Tang *et al.*, 2015). This specific localization pattern displays great interspecies variance, as demonstrated in rat (Eberhorn *et al.*, 2006) and cat motor nuclei (Bohlen *et al.*, 2017), where MIF motoneurons tend to be more interspersed within the abducens nucleus (Hernández *et al.*, 2019).

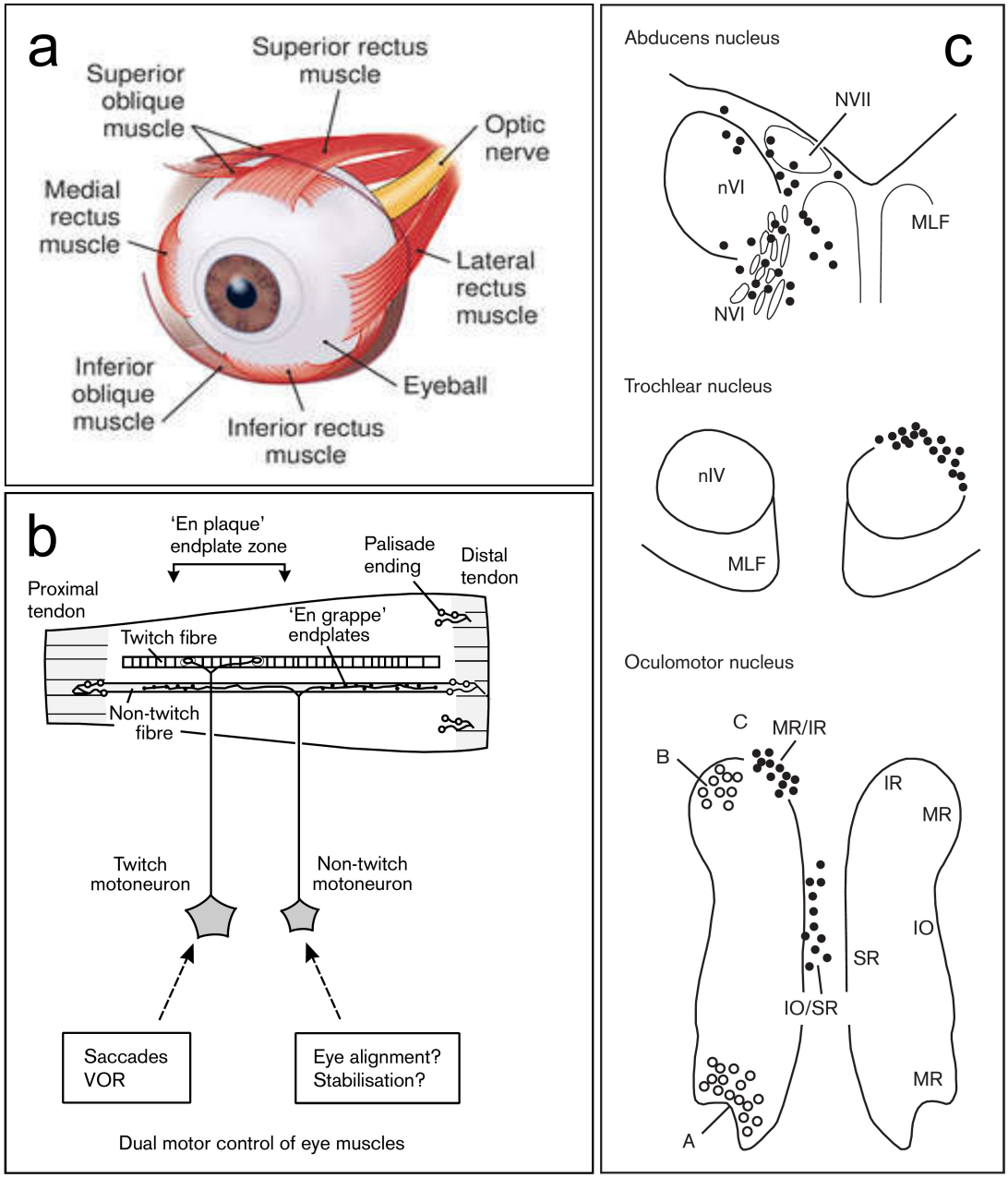

Figure 2: Extraocular muscles and their innervation. **a.** Six extraocular muscles on the left eye, figure taken from (Liu *et al.*, 2016) with permission. *Copyright © 2016, IEEE.* **b.** Singly- and multiply-innervated muscle fiber innervation by their respective motoneurons, named here as twitch (SIF) and non-twitch (MIF), respectively. **c.** Localization of MIF motoneurons in the abducens (nVI), trochlear (nIV), and oculomotor (nIII) nuclei. Note that MIF motoneurons in the nIII are found in C- (MR/IR) and S- (IO/SR) groups. Medial rectus SIF-motoneurons are found within the A and B groups (open circles). Figures (**b&c**) taken with permission from (Büttner-Ennever & Horn, 2002a).

Major histochemical differences between MIF and SIF motoneurons have been outlined by combined tract-tracing and histochemical studies in monkey and rat, which also served to identify the homologous neuronal groups in humans (Eberhorn *et al.*, 2005; Eberhorn *et al.*, 2006; Horn *et al.*, 2008; Horn *et al.*, 2018). SIF motoneurons of all extraocular motor nuclei are ensheathed by a condensed extracellular

matrix, called perineuronal nets (PN) and express the calcium-binding protein parvalbumin (PAV), while MIF motoneurons lack both features (Eberhorn *et al.*, 2005; Büttner-Ennever, 2006; Eberhorn *et al.*, 2006; Horn *et al.*, 2008). This characterization is found across species such as mouse (Bohlen *et al.*, 2019), rat (Eberhorn *et al.*, 2006), cat (Bohlen *et al.*, 2017), monkey (Eberhorn *et al.*, 2005; Büttner-Ennever, 2006; Horn *et al.*, 2008) and human (Horn *et al.*, 2008; Horn *et al.*, 2018). Clear anatomical segregation of the MIF and SIF motoneurons with differently weighed premotor inputs combined with histochemical differences led to the assumption that MIF motoneurons participate only in gaze holding and slow eye movement types, whereas SIF motoneurons participate in all eye movements including high-velocity saccades (Ugolini *et al.*, 2001; Büttner-Ennever & Horn, 2002b). However, this view was challenged by recent electrophysiological recordings in the cat abducens and oculomotor nuclei, where all motoneuron types were shown to participate in all types of eye movements (Hernández *et al.*, 2019; Carrero-Rojas *et al.*, 2021). Nevertheless, there is accumulating evidence that MIF and SIF motoneurons have differences in their electrophysiological properties such as firing rates, activation thresholds and eye-related sensitivities (Hernández *et al.*, 2019; Carrero-Rojas *et al.*, 2021). It is also considered that extraocular motoneurons lie on a continuous spectrum in terms of variance of these characteristics, with MIF motoneurons corresponding to the population with lowest firing levels, eye movement-related sensitivities and firing thresholds, and SIF motoneurons to the population with the highest firing levels and firing thresholds (Dietrich *et al.*, 2017; Horn & Straka, 2021).

1.2. Projections to the extraocular motor neurons

In addition to the histochemical and electrophysiological differences, MIF and SIF motoneurons can be delineated by synapses associated with their membranes in terms of synaptic density and premotor connections. For instance, an electron microscopic study of medial rectus motoneurons demonstrated a lower density of synapses on the membranes of MIF motoneurons compared to SIF motoneurons (Erichsen *et al.*, 2014). Additionally, MIF and SIF motoneurons differ in the origins of the premotor inputs (Ugolini *et al.*, 2006). In general, MIF motoneurons were demonstrated to receive synaptic inputs from brainstem regions associated with gaze-holding and smooth pursuit, whereas SIF motoneurons receive monosynaptic connections from the saccadic premotor burst neurons (Ugolini *et al.*, 2006). For instance, MIF motoneurons of the abducens nucleus receive synaptic inputs from the nucleus prepositus hypoglossi (NPH) and medial vestibular nucleus (MVN), both premotor neurons involved in gaze-holding and smooth pursuit. However, they are spared from synaptic inputs from the saccadic premotor burst neurons of the paramedian pontine reticular formation (PPRF) and dorsal paragigantocellular nucleus (PGD) (Büttner-Ennever *et al.*, 1996; Wasicky *et al.*, 2004; Ugolini *et al.*, 2006). Likewise, the pretectum provides input to the C-group of the oculomotor nucleus, which does not receive inputs from the saccadic premotor neurons (Büttner-Ennever *et al.*, 1996; Wasicky *et al.*, 2004; Ugolini *et al.*, 2006). These observations regarding differential synaptic connectivity of MIF and SIF motoneurons formed the view that they serve distinct functional roles in eye movement control (Büttner-Ennever & Horn, 2002a).

1.3. Premotor circuitry of the oculomotor system

Saccadic premotor burst neurons

Supranuclear commands for the horizontal and vertical components of conjugate saccades originate in different regions of the brainstem. For the horizontal saccades, the excitatory premotor burst neurons (EBN) are located in the paramedian pontine reticular formation (PPRF) rostral to the abducens nucleus, and they innervate the lateral rectus motoneurons and internuclear neurons (INT) in the abducens nucleus (Strassman *et al.*, 1986a; Horn *et al.*, 1996). The inhibitory burst neurons (IBN) are located in the dorsal paragigantocellular nucleus (PGD) in the medullary reticular formation caudal and ventromedial to the abducens nucleus (Fig. 3a) (Strassman *et al.*, 1986b). EBNs in the PPRF utilize glutamate (McElligott & Spencer, 2000; Horn, 2006) and IBNs in the PGD utilize glycine as their transmitter (Spencer *et al.*, 1989). EBNs of the PPRF project to the ipsilateral abducens nucleus SIF motoneurons as well as nucleus prepositus hypoglossi (NPH) and the adjacent medial vestibular nucleus (MVN) monosynaptically (Ugolini *et al.*, 2006). IBNs also project to the abducens nucleus SIF motoneurons, however, contralaterally (Fig. 3b). During ipsiversive saccades, ipsilateral IBNs ensure the release of contraversive eye muscles, by not only inhibiting the contralateral EBNs, but also the contralateral IBNs (Fig. 3b) (Strassman *et al.*, 1986a; b).

For horizontal saccades, EBNs make comparable excitatory, monosynaptic connections with the motoneurons and INTs in the ipsilateral abducens nucleus (nVI) and provide the main source of excitatory drive for the saccade-related pulse of motor neuron activity for the lateral rectus muscle (Strassman *et al.*, 1986a). IBNs almost identically match the firing patterns of the EBNs to counteract contralateral EBN and IBN activity (Fig. 3b) (Strassman *et al.*, 1986b).

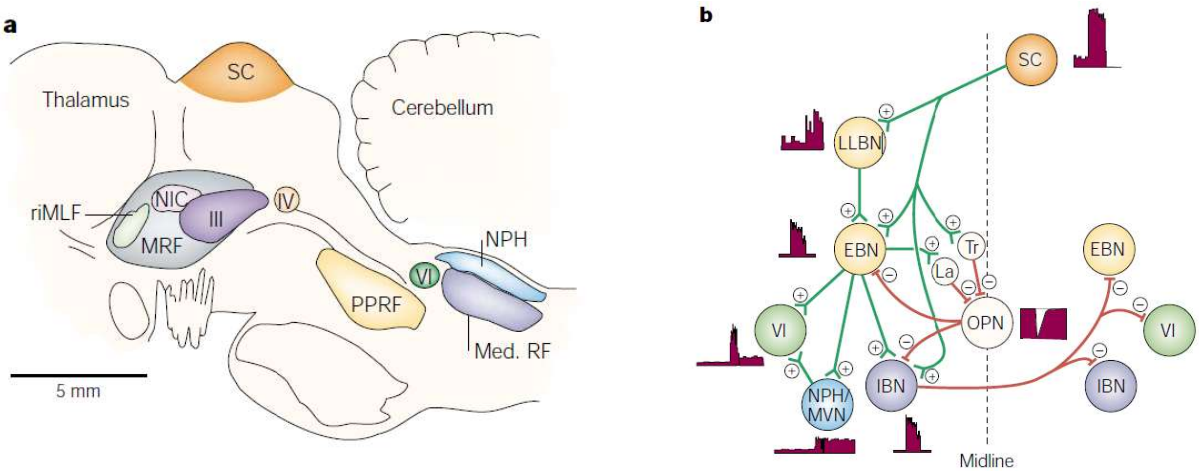

Figure 3: Location and connections of the brainstem saccade-generator neurons and their discharge characteristics. **a.** Illustration of a monkey brainstem in the sagittal plane, displaying brainstem areas involved in saccade generation. III, oculomotor nucleus; IV, trochlear nucleus; VI, abducens nucleus; Med. RF, medullary reticular formation; MRF, midbrain reticular formation; NIC, interstitial nucleus of Cajal; NPH, nucleus prepositus hypoglossi; PPRF, paramedian pontine reticular formation; riMLF, rostral interstitial nucleus of the medial longitudinal fasciculus; SC, superior colliculus. **b.** A schematic diagram of horizontal saccadic circuit and firing characteristics of neuronal types involved. VI, abducens motor neuron; EBN, excitatory burst neuron; IBN, inhibitory burst neuron; LLBN, long-lead burst neuron; NPH/MVN, neurons in nucleus prepositus hypoglossi or medial vestibular nucleus; OPN, omnipause neuron; SC, superior colliculus. Green lines represent excitatory connections; red lines represent inhibitory connections. Saccades are initiated by a trigger signal (Tr) that inhibits the OPNs. The OPNs are prevented from resuming their tonic discharge during the generation of the saccade command by the activity of 'latch' neurons (La). Figure taken with permission from (Sparks, 2002).

For vertical/torsional saccades, the premotor BNs, which project to the motoneurons of the oculomotor nucleus and trochlear nucleus, are located in the mesencephalic reticular formation, in the rostral interstitial nucleus of the medial longitudinal fascicle (RIMLF) (Büttner *et al.*, 1977; Horn & Büttner-Ennever, 1998). The EBNs within the RIMLF are glutamatergic, whereas IBNs of the vertical saccadic system are GABAergic, and are found in the interstitial nucleus of Cajal (INC) in primates (Horn *et al.*, 2003b). In cat, GABAergic IBNs are housed within the RIMLF together with EBNs (Spencer & Wang, 1996; Sugiuchi *et al.*, 2013).

Omnidirectional pause neurons (omnipause neurons)

During inter-saccadic intervals and slow, non-saccadic eye movements, the burst neurons of both the horizontal and the vertical system are inhibited bilaterally by the glycinergic omnipause neurons (OPN), which are located in the pontine reticular formation around the midline in the raphe interpositus nucleus (RIP) (Büttner-Ennever *et al.*, 1988). OPNs ensure the stability of the saccadic system by tonically inhibiting both EBNs and IBNs, except during saccades (Optican, 2008). OPNs discharge tonically in a reciprocal pattern to the BNs during intersaccadic periods and pause completely for saccades in all directions (Fig. 3b) (Cohen & Henn, 1972; Luschei & Fuchs, 1972; Keller, 1974; Evinger *et al.*, 1982).

OPNs receive monosynaptic projections from several sources including the superior colliculus, cerebellum and possibly central mesencephalic reticular formation (cMRF) (Shinoda *et al.*, 2011; Wang *et al.*, 2013; 2017). Several hypotheses regarding the role of OPNs have been presented, including the role of gatekeeper for saccades, a role in the determination of saccade duration or arousal of the orienting systems (Optican, 2008).

Superior colliculus projections to the premotor neurons

The superior colliculus (SC) plays a role in saccade initiation, and its lesion abolishes the saccade generation to the contralateral side, which later recovers only with a prolonged latency (Sparks *et al.*, 2000; Puri & Shaikh, 2017). Fixation neurons in the rostral SC project to the OPNs in monkey and show a similar firing pattern (Munoz & Wurtz, 1992; 1993; Büttner-Ennever *et al.*, 1999). However, OPNs fire at a higher and more regular level than SC fixation neurons, and also synchronize more accurately with the saccade initiation and cessation than SC fixation neurons (Everling *et al.*, 1998) suggesting additional inputs to the OPNs that regulate saccadic parameters more precisely. During saccades, OPNs receive an indirect disynaptic input via the inhibitory neurons of the caudal SC region, which stops the OPN activity, in contrast to preventing saccades with the help of monosynaptic excitation from the rostral projection (Büttner-Ennever *et al.*, 1999; Shinoda *et al.*, 2011).

Notably, OPNs and IBNs have an interesting relationship through different SC areas which suggests a possible role of IBNs in initiating saccades by actively inhibiting the tonic inhibition of the OPNs (Shinoda *et al.*, 2011). IBNs receive monosynaptic excitation from the contralateral caudal SC and disynaptic inhibition via contralateral IBNs from the ipsilateral caudal SC, while IBNs also receive disynaptic inhibition from the fixation neurons in rostral SC via OPNs (Shinoda *et al.*, 2011). On the other hand, OPNs receive disynaptic inhibition from the caudal SC, which is mediated by IBNs, overall suggesting a role of IBNs in saccade initiation (Shinoda *et al.*, 2011).

Saccadic integrator neurons

Saccadic velocity to position integrator neurons operate to transform the eye velocity and eye position information to attain and maintain a new eye position, respectively (Moschovakis, 1997; Sanchez & Rowe, 2018). Saccadic premotor BNs project to the neural integrators (Moschovakis, 1997) and consecutively, the calculated tonic signal is conveyed to the motoneurons, providing the eye position signal (Moschovakis, 1997). Horizontal neural integrators are located at the NPH and MVN, whereas vertical and torsional integrators are found in the interstitial nucleus of Cajal (INC) (Sanchez & Rowe, 2018). Dysfunction of these neurons leads to the inability to maintain eye positions after saccades (Sparks, 2002; Leigh & Zee, 2015; Kim *et al.*, 2016).

Cerebellar neurons of the oculomotor system

The cerebellum plays a role in the fine-tuning of the eye movements and stabilization of images on the fovea by adjusting precision and accuracy (Straube *et al.*, 2001; Watanabe & Munoz, 2011). There are several important cerebellar regions for eye movement control: the flocculus, paraflocculus and the nodulus are involved in the vestibular responses, smooth pursuit and gaze holding, whereas the dorsal cerebellar vermis (lobules VI and VII), and caudal fastigial nucleus, which is referred as fastigial oculomotor region (FOR) are involved in the saccadic control (Robinson & Fuchs, 2001; Kheradmand & Zee, 2011). Particularly, FOR is known to project to the PPRF and RIMLF, and is thought to influence saccade initiation (Noda *et al.*, 1990; Kheradmand & Zee, 2011). It has been also proposed that a direct projection from FOR to OPNs might play a role in ending a saccade (Kheradmand & Zee, 2011). Lastly, FOR projects to IBNs alongside OPNs, providing the inhibition during ipsilateral saccades (Fuchs *et al.*, 1993).

Y-group

The Y-group is a nucleus located in the cerebellar white matter at the level of the cerebellomedullary junction with roles in smooth pursuit generation and vertical vestibuloocular reflex (VOR) modulation (Goldberg *et al.*, 2012). Y-group contributes to the eye movements through vestibular and visual signals mediated by the cerebellar flocculus, and in the event of an isolated lesion of the circuitry, eye movement disorders such as nystagmus can be observed (Marti *et al.*, 2008). The dorsal portion of the Y-group (Yd) contains premotor neurons, which project to the motoneurons for up-gaze in the contralateral oculomotor nucleus (nIII), as well as to the motoneurons in ipsilateral nIII and trochlear nuclei (nIV) involved in downgaze (Gacek, 1977; Carpenter & Cowie, 1985). A subpopulation of Yd that is associated with calretinin (CR) expression is excitatory and projects to the contralateral nIII. The CR-negative population is presumed to inhibit the ipsilateral nIII. Premotor neurons in Yd receive disynaptic inputs from the superior vestibular nucleus (SVN) and caudal MVN related to head velocity signals (Blazquez *et al.*, 2000). Furthermore, Yd receives a strong inhibitory (GABAergic) input from Purkinje cells of the flocculus and ventral paraflocculus (Partsalis *et al.*, 1995).

2. Physiological properties of the neurons in the oculomotor system

2.1. Firing patterns of the oculomotor neurons and their translation into eye movement types

Ocular motoneurons employ burst/tonic (i.e. pulse/step) firing patterns (see Fig. 3&4). The burst component corresponds to the saccade whereas tonic firing corresponds to the fixation or intersaccadic interval. Motoneurons generate a high-frequency burst of spikes (a pulse) immediately before saccades, to stimulate the agonist extraocular muscles in the direction of the eye movement. This signal originates from the saccadic premotor BNs. As a result, burst firing approximately defines the temporal limits of saccade duration. During the fixation intervals between saccades, motoneurons discharge at a constant

rate (tonic), which correlates linearly to the eye position (i.e. higher frequency with fixation point towards on-direction of the respective muscle). This position signal comes from the integrator neurons located in the NPH for the horizontal component and the interstitial nucleus of Cajal for the vertical component of saccades (Moschovakis, 1997; Saito & Sugimura, 2020). These neurons receive signals from the BNs and translate them into a position signal by mathematical integration, and then provide the gaze holding and eye position information to the motoneurons (Cannon *et al.*, 1983).

2.2. Parameters of eye movements as provided by the brainstem premotor neurons

Pulse/step generators in the brainstem receive the main input from the superior colliculus (SC), which receives signals from various cortical and subcortical areas (Sparks, 2002; Basso & May, 2017; Matsumoto *et al.*, 2018). Although the SC provides direct or indirect output to all premotor areas involved in the eye and head movements, individual SC neurons do not encode saccadic parameters such as the *amplitude* or *velocity* by the number or the rate of spikes (Sparks, 2002). The *amplitude* of a saccade is determined by, and is linearly correlated to, the duration of bursting in the premotor BNs. The determining factor of the saccade *amplitude* is the number of spikes generated by the BNs. The overall *duration* of a saccade, on the other hand, relates directly to the bursting duration of BNs. Lastly, the saccadic *velocity* (degrees per second) is defined by the peak firing rate of the BNs. Despite providing the main input to the premotor brainstem areas for saccade generation, the role of the SC in determining saccadic parameters is not fully understood, as saccades remain relatively intact in isolated lesions of the SC despite some reports suggesting otherwise (Isa & Sasaki, 2002; Sparks, 2002; Gandhi & Katnani, 2011). However, from lesion studies and mathematical models, it is clear that the dysfunction in the brainstem saccade-generator circuit is sufficient for eye movement-related symptoms in many disorders (Suzuki *et al.*, 1995; Moschovakis *et al.*, 1996; Suzuki *et al.*, 1999; Ramat *et al.*, 2005).

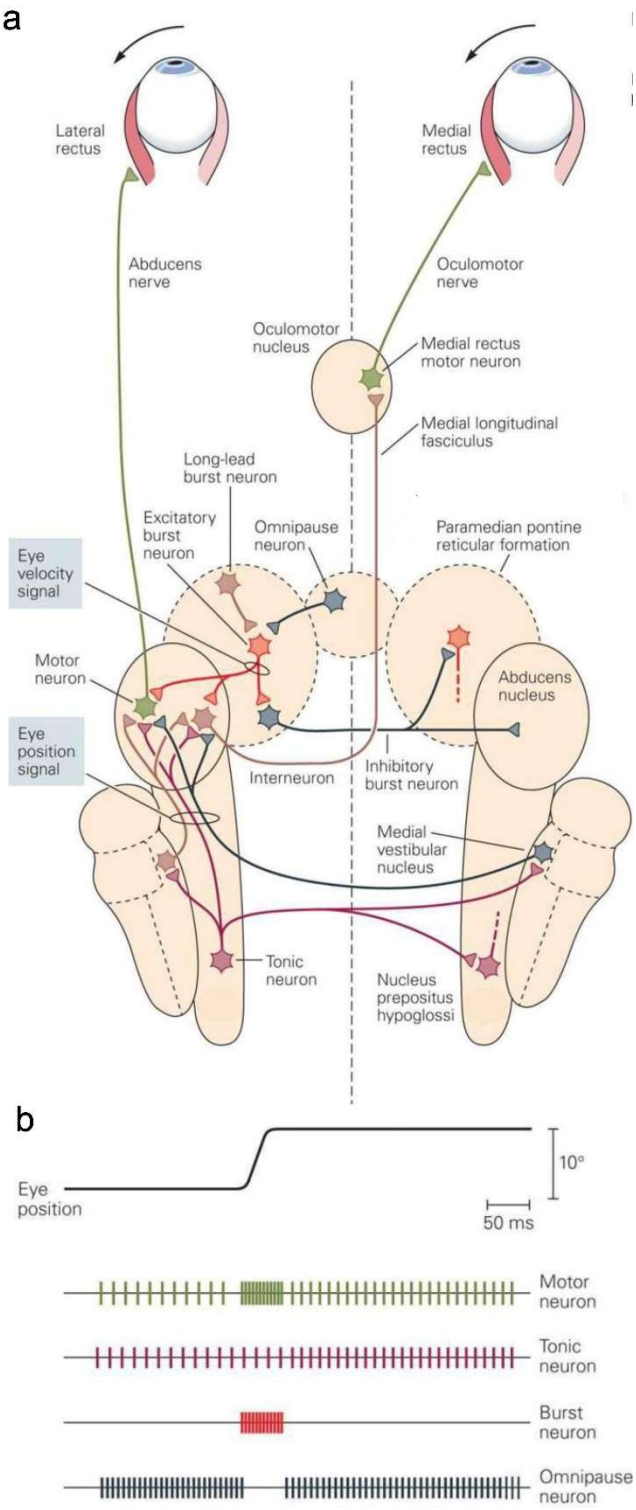

Figure 4: Summary diagram depicting premotor circuit for horizontal saccades and firing patterns of the principal neurons generating saccades. **a**. The saccade velocity arises from excitatory burst neurons (EBN) in the paramedian pontine reticular formation (PPRF) that project to motoneurons and internuclear neurons (INT) in the abducens nucleus. The abducens motoneurons project to the ipsilateral lateral rectus muscles, whereas the INTs project to the contralateral medial rectus motoneurons by axons that cross the midline and ascend in the medial longitudinal fasciculus. The EBNs also drive ipsilateral inhibitory burst neurons (IBN) that inhibit contralateral abducens motoneurons and the EBNs. Eye position component. This component arises from a neural integrator consisting of neurons distributed throughout the medial vestibular nucleus (MVN) and nucleus prepositus hypoglossi (NPH) on both sides of the brainstem. These neurons receive velocity signals from the EBNs and integrate this velocity signal to a position signal. The position signal excites the ipsilateral abducens neurons and inhibits the contralateral abducens neurons. Grey neurons are inhibitory; all other neurons are excitatory. The vertical dashed line represents the midline of the brainstem. **b**. Different neurons provide different information for the horizontal saccades. The motoneurons provide both position and velocity signals. The tonic neurons (NPH) signal only the eye position. The EBNs (PPRF) signal only the eye velocity. The omnipause neurons (OPNs) discharge at a high rate except immediately before, during, and just after the saccades. Figure taken with permission from (Kandel *et al.*, 2013).

In summary, healthy saccades with the correct parameters require well-timed and precise interactions of the EBNs, IBNs and OPNs. As observed in some neurodegenerative diseases, any lesion or dysfunction in the premotor saccadic network causes multiple eye movement disorders. These disorders are not necessarily correlated with neuronal loss. The broader implications of the clinical observations regarding

irregular eye movements, and the hypotheses derived from those investigations will be further elaborated in *Chapter 5: "Hypotheses stemming from clinical studies of eye movement disorders"*.

2.3. Irregular eye movements as a result of dysfunction in the brainstem saccadic generator

Lesions in the cortical oculomotor regions, such as the frontal and parietal eye fields, affect the accuracy and latency in visual search and cause problems in visually guided and remembered saccades, such as seen during anti-saccade tasks (Pierrot-Deseilligny *et al.*, 2002; Lynch & Tian, 2006; Leigh & Zee, 2015). On the other hand, dysfunction in the brainstem saccadic generator circuit yields motor symptoms, i.e. outcomes directly relevant to the calculation of saccadic parameters (Leigh & Zee, 2015). In general terms, abnormalities in saccadic velocity indicate dysfunction in the brainstem premotor saccade generator circuit, whereas abnormalities in saccadic accuracy point to cerebellar disorders (Leigh & Zee, 2015). For instance, lesions introduced in the EBNs of the PPRF or RIMLF abolish, or dramatically slow, saccades in the horizontal and vertical axes, respectively (Cohen *et al.*, 1968; Büttner *et al.*, 1977; Henn *et al.*, 1984). Similarly, lesions of the motoneurons result in slowed saccades, or in a limited range of eye movements (Leigh & Zee, 2015). Dysfunction of the OPNs is correlated with slow saccades in all directions (Kaneko, 1996; Miura & Optican, 2006), or possibly the lack of intersaccadic interval in some disorders of saccadic oscillations, such as opsoclonus or ocular flutter (Cogan, 1954; Leigh & Zee, 2015). Interestingly, the saccade velocity might exceed normal speeds in patients with ocular flutter and opsoclonus, which results in prematurely concluded, therefore inaccurate saccades (Leigh & Zee, 2015). As fine-tuning and calibration of the saccade fidelity is achieved by oculomotor cerebellar regions, lesions in the cerebellar dorsal vermis and fastigial nucleus can yield saccadic hypometria and hypermetria, respectively (Leigh & Zee, 2015). However, isolated lesions of the cerebellum do not affect saccade velocity (Leigh & Zee, 2015).

3. Neuronal substrates of fast-firing in the oculomotor system

3.1. The action potential and neuronal excitability

<u>The action potential</u>

When not actively "firing", neuronal membranes rest at negative voltages of typically -70 mV, which is called the resting membrane potential. An action potential (AP) is the rapid significant rise and fall of this membrane potential, which is characterized by four phases: rest, depolarization, repolarization and hyperpolarization (undershoot) stages (Fig. 5). These stages are mainly defined by the antagonistic activity of the sodium and potassium channel activities. Firstly, in the resting state, sodium (Na^+) ions are more concentrated at the outside of the neuronal membrane, and the potassium (K^+) ions are more within the cytosol. The chemical and electrostatic gradients are maintained by the semi-permeable cellular membrane, and additionally by the help of ion pumps. In response to a stimulating current,

sodium channels open, allowing Na^+ influx, rapidly depolarizing the neuronal membrane towards positive values. If the initial stimulation is substantial enough, the membrane voltage exceeds a "threshold" and an action potential can take place. Sub-threshold stimuli cannot initiate an action potential whereas supra-threshold stimuli will initiate an action potential. However, the commonality of all APs is the all-or-none property, meaning that once the membrane potential reaches the AP threshold, AP generation and propagation can no longer be stopped in healthy neurons (Kandel *et al.*, 2013; McCormick, 2013).

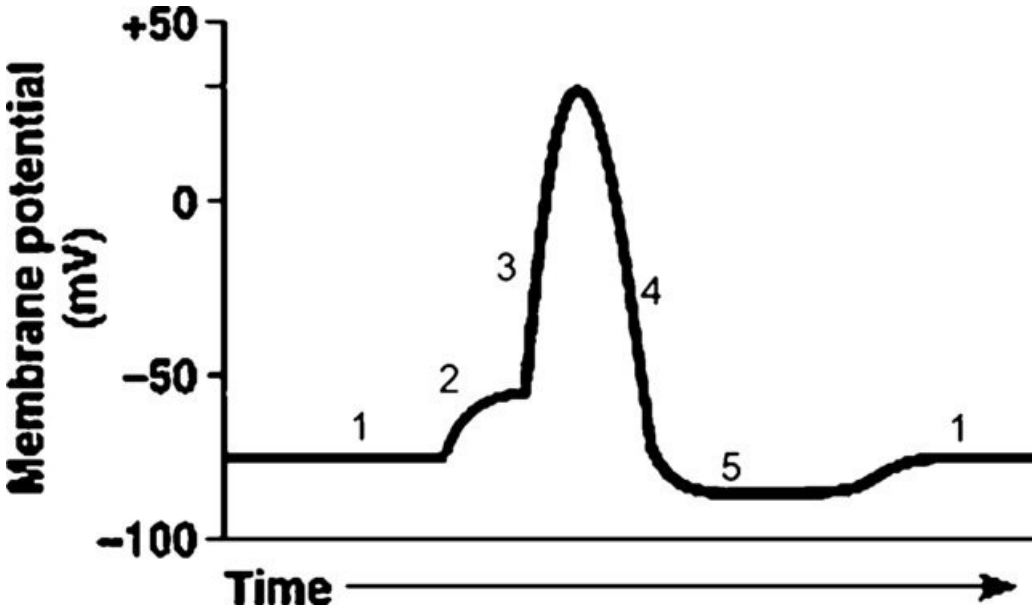

Figure 5: The action potential and its major phases. 1- Resting membrane potential. 2- Small depolarizations could cause the membrane potential to reach the firing threshold. 3- Voltage-gated sodium (Na^+) channels open and Na^+ influx depolarizes the cell membrane. Late at this stage voltage-gated potassium (K^+) channels open. 4- Repolarizing effect of K^+ efflux lowers the membrane potential. 5- The hyperpolarized (undershoot) stage is caused by the delay in K^+ channel inactivation. Figure taken with permission from (Nichols *et al*., 2013).

During depolarization, voltage-gated potassium channels (Kv) start to open. These channels allow K^+ efflux in a voltage-dependent manner, and in principle counteract the depolarization effect of the Na^+ influx. Opening of Kv channels begins with the subunits with lower-voltage activation (i.e. Kv1, Kv7) and is followed by other potassium channel subunits with rapid kinetics (i.e. Kv3) at highly depolarized stages. These subunits enable a high rate of K^+ efflux, which in turn acts as the major repolarizing force during AP generation. Voltage-gated potassium channel subunits are the major regulators of neurons' ability to return to the resting membrane potential, in terms of speed and shape of the AP, as well as the regulation of the resting membrane potential and firing threshold itself. In this third "repolarization" stage, Na^+ channels are rapidly deactivated in conjunction with the rapid activation of fast Kv channels, driving the membrane potential steeply towards negative values. The more negative the membrane

potential is, the higher the ratio of voltage-gated potassium channel inactivation becomes. However, due to a delay in the inactivation kinetics of the potassium channels, the membrane potential continues to drop even after reaching the resting membrane potential, which is defined as the "undershoot" or the "hyperpolarization" stage. The extremely low membrane potential is then brought back up to the resting membrane potential by other low-voltage activated or hyperpolarization-activated ion channels (see *Chapter 4*), thereby completing the cycle of the action potential generation. In the hyperpolarized state, a neuron is in the refractory period, during which the membrane is unable to generate subsequent action potentials until Na^+ and K^+ ions are redistributed with the help of sodium-potassium pumps (Hodgkin & Huxley, 1952a; b; Kandel *et al.*, 2013; McCormick, 2013).

Neuronal excitability

The firing pattern and the overall excitability of neurons are determined by the ion channel expression on the neuronal membrane along with the transmitter inputs they receive and transmitter receptors they express (Catterall, 1984). As seen in cardiac muscles and the central pattern generators, ion channels can be predominantly responsible for maintaining action potentials, without requiring post-synaptic excitation as the main source of spike initiation and regulation (Baruscotti *et al.*, 2005). Similarly, the membrane excitability and firing patterns are heavily dependent on the ion channel proteins embedded in the neuronal cell membrane. In other words, the characteristics of ion channel-protein content predetermine the spike frequency and type (i.e. bursting, tonic, pace-making, etc.) in response to an excitatory stimulus or to the cessation of inhibitory inputs. Within the scope of this thesis, voltage-gated potassium channel families Kv1 and Kv3, voltage-gated calcium channel family Cav3 and hyperpolarization-activated cyclic nucleotide-gated channel families HCN1-2 will be examined on the motoneurons and premotor neurons of the oculomotor system as the major contributors/regulators of their firing characteristics. These ion channel types were discovered to be of major importance in neurons with similar characteristics to neurons of the oculomotor system, such as the auditory system (Johnston *et al.*, 2010; Khurana *et al.*, 2012). In addition, these ion channels were identified as valuable candidates through mathematical modelling approaches to explain premotor neuron behavior, and potentially, dysfunction in pathologies (Miura & Optican, 2006).

3.2. Potassium channels and fast-firing capability

Voltage-gated potassium channel Kv1 family opens at sub-threshold voltages, and its fast kinetics allows small perturbations on the membrane by excitatory potentials to be mitigated (Fig. 6). In this sense, Kv1 subunits, therefore, assume the role of a high-pass filter for the action potential generation, which is highly critical for neural circuits that are required to be synchronized, as found in the auditory system (Johnston *et al.*, 2010). Kv1 activity blocks small perturbations in the membrane potential to generate an action potential, promoting selective firing. By mitigating K^+ accumulation below the AP threshold, Kv1 subunits also contribute to the determination of the firing (AP) threshold, which increases directly

proportional to Kv1 (or other low-voltage activated potassium channel) expression levels. This property translates into the regulation of neuronal excitability, as the reduced expression of low-voltage activated potassium channels yields increased spontaneous activity upon small membrane potential perturbations. On the contrary, increased expression of Kv1 subunits yields more difficult and therefore more selective action potential initiation, resulting in more tightly controlled spike generation by the excitatory neurotransmission, in terms of spike frequency and timing. When the activity of these channels is blocked by selected neurotoxins, such as dendrotoxin (DTX), multiple APs are generated as a response to a single excitatory postsynaptic potential (EPSP). Moreover, reduced Kv1 activity, by either blockage or knocking out the gene, results in increased variance (jitter) in neuronal response to a repetitive stimulation (Gittelman & Tempel, 2006; Klug & Trussell, 2006).

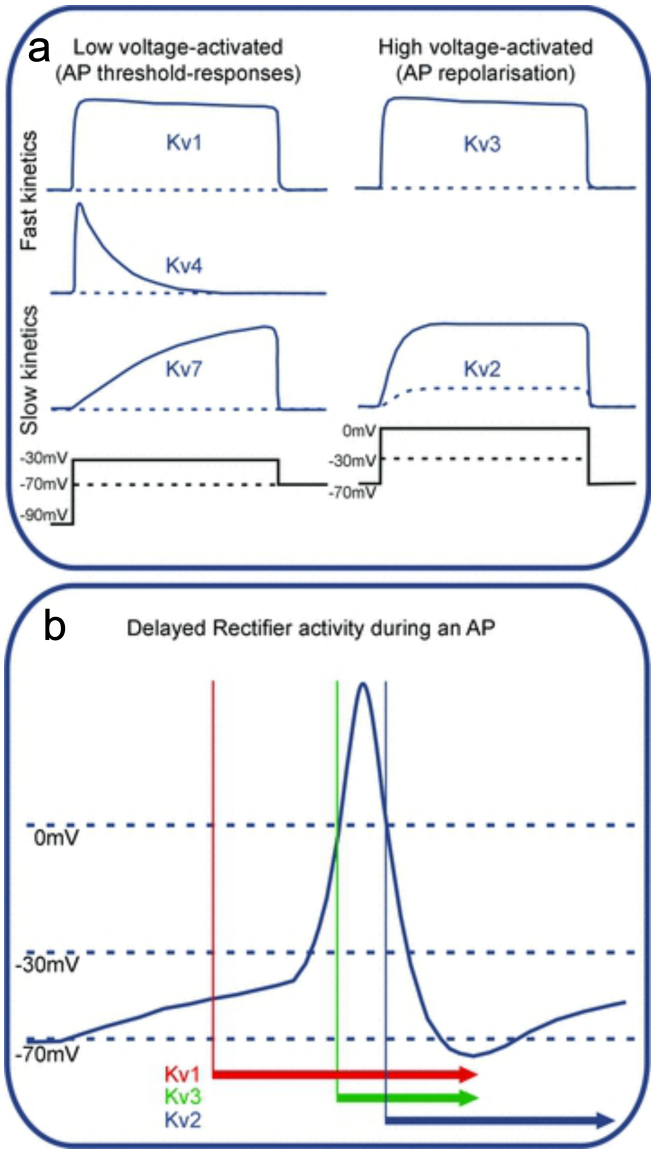

Figure 6: **a**. Voltage-dependent activation kinetics of the voltage-gated potassium channels as seen in voltage-clamp experiments. These channels can be grouped as low-voltage-activated (LVA) (Kv1, Kv4 and Kv7), and high-voltage-activated (HVA) channels (Kv3 and Kv2); or they can be grouped in terms of their activity kinetics, such as Kv channels with fast kinetics (Kv1, Kv4 and Kv3) and slow kinetics (Kv7 and Kv2). **b.** Activity of Kv channel subunits during action potential (AP) generation, as seen in current-clamp experiments. LVA channels open upon small depolarizations from the resting membrane potentials around −70mV to around −30mV, thereby regulating the AP threshold. HVA channels activate late, only during AP generation, therefore, these channels contribute mainly to the repolarization. Kv1 channels would activate with small perturbations, while Kv3 activity would be delayed until higher voltages are reached. Kv2 channels open even later due to their slow kinetics, which also means slower inactivation and longer activity. Note that this diagram describes a concept, and is an oversimplification, aiming at visualizing discussed Kv kinetics. Figure taken with permission from (Johnston *et al.*, 2010).

Voltage-gated potassium channel Kv3 family on the other hand opens at positive potentials late in the depolarization stage of the AP (Fig. 6) and counteracts the depolarization caused by Na^+ influx rapidly. Kv3 is therefore the major contributor to shortening the AP width with its rapid kinetics (Brew & Forsythe, 1995). Moreover, its rapid deactivation during the falling phase (repolarization) of the AP contributes to a shortening of the after-hyperpolarization stage and thus the refractory period. Short APs also minimize the Nav inactivation and therefore assist the maintained firing and overall increased excitability. The critical role of the Kv3 family can be demonstrated with the chemical blockage via the application of 1-3mM tetraethylammonium (TEA), which yields extremely broad APs and abolishes the high-frequency firing capabilities of neurons (Brew & Forsythe, 1995; Wang *et al.*, 1998).

3.3. The fast-firing module and co-regulated properties

The capacity of neurons for sustained fast and precise firing is essential for many circuits in the brain, and especially for the sensory and motor systems, such as the oculomotor circuitry. Regulation of fast and precisely-timed firing patterns within the individual ocular motor and premotor nuclei allows for the coordinated relay of signals, which translates into correctly calculated and calibrated eye positions and displacements at the motor level. Therefore, it is of utmost importance to identify the biophysiological contributors, which constitute the capacity for fast, precisely-timed and persistent firing in neurons of the oculomotor system. This characterization in turn would allow further anatomical identification and categorization of the neuronal groups with distinct firing patterns within the oculomotor system. Furthermore, the histochemical identification of the etiology for instabilities observed in many disorders with oculomotor symptoms relies on this characterization and understanding of how the healthy neurons undertake the required biophysiological function.

In order to identify what the main biophysiological contributors to sustained high firing rates are, Kodama et al. (2020) took advantage of the mouse medial vestibular nucleus (MVN) neuronal subpopulations with differential firing characteristics. This model organism has a particular advantage, as a combined analysis of anatomy, electrophysiology and genetic profiling is viable to correlate the different firing behaviors of these neurons to distinct co-expression patterns of genes. This study included, but was not limited to, the investigation of the voltage-gated ion channel families, neurofilaments and calcium-binding proteins (Kodama *et al.*, 2020). Interestingly, the authors identified a group of genes related to ion channel, synaptic and cytoskeletal gene expression that is correlated to the coordination of biophysical properties required to maintain the high rates of firing and transmitter release (Kodama *et al.*, 2020). Regarding the ion channel expression, Kv1.1, Kv3.1 and Nav1.6 co-expression is covaried and is linearly correlated with the fast-firing capacity of the various MVN neuron subpopulations with fast, albeit varied, firing rates (Kodama *et al.*, 2020).

3.4. Transmitter-related proteins and the firing regulation

In addition to the membrane proteins and the extracellular matrix, the neuronal responses to post-synaptic stimuli are defined by the presynaptic transmitters involved in conjunction with the postsynaptic receptors. On the presynaptic side, the frequency of transmitter release from the source of stimulation, the number and density of synaptic terminals, the type of transmitter and the characteristics of its reuptake may play a major role. On the postsynaptic side, the evoked responses rely on how these signals are translated. These depend on the transmitter receptor types, the ions they are permeable to, the amount or density of these receptors on the membrane, and finally the temporal summation of the effects caused by the ion exchange in these receptors (Giuliodori & Zuccolilli, 2004; Kandel *et al.*, 2013).

Glutamate as the major excitatory transmitter of the oculomotor system

Apart from acetylcholine, the neurotransmitter of ocular motoneurons, the major excitatory neurotransmitter utilized by the premotor neurons of oculomotor circuitry is glutamate (Horn, 2006). Upon its release into the synaptic cleft, the postsynaptic response to glutamate is mediated by AMPA, NMDA, kainate and/or metabotropic receptors (Traynelis *et al.*, 2010). Ionotropic glutamate receptors (AMPA, NMDA and kainate) initiate depolarizing EPSPs by increasing the membrane permeability for mainly sodium and potassium ions (Dingledine *et al.*, 1999; Traynelis *et al.*, 2010). The effects of glutamatergic stimulation on neuronal excitability and firing regulation are well documented, especially in the motoneurons of oculomotor circuitry (Durand *et al.*, 1987; Torres-Torrelo *et al.*, 2012). Glutamate modulates the firing rate of the extraocular motoneurons by decreasing the voltage threshold depending on cell size (Torres-Torrelo *et al.*, 2012). In motoneurons, glutamate predominantly impacts the burst component of the phasic/tonic discharge; however, the intrinsic active membrane properties such as collaboration with Nav and Kv channels are required for achieving fast firing rates, as shown in spinal motoneurons (Iwagaki & Miles, 2011; Torres-Torrelo *et al.*, 2012).

Glutamate is involved in about 90% of the synapses in the adult human brain (Braitenberg & Schüz, 1998). Postsynaptic responses to glutamatergic excitation are regulated by the differences in the release of this transmitter into the synaptic cleft by different presynaptic vesicular glutamate transporter subunits (i.e. vGlut1-3) or by different kinematics of glutamate transmitter receptors at the postsynaptic sites of their targets (Dingledine *et al.*, 1999; Vigneault *et al.*, 2015). To elaborate, vGlut2 exhibits higher transport probability and faster synaptic release compared to vGlut1, which may play a major role in tightly controlled and highly-active circuits such as the oculomotor system (Fremeau *et al.*, 2004). On the postsynaptic side of glutamatergic transmission, the speed and duration of the responses to glutamate are defined by the type of glutamate receptors (Traynelis *et al.*, 2010). Overall, it is accepted that the AMPA receptors initiate more rapid and transient responses, whereas NMDA receptors mediate slower and more prolonged responses, as demonstrated in the motoneurons of the cat abducens nucleus (Durand *et al.*, 1987; Traynelis *et al.*, 2010). NMDA receptors additionally allow for the Ca^{2+} influx, which might have secondary consequences in terms of neuronal excitability and cellular responses due to the role of

Ca^{2+} as a secondary messenger in cell signaling (Lau *et al.*, 2009). Furthermore, expression profiles of the AMPA and NMDA receptors might assume a functional role in the organization of the ocular motoneurons as demonstrated in the abducens nucleus of Xenopus laevis larvae, where the motoneurons could be divided into two subgroups in terms of their predominant activation through the AMPA or NMDA receptors (Goetz *et al.*, 2009; Dietrich *et al.*, 2017).

Glycine and GABA as the major inhibitory transmitters of the oculomotor system

The simplest amino acid glycine acts as a major inhibitory neurotransmitter in the brainstem, spinal cord and inner retina (Rajendra *et al.*, 1997; Benarroch, 2011). In the adult nervous system, glycine exerts fast postsynaptic inhibition that is important for the control of excitability of the motoneurons, auditory processing, pain transmission in the dorsal horn, and other functions (Benarroch, 2011). On the other hand, the other major inhibitory neurotransmitter γ-aminobutyric acid (GABA) constitutes at least 40% of the inhibitory transmitters in the entirety of the mammalian brain (Bowery & Smart, 2006).

Both GABA and glycine exert inhibitory effects through their receptors by increasing the membrane permeability to chloride (Cl^-) ions, thereby causing an inhibitory postsynaptic potential (IPSP). Binding of ligands to the glycine receptors elicits the opening of the Cl^- channels, which is similar to that of GABA acting on the ionotropic $GABA_A$ receptors (Betz *et al.*, 1991; Goetz *et al.*, 2009). However, glycine receptors generally have faster inhibitory kinetics than the $GABA_A$ receptors and GABAergic responses decay more slowly than glycinergic responses in the motoneurons (O'Brien & Berger, 1999; Russier *et al.*, 2002). Glycine and GABA are not exclusive and can be co-released, which plays a role in determination of the strength and timing of the postsynaptic hyperpolarization (O'Brien & Berger, 1999). Co-release of glycine and GABA may affect the temporal profile of the postsynaptic effects with immediate effects undertaken by glycinergic IPSPs, which is later dominated by the effects of the $GABA_A$ receptors, thus optimizing the inhibition of motoneuron function (O'Brien & Berger, 1999; Russier *et al.*, 2002). Furthermore, glycine has synaptic interactions with glutamate, which regulate neuronal excitability both during development and in the adult nervous system (Benarroch, 2011). For instance, glycine is a required co-agonist along with glutamate for the NMDA receptors (Cummings & Popescu, 2015).

The resulting change in the membrane potential (IPSP) elicited by glycine or $GABA_A$ receptor activation depends on the transmembrane Cl^- concentration, which is determined by the activity of the K^+-Cl^- cotransporter 2 (KCC2) (Rivera *et al.*, 1999). KCC2 extrudes Cl^- from the cell, thereby maintaining chloride homeostasis in neurons (Chamma *et al.*, 2012). Therefore, KCC2 indirectly determines the polarity and efficacy of glycine and $GABA_A$ receptors (Chamma *et al.*, 2012). In mature neurons, where a low intracellular Cl^- concentration is maintained by KCC2, the activation of glycine receptors elicits an influx of Cl^-, leading to a fast hyperpolarization and postsynaptic inhibition. Furthermore, through the elevated glutamate levels, the NMDA receptor activity downregulates KCC2, also resulting in a

depolarizing (reversed) $GABA_A$ receptor activity, which suggests more versatility of the $GABA_A$ receptor activity in firing regulation (Lee *et al.*, 2011).

Apart from problems in the neuronal excitability presented by abnormal KCC2 activity, dysfunction of the glycinergic transmission can cause hyperexcitability. For instance, mutated proteins at the presynaptic sites, such as glycine transporters, or at the postsynaptic sites, such as glycine receptors, result in severe motor hyperexcitability problems in the spinal cord and the brainstem (Harvey *et al.*, 2008). Mice knockout models lacking the glycine transporter subtype 2 (GlyT2) die shortly after birth due to motor deficiencies, which present similarly to symptoms observed in human hyperekplexia, a neurological disorder presenting with startle responses to stimuli (Latal *et al.*, 2010). On the other hand, due to the reversal in the role of GABA from excitatory to inhibitory during development, abnormal GABAergic transmission due to the malfunction of transporters or transmitter receptors may lead to problems with neuronal excitability and excitotoxicity (Ben-Ari *et al.*, 2012). For instance, the role of $GABA_A$ receptors in the modulation of excitability was shown in tonic-clonic seizures (Loup *et al.*, 2000). Furthermore, both $GABA_A$ receptors and transporters in GABAergic terminals, which employ glutamate decarboxylase (GAD) enzyme, were implicated in the pathophysiology of motoneurons in amyotrophic lateral sclerosis (ALS) (Carunchio *et al.*, 2008; Venugopal *et al.*, 2021). As glycine and GABA are differentially employed by the horizontal and vertical eye movement circuits, the physiological implications of dysfunction in neurotransmission by these transmitters are important for the disorders that affect one of these systems selectively (Spencer & Baker, 1992; Spencer *et al.*, 1992).

3.5. Calcium-binding proteins, perineuronal nets and firing regulation

Calcium homeostasis and calcium-binding proteins

Neurons strictly maintain cytosolic calcium levels around 200 nM, and also a 20,000- to 100,000-fold gradient between their intracellular (cytosolic) and extracellular Ca^{2+} concentration (Zhou *et al.*, 2013). The intracellular Ca^{2+} levels are tightly controlled by the uptake and release by the endoplasmic reticulum, as Ca^{2+} is a potent tool of cell signaling as a secondary messenger (Zhou *et al.*, 2013). Moreover, the steep Ca^{2+} concentration gradient provides an excellent opportunity for signal transduction, which neurons utilize to a great extent, as every change in the Ca^{2+} concentration can be easily detected and propagated (Grzybowska, 2018). Ca^{2+} signaling tends to be rapid, localized and propagated as spikes, waves, or oscillations. Keeping excess Ca^{2+} out of the cytosol is vital because free Ca^{2+} ions are also potentially toxic (Grzybowska, 2018).

Calcium homeostasis in the cytosol is achieved by either removal of Ca^{2+} by the endoplasmic reticulum, or by binding free Ca^{2+} with so-called calcium-binding proteins. These include calexcitin, calmodulin, calbindin, calretinin and parvalbumin, which serve a buffering purpose and tight/rapid control of the unbound Ca^{2+} concentration within the cytosol (Nelson *et al.*, 1996). Neurons with high activity levels and metabolism requirements, such as those of the oculomotor circuitry, often express calcium-binding

proteins (de la Cruz *et al.*, 1998; Horn, 2006). OPNs, saccadic BNs and SIF motoneurons express parvalbumin, and subpopulations of EBNs in the RIMLF and the Y-group governing up-gaze, express calretinin in addition to parvalbumin (Horn *et al.*, 1994; Horn *et al.*, 1996; Horn & Büttner-Ennever, 1998; Horn *et al.*, 2003a; Ahlfeld *et al.*, 2011). Purkinje cells employ calbindin and calmodulin as well as parvalbumin (Garcia-Segura *et al.*, 1984; Ikeshima *et al.*, 1993; Brandenburg *et al.*, 2021). Parvalbumin, for example, when combined with staining for the perineuronal nets, serves as a marker of fast-spiking GABAergic interneurons in the cortex (Härtig *et al.*, 1992; Härtig *et al.*, 1994; Härtig *et al.*, 1999). Alongside serving as traditional anatomical markers of fast-spiking neurons within the central nervous system, the expression of calcium-binding proteins may be significant regarding biophysiological function and the regulation of firing in neurons. For instance, calexcitin was found to enhance membrane excitability by interacting with voltage-gated potassium channels (Nelson *et al.*, 1996). Whether or not the selective expression of calretinin within premotor subpopulations mainly involved in up-gaze signifies a distinction in their biophysiological properties, remains to be further investigated.

Perineuronal nets

Perineuronal nets (PN) are specialized extracellular matrix formations that envelop the soma and proximal dendrites of neurons in the nervous system (Fig. 7, left). PNs are composed of a condensed matrix of chondroitin sulfate proteoglycan molecules, which are composed of various proteins including aggrecan, brevican, neurocan, phosphacan and hyaluronan (Fig. 7, right). In the literature, PNs are often referred to by their roles in the context of development, neuroplasticity, synaptic plasticity, synaptic and network stabilization and neuroprotection (Wingert & Sorg, 2021). However, they also contribute to the anchoring of AMPA receptors and ion channels to the membrane to act as lateral diffusion barriers. Finally, they may serve as cation buffers around the cell membrane (Härtig *et al.*, 1999). These latter functions are particularly important in the research of the modulators of excitability in neurons of the oculomotor system, as they imply the biophysiological regulation of high metabolic activity and fast-firing capabilities (Balmer, 2016).

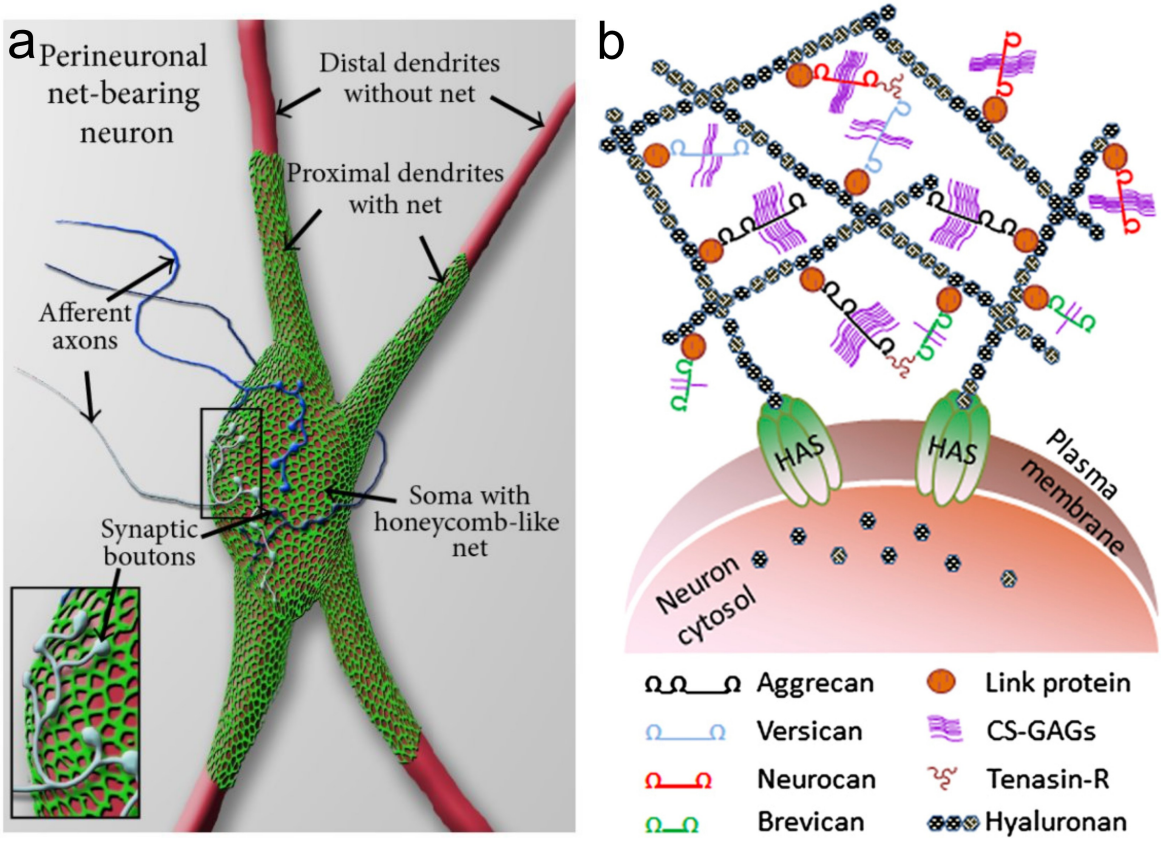

Figure 7: Scheme of a neuron (**a**) enveloped by perineuronal nets (PNs) and molecular structure of PNs (**b**). **a**. A neuronal cell body with its proximal dendrites (red) covered by a typical reticular, honeycomb-like net (green). More distally, dendrites are devoid of nets. The holes in the perineuronal nets are occupied by synaptic boutons of afferent axons (insert, blue) that target the neuron. Figure taken from (de Winter *et al.*, 2016; open access article distributed under the Creative Commons Attribution License CC BY 4.0). **b**. The PNs consist of multiple proteins: hyaluronan, secreted by membrane-bound hyaluronan synthase (HAS), binds to proteins such as aggrecan, brevican, versican, and neurocan. Figure taken from (Tsien, 2013; open access article distributed by PNAS under the Creative Commons Attribution License CC BY/CC BY-NC-ND).

In cortical and subcortical areas, as well as deep cerebellar nuclei, PNs are often found surrounding GABAergic (inhibitory) interneurons containing the calcium-binding protein parvalbumin (Härtig *et al.*, 1994; Morris & Henderson, 2000; Wingert & Sorg, 2021). However, PNs are also shown to envelop the excitatory neurons, as seen in various neurons of the oculomotor circuitry such as excitatory premotor BNs, SIF motoneurons and INTs of the abducens nucleus (Horn *et al.*, 2003a; Horn *et al.*, 2008; Horn *et al.*, 2018). PNs also envelop various inhibitory neurons in the oculomotor circuit, such as OPNs and the IBNs, which is in accordance with the observation that PNs envelop neurons with high metabolic activity (Horn *et al.*, 2003a). Moreover, PNs are not found enveloping modulatory neurons in the raphe nuclei (Hobohm *et al.*, 1998), urocortin-immunopositive non-preganglionic Edinger-Westphal nucleus neurons (Horn *et al.*, 2008) or the MIF motoneurons with known weaker firing characteristics (Eberhorn *et al.*,

2005; Horn *et al.*, 2018; Hernández *et al.*, 2019). These findings are interesting, as the presence of PNs is often associated with the voltage-dependent potassium channel subunit Kv3.1b expression in parvalbumin immunopositive fast-firing neurons (Härtig *et al.*, 1994; Härtig *et al.*, 1999).

4. Low-voltage activated ion channels and the post-inhibitory rebound (PIR) bursting phenomenon in the saccadic premotor neurons

4.1. Post-inhibitory rebound bursting

Post-inhibitory rebound (PIR) bursting is a biophysical property of some neurons that must develop a quick increase in their discharge after being disinhibited. With PIR, a neuron is capable of firing at high rates spontaneously and without stimulation when released from inhibition. PIR usually occurs due to a low membrane threshold potential of neurons, and combined with the lack of required excitatory stimulus, they can generate spontaneous bursts immediately upon release from inhibition (Enderle & Engelken, 1995). This was, for example, shown for the central pattern generators in swimming leech (Angstadt *et al.*, 2005). PIR is thought to be of fundamental physiological significance to the generation of saccades, as it ensures a rapid increase in BN discharge frequency after inhibition by OPNs, which is essential for strong eye muscle contraction. This burst discharge of the premotor BNs is necessary, as it provides the phasic component of eye movement signals to the motoneurons in order to overcome the mechanical hindrances to movement in the orbit, and rapidly rotate the globe from one position to another during saccades.

Typically, neurons can generate two distinct patterns of discharge in response to the depolarizing stimulus. Regular (tonic) firing is elicited when the neuron is depolarized from a resting membrane potential around -55 mV. In contrast, when the membrane potential is below -70 mV, as seen during sustained hyperpolarization, the same stimulus triggers a high-frequency burst (post-inhibitory burst). Membrane depolarization following the hyperpolarization below -70 mV occurs in two steps, each regulated by two distinct ion conductances – H-currents (I_h) and T-currents (I_T) (Fig. 8). These two conductances carry out the role of bringing the membrane potential up to the level where sodium conductance (I_{Na}) is promoted, readily ascending the potential above the threshold, and thereby generating an action potential. The primary stage of recovery from the hyperpolarized state involves hyperpolarization-activated cyclic nucleotide-gated (HCN) channels (Fig. 8). Therefore, HCN channels are thought to be important in building up the PIR response by allowing cation influx (I_h) at extreme hyperpolarized voltages, reducing the membrane resistance and rescuing the neuronal membrane towards the threshold voltage. The second PIR stage immediately subsequent to hyperpolarization, is mediated by the low-threshold Ca^{2+} currents (T-currents, I_T) carried out by the voltage-gated calcium channel family Cav3 (Fig. 8). Cav3 family is low-voltage activated, in contrast to other members of voltage-gated calcium channels. Several intricate properties of these channels are further explained in *Chapter*

4.3. Depolarizing effects of the increased or decreased I_h and I_T conductances on the burst intensity are depicted in Fig. 11 (*Discussion Chapter 2*). Other ion conductances, such as calcium-activated potassium (K_{Ca}) conductance, could indirectly affect I_h activation by increasing the strength of after-hyperpolarization, as the strength of rebound bursting is proportional to the magnitude and duration of hyperpolarization (Wang *et al.*, 2016).

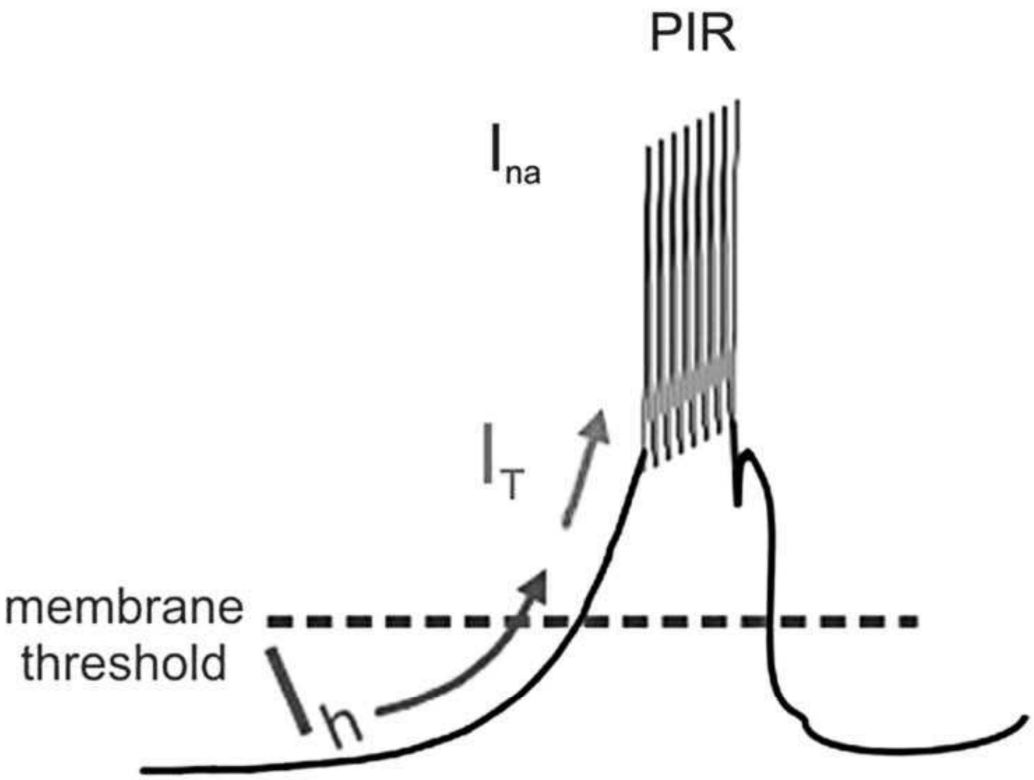

Figure 8: Low-threshold spiking, post-inhibitory rebound burst mechanism, and the currents that enable the bursting. The H-current (I_h) pacemaker raises the membrane potential to the threshold for the T-type calcium current activation. T-current (I_T) brings the membrane potential to the depolarization stage, where sodium-potassium spikes become prominent. Subsequently, H-current deactivates and T-current inactivates due to the high membrane potential. I_{na} represents sodium currents. Figure taken with permission from (Shaikh *et al.*, 2008).

4.2. Hyperpolarization-activated cyclic nucleotide-gated (HCN) channels

HCN channels are non-selective voltage-gated cation channel proteins located on predominantly neuronal and cardiac cell membranes. HCN channels are sometimes referred to as pacemaker channels because they help to generate pacemaking rhythmic or oscillatory activity within groups of heart and brain cells (Baruscotti *et al.*, 2005; Benarroch, 2013). In the brain, HCN channels have a major role in controlling neuronal excitability, dendritic integration of synaptic potentials, synaptic transmission, and rhythmic oscillatory activity in individual neurons and neuronal networks (Benarroch, 2013).

HCN channels, which are permeable to Na^+ and K^+, are activated by the membrane hyperpolarization and are constitutively open at voltages near the resting membrane potential. HCN channels were shown to regulate the resting membrane potential of neurons, thereby indirectly regulating neuronal excitability (Wang *et al.*, 2016). Their role in the PIR phenomenon is also demonstrated in the rat medial geniculate nucleus, so that although PIR is basically carried out by T-currents (I_T by Cav3), the blockage of HCN channels hyperpolarizes the resting membrane potential, and thus represses the PIR phenomenon (Wang *et al.*, 2016). Therefore, the membrane resistance introduced by the HCN blockage enhances the effectiveness of hyperpolarization (Wang *et al.*, 2016).

4.3. Cav3 channel family

T-type (transient opening) calcium channels are low voltage-activated (LVA) calcium channels that become inactivated during extreme cell membrane hyperpolarization, but then open to depolarization. T-type channels activate upon small depolarization of the membrane, allowing a rapid influx of Ca^{2+} into neurons at the beginning of an action potential (when the electrochemical gradient is actively pushing cation entry) (Senatore & Spafford, 2015; Rossier, 2016). Alternatively, a brief hyperpolarization promotes recovery of T-type channels from inactivation, and upon release from the hyperpolarizing influence, they depolarize the membrane to generate an LVA Ca^{2+} spike and rebound depolarization that drives a burst of Na^+ spikes (post inhibitory rebound burst) (Molineux *et al.*, 2006). The activation of T-type calcium channels overlaps around the same range of voltages as voltage-gated sodium channels, which is at about -55 mV. Therefore, they play a role in regulating excitability and pacemaking at subthreshold voltages.

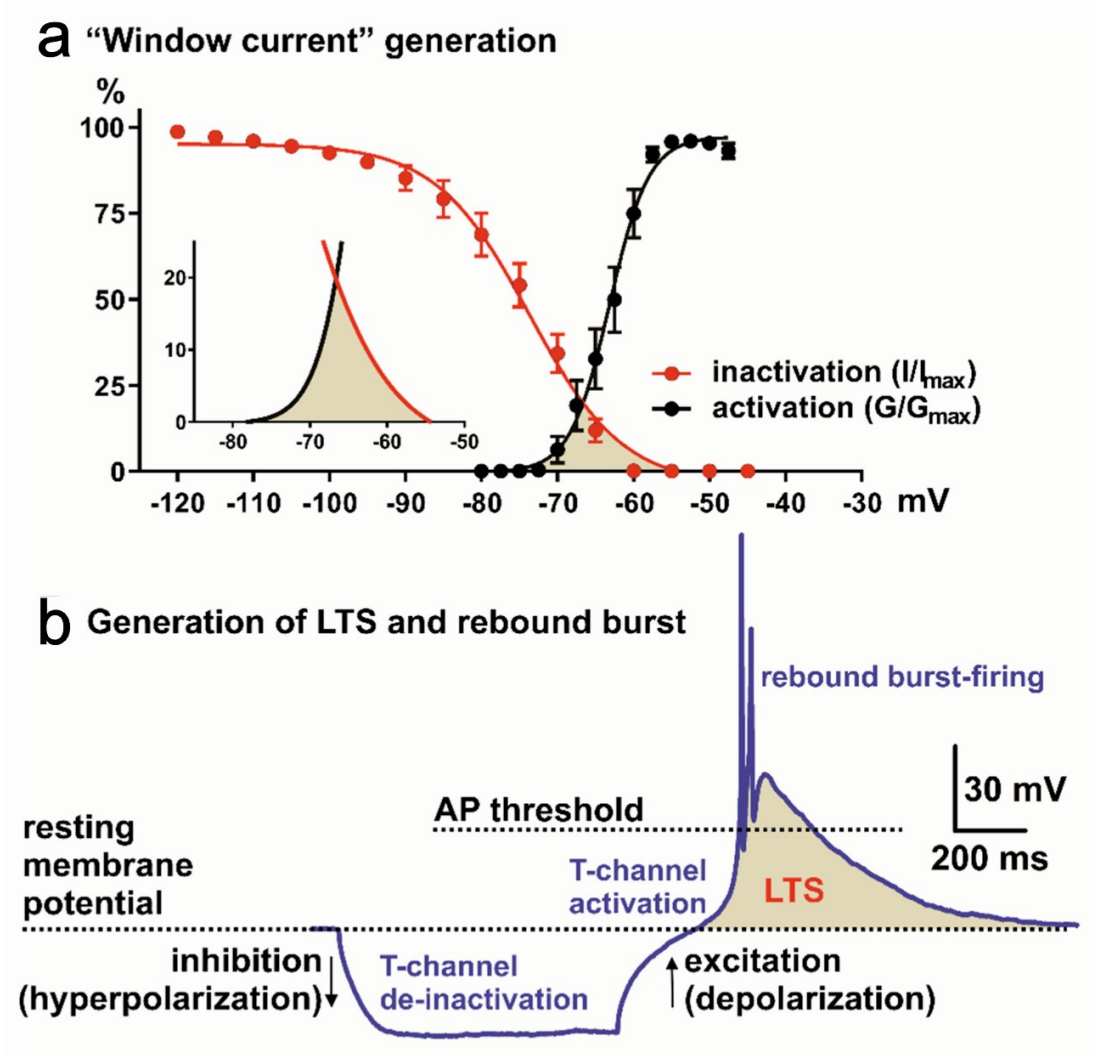

Figure 9: **a.** "Window" current generation, red trace—steady-state inactivation and black—steady-state activation T-channel (T-type Ca^{+2} channel; Cav3 channel) kinetics. Inset in A is an enlarged "window" current (shaded area) generated by the overlap between steady-state activation (black) and inactivation (red) curves. **b.** Role of the T-channels in LTS (low-threshold spike, shaded area) and the rebound burst generation. Note that in most systems, LTS and burst-firing cannot be generated from the resting membrane potential, but the neuronal cell membrane is required to be hyperpolarized in order to allow T-channel de-inactivation (recovery from inactivation). AP: Action potential. Figure taken from (Timic Stamenic & Todorovic, 2022; published under an open access Creative Common CC BY license).

Their rapid, voltage-dependent inactivation and their slow deactivation make the gating characteristics of T-type Ca^{2+} channels distinct from other Ca^{2+} channels such as L-type Ca^{2+} channels (Rossier, 2016). They generally increase neuronal excitability, as they are members of a family of inward-permeating cation channels such as voltage-gated sodium channels (Senatore & Spafford, 2015). When activation and inactivation curves of T-type Ca^{2+} channels overlap, a sustained flux of calcium through the channels is possible for up to minutes in this window around the resting membrane potential (Fig. 9). During this "window" current, a significant proportion of channels are already activated but not yet completely

inactivated (Crunelli *et al.*, 2005). By generating action potential-independent sustained Ca^{2+} elevations near the resting conditions, T-type channels control a multitude of cellular and physiological functions, such as (low-threshold) vesicular exocytosis (Weiss & Zamponi, 2013).

5. Hypotheses stemming from the clinical studies of eye movement disorders

5.1. Predictions of the neuromimetic mathematical models of the saccadic circuitry

Ocular flutters or oscillations, such as seen in opsoclonus-myoclonus-ataxia syndrome, are abnormal eye movements consisting of uncontrolled, repetitive, irregular and involuntary bursts of horizontal saccades without intersaccadic intervals (Cogan, 1954; Daye *et al.*, 2013; Leigh & Zee, 2015). According to one view based on neuromimetic mathematical models of the oculomotor function, this phenomenon can be explained as an instability in positive feedback loops involving the EBNs and IBNs (Ramat *et al.*, 2005; Daye *et al.*, 2013). However, in order for oscillations to be generated as a result of these positive feedback loops, neurons must have PIR bursting (Daye *et al.*, 2013).

An explanation of oscillations by the intrinsic membrane properties is expanded further by the observations in opsoclonus cases. One hypothesis regarding the cause of the symptoms has been dysfunction of the OPNs, despite the fact that no abnormalities found in two opsoclonus cases (Ridley *et al.*, 1987). However, Ramat et al. (2008) and Shaikh et al. (2008) provided mathematical-modelling based evidence to demonstrate that the opsoclonus symptoms could be reproduced by reducing the inhibition provided by OPNs alone, or by dysregulation of ion channels in the BNs (Ramat *et al.*, 2007; Shaikh *et al.*, 2008). These hypotheses imply that without neuronal loss of the OPNs or BNs, dysregulation of transmitter activity or changes in the membrane excitability of OPNs and/or BNs could produce the symptoms, despite the normal morphology of these neurons. Alternatively, increased $GABA_A$ receptor sensitivity in these neuronal groups could explain the eye movement characteristics observed in opsoclonus (Optican & Pretegiani, 2017b).

Simulation studies of saccades generated with a conductance-based mathematical model involving neuronal characteristics such as PIR and a firing threshold (Miura and Optican, 2003) demonstrated that the inclusion of I_T (Cav3 family) in the model was sufficient to simulate the saccade slowing after OPN lesion (Kaneko, 1996; Soetedjo *et al.*, 2002; Miura & Optican, 2006). Additionally, the possible effects of reduced glycinergic transmission on the EBNs were demonstrated as a possible contributor to saccadic slowing, since it would not only reduce the hyperpolarization of the EBNs before saccades, but also might reduce the glutamatergic saccadic drive through the NMDA receptor activity, which is dependent on glycine as co-agonist (Miura & Optican, 2006; Cummings & Popescu, 2015).

Another example of the saccadic slowing with the associated curved and irregular saccadic trajectories is found in patients with progressive supranuclear palsy (PSP, *see* *Discussion Chapter 6.1*), which is a neurodegenerative disease with midbrain tissue loss resulting in saccadic slowing particularly in the

vertical axis (Login, 1982; Shaikh *et al.*, 2017). Using a similar single-compartment neuromimetic model of the burst generators (Miura & Optican, 2006), Shaikh et al (2017) predicted and successfully recreated the cause of saccadic slowing in PSP as observed in patients, as a dysfunction of primarily both EBNs and IBNs and possibly of the OPNs at later stages (Shaikh *et al.*, 2017). The authors matched the characteristics of saccades in PSP in their model with the lack of PIR phenomenon in EBNs and IBNs of the vertical saccadic circuitry (Shaikh *et al.*, 2017).

The current state of knowledge on and inquiry about the possible etiology of various saccadic disorders lack the necessary information on the histochemical composition of neurons in the oculomotor circuitry. For instance, PIR bursting is predicted with a neuromimetic model of the brainstem saccadic circuitry, which successfully reproduces irregular eye trajectories in multiple disorders. However, the cellular machinery required to achieve this phenomenon is not elucidated in the neurons of oculomotor circuitry. As multiple disciplines such as clinical neuroscience, computational neuroscience and physiology converge on deciphering the inner workings of the oculomotor circuitry, the lack of established expression profiles for its neurons presents a hindrance to the future of oculomotor research.

5.2. Lessons from neurodegenerative diseases

To emphasize the rationale behind the approach being established in this thesis even further, it is necessary to extract valuable lessons from the studies of various neurodegenerative disorders. Several neurodegenerative diseases present with varying degrees of oculomotor abnormalities (Anderson & MacAskill, 2013). These include Parkinson's disease (PD), Alzheimer's disease (AD), amyotrophic lateral sclerosis (ALS), Huntington's disease (HD), and the spinocerebellar ataxias (SCA). Some diseases display more prominent and selective symptoms, such as the vertical saccadic impairment in progressive supranuclear palsy (PSP) and Niemann Pick Disease Type C (NPC), the horizontal saccadic impairment in Gaucher disease (Thurtell *et al.*, 2007; Salsano *et al.*, 2012) and the loss of intersaccadic intervals in opsoclonus (Wong *et al.*, 2001; Wong, 2007). However, regardless of their direct or selective impact on eye movements, there are many lessons that motivated the approach used in the research presented in this thesis.

Neuronal loss is not a prerequisite for the emergence of oculomotor symptoms. As observed in Huntington's disease and various spinocerebellar ataxias, neurological symptoms are rather due to neuronal dysfunction, than to neuronal cell loss, and they usually precede any neuronal cell loss (Jeub *et al.*, 2006). In SCA3, resting membrane potentials were reduced, and a hyperpolarizing shift of the activation curve of the delayed rectifier potassium current was observed, tying the dysfunction to an abnormal Kv activity (Jeub *et al.*, 2006). On the other hand, Huntington's disease mouse models showed altered physiological properties such as depolarized resting membrane potentials and higher input resistance, abnormal action potentials and a reduction of K^+ influx and efflux (Ariano *et al.*, 2005; Jeub *et al.*, 2006). Along with an observed NMDA receptor hyperactivity both in the hippocampus and in

striatal neurons, these changes are considered to cause neuronal dysfunction due to excitotoxicity (Jeub *et al.*, 2006).

Profiles of ion channels and transmitter receptor expression are linked to excitotoxicity and neurodegeneration. Over-excitation of neurons with high glutamate concentrations or prolonged stimulation has toxic effects, which is known as excitotoxicity (Kandel *et al.*, 2013). Excitotoxicity can be caused by different factors, such as increased NMDA receptor activity or expression, causing glutamatergic toxicity, increased neuronal excitability through ion channel regulation and the like (Jeub *et al.*, 2006). For instance, the downregulation of the K^+ concentration is linked to the dendritic degeneration observed in SCA1 (Chopra *et al.*, 2018). Furthermore, in ALS, an increased expression of P/Q type calcium channels (Cav2.1) is linked to selective neurodegeneration (Miles *et al.*, 2004). As calcium metabolism and Cav channel expression are linked to the firing characteristics of neurons, differential expression of calcium-binding proteins was also investigated for its role in neurodegeneration (Fairless *et al.*, 2019). However, calretinin and parvalbumin were shown to be not reliable markers of selective vulnerability to neurodegeneration (Laslo *et al.*, 2000; Fairless *et al.*, 2019).

Differential firing patterns contribute to selective neuronal vulnerability. Selective vulnerability of neurons to neurodegeneration is the phenomenon that a population of neurons shows differential susceptibility to degeneration under comparable genetic or microenvironment conditions. The first prominent example is the selective vulnerability of the dopaminergic neurons of substantia nigra pars compacta in PD. Interestingly, surviving neurons were found to express increased NMDA receptor subunit 1 (NMDAR1) levels, and displayed up to double their base bursting rates, which might contribute to the selective vulnerability of these neurons (Roselli & Caroni, 2015). Another impactful discovery is the finding that selective neurodegeneration of the motoneurons that innervate tongue muscles in ALS is correlated to differential expression of Cav channels (Miles *et al.*, 2004). In comparison to the ocular motoneurons, these neurons display a 3.5-fold increase in P/Q type calcium currents (by Cav2.1), which might also imply distinct firing patterns for the cause of selective neurodegeneration (Miles *et al.*, 2004). It must be noted that tonic and bursting firing patterns employ distinct Cav channel types (Roselli & Caroni, 2015). In ALS, fast-fatigable motoneurons with high firing threshold and burst spiking are particularly susceptible, which is linked to higher expression of calcium-activated SK channels, as also seen in the dopaminergic neurons of substantia nigra pars compacta (Wolfart *et al.*, 2001; Saxena & Caroni, 2011). In contrast, slow motoneurons, which exhibit low recruitment thresholds and a tonic firing, are less vulnerable as seen in mouse models of ALS (Pun *et al.*, 2006; Saxena *et al.*, 2013; Roselli & Caroni, 2015).

Accumulation of proteins may contribute indirectly to neurodegeneration through their alteration of ion channel expression. Protein aggregates or misfolded protein inclusions in neurodegenerative diseases is a common phenomenon and has been traditionally thought to be responsible for disease progression and physiological changes in brain tissue leading to neuronal toxicity and cell loss (Ross & Poirier, 2004). These include tau protein, amyloid β, α-synuclein and prions. However, there is only a weak direct

correlation between manifested severity of neurodegeneration and the number and density of plaques and tangles (McLean *et al.*, 1999; Roselli & Caroni, 2015). Recently, evidence emerged implying that the indirect effect of protein aggregates on ion channel regulation and excitotoxicity could be responsible for neuronal dysfunction (Kourie & Henry, 2001). For instance, dipeptidyl peptidase 10 (DPP10), a protein that facilitates Kv4 channel surface expression and neuronal excitability, is observed in neurofibrillary tangles and plaques of AD and PSP (Chen *et al.*, 2014). Likewise, amyloid B is shown to be involved in Kv channel function, and its physiological role in controlling neuronal excitability could be the underlying cause of neurodegeneration (Campolongo *et al.*, 2013).

6. Aim of the Thesis

This thesis aims primarily to build a bridge between histochemistry and electrophysiology in neurons of the oculomotor circuitry with known functions by demonstrating different ion channel and transmitter profiles of functionally distinct populations at the motor and premotor levels. Histochemical characterization of these neurons in macaque monkeys in terms of the transmitter or ion channel expression will subsequently allow for the post-mortem investigation of clinical cases with oculomotor symptoms in order to illuminate the biophysiological etiology and progression of oculomotor disorders. In this endeavor, specific lines of questions were addressed in the published material in order to establish this methodology as a valid tool for connecting biophysiological properties of the neurons in the oculomotor system to histochemistry and mathematical models. These are:

1- Is it possible to demonstrate the fast-firing capabilities of various neuronal populations in the oculomotor circuit with histochemical examination in terms of voltage-gated ion channels?

2- Is it possible to address the conflicting electrophysiology and anatomy data in terms of functional segregation views of MIF and SIF motoneurons with a histochemical identification of ion channel and transmitter-related protein expression in these groups?

3- Is it possible to investigate the validity of hypotheses put forward by the mathematical models, which are based on clinical data, with the immunohistochemical method?

4- Is it possible to provide valuable data, in return, to the computational neuroscience field applicable to the developed neuromimetic models of eye movement pathways in terms of intrinsic membrane properties and transmitter content of interconnections in the oculomotor system?

5- Is it possible to identify ion channel and transmitter-related markers that can be further used to delineate different firing characteristics (i.e. tonic, burst, burst/tonic, fast or slow) of populations or sub-populations within the oculomotor circuitry?

In order to address these questions, particular emphasis was placed on the motoneurons of the abducens and trochlear nuclei, premotor BNs of the RIMLF and PGD, OPNs and the Y-group neurons. Previously established anatomical, histochemical and electrophysiological differences between MIF and SIF

motoneurons were investigated by the immunolabeling of various ion channel and transmitter-related proteins. These will include voltage-gated potassium channels for fast-firing capability, low-voltage activated cation channels for post-inhibitory bursting capability, and finally excitatory and inhibitory transmitter inputs and post-synaptic receptor expression for differences in connectivity and excitability. Furthermore, the premotor neurons with distinct firing patterns were histochemically examined for the aforementioned ion channel protein expression in order to detect the potential differences and test hypotheses based on the mathematical models. Ultimately, this thesis aims to lay the groundwork in the non-human primate brain for an eventual paradigm shift in the assessment of the etiology in saccadic and other eye movement disorders. The post-mortem analysis of channelopathy in human as a cause for saccadic disorders and neurodegenerative disorders with oculomotor symptoms, will not only allow for the pharmacological intervention targeting the probable ion channel dysfunction, but also open a door for more accurate modeling of complex motor systems.

Results

Paper 1, pp 32-39:

Potassium channels in omnipause neurons (2019)

Paper 2, pp 40-67:

Transmitter and ion channel profiles of neurons in the primate abducens and trochlear nuclei (2021)

Paper 3, pp 68-82:

Saccadic premotor burst neurons and histochemical correlates of their firing patterns in rhesus monkey (2022)

Paper 4, pp 83-99:

Histochemical characterization of the vestibular y-group in monkey (2021)

1. Potassium channels in omnipause neurons

Mayadali ÜS, Lienbacher K, Mustari M, Strupp M, Horn AKE. Potassium channels in omnipause neurons. Prog Brain Res. 2019; 249:117-123. doi: 10.1016/bs.pbr.2019.04.017. Epub 2019 Jun 7. PMID: 31325972.

With permission of Elsevier

GSN affiliated co-authors:

- Prof. Dr. Michael Strupp; Regular member MCN, GSN associate faculty
  Ludwig-Maximilians-University Munich, University Clinic Großhadern, Dept. of Neurology and IFB-LMU
  Marchioninistr. 15, D-81377 Munich, Germany
  michael.strupp@med.uni-muenchen.de
  +49 (0)89 / 4400-73678
- Prof. Dr. Anja Horn-Bochtler; GSN associate faculty
  Chair of Vegetative Anatomy, Institute of Anatomy, Faculty of Medicine, LMU, Pettenkoferstr. 11 D-80336 Munich, Germany
  anja.bochtler@med.uni-muenchen.de
  +49 (0)89 / 2180-72667

CHAPTER

Potassium channels in omnipause neurons

8

Ümit S. Mayadali[a,b,d,*], Karoline Lienbacher[a,b], Michael Mustari[e,f], Michael Strupp[b,c,d], Anja K.E. Horn[a,d]

[a]*Institute of Anatomy and Cell Biology I, Ludwig-Maximilian University (LMU), Munich, Germany*
[b]*German Center for Vertigo and Balance Disorders, LMU, Munich, Germany*
[c]*Department of Neurology, LMU, Munich, Germany*
[d]*Graduate School of Systemic Neurosciences (GSN), LMU, Munich, Germany*
[e]*Washington National Primate Research Center, University of Washington, Seattle, WA, United States*
[f]*Department of Ophthalmology, University of Washington, Seattle, WA, United States*
**Corresponding author: Tel.: +49 89-2180-72668, e-mail address: umit.mayadali@med.uni-muenchen.de*

Abstract

Potassium (K^+) channels are major contributors to fast and precise action potential generation. The aim of this study was to establish the immunoreactivity profile of several potassium channels in omnipause neurons (OPNs), which play a central role in premotor saccadic circuitry. To accomplish this, we histochemically examined monkey and human brainstem sections using antibodies against the voltage gated K^+-channels $K_V1.1$, $K_V3.1b$ and K^+-Cl^- cotransporter (KCC2). We found that OPNs of both species were positive for all three K^+-antibodies and that the staining patterns were similar for both species. In individual OPNs, $K_V3.1b$ was detected on the somatic membrane and proximal dendrites, while $K_V1.1$ was mainly confined to soma. Further, KCC2 immunoreactivity was strong in distal dendrites, but was weak in the somatic membrane. Our findings allow the speculation that the alterations in K^+-channel expression in OPNs could be the underlying mechanism for several saccadic disorders through neuronal and circuit-level malfunction.

Keywords

Saccade, Fast-firing neurons, Perineuronal nets, Immunohistochemistry, $K_V1.1$, $K_V3.1b$, Potassium-chloride cotransporter, Monkey, Human

Progress in Brain Research, Volume 249, ISSN 0079-6123, https://doi.org/10.1016/bs.pbr.2019.04.017

1 Introduction

The generation and accurate execution of saccades relies on the timely interaction of premotor burst neurons and omnipause neurons (OPNs) in the brainstem (Leigh and Zee, 2015). During fixation and non-saccadic eye movements, OPNs prevent burst neurons from firing via a continuous tonic inhibition with frequencies approaching 200 Hz (Gandhi and Keller, 1999). Conceivably, a malfunction of the OPN firing pattern could result in saccadic disorders such as saccadic intrusions/oscillations (e.g., ocular flutter, opsoclonus) or saccadic slowing (Leigh and Kennard, 2004). Although some histochemical properties of OPNs that may contribute to the firing characteristics have been studied (Horn et al., 2003), not much is known about their ion channel expression profiles. Investigation of ion channels in OPNs would not only provide essential parameters of the saccadic circuitry, but also would enable the investigation of possible mechanisms of OPN failure that could contribute to saccadic intrusions/oscillations or slowing (Shaikh et al., 2008).

Due to their central role in determining and maintaining membrane potentials in highly active neurons (Johnston et al., 2010), it is reasonable to assume that voltage-gated potassium channel subunits (K_V) contribute significantly to OPN firing characteristics. Therefore, we provide here $K_V1.1$, $K_V3.1b$ and K^+-Cl^- cotransporter (*KCC2*) expression profiles of OPNs in monkey and human tissue specimen.

2 Methods

Five monkey brainstems (three *Macaca nemestrina,* obtained from Washington National Primate Research Center, two *Macaca mulatta* sections from previous studies—all fixed with 4% paraformaldehyde), and four post mortem human cases (fixed in 10% formaline) with no prior oculomotor symptoms obtained from the Reference Center for Neurodegenerative Disorders of the LMU were examined. Free-floating monkey brainstem sections were processed for the simultaneous immunofluorescence detection of one K^+ channel together with either SMI-32, a non-phosphorylated neurofilament (NP-NF) marker, or perineuronal net (PNN) marker hyaluronan and proteoglycan link protein 1 (HAPLN1), or with γ-aminobutyric acid (GABA)-A receptor ($GABA_AR$). Sections were subsequently visualized with a laser-scanning confocal microscope (Leica SP5, Mannheim, Germany) as described previously (May et al., 2016). Paraffin sections from human and monkey brainstems were processed for the detection of one K^+ channel together with either SMI-32 or PNN marker aggrecan (ACAN) using an immunoperoxidase protocol (see Table 1). The specificity of antibodies was validated by antibody-antigen preabsorption tests (data not shown). Since K^+ channels have been extensively

Table 1 Overview of the antibodies used in this study.

Antibody antigen	Dilution IF	Dilution IHC	Immunogen	Antibody details
K_V1.1	1:250	1:500 (human) 1:750 (monkey)	AA residues 416–495 of mouse KCNA1	Alomone APC-009 rabbit polyclonal
K_V3.1b	1:2000	1:6000	Residues 567–585 of rat K_V3.1b, KCNC1	Alomone APC-014 rabbit polyclonal
KCC2	1:500	1:4000	Residues 932–1043 of rat KCC2	Millipore 07-432 rabbit polyclonal
SMI-32 (NP-NF)	1:2500	1:2500	Neurofilament heavy polypeptide, 200 kDa	Sternberger 801701 mouse monoclonal
ACAN	–	1:75	Purified human articular cartilage aggrecan	Acris SM1353 mouse monoclonal
HAPLN1	1:100	1:400	Residues 16-354 of human HAPLN1	R&D AF2608 goat polyclonal

IF: immunofluorescence; IHC: immunohistochemistry; NP-NF: non-phosphorylated neurofilaments; ACAN: aggrecan; HAPLN1: hyaluronan and proteoglycan link protein 1.

studied in the auditory nuclei, the medial superior olive (MSO) in the same sections served as the internal positive control for both species (Johnston et al., 2010; Mathews et al., 2010).

3 Results

In monkey and human, OPNs were identified at the level of the traversing fibers of the abducens nerve by either SMI-32 or PNN immunostaining, which outlines their characteristic morphology (Figs. 1A and 2A,F) (Horn et al., 2003). The MSO was located ventrolateral to the OPNs in the same sections (Fig. 1B).

K_V1.1: OPNs showed positive K_V1.1 immunoreactivity in both monkey and human (Figs. 1A and 2A–D). Notably, K_V1.1 labeling in the OPNs was confined to the soma in both species, while K_V1.1 immunoreactivity in MSO neurons extended to somatic and dendritic membranes (Figs. 2E and 3D).
K_V3.1b: OPNs exhibited strong K_V3.1b immunoreactivity in both species (Figs. 2F–I and 3B). Confocal microscopy revealed that K_V3.1b expression was primarily present in the cell membrane of soma and proximal dendrites and moderately in the cytoplasm (Figs. 2G–I and 3B). A similar pattern of K_V3.1b immunoreactivity was found in MSO neurons of both species (Figs. 2J and 3E).

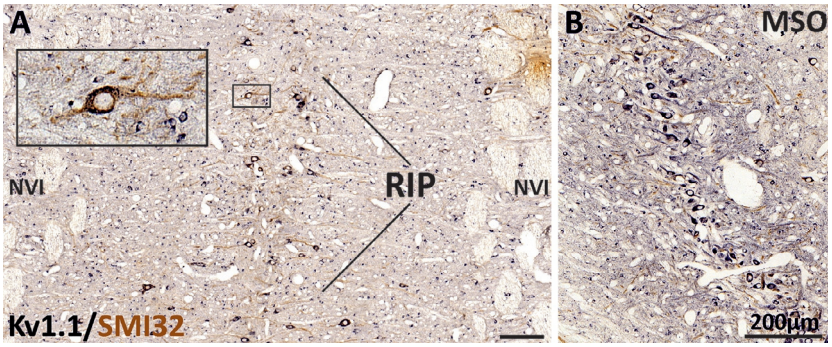

FIG. 1

Overview of OPNs located within raphe interpositus (RIP) (A), between traversing fibers of the abducens nerve (NVI) and medial superior olive (MSO, B) found ventrolateral to the OPNs on the same frontal section of a monkey pontine brainstem. Scale bars = 200 µm.

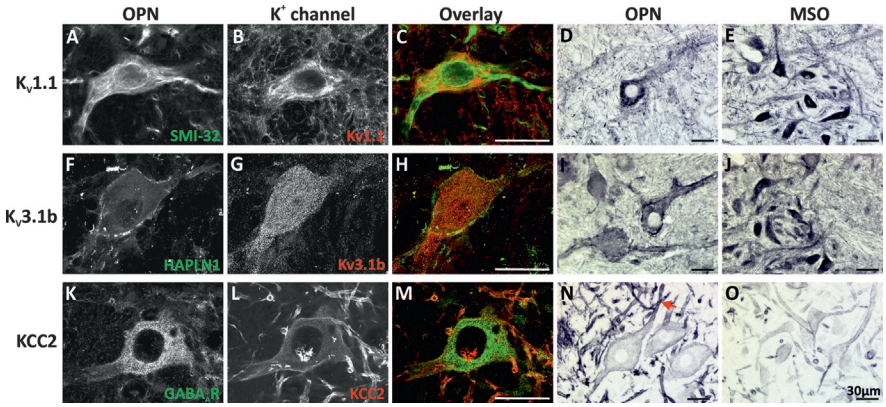

FIG. 2

K^+ channels in monkey OPNs: $K_V1.1$ labeling in OPNs identified by either SMI-32 (A, C) or HAPLN1 immunostaining (F, H) was confined to the somatic cytoplasm (A–D), while $K_V3.1b$ was primarily found in the cell membrane of the soma and proximal dendrites (F–H). MSO neurons within the same section showed strong somatic and dendritic immunoreactivity for $K_V1.1$ and $K_V3.1b$ (E, J). KCC2 immunoreactivity was weak in the somatic membranes (L, N), but strong in the dendrites of OPNs (L, N, arrow) similar to that of MSO neurons (O). A strong co-expression of $GABA_A$-Receptor immunoreactivity was present in OPNs (K). Scale bars = 30 µm.

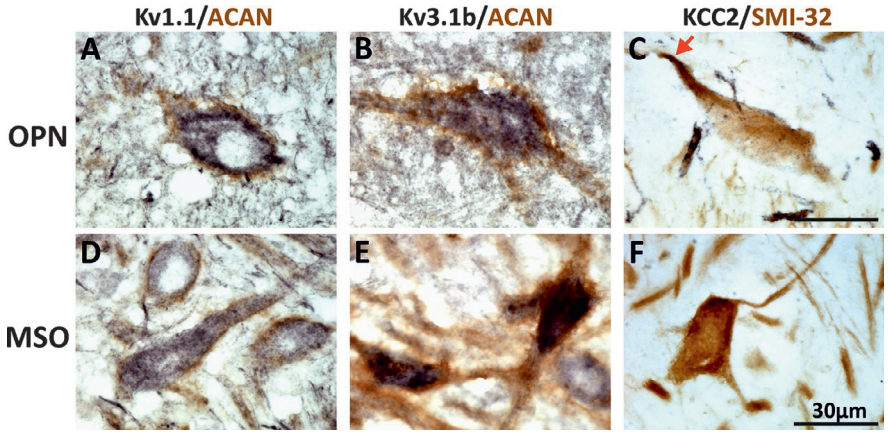

FIG. 3

K^+ channels in human OPNs: Immunostaining for $K_V1.1$ and $K_V3.1b$ (A–B) in human OPNs that were outlined by ACAN (aggrecan, brown) were similar to those of monkey OPNs. Comparable to KCC2 expression in monkey OPNS, KCC2 immunoreactivity was stronger in dendrites (C, arrow) than somatic membrane. MSO neurons on the same sections as the $K_V1.1$, $K_V3.1b$ and KCC2 stainings are shown in their respective columns (D–F). Scale bars = 30 µm.

KCC2: Strong KCC2 immunoreactivity was present in the dendrites of OPNs, whereas in their somatic membranes the signal was weak (Figs. 2K–N and 3C). The KCC2 positive OPNs co-expressed $GABA_AR$ immunoreactivity (Fig. 2K–M). KCC2 staining patterns of the OPNs were similar to that of MSO neurons, but the latter expressed less overall immunoreactivity (Figs. 2O and 3F).

4 Discussion

This study demonstrates by specific immunohistochemical staining that saccadic OPNs in monkey and human express the potassium channels $K_V1.1$, $K_V3.1b$ and KCC2. Expression of K_V1 and K_V3 subunits in particular, suggests a direct contribution to the fast and precise firing properties of OPNs, as previously demonstrated in auditory brainstem circuitry (Johnston et al., 2010; Mathews et al., 2010). For instance, K_V1 subunits are known to raise the action potential firing threshold and to reduce the time constant by opening with only small perturbations (Johnston et al., 2010). K_V3 subunits, on the other hand, facilitate high firing rates by opening only at high membrane potentials, and short refractory periods by their fast closure kinetics (Kaczmarek and Zhang, 2017). Specifically, $K_V3.1b$ expression is often found in neurons with fast-firing properties that contain the calcium-binding protein

parvalbumin, and that are ensheathed by PNNs (Härtig et al., 1999) as seen in OPNs (Horn et al., 2003). Further, KCC2 maintains chloride homeostasis in neurons and determines the polarity and efficacy of $GABA_AR$ and glycine receptors (Chamma et al., 2012). As GABAergic and glycinergic input to the OPNs had been already found (Horn et al., 1994), the co-expression of KCC2 and $GABA_AR$ in OPNs in the present study is in line with the functional implications of the transporter (Fig. 2K–M) (Chamma et al., 2012).

These findings on OPNs have clinical implications as irregularities in all of the tested potassium channels result in disorders related to neuronal excitability (Kaczmarek and Zhang, 2017; Shieh et al., 2000; Vinay and Jean-Xavier, 2008). Such a failure of a key cell group in the saccadic circuitry could manifest itself as saccadic flutter/oscillations, as suggested by Shaikh et al. (2008). Therefore, investigation of potassium channel expression in OPNs (or other functional groups of the saccadic circuitry) in such saccadic disorders as found in autoantibody-mediated autoimmune disorders, paraneoplastic syndromes and brainstem encephalitis (Torres-Vega et al., 2016; Tüzün et al., 2010) would provide valuable insight into their pathophysiology.

Acknowledgments

We thank Christine Unger and Ahmed Messoudi, MPh for their excellent technical assistance, and Prof. Dr. med. Waschke for his continuous support. This work was supported by BMBF (IFB-01E0901, Brain-Net-01GI0505) and National Institutes of Health (EY06069; P51 OD010425).

References

Chamma, I., Chevy, Q., Poncer, J.C., Levi, S., 2012. Role of the neuronal K-cl co-transporter KCC2 in inhibitory and excitatory neurotransmission. Front. Cell. Neurosci. 6, 5.

Gandhi, N.J., Keller, E.L., 1999. Comparison of saccades perturbed by stimulation of the rostral superior colliculus, the caudal superior colliculus, and the omnipause neuron region. J. Neurophysiol. 82, 3236–3253.

Härtig, W., Derouiche, A., Welt, K., Brauer, K., Grosche, J., Mäder, M., Reichenbach, A., Brückner, G., 1999. Cortical neurons immunoreactive for the potassium channel Kv3.1b subunit are predominantly surrounded by perineuronal nets presumed as a buffering system for cations. Brain Res. 842, 15–29.

Horn, A.K.E., Büttner-Ennever, J.A., Wahle, P., Reichenberger, I., 1994. Neurotransmitter profile of saccadic omnipause neurons in nucleus raphe interpositus. J. Neurosci. 14, 2032–2046.

Horn, A.K.E., Brückner, G., Härtig, W., Messoudi, A., 2003. Saccadic omnipause and burst neurons in monkey and human are ensheathed by perineuronal nets but differ in their expression of calcium-binding proteins. J. Comp. Neurol. 455, 341–352.

Johnston, J., Forsythe, I.D., Kopp-Scheinpflug, C., 2010. Going native: voltage-gated potassium channels controlling neuronal excitability. J. Physiol. 588, 3187–3200.

Kaczmarek, L.K., Zhang, Y., 2017. Kv3 channels: enablers of rapid firing, neurotransmitter release, and neuronal endurance. Physiol. Rev. 97, 1431–1468.
Leigh, R.J., Kennard, C., 2004. Using saccades as a research tool in the clinical neurosciences. Brain 127, 460–477.
Leigh, R.J., Zee, D.S., 2015. The Neurology of Eye Movements, fifth ed. Oxford University Press, New. York.
Mathews, P.J., Jercog, P.E., Rinzel, J., Scott, L.L., Golding, N.L., 2010. Control of submillisecond synaptic timing in binaural coincidence detectors by Kv1 channels. Nat. Neurosci. 13, 601–609.
May, P.J., Warren, S., Bohlen, M.O., Barnerssoi, M., Horn, A.K., 2016. A central mesencephalic reticular formation projection to the Edinger-Westphal nuclei. Brain Struct. Funct. 221, 4073–4089.
Shaikh, A.G., Ramat, S., Optican, L.M., Miura, K., Leigh, R.J., Zee, D.S., 2008. Saccadic burst cell membrane dysfunction is responsible for saccadic oscillations. J. Neuroophthalmol. 28, 329–336.
Shieh, C.C., Coghlan, M., Sullivan, J.P., Gopalakrishnan, M., 2000. Potassium channels: molecular defects, diseases, and therapeutic opportunities. Pharmacol. Rev. 52, 557–594.
Torres-Vega, E., Durán-Moreno, M., Sánchez Del Pino, M., Yáñez, Y., Cañete, A., Castel, V., López-Cuevas, R., Vílchez, J.J., Dalmau, J., Graus, F., García Verdugo, J.M., Bataller, L., 2016. Immunoproteomic studies on paediatric opsoclonus-myoclonus associated with neuroblastoma. J. Neuroimmunol. 297, 98–102.
Tüzün, E., Kürtüncü, M., Lang, B., Içöz, S., Akman-Demir, G., Eraksoy, M., Vincent, A., 2010. Bickerstaff's encephalitis and Miller Fisher syndrome associated with voltage-gated potassium channel and novel anti-neuronal antibodies. Eur. J. Neurol. 17, 1304–1307.
Vinay, L., Jean-Xavier, C., 2008. Plasticity of spinal cord locomotor networks and contribution of cation-chloride cotransporters. Brain Res. Rev. 57, 103–110.

2. Transmitter and ion channel profiles of neurons in the primate abducens and trochlear nuclei

Mayadali ÜS, Fleuriet J, Mustari M, Straka H, Horn AKE. Transmitter and ion channel profiles of neurons in the primate abducens and trochlear nuclei. Brain Struct Funct. 2021 Sep; 226(7):2125-2151. doi: 10.1007/s00429-021-02315-7. Epub 2021 Jun 28. PMID: 34181058; PMCID: PMC8354957

Open Access

GSN affiliated co-authors:

- Prof. Dr. Hans Straka; MCN Board member, GSN core faculty
  Ludwig-Maximilians-University Munich, Dept. Biology II, Division Neurobiology
  Großhaderner Straße 2, D-82152 Planegg-Martinsried, Germany
  straka@lmu.de
  +49 (0)89 / 2180-74307
- Prof. Dr. Anja Horn-Bochtler; GSN associate faculty
  Chair of Vegetative Anatomy, Institute of Anatomy, Faculty of Medicine, LMU, Pettenkoferstr. 11 D-80336 Munich, Germany
  anja.bochtler@med.uni-muenchen.de
  +49 (0)89 / 2180-72667

Brain Structure and Function (2021) 226:2125–2151
https://doi.org/10.1007/s00429-021-02315-7

ORIGINAL ARTICLE

Transmitter and ion channel profiles of neurons in the primate abducens and trochlear nuclei

Ümit Suat Mayadali[1,2] · Jérome Fleuriet[3,4] · Michael Mustari[3] · Hans Straka[5] · Anja Kerstin Ellen Horn[1]

Received: 19 February 2021 / Accepted: 4 June 2021 / Published online: 28 June 2021

Abstract

Extraocular motoneurons initiate dynamically different eye movements, including saccades, smooth pursuit and vestibulo-ocular reflexes. These motoneurons subdivide into two main types based on the structure of the neuro-muscular interface: motoneurons of singly-innervated (SIF), and motoneurons of multiply-innervated muscle fibers (MIF). SIF motoneurons are thought to provoke strong and brief/fast muscle contractions, whereas MIF motoneurons initiate prolonged, slow contractions. While relevant for adequate functionality, transmitter and ion channel profiles associated with the morpho-physiological differences between these motoneuron types, have not been elucidated so far. This prompted us to investigate the expression of voltage-gated potassium, sodium and calcium ion channels (*Kv1.1*, *Kv3.1b*, *Nav1.6*, *Cav3.1–3.3*, *KCC2*), the transmitter profiles of their presynaptic terminals (*vGlut1* and *2*, *GlyT2* and *GAD*) and transmitter receptors (*GluR2/3*, *NMDAR1*, *GlyR1α*) using immunohistochemical analyses of abducens and trochlear motoneurons and of abducens internuclear neurons (INTs) in macaque monkeys. The main findings were: (1) MIF and SIF motoneurons express unique voltage-gated ion channel profiles, respectively, likely accounting for differences in intrinsic membrane properties. (2) Presynaptic glutamatergic synapses utilize vGlut2, but not vGlut1. (3) Trochlear motoneurons receive GABAergic inputs, abducens neurons receive both GABAergic and glycinergic inputs. (4) Synaptic densities differ between MIF and SIF motoneurons, with MIF motoneurons receiving fewer terminals. (5) Glutamatergic receptor subtypes differ between MIF and SIF motoneurons. While NMDAR1 is intensely expressed in INTs, MIF motoneurons lack this receptor subtype entirely. The obtained cell-type-specific transmitter and conductance profiles illuminate the structural substrates responsible for differential contributions of neurons in the abducens and trochlear nuclei to eye movements.

Keywords Voltage-gated potassium channels · Low-voltage activated calcium channels · Glutamate · GABA · Glycine · Extraocular motoneurons · Internuclear neurons

✉ Anja Kerstin Ellen Horn
Anja.Bochtler@med.uni-muenchen.de

1 Institute of Anatomy and Cell Biology, Dept. I, Ludwig-Maximilians-University Munich, Pettenkoferstrasse 11, 80336 Munich, Germany

2 Graduate School of Systemic Neurosciences, Ludwig-Maximilians-University Munich, Planegg-Martinsried, Germany

3 Washington National Primate Research Center, Department of Ophthalmology, University of Washington Seattle, Seattle, WA, USA

4 Intensive Care Unit, Raymond Poincaré Hospital, Assistance Publique-Hôpitaux de Paris, Garches, France

5 Department of Biology II, Ludwig-Maximilians-University Munich, Planegg-Martinsried, Germany

Introduction

Extraocular muscles and innervation by motoneurons in the abducens and trochlear nuclei

Extraocular muscles are responsible for diverse types of eye movements including saccades, smooth pursuit, vestibulo-ocular and optokinetic reflexes, and for fixation (Leigh and Zee 2015). The variation of speed and persistence of these eye movements derive from the contraction of distinct muscle fiber types and their endowment with fast or slow myosin heavy chain isoforms, the number of mitochondria in the sarcoplasm, number and distribution of nerve endings along muscle fibers and the activity of associated motoneurons (Hoh 2020; Horn and Straka 2021). Extraocular

muscle fibers can be grouped into one of two main categories according to their innervation patterns: Fast-contracting, fatigable twitch type muscle fibers are innervated by a single *en plaque* ending near the middle of the muscle belly (SIF), whereas slow-contracting, non-fatigable non-twitch type muscle fibers are synaptically contacted along the entire length of the fiber by multiple *en grappe* nerve endings (MIF). In addition, MIFs are also associated with another type of nerve terminal, the palisade endings, which are located at the proximal and distal myotendinous junctions. Whether these unique eye muscle specializations have a sensory or motor function is still being debated (Lienbacher and Horn 2012; Zimmermann et al. 2013).

Eye movements result from coordinated contractions of largely synergistic extraocular muscles through task-specific cooperation by MIFs and SIFs. For horizontal eye movements, lateral rectus muscles are activated by motoneurons in the ipsilateral abducens nucleus (nVI), located in the hindbrain pontine tegmentum; and for vertical and torsional eye movements, by motoneurons in the oculomotor (nIII) and trochlear (nIV) nuclei located in the mesencephalon and rostral hindbrain, respectively (Horn and Straka 2021). The abducens nucleus as an entity consists of four distinct neuronal subtypes: cholinergic motoneurons targeting (1) singly- (SIF) and (2) multiply-innervated (MIF) lateral rectus muscle fibers, (3) glutamatergic internuclear neurons (INT) and (3) paramedian tract neurons (PMT) (Horn et al. 2018; Nguyen and Spencer 1999). While MIF and SIF motoneurons collectively elicit eye muscle contraction, INTs provide the concomitant activation of synergistic medial rectus motoneurons in the contralateral nIII for the generation of conjugate eye movements in the horizontal plane (Büttner-Ennever and Akert 1981). Lastly, PMT neurons presumably send an efference copy of premotor commands to the cerebellar floccular region (Büttner-Ennever 1992; Horn et al. 2018).

The trochlear nucleus, which innervates the contralateral superior oblique muscle, forms one of the final motor elements of the vertical/oblique eye movement circuitry and mainly contains MIF and SIF motoneurons, with only a few internuclear neurons (Ugolini et al. 2006). The two distinct MIF and SIF motoneuronal populations in the abducens and trochlear nuclei were initially demonstrated by tract-tracing from distinct muscle target sites (Büttner-Ennever et al. 2001). In both nuclei, SIF and MIF motoneurons can be retrogradely labeled by tracer injections into the belly of the lateral rectus or superior oblique muscle (Büttner-Ennever et al. 2001; Ugolini et al. 2006). On the other hand, MIF motoneurons can be labeled selectively by tracer injections into the myotendinous junctions of both muscles, which exclusively contain *en grappe* endings (Büttner-Ennever et al. 2001; Ugolini et al. 2006). MIF motoneurons are small or medium-sized neurons clustered in a dorsal cap of the trochlear nucleus. In the abducens nucleus, MIF motoneurons, which form up to 20% of the entire motoneuronal population, are more distributed and accumulate at the medial, dorsal and ventral borders (Eberhorn et al. 2005; Horn et al. 2018; Hernández et al. 2019).

Histochemical and functional segregation of SIF and MIF motoneurons

MIF and SIF motoneurons in the abducens nucleus form distinct functional subgroups based on differential origins of premotor inputs (Ugolini et al. 2006). Rabies virus injection into the belly of the lateral rectus muscle results in retrograde transneuronal labeling of all premotor cell groups, such as the nucleus prepositus hypoglossi, premotor burst neurons in the paramedian pontine reticular formation (PPRF) and dorsal paragigantocellular nucleus; injection into the myotendinous junction results in transneuronal labeling of premotor neurons involved in gaze-holding and smooth pursuit, but fails to outline other premotor neurons, such as saccade-related burst neurons in the PPRF (Ugolini et al. 2006). This suggests that SIF motoneurons are more involved in targeted eye movements, whereas MIF motoneurons are more suitable to stabilize the eyes around the primary position during fixation of a target (Büttner-Ennever et al. 2001; Dean 1996).

Combined tract-tracing and histochemical studies in monkey have outlined major histochemical differences between MIF and SIF motoneurons, which also served to identify homologous neuronal groups in humans (Horn et al. 2008, 2018). Cholinergic SIF motoneurons of all extraocular motor nuclei are ensheathed by a condensed extracellular matrix, called perineuronal nets (PN) and express the calcium-binding protein parvalbumin (PAV), while MIF motoneurons lack both features (Büttner-Ennever 2006; Eberhorn et al. 2005, 2006; Horn et al. 2008). PNs, together with the expression of PAV, are markers for fast-spiking neurons with high metabolic demands (Härtig et al. 1999; Kodama et al. 2020). In this regard, SIF motoneurons and abducens INTs share similar histochemical profiles (Horn et al. 2018). In addition, an electron microscopic study of medial rectus motoneurons demonstrated a differential density of various types of synaptic contacts on MIF versus SIF motoneurons (Erichsen et al. 2014). The rather tonic firing properties of MIF motoneurons, as demonstrated in frogs, support the idea that MIF motoneurons are particularly suitable for slow changes and tonic maintenance of eye position (Dieringer and Precht 1986; Eberhorn et al. 2005).

At variance with a task-separation of SIF and MIF motoneurons, a number of studies in different species have challenged such a functional segregation. For instance, vestibulo-ocular responses of abducens motoneurons in larval *Xenopus laevis* demonstrated that motoneurons are not segregated

into two clearly distinct groups in terms of firing characteristics; instead, these neurons rather form a continuum with respect to firing rate and activation threshold (Dietrich et al. 2017). Potentially, these motoneuron populations may also form a gradient with respect to specific glutamatergic receptor subtypes (i.e., NMDA or AMPA) mediating vestibular excitatory inputs (Dietrich et al. 2017). In addition, four different motoneuronal types were identified in the rat oculomotor nucleus with respect to discharge characteristics in vitro, where, however, none of the subgroups corresponds to anatomically identified MIF motoneurons (Nieto-Gonzales et al. 2007). A distinct, task-specific separation has also been challenged based on recordings in alert cats, where both SIF and MIF motoneurons were recruited regardless of the eye movement type. In addition, both types contribute with a burst/tonic discharge pattern to all eye movement behaviors (Hernández et al. 2019). However, MIF motoneurons exhibit lower discharge thresholds, lower eye movement sensitivities and overall reduced firing rate levels (Hernández et al. 2019). Collectively, these results suggest that the duality of MIF and SIF motoneurons based on the structure of the neuro-muscular interface is likely too simplistic, and thus requires further fine-tuning according to presynaptic transmitter profile, postsynaptic receptor identity and ion channel composition.

Aim of the study

The apparent discrepancy between electrophysiological and anatomical/histochemical findings in regard to MIF and SIF motoneurons prompted us to investigate potential histochemical differences between the two types by analyzing molecular characteristics known to define intrinsic membrane and/or synaptic properties. Therefore, this study aims at investigating differences in excitatory and inhibitory synaptic inputs, transmitter receptors and voltage-gated ion channels using the previously established histochemical identification scheme of classifying neurons in the abducens and trochlear nuclei.

Materials and methods

Brain tissue

Brainstem sections of one new macaque (Case M1) and five previously described macaque monkeys (Cases M2–6) were used in this study (Ahlfeld et al. 2011; Lienbacher et al. 2011; Table 1). Frozen sections from three cases (M1–3) and paraffin sections from three other cases (M4–6) were used. All animals had been similarly fixed by transcardial perfusion with 4% paraformaldehyde (PFA) in 0.1 M phosphate buffer (PB; pH 7.4).

The *Macaca mulatta* specimen (M1) received an injection with the tract-tracer wheatgerm agglutinin (WGA; 10 µL 5%; EY Laboratories) into the myotendinous junction of the lateral rectus muscle of one eye to retrogradely label MIF motoneurons. After three days of survival, the animal was sacrificed with an overdose of pentobarbital (90 mg/kg body weight) and transcardially perfused with 0.9% saline followed by 2–3 L of 4% PFA in 0.1 M PB (pH 7.4). The extracted brainstem of this specimen, as well as two additional *Macaca nemestrina* specimens (M2 and M3), were similarly prepared for sectioning on a freezing microtome by immersion in increasing concentrations of 10–30% sucrose dissolved in 0.1 M PB solution. Frozen brainstems were cut

Table 1 Summary of experimental protocols, histological procedures and immunohistochemical details for tissue obtained from six macaque monkeys (cases M1–M6)

Case	Injection	Section Type	Fluorescence	Immunohistochemistry
M1	WGA; 10µl 5%	Frozen (40µm)	**WGA**, **ACAN**, **Kv1.1, Kv3.1b**	*WGA, ACAN*
M2	-	Frozen (40µm)	**ACAN**, **ChAT**, **Kv1.1, Kv3.1b**	-
M3	-	Frozen (40µm)	*ACAN, ChAT, Kv1.1, Kv3.1b*	-
M4	-	Paraffin (5µm/10 µm)	-	**ACAN**, **ChAT**, *Kv1.1, Kv3.1b,* **vGlut1**, **vGlut2**, **SMI-32**, **GluR2/3**, *NMDAR1, CR*, *GlyT2, GAD*, **GlyR1α**, *KCC2, PAV*
M5	-	Paraffin (5µm)	-	**ACAN**, **ChAT**, **Kv1.1**, **Kv3.1b**, **Nav1.6**, **vGlut1**, **vGlut2**, *SMI-32,* **GluR2/3**, **NMDAR1**, **CR**, **GlyT2**, **GAD**, *GlyR1α*, **KCC2**, **PAV**, **Cav3.1**, **Cav3.2**, **Cav3.3**
M6	-	Paraffin (7µm)	-	**ACAN**, **ChAT**, *Kv1.1, Kv3.1b,* **vGlut1**, **vGlut2**, **SMI-32**, *GluR2/3,* **NMDAR1**, **CR**, *GlyT2, GAD*, **GlyR1α**, **KCC2**, *PAV*

Antibodies in gray italics denote histochemical tests that were not illustrated in the figures. Antibodies in bold denote IHC labeling shown in the figures. Colors of antibodies match the visualized chromogen of a particular antibody staining

IF immunofluorescence; *IHC* immunohistochemistry (peroxidase)

with a Leica cryostat at 40 µm thickness in the transverse plane, and used for immunofluorescence staining.

Brainstems from three additional *Macaca mulatta* cases from previous projects, which were embedded in paraffin, were also included in the analysis (Zeeh et al. 2020). Thin serial sections (5 µm (M4, M5), 7 µm (M6), 10 µm (M4)) were cut and immunostained after deparaffination, rehydration and antigen retrieval protocols. In brief, antigen retrieval was accomplished by rinsing the rehydrated sections in distilled water and reacting in 0.01 M sodium citrate buffer (pH 6.0) at 1160 W power in a microwave (AEG, Micromat) three times for 3 min, each. After cooling to room temperature, sections were transferred to a Tris buffered saline (TBS; pH 7.4) for subsequent immunoperoxidase-based staining.

All experimental procedures conformed to the State and University Regulations on Laboratory Animal Care, including the Principles of Laboratory Animal Care (NIH Publication 85-23, Revised 1985), and were approved by the Animal Care Officers and Institutional Animal Care and Use Committees at the University of Washington, where all surgical interventions were made.

Antisera

Choline acetyltransferase (ChAT)

Cholinergic motoneurons were detected with an affinity-purified polyclonal goat anti-ChAT antibody (Cat #: AB144P; RRID: AB_2079751; Chemicon, Temecula, CA, USA) directed against the whole enzyme isolated from the human placenta, which is identical to the enzyme expressed in the brain (Bruce et al. 1985). This antibody recognizes a 68–70 kDa protein. The appearance and distribution of ChAT-immunopositive neurons identified with this antibody in the present study comply with the respective results of previous studies (Eberhorn et al. 2005; Horn et al. 2018). A 1:75 dilution was used for the immunoperoxidase-based method and a 1:25 dilution for the immunofluorescence-based detection.

Wheat germ agglutinin (WGA)

The tracer wheat germ agglutinin (WGA; EY Labs, San Mateo, CA, USA) was detected with a polyclonal goat antibody (Cat #: SM1353AS-2024; RRID: AB_2315611; Vector, Burlingame, CA, USA). A 1:5000 dilution was used for the immunofluorescence-based detection.

Aggrecan (ACAN)

Perineuronal nets were detected with the monoclonal mouse anti-aggrecan antibody (Cat #: SM1353; RRID: AB_972582; Acris Antibodies GmbH, Herford, Germany), which was developed to identify human aggrecan protein, a proteoglycan component of the cartilage matrix. A 1:75 dilution was used for the immunoperoxidase-based method and a 1:25 dilution for the immunofluorescence-based detection.

Voltage-gated potassium channel subunits Kv1.1 and Kv3.1b

The voltage-gated potassium channel subfamily A member 1 (KCNA1) subunit was detected with a polyclonal rabbit antibody (Cat #: APC-009; RRID: AB_2040144; Alomone Labs, Jerusalem, ISRAEL). This antibody recognizes the intracellular Kv1.1 C-Terminus epitope, corresponding to amino acid residues 416–495 of the mouse (*Mus musculus*) Kv1.1 protein. In this study, a 1:750 dilution was used for the immunoperoxidase-based method and a 1:250 dilution for the immunofluorescence-based detection.

The antibody against Kv3.1b amino acid residues 567–585, corresponding to the C-terminus of the voltage-gated potassium channel subunit KCNC1 (RRID: AB_2040166) was raised in rabbit (Weiser et al. 1995). In this study, a 1:6000 dilution was used for the immunoperoxidase-based method and a 1:2000 dilution for the immunofluorescence-based method.

Voltage-gated sodium channel subunit Nav1.6

The voltage-gated sodium channel type VIII alpha subunit (SCNA8) was detected with a polyclonal rabbit antibody (Cat #: ASC-009; RRID: AB_2040202; Alomone Labs, Jerusalem, ISRAEL). This antibody recognizes amino acid residues 1042–1061 of the rat Nav1.6 peptide. In this study, a 1:500 dilution was used.

Low-voltage activated calcium channel subunits (Cav3.1, Cav3.2, Cav3.3)

Voltage-dependent T-type calcium channel subunits Cav3.1 (CACNA1G, α1G; Cat #: ACC-021; RRID: AB_2039779), Cav3.2 (CACNA1H, α1H; Cat #: ACC-025; RRID: AB_2039781) and Cav3.3 (CACNA1I, α1H; Cat #: ACC-009; RRID: AB_2039783) were detected with polyclonal rabbit antibodies from (Alomone Labs, Jerusalem, ISRAEL). The Cav3.1 antibody recognizes intracellular amino acid residues 1–22 of the rat CACNA1G at the N-terminus. The Cav3.2 antibody recognizes amino acid residues 581–595 of the rat CACNA1H at the intracellular loop between domains D1 and D2. The Cav3.3 antibody recognizes amino acid residues 1053–1067 of the rat Cav3.3 between the intracellular domains II and III. In this study, a 1:1000 dilution was used for all three antibodies.

AMPA receptor GluR2/3

Glutamate receptors (GluR) 2 and 3 were detected with a polyclonal rabbit antibody (Cat #: AB1506; RRID: AB_90710; Chemicon, Temecula, CA, USA), which recognizes the C-terminus (EGYNVYGIESVKI) of the rat GluR2 peptide, which is nearly identical with the C-terminus of GluR3. Here, a 1:500 dilution was used.

NMDA receptor 1

The NMDA receptor 1 (*N*-methyl-D-aspartate receptor channel, subunit zeta-1) was detected with a monoclonal mouse antibody (Cat #: MAB363; RRID: AB_94946; Chemicon, Temecula, CA, USA), which recognizes amino acid residues 660–811 located in the extracellular loop between transmembrane regions III and IV of the NMDAR1. In this study, a 1:1000 dilution was used.

Glutamate decarboxylase (GAD65/67) and glycine transporter 2 (GlyT2)

GABAergic synaptic terminals were detected by a polyclonal rabbit anti-glutamate decarboxylase 65 and 67 (GAD65/67) antibody (Cat #: AB1511; RRID; AB_90715; Chemicon, Temecula, CA, USA), which recognizes C-terminus residues 572–585. GAD65 is membrane-anchored (585 a.a.) and is responsible for vesicular GABA production, whereas GAD67 is located in the cytoplasm (594 a.a.) and is responsible for a significant cytoplasmic GABA production. A 1:2000 dilution was used.

Glycinergic synaptic terminals were detected by a polyclonal sheep antibody (Cat #: AB1771; RRID: AB_90945; Chemicon, Temecula, CA, USA), which recognizes a synthetic peptide from the C-terminus of the glycine transporter 2 as predicted from the cloned rat GlyT2. A 1:5000 dilution was used.

Glycine receptor 1α

Glycine receptor 1α was detected by a monoclonal (clone mAb4a) mouse antibody (Cat #: 146 011; RRID: AB_887722; Synaptic Systems, Göttingen, Germany), which recognizes amino acid residues 96–105 from the rat glycine receptor α1. A 1:300 dilution was used.

K^+/Cl^- cotransporter (KCC2)

The potassium chloride symporter 2 (KCC2) was detected by a polyclonal rabbit antibody (Cat #: 07-432; RRID: AB_310611; Chemicon, Temecula, CA, USA), which recognizes amino acid residues 932–1043 of the rat KCC2 at the N-terminus. A 1:4000 dilution was used.

Calretinin (CR) and parvalbumin (PAV)

The calcium-binding protein calretinin (CR) was detected with a polyclonal rabbit antibody (Cat #: 7699/3H; RRID: AB_10000321; Swant, Marly, Fribourg, Switzerland) as described previously (Fairless et al. 2019). The calcium-binding protein parvalbumin (PAV) was detected with a monoclonal mouse antibody (Cat #: 235; RRID: AB_10000343; Swant, Marly, Fribourg, Switzerland). In this study, a 1:2500 dilution was used for both antibodies.

Vesicular glutamate transporters (vGlut1 and vGlut2)

The vesicular glutamate transporter 1 (vGlut1/ SLC17A7) was detected with a polyclonal rabbit antibody (Cat #: 135 303; RRID: AB_887875; Synaptic Systems, Göttingen, Germany). The vesicular glutamate transporter 2 (vGlut2/ SLC17A6) was detected with a monoclonal mouse antibody (Cat #: MAB5504; RRID: AB_2187552; Chemicon, Temecula, CA, USA). Both, vGlut1 and vGlut2 mediate the uptake of glutamate into synaptic vesicles at the presynaptic nerve terminals of excitatory neurons, and usually show complementary expression patterns (Fremeau et al. 2004). In this study, a 1:3000 dilution for vGlut1 and a 1:4000 dilution for vGlut2 were used.

The specificities of all antibodies were validated with the first antibody omission control and pre-absorption control tests.

Staining methods

Combined immunofluorescence labeling of tracer-stained motoneurons

Transverse sections through the pontomedullary junction were processed for different combinations of immunofluorescence staining. For simultaneous detection of WGA and PNs, floating sections of case M1 were incubated in 5% normal donkey serum in 0.1 M Tris-buffered saline (TBS; pH 7.4), containing 0.3% Triton X-100 (NDS-TBS-T) for 1 h at room temperature. Subsequently, the sections were processed with a mixture of mouse anti-ACAN (1:25), goat anti-WGA (1:250) and optionally one of the voltage-gated potassium channel markers (rabbit anti-Kv1.1, 1:250 or rabbit anti-Kv3.1b, 1:2000) in NDS-TBS-T for 48 h at 4 °C. After washing three times in 0.1 M TBS, the sections were treated with a mixture of Cy3-conjugated donkey anti-rabbit IgG (1:200; Dianova), Alexa Fluor 488-tagged donkey anti-mouse IgG (1:200; Molecular Probes, Eugene, OR, USA) and DyLight 512 tagged donkey anti-goat IgG (1:100, Dianova) for 2 h at room temperature. After a short rinse in

distilled water, sections were dried and coverslipped with DPX mounting medium (Gel/Mount; Biomeda, San Francisco, CA, USA) and stored in darkness at 4 °C.

Single and double immunoperoxidase stainings of consecutive paraffin sections

For single immunoperoxidase staining, paraffin-embedded brainstem sections of cases M4, M5 and M6 were washed in 0.1 M TBS (pH 7.4) and treated with 1% H_2O_2 in TBS for 30 min to block endogenous peroxidase activity subsequent to deparaffination, rehydration and antigen retrieval protocols. Sections were then processed with a primary antibody of choice (see Methods, Table 2) in 0.1 M TBS (pH 7.4), containing 0.3% Triton X-100 (NDS-TBS-T) in humid chambers for 48 h at 4 °C. Subsequent to primary antibody incubation, all markers were visualized by the binding of biotinylated secondary antibodies (1:200; Vector Lab) followed by extravidin-peroxidase (1:1000; Sigma) and diaminobenzidine (DAB)

Table 2 Summary of primary antibodies and dilutions for the immunolabeling

Antibody	Host	Antigen	Manufacturer	Antibody registry number (RRID)	Dilution
WGA	Goat/polyclonal	Wheat germ agglutinin	EY Labs, San Mateo,CA, USA	AB_2315611	1:250 (IF)
ACAN	Mouse/monoclonal	Aggrecan	Acris Antibodies GmbH, 32052 Herford, Germany	AB_972582	1:25 (IF), 1:75 (IHC)
ChAT	Goat/polyclonal	Choline acetyltransferase	Chemicon, Temecula, CA, USA	AB_2079751	1:25 (IF), 1:50 (IHC)
Kv1.1	Rabbit/polyclonal	Voltage-gated potassium channel 1.1	Alomone Labs Jerusalem BioPark (JBP)	AB_2040144	1:250 (IF), 1:750 (IHC)
Kv3.1b	Rabbit/polyclonal	Voltage-gated potassium channel 3.1b	(Weiser, Bueno et al. 1995)	Härtig (AB_2040166)	1:2000 (IF), 1:6000 (IHC)
Nav1.6	Rabbit/polyclonal	Voltage-gated sodium channel 1.6	Alomone Labs Jerusalem BioPark (JBP)	AB_2040202	1:500 (IHC)
vGlut1	Rabbit/polyclonal	Vesicular glutamate transporter 1	Synaptic Systems, Göttingen, Germany	AB_887875	1:3000 (IHC)
vGlut2	Mouse/monoclonal	Vesicular glutamate transporter 2	Chemicon, Temecula, CA, USA	AB_2187552	1:4000 (IHC)
SMI-32	Mouse/monoclonal	Nonphosphorylated neurofilament marker H	SM1353, Acris Antibodies	AB_2715852	1:2500 (IHC)
GluR2/3	Rabbit/polyclonal	Glutamate (AMPA) receptor 2/3	Chemicon, Temecula, CA, USA	AB_90710	1:500 (IHC)
NMDAR1	Mouse/monoclonal	(NMDA) receptor 1	Chemicon, Temecula, CA, USA	AB_94946	1:1000 (IHC)
CR	Rabbit/polyclonal	Calretinin	Swant, Marly, Fribourg, Switzerland	AB_10000321	1:2500 (IHC)
GlyT2	Sheep/polyclonal	Glycine transporter 2	Chemicon, Temecula, CA, USA	AB_90945	1:5000 (IHC)
GAD	Rabbit/polyclonal	Glutamate decarboxylase 65 and 67	Chemicon, Temecula, CA, USA	AB_90715	1:2000 (IHC)
GlyR1α	Mouse/monoclonal	Glycine receptor 1α	Synaptic Systems, Göttingen, Germany	AB_887722	1:300 (IHC)
KCC2	Rabbit/polyclonal	Potassium-chloride cotransporter 2	Chemicon, Temecula, CA, USA	AB_310611	1:4000 (IHC)
Cav3.1	Rabbit/polyclonal	T-type voltage-gated calcium channel 3.1	Alomone Labs Jerusalem BioPark (JBP)	AB_2039779	1:1000 (IHC)
Cav3.2	Rabbit/polyclonal	T-type voltage-gated calcium channel 3.2	Alomone Labs Jerusalem BioPark (JBP)	AB_2039781	1:1000 (IHC)
Cav3.3	Rabbit/polyclonal	T-type voltage-gated calcium channel 3.3	Alomone Labs Jerusalem BioPark (JBP)	AB_2039783	1:1000 (IHC)
PAV	Mouse/monoclonal	Parvalbumin	Swant, Marly, Fribourg, Switzerland	AB_10000343	1:2500 (IHC)

as a chromogen to yield a brown colored, or DAB-Nickel as chromogen to yield a black colored precipitate.

Series of paraffin sections from cases M4, M5 and M6 were processed for concomitant detection of ChAT-immunopositive motoneurons and ACAN-containing PNs as described previously (Horn et al. 2018). Combined detection of two primary antibodies was carried out similarly to the single staining in a sequential manner, where the first antigen was detected by the reaction with DAB-Ni yielding a black precipitate. Subsequently, sections were treated with 1% H_2O_2 in TBS for 30 min as the first step of the second round of staining with the same serum. In these cases, the second antigen was detected with a simple DAB reaction protocol yielding a brown precipitate.

For preservation and scanning, sections were extensively washed with TBS (pH 7.4), briefly rinsed in distilled water, air-dried and cover-slipped with DPX mounting medium (Sigma-Aldrich, Steinheim, Germany).

Analysis of stained sections

Sections containing fluorescent labeling were examined with a Leica microscope DMRB (Bensheim, Germany) equipped with appropriate filters for red fluorescent Cy3 (N2.1), green fluorescent Alexa 488 (I3), or blue fluorescence imaging capability. Images from selected preparations were captured with a laser-scanning confocal microscope (Leica SP5, Mannheim, Germany) at 10× or 63× magnification. Triple imaging for Dylight, Alexa 488 and Cy3 fluorophores were sequentially performed at 405, 488 or 543 nm excitation wavelength, respectively. Z-stack series were collected every 0.5 µm (at 63×) or 2 µm (at 10×) for each section. Image stacks were processed with Fiji/ImageJ software (https://imagej.net/Fiji, SCR_003070). Contrast and brightness of the final composite images were adjusted to reflect the appearance of the labeling, as seen through the microscope using Fiji software.

Brightfield images of paraffin-embedded sections were captured either with a digital camera (Microfire; Optronics, USA) using PictureFrame 2.2 software (Optronics, USA) or with a slide scanner (Mirax MIDI, Zeiss), equipped with a Plan-Apochromat objective (Zeiss, 20×). The digitized images were viewed and captured with the free software Panoramic Viewer (3DHistech; 1.152.3) and Case Viewer (3DHistech; v2.2). Corresponding detailed views of equally arranged and magnified images of adjacent sections were analyzed on the computer screen. The same neurons were identified by their location with the help of anatomical landmarks, such as blood vessels.

Quantification of immunopositive puncta and statistical analysis

For quantification, images were captured with a slide scanner (Mirax MIDI, Zeiss), equipped with a Plan-Apochromat objective (Zeiss, 20×), loaded into Fiji software, followed by a conversion into RGB format and sharpening for better edge detection. Neurons to be investigated were identified using consecutive PN/ChAT-stained sections. Somatic perimeters of labeled neurons in the adjacent sections were measured using manual selection with the freehand tool after setting the corresponding scale. Finally, immunopositive puncta were manually counted, and number of puncta per µm perimeter were calculated by dividing the number of puncta by the measured somatic perimeter for each neuron. Quantification of somatic versus dendritic glutamatergic inputs was performed on a 10 µm thick section from case M4 stained for vGlut2 and ChAT antibodies. Only dendrites in continuation with the soma were included in the analysis. vGlut2-immunopositive puncta were counted along a hand-drawn line of the perimeters and the associated dendrite(s). For comparative quantification of transmitter inputs to the different neuronal populations in nVI and nIV, the density of vGlut2-, GlyT2- and GAD65/67-immunopositive puncta were counted along the somatic perimeters in two to three 5 µm thick sections at different levels of the respective nuclei of two cases.

All data sets showed a normal distribution according to the Kolmogorov–Smirnov Test of Normality, which is a prerequisite for subsequent *t*-Test analyses of different sized samples. Two-tailed Student's *t*-Test for two independent means was performed for each comparison (i.e., MIF versus SIF motoneurons, or dendritic versus somatic locations) to assess differences in mean numbers of synaptic terminals (puncta/µm) between populations.

Results

MIF and SIF motoneurons differ in voltage-gated potassium channel profiles

Differential Kv1.1 and Kv3.1b channel distribution in neurons of the abducens and trochlear nuclei

As previously shown, WGA-injection into the myotendinous junction of the lateral rectus muscle (case M1) resulted in retrogradely labeled, small to medium-sized MIF motoneurons mainly in the periphery of the abducens nucleus (Büttner-Ennever et al. 2001). These neurons lack aggrecan (ACAN)-based perineuronal nets (PN) in contrast to SIF motoneurons and INTs (Eberhorn et al. 2005) (Table 1; Fig. 1a–c). Combined immunofluorescence detection of

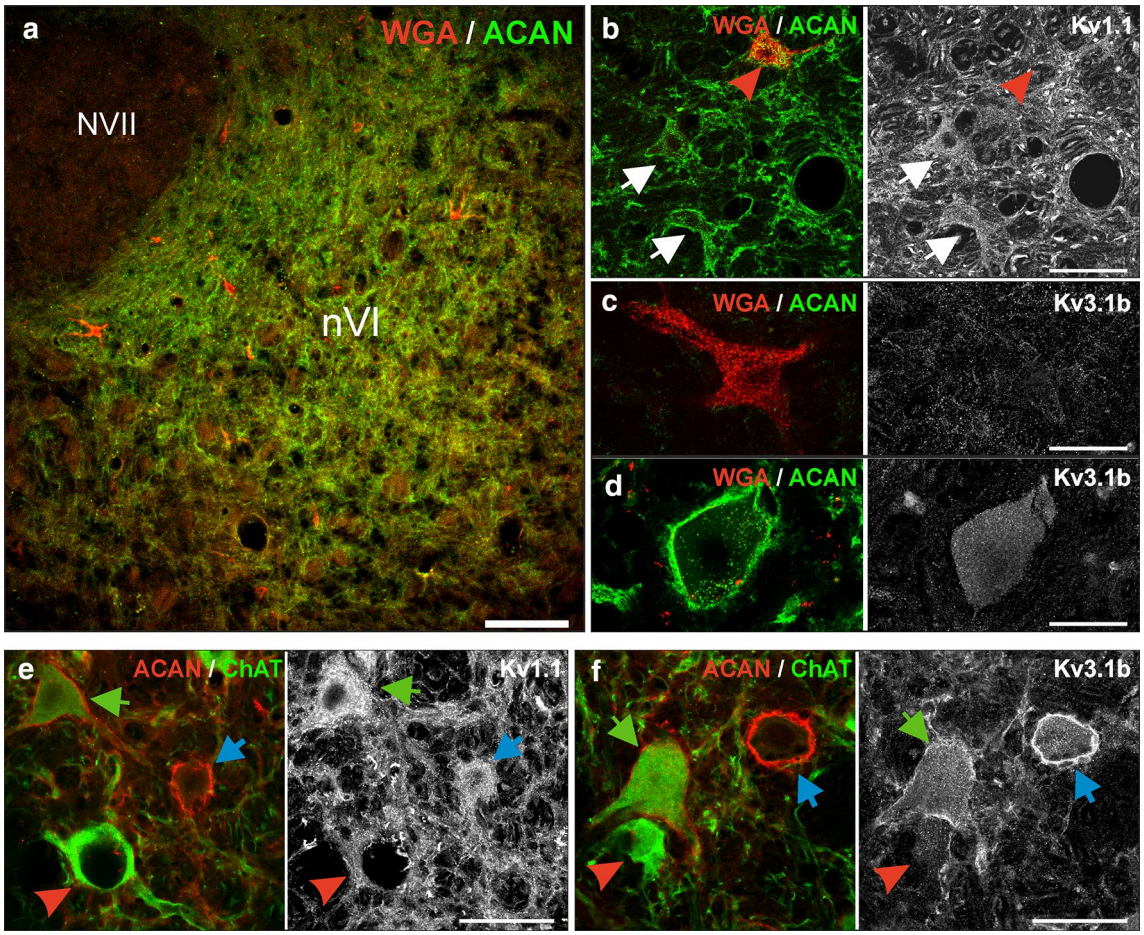

Fig. 1 Immunofluorescent detection of Kv1.1 and Kv3.1b in the abducens nucleus. **a** Transverse section through the abducens nucleus (nVI) depicting retrogradely labeled motoneurons (MNs) of multiply-innervated muscle fibers (MIF) (red) after injection of wheat germ agglutinin (WGA) into the myotendinous junction of the lateral rectus muscle. These cells lack aggrecan (ACAN)-based perineuronal nets (PN) (green). **b** Detailed view of a different section (left) demonstrating WGA-labeled MIF MNs (red arrowhead) and PN-bearing SIF MNs or internuclear neurons (INT) (white arrows) both of which lacked WGA labeling; SIF MNs or INTs (right) express strong immunoreactivity for Kv1.1 (white arrows), whereas MIF MNs exhibit a weak Kv1.1 signal (red arrowhead). **c** Close-up of a WGA-labeled MIF MN (left) lacking Kv3.1b-immunoreactivity (right). **d** Close-up of a PN-immunopositive SIF MN or INT (left) with strong Kv3.1b-immunoreactivity (right). **e, f** Close-up examples of abducens neurons following triple immunofluorescence staining for ACAN (red), choline acetyltransferase (ChAT) (green) and Kv1.1 (**e**, white) or Kv3.1b (**f**, white) in two different cases; note in **e** the strong Kv1.1-immunoreactivity in SIF MNs (green arrows) and INTs (blue arrows) visible as somatic staining around the cell nucleus. By comparison, there are low levels of Kv1.1-immunoreactivity in MIF MNs (red arrowhead); SIF MNs (green arrows) and INTs (blue arrows) in **f** express very strong Kv3.1b-immunoreactivity, which is absent in MIF MNs (red arrowheads). NVII, facial nerve. Scale bar represents 200 µm in **a**, 50 µm in **b** and 30 µm in **c**–**f**

WGA and ACAN, as well as selected Kv channels, revealed a weak labeling of Kv1.1 ion channels in MIF motoneurons, (Fig. 1b, red arrowhead), while ACAN-immunopositive SIF motoneurons or INTs, which were not labeled by tracer injections into the myotendinous junction of the muscle, showed a strong Kv1.1 signal within their soma (Fig. 1b, white arrows). Kv3.1b-immunoreactivity was absent in retrogradely labeled MIF motoneurons (Fig. 1c) but was present in all ACAN-immunopositive neurons (Fig. 1d). In additional cases (M2, M3; Table 1), a second approach using triple immunofluorescence for Kv channels, ACAN and choline acetyltransferase (ChAT) was applied, which allowed a distinction between SIF motoneurons and INTs (Fig. 1e, f). SIF motoneurons, defined by ChAT- and PN-immunopositivity, exhibited intense Kv1.1- and Kv3.1b-immunofluorescence (Fig. 1e, f, green arrows). Kv1.1-immunolabeling appeared as strongly stained clusters within the cytoplasm only sparing the nucleus, while the signal along the membrane was weak (Fig. 1e; green arrow). In contrast, the Kv3.1b labeling was strongest along the membranes of the soma and proximal dendrites, while weak immunoreactivity was observed within the somatic cytoplasm (Fig. 1f, green arrow). As reported above, ChAT-immunopositive but ACAN-immunonegative MIF motoneurons showed

no Kv3.1b-immunoreactivity (Fig. 1f, red arrowhead). In addition, the low level of Kv1.1-immunopositivity did not present as clustered signals around the cell nucleus and was barely detectable along the somatic membrane (Fig. 1e, red arrowhead). Finally, ChAT-immunonegative INTs, which were densely ensheathed by PNs, were strongly labeled by antibodies directed against both Kv1.1 and Kv3.1b (Fig. 1e,f, blue arrows). In fact, INTs stood out within the abducens nucleus by their prominent PN and Kv3.1b-immunolabeling (Fig. 1e, f, blue arrows).

To confirm the lack of Kv3.1 expression in MIF motoneurons, the general presence of Kv channels was validated by the more sensitive immunoperoxidase staining using selected sets of three consecutive 5 or 7 µm paraffin sections through the abducens and trochlear nuclei in three additional cases (Figs. 2, 3; Case M4, M5, M6; see Table 1). With this method, Kv1.1- and Kv3.1b-immunoreactivity was detected as black DAB-Ni precipitate (Figs. 2a–c, 3a–c, left and right columns) on sections adjacent to the one immunostained for the PN marker ACAN (black) and the motoneuron marker ChAT (brown; Figs. 2a–c, 3a–c, middle columns). Using ACAN/ChAT-immunostaining, MIF MNs were identified by the positive ChAT, but negative ACAN labeling (red arrowheads), SIF MNs were identified by positive ChAT and ACAN labeling (green arrows), and INTs in the abducens nucleus were identified by negative ChAT, but positive ACAN labeling (Fig. 2c, blue arrows) for evaluation of the same neurons on adjacent sections. Varying intensities of somatic immunoreactivity for Kv1.1 were detected in both the abducens and trochlear nuclei (Figs. 2a, b, 3a, b, left columns), whereas the Kv3.1b-immunolabeling was generally uniform in the cytoplasm, with a predominant localization along the somatic and proximal dendritic membrane (Figs. 2a,b, 3a, b, right columns). Unlike scattered abducens MIF motoneurons, trochlear MIF motoneurons are clustered in a dorsal cap facilitating identification by the lack of ACAN-immunopositive PNs (Fig. 3a, red dashed line boundaries). In both motor nuclei, the ChAT-immunopositive PN-ensheathed SIF motoneurons showed strong Kv3.1b-immunostaining, a feature that was clearly absent from MIF motoneurons (Figs. 2b, 3b, middle and right columns, red arrowheads). Kv1.1-immunolabeling was equally strong in SIF motoneurons, but only weakly expressed in MIF motoneurons (Figs. 2b,c, 3b, left columns, green arrows and red arrowheads, respectively). As demonstrated by immunofluorescence staining (see above), ChAT-immunonegative abducens INTs exhibited a very strong immunoreactivity for Kv3.1b and ACAN, which rendered them clearly visible even in the overview (Fig. 2a, c, middle and right columns; blue arrows). Their Kv1.1-immunolabeling was also strong and comparable to that of SIF motoneurons (Fig. 2a, c, left and middle columns, blue arrows). The specificity and localization of Kv1.1- and Kv3.1b-immunolabeling were qualitatively confirmed by visualization of the well-known expression pattern in medial superior olivary (MSO) neurons (Fig. 3c) (Mayadali et al. 2019; Nabel et al. 2019), where strong labeling was observed for both subunits, as well as for the PN marker ACAN, but not for ChAT, as expected for these neurons.

Nav1.6 subunit in neurons of the abducens and trochlear nuclei

The expression of the sodium channel subunit Nav1.6 is usually tightly correlated with the expression pattern of Kv3.1b subunits in agreement with a fast-spiking capacity for these neurons (Gu et al. 2018; Kodama et al. 2020). Therefore, expression of this sodium channel subunit was evaluated in SIF and MIF motoneurons in both, the abducens and trochlear nuclei (Figs. 2d, 3d, green arrows), and in abducens INTs (Fig. 2d, blue arrow). However, simultaneous expression of Kv3.1b and Nav1.6 was only found for SIF motoneurons and INTs, whereas only Nav1.6 expression was present in MIF motoneurons, which lacked Kv3.1b (Figs. 2d, 3d, red arrows).

Excitatory transmitters and receptors in the abducens and trochlear nuclei

Glutamatergic synapses onto abducens and trochlear neurons utilize vGlut2, but not vGlut1

Glutamatergic inputs to cell groups in the motor nuclei were investigated on consecutive paraffin sections (Case M4, M5, M6) by immunostaining for the vesicular glutamate transporters 1 and 2 (vGlut1, vGlut2) known to be present in synaptic boutons (Fremeau et al. 2001). Combined immunostaining for either ChAT or non-phosphorylated neurofilament (SMI-32) were used as a marker for motoneurons (Figs. 4a, 5a, brown label). Numerous vGlut2-immunopositive puncta were present in both the abducens (Fig. 4a, right column) and trochlear nucleus (Fig. 5a, right column), most likely representing glutamatergic terminals. In contrast, no vGlut1-immunopositive puncta were found in either one of the two motor nuclei but occurred in abundance in adjacent areas, thus forming a sharp contrast that visually dissociated each nucleus clearly from the surrounding tissue (Figs. 4a, 5a, black label, left columns). While vGlut2-immunopositive puncta were observed along the somatic membrane of all neurons in the two nuclei, they were more concentrated on dendrites, as seen on thicker sections (7–10 µm; cases M4, M6), however, demonstrated in detail here only for the abducens nucleus (Fig. 5b). Accordingly, systematic quantification of

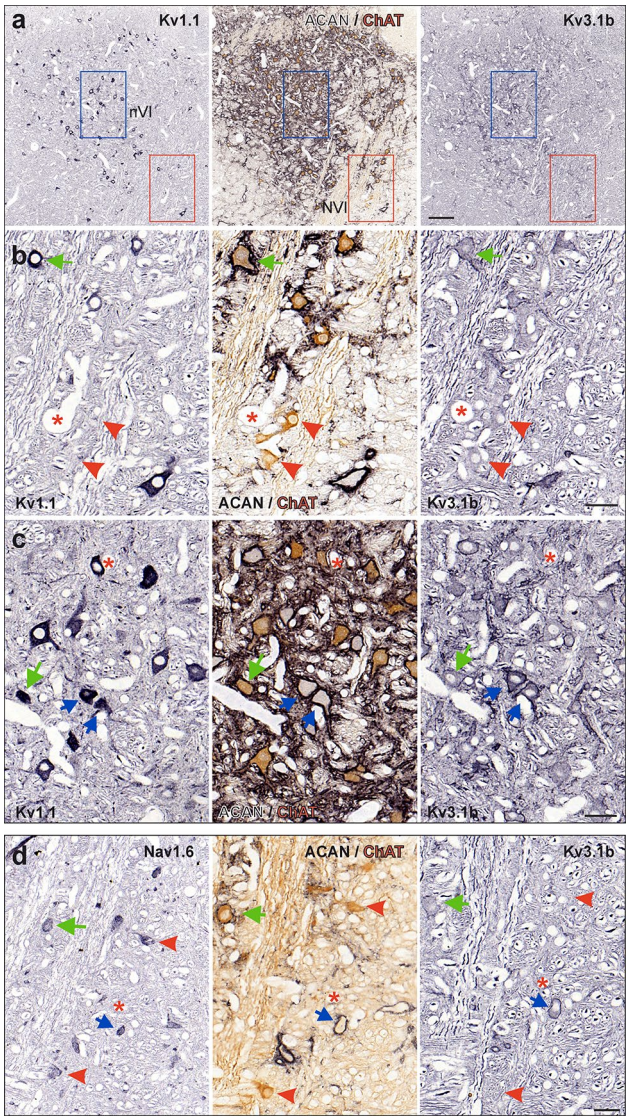

Fig. 2 Immunoperoxidase labeling of Kv1.1, Kv3.1b and Nav1.6 proteins in the abducens nucleus. **a** Consecutive coronal paraffin sections through the abducens nucleus (nVI) immunostained for Kv1.1 (left), Kv3.1b (right), combined aggrecan (ACAN)-based perineuronal nets (PN; black) and choline acetyltransferase (ChAT; brown, middle), respectively. Note the regional variability in the intensity of Kv1.1-immunolabeling within the nucleus; colored boxes indicate the areas illustrated at higher magnification in b (red) and c (blue), respectively. **b** Close-up comparing Kv1.1 and Kv3.1b expression in motoneurons (MNs) of multiply-innervated muscle fibers (MIF) (red arrowheads) and singly-innervated muscle fibers (SIF) (green arrow). **c** Close-up of Kv1.1 and Kv3.1b expression in internuclear neurons (INTs) (blue arrows) and SIF MNs (green arrow). **d** Close up of Nav1.6-immunolabeling related to Kv3.1b expression in three abducens neuronal populations (SIF MNs: green arrow; MIF MNs: red arrowheads; INTs: blue arrow). Scale bar represents 200 µm in **a**, and 50 µm in **b–d**

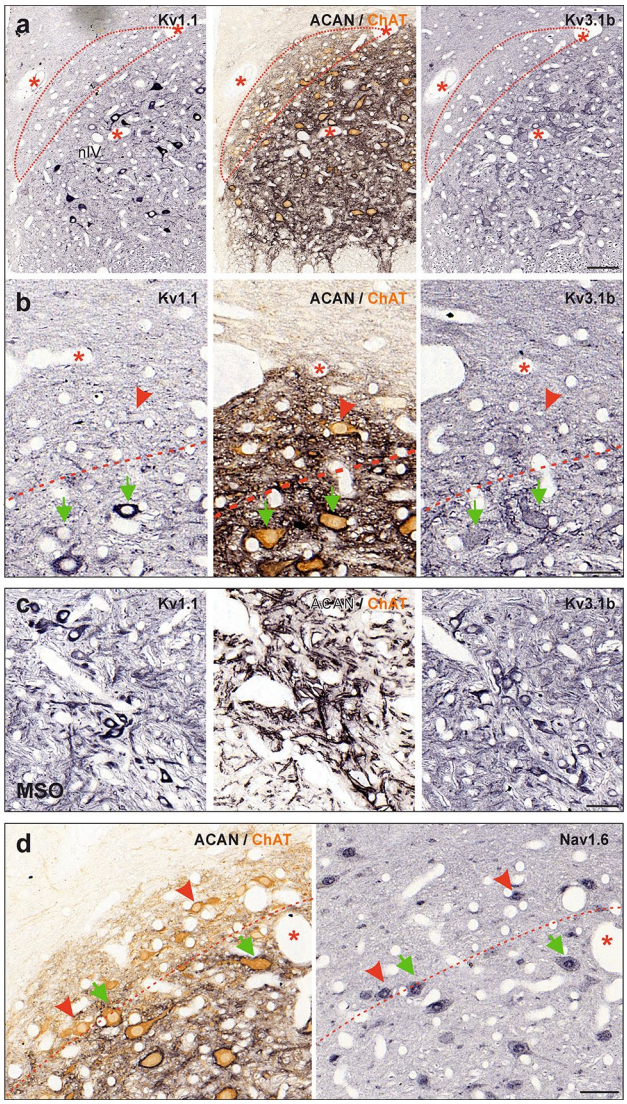

Fig. 3 Immunoperoxidase labeling of Kv1.1, Kv3.1b and Nav1.6 proteins in the trochlear nucleus. **a, b** Consecutive coronal paraffin sections depicting an overview (**a**) and close-up from a different section (**b**) through the trochlear nucleus (nIV) immunostained for Kv1.1 (left), Kv3.1b (right), combined aggrecan (ACAN)-based perineuronal nets (PN; black) and choline acetyltransferase (ChAT; brown, middle), respectively; the red dashed lines delineate the dorsal cap of nIV containing motoneurons of multiple-innervated muscle fibers (MIF MN); note the regional variability in the intensity of Kv1.1-immunolabeling within the nucleus. **c** Medial superior olivary (MSO) neurons adjacent to the abducens nucleus on the same section as a positive control for the immunohistochemical specificity of the antibody staining. **d** Close-up of Nav1.6-immunolabeling in MIF (red arrowheads) and SIF MNs (green arrows) in nIV. Red dashed lines indicate the tentative boundary between SIF and MIF MNs. Scale bar represents 100 µm in **a** and 50 µm in **b–d**

the immunostaining in the abducens nucleus revealed that the mean density of vGlut2-immunopositive puncta was significantly higher along the dendritic, as compared to the somatic membrane, of both MIF ($p < 0.01$, *t*-test) and SIF ($p < 0.001$, *t*-test) motoneurons (Fig. 6a, right).

In the abducens nucleus, vGlut2-immunopositive puncta were found along the somatic membrane of all three types of neurons (Fig. 4b, c). However, MIF motoneurons had

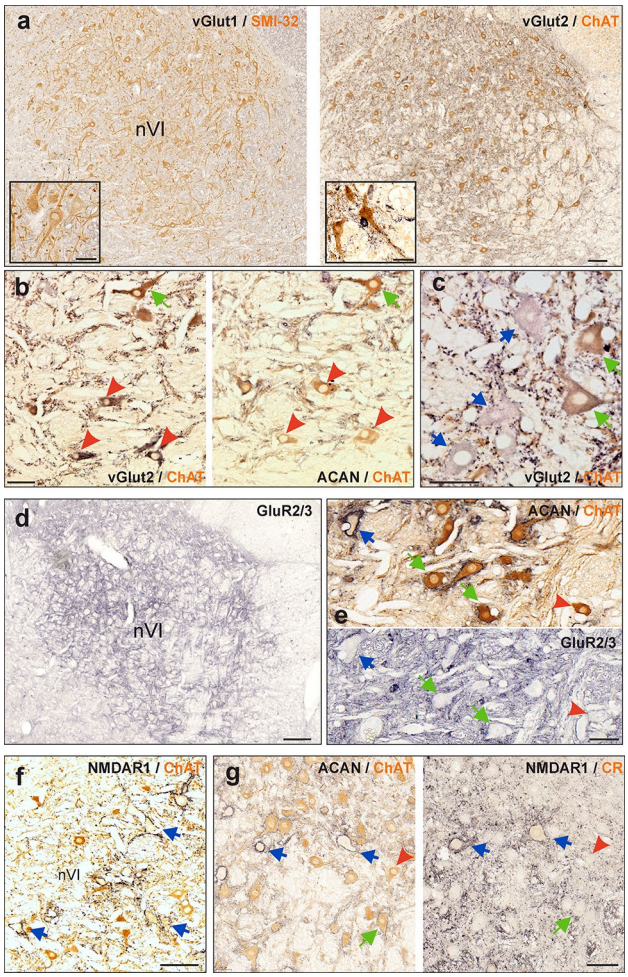

Fig. 4 Immunohistochemistry of glutamatergic synapses onto abducens neurons. **a**–**g** Consecutive coronal paraffin sections illustrating glutamatergic presynaptic terminals (**a**–**c**) and postsynaptic receptors (**d**–**g**) of abducens (nVI) neurons identified by immunoperoxidase labeling (black). **a** Neurons in nVI immunostained for the vesicular glutamate transporter 1 (vGlut1) (black) and non-phosphorylated neurofilament with SMI32-antibody (brown; left), vGlut2 (black) and choline acetyltransferase (ChAT) (brown; right). Close-up examples of labeled neurons are illustrated in the insets in **a**. Close-up of vGlut2-positive terminals on MIF (**b**, red arrowheads) and SIF (**b, c,** green arrows) motoneurons (MNs) and internuclear neurons (INTs) (**c**, blue arrows) in nVI. **d** AMPA receptor GluR2/3-immunoreactivity in nVI. **e** Close-up of consecutive sections depicting GluR2/3-immunoreactivity of MIF (red arrowhead) and SIF (green arrows) MNs and INTs (blue arrow) in nVI. **f,g** NMDAR1-immunoreactivity in nVI; combined NMDAR1 and ChAT-immunostaining (brown) highlighting INTs with intense NMDAR1 labeling (**f**, blue arrows). Consecutive sections depicting ChAT-negative INTs (**g**, blue arrows) with weak calretinin (CR)-immunolabeling (**g**, right, brown) and strong somatic and dendritic NMDAR1 labeling; note that punctate labeling of NMDAR1 occurs on SIF MNs (**g**, green arrow), whereas MIF MNs exhibit no labeling (**g**, red arrowhead). Red arrowheads depict MIF MNs, green arrows depict SIF MNs and blue arrows depict INTs. Scale bar indicates 200 µm in **a, d**, 100 µm in **f** and 50 µm in **b, c, e, g** as well as for insets in **a**

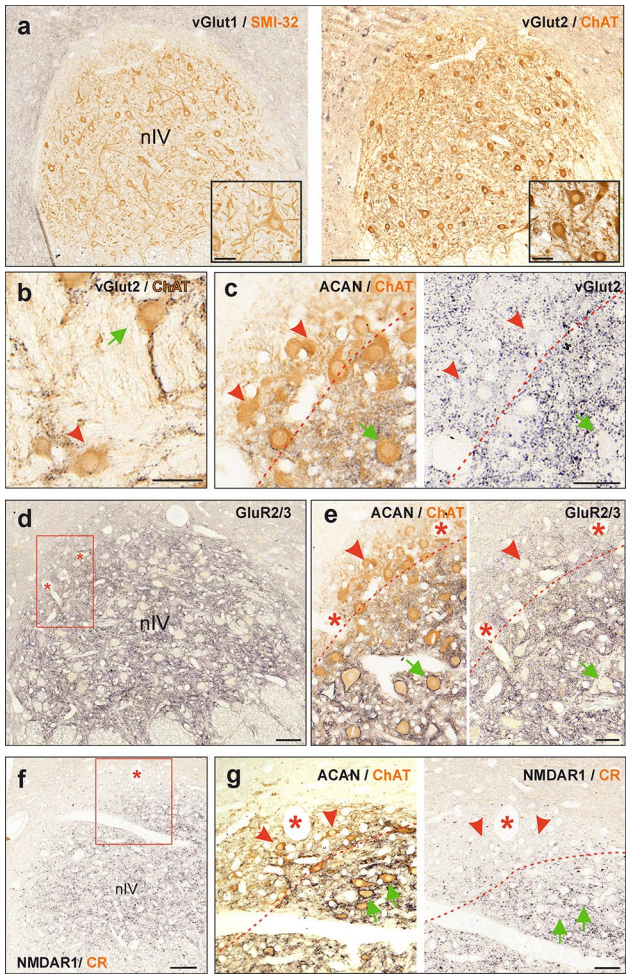

Fig. 5 Immunohistochemistry of glutamatergic synapses onto trochlear neurons. **a**–**g** Consecutive coronal paraffin sections illustrating glutamatergic presynaptic terminals (**a**–**c**) and postsynaptic receptors (**d**–**g**) of trochlear (nIV) neurons identified by immunoperoxidase labeling (black). **a** Neurons in nIV immunostained for the vesicular glutamate transporter 1 (vGlut1) (black) and non-phosphorylated neurofilament with SMI32-antibody (brown) on the left, and for vGlut2 (black) and choline acetyltransferase (ChAT) (brown) on the right. Close-up examples are illustrated in the insets in **a**. **b** Example of somatic and dendritic distribution of vGlut2-immunopositive terminals on a SIF MN (green arrow) in nIV found on a 10 µm section. **c** Close-up of vGlut2-positive terminals on SIF (green arrow) within nIV and MIF MNs (red arrowheads) located within the dorsal cap of nIV. **d** AMPA receptor GluR2/3-immunoreactivity in nIV. **e** Close-up of the area outlined by the box in **d**, depicting weaker GluR2/3-immunolabeling in MIF MNs (red arrowhead) within the dorsal cap of nIV (right panel), as compared to SIF MNs (green arrow). **f** Combined NMDAR1- and CR-immunostaining in nIV. **g** Close-up of the area outlined by the box in **f** depicting NMDAR1 labeling only in SIF MNs (green arrows), but not in MIF MNs (red arrowheads) within the dorsal cap of nIV. Red arrowheads and green arrows depict MIF and SIF MNs, respectively. Red dashed lines indicate the tentative border delineating the dorsal cap of nIV. Scale bar indicates 200 µm in **a**, 100 µm in **d, f** and 50 µm in **b, c, e, g** as well as for insets in **a**

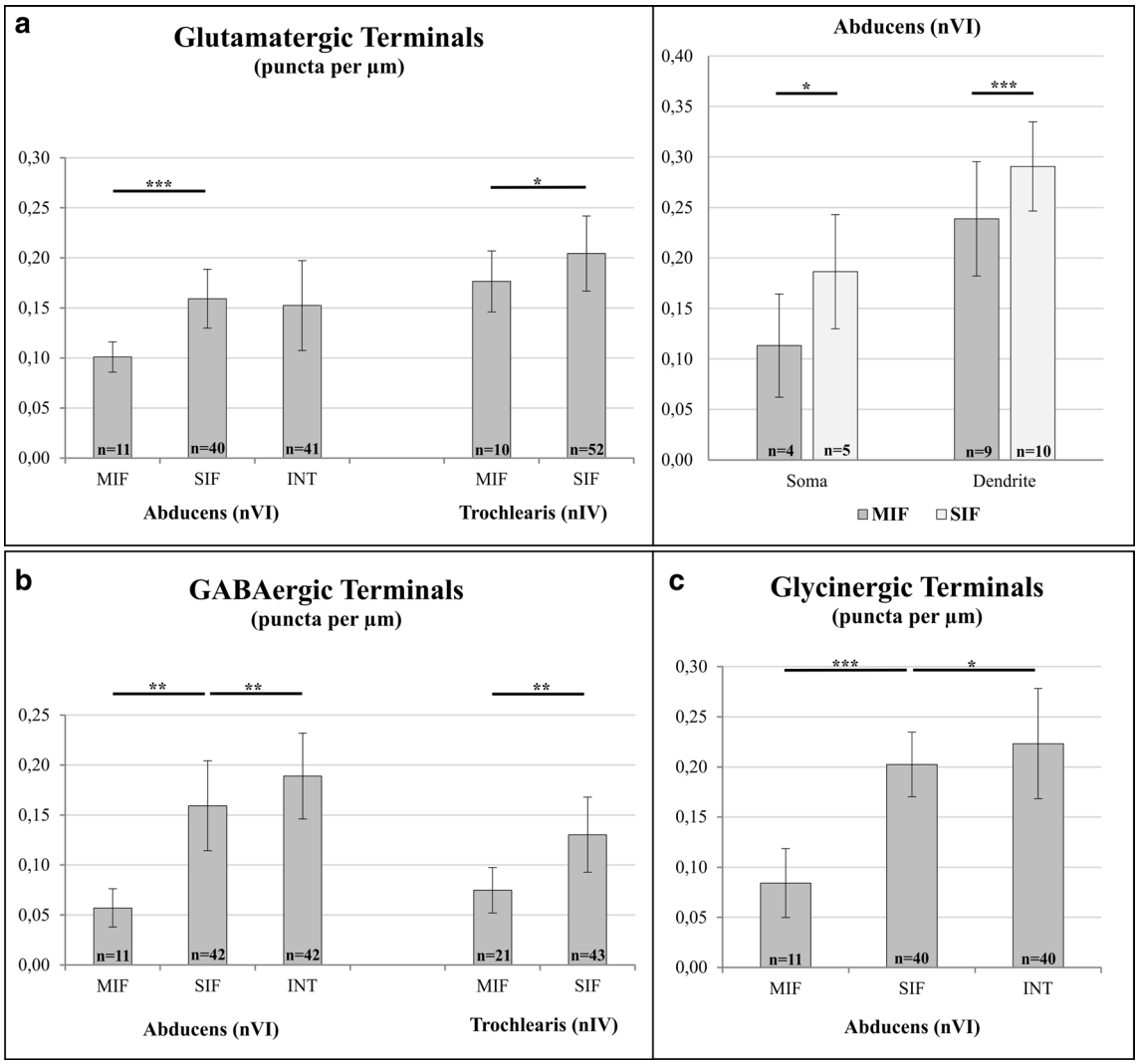

Fig. 6 Quantification of vGlut2, GAD- and GlyT2-immunopositive puncta and statistical analysis. **a** Immunopositive glutamatergic terminals surrounding different types of neurons in the abducens (nVI) and trochlear (nIV) nuclei, quantified as numbers of puncta along the somatic membrane (puncta/µm) (left, obtained from 5 µm thick sections) and for comparison between dendritic and somatic locations (right, obtained from 10 µm thick section). **b, c** Immunopositive GABAergic (**b**) and glycinergic (**c**) synaptic structures quantified as number of puncta/µm along the somatic membrane of nVI and nIV neurons (obtained from 5 µm thick sections). Number (*n*) of analyzed neurons/measurements are indicated within the bars. Significant statistical differences between puncta/µm according to two-tailed *t*-test for two-independent means; $*p<0.05$, $**p<0.01$, $***p<0.001$

significantly fewer somatic glutamatergic inputs than SIF motoneurons ($p<0.001$, *t*-test) per membrane length (Figs. 4b, red arrowheads, 6a, left). The density of vGlut2-immunopositive puncta per membrane length of INTs was similar to and not significantly different ($p=0.43$, *t*-test) from, that of SIF motoneurons (Figs. 4c, blue arrows, 6a, left; Table 3).

The number of vGlut2-immunopositive puncta on both MIF and SIF motoneurons appeared to be similar between the trochlear and abducens nucleus (Figs. 4b, 5c, red arrowheads and green arrows). In fact, quantification of the magnitudes did not reveal any significant difference in the extent of the vGlut2-immunopositivity around the somata of motoneurons in the trochlear nucleus, as compared to those encountered in the abducens nucleus (Fig. 6a, left). This was true for MIF ($p=0.11$, *t*-test) and for SIF motoneurons ($p=0.12$, *t*-test).

Differential expression of glutamatergic receptors by MIF and SIF motoneurons in the abducens and trochlear nuclei

Ionotropic AMPA receptors, composed of several different subunits, cause a Na^+ influx (and K^+ efflux) upon glutamate binding, thereby exciting the neuron. The additional

Table 3 Qualitative summary of immunohistochemical results (− no labeling, + weak, + + moderate, + + + strong labeling)

	Abducens			Trochlearis	
	MIF	SIF	INT	MIF	SIF
Kv1.1	+	+ + +	+ + +	+	+ + +
Kv3.1b	−	+ +	+ + +	−	+ +
Nav1.6	+	+	+	+	+
KCC2	+	+	+	+	+
Cav3.1	+ + +	−	−	+ + +	+/−
Cav3.2	+	+ +	+ +	+	+ +
Cav3.3	+	+	+	+	+
vGlut1	−	−	−	−	−
vGlut2	+ +	+ + +	+ + +	+ +	+ + +
GlyT2	+	+ +	+ +	−	−
GAD 65/67	+	+ +	+ +	+	+
GluR2/3	+	+ +	+ +	+	+ +
NMDAR1	−	+	+ + +	−	+
GlyR1a	+	+	+	−	−

permeability for Ca^{2+} ions is prevented by the presence of GluR2 subunits, as a component of the AMPA receptor (Wollmuth 2018). Therefore, antibodies directed against the subunits GluR2 and GluR3 (GluR2/3) were used to test the presence of these calcium-impermeable AMPA receptors in abducens and trochlear neurons. GluR2/3-immunolabeling was encountered in the neuropil and along the membrane of neurons in both motor nuclei (Figs. 4d, 5d). While immunolabeling was more intense around SIF motoneurons and INTs within the core region of the abducens nucleus (Fig. 4e, green and blue arrows, respectively; Table 3), MIF motoneurons located at the medial border expressed a weaker labeling (Fig. 4e, red arrowheads). This differential labeling pattern was even more pronounced for SIF and MIF motoneurons in the trochlear nucleus (Fig. 5e, green arrows and red arrowheads, respectively), where the intensity of the GluR2/3-immunolabeling clearly subsided towards the dorsal cap, which contains MIF motoneurons.

Ionotropic NMDA receptors allow the influx of Ca^{2+}-ions in addition to Na^{+} and K^{+} exchange across the membrane upon glutamate binding and thus promote more extended postsynaptic responses than AMPA receptors (Dingledine et al. 1999). Therefore, immunolabeling of the NMDAR1 subunit was evaluated in neurons of the abducens and trochlear nuclei (Figs. 4f, g, 5f, g; Table 3). In the abducens nucleus, the strongest NMDAR1-immunostaining was found along the somatic and dendritic membrane of ChAT-immunonegative INTs (Fig. 4f, g, blue arrows). Albeit much less abundant as compared to INTs, NMDAR1 was also present along the membrane of SIF motoneurons in punctate form (Fig. 4g, green arrow), suggesting the presence of numerous synapses endowed with this glutamate receptor subtype. In contrast, MIF motoneurons failed to show any NMDAR1-immunolabeling (Fig. 4g, red arrowhead). NMDAR1-immunolabeling in the trochlear nucleus was similar to that of the abducens nucleus with clear punctate immunolabeling associated with SIF motoneuronal membranes (Fig. 5f, g, green arrows), whereas MIF motoneurons were clearly spared by NMDAR1-immunolabeling (Fig. 5f, g, red arrowheads).

Inhibitory transmitters and receptors in neurons of the abducens and trochlear nuclei

Differential glycinergic and GABAergic inputs to abducens and trochlear neurons

A previous study reported a comparable extent of GABAergic inputs to trochlear MIF and SIF motoneurons, while glycinergic inputs to both motoneuronal types were absent (Zeeh et al. 2015). Consequently, the different abducens neuron types were analyzed here for the presence of the respective inhibitory synaptic structures. Glycinergic and GABAergic inputs to abducens neurons were visualized on consecutive 5 µm sections through immunolabeling of the glycine transporter 2 (GlyT2) and glutamate decarboxylase (GAD), respectively (Fig. 7; Table 3). Numerous GlyT2- and GAD-immunopositive puncta were distributed throughout the abducens nucleus (Fig. 7a–c, left and middle columns, respectively). The weak background labeling of the somata found by GlyT2-immunostaining was used for proper identification and visualization of the same neurons on adjacent sections (Fig. 7a–c, left column).

Using cell types determined by ChAT and ACAN staining (Fig. 7a–c, right), we found that while GlyT2-immunopositive puncta were present to a comparable extent along the somatic membrane of SIF motoneurons and INTs in the abducens nucleus (Fig. 7c, left column; green arrows and blue arrows, respectively), considerably fewer puncta were observed along the somatic membrane of MIF motoneurons (Fig. 7b, left column, red arrowheads). Quantification revealed a two to three-fold (240.7%; $p < 0.001$, *t*-test) difference between average numbers of GlyT2-immunopositive puncta surrounding SIF motoneurons as compared to MIF motoneurons (Fig. 6c). INTs had a significantly higher number (10.2%; $p < 0.05$, *t*-test) of glycinergic inputs as compared to SIF motoneurons (Fig. 6c). In general, GlyT2-immunopositive puncta were observed in greater abundance on the dendrites of MIF motoneurons, however, quantitative confirmation of differences between somatic versus dendritic labeling was not possible using 5 µm paraffin sections.

The pattern of GAD-immunolabeling in the abducens nucleus was similar to that of GlyT2-immunolabeling.

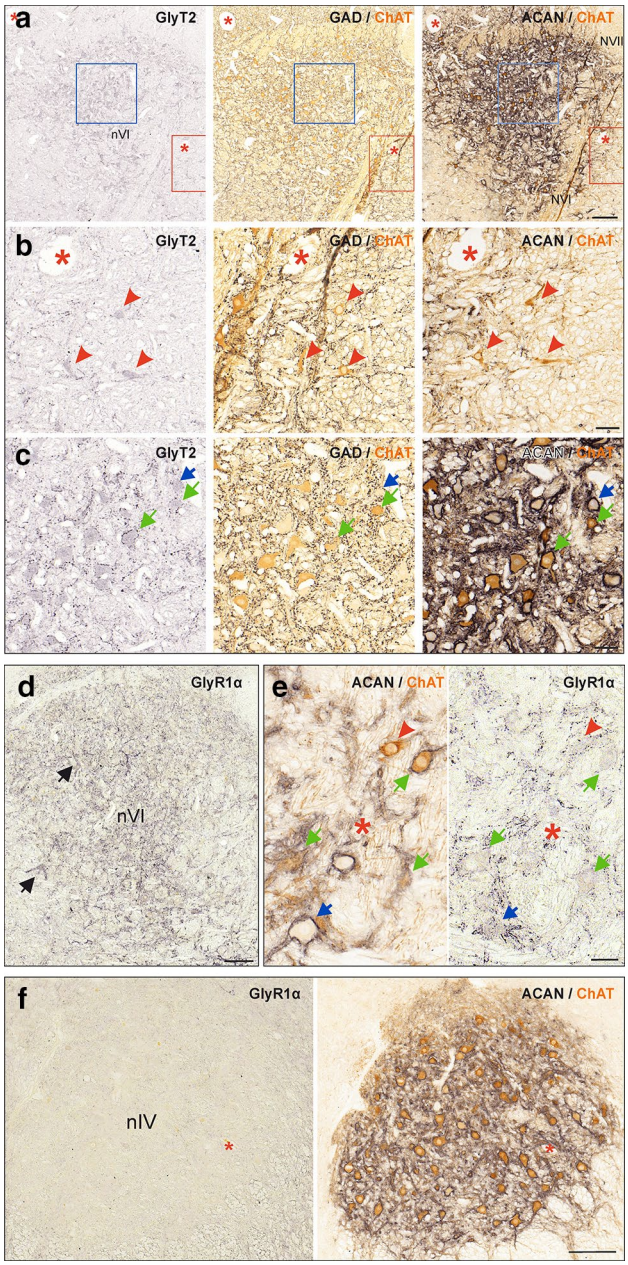

Fig. 7 Inhibitory transmitter profile of synapses onto abducens and trochlear neurons. **a–c** Consecutive coronal paraffin sections illustrating presynaptic glycinergic (left) and GABAergic terminals (middle; black) onto choline acetyltransferase (ChAT)- and aggrecan (ACAN)-immunopositive (right) SIF MNs (**c**, green arrows), onto ACAN-immunonegative MIF MNs (**b**, red arrowheads) and onto ChAT-immunonegative INTs (**c**, blue arrow) in the abducens nucleus (nVI). Colored boxes indicate the areas illustrated at higher magnification in b (red) and c (blue), respectively. Immunolabeling for the glycine transporter 2 (GlyT2) in an overview (**a**) and higher magnification (**b**,**c**, left, black) reveals few glycinergic synapses on MIF MNs (**b**, red arrowheads), and more numerous synapses on SIF MNs (**c**, green arrows) and INTs (**c,** blue arrows) in nVI. Immunolabeling for GAD in an overview (**a**, middle) and higher magnification (**b**,**c**, middle) in nVI shows fewer GAD-immunopositive terminals on MIF MNs (**b**, red arrowheads), compared to more abundant terminals on SIF MNs (**c**, green arrows) and INTs (**c**, blue arrow). **d–f** glycine receptor (GlyR1α)-immunolabeling in the nVI and the trochlear nucleus (nIV). Only nVI neurons express GlyR1α that is visible as punctate staining (**d, e**, right). Note the stronger dendritic than somatic immunolabeling (**d**, black arrows) more clearly seen in the close-up (**e**) with GlyR1α-immunopositive puncta along the membrane of SIF (green arrows), MIF MNs (red arrowheads) and INTs (blue arrows). Note that GlyR1α-immunolabeling is absent in nIV neurons (**f**). Scale bar represents 200 µm in **a, d, f,** and 50 µm in **b, c, e**

GAD-immunopositive puncta were abundant around the somata of SIF motoneurons and INTs, while fewer puncta were found around MIF motoneurons (Fig. 7b, c, middle column, green arrows, blue arrow and red arrowheads, respectively). Quantification revealed up to three times (279.1%; $p < 0.01$, *t*-test) as many GAD-immunopositive puncta surrounding SIF motoneurons as compared to MIF motoneurons (Fig. 6b). With respect to GlyT2-immunopositive puncta, INTs were consistently surrounded by a significantly higher number of GAD-immunopositive puncta (18.7%; $p < 0.01$, *t*-test) as compared to SIF motoneurons (Fig. 6b).

To compare the extent of GAD-immunostaining around abducens and trochlear neurons, immunohistochemistry was performed on trochlear motoneurons using consecutive 5 µm paraffin sections of the same case (M5). The respective analysis yielded GAD-immunopositive puncta on both MIF and SIF motoneurons (not shown) in agreement with a previous report (Zeeh et al. 2015). Quantitative analyses of MIF and SIF trochlear motoneurons demonstrated significantly fewer ($p < 0.01$, *t*-test) GAD-immunopositive puncta around MIF as compared to SIF motoneurons (Fig. 6b).

Differential expression of glycine receptor 1α in abducens and trochlear neurons

The differential organization of glycinergic synaptic structures innervating MIF and SIF abducens motoneurons were complemented by an evaluation of the expression of the glycine receptor subunit 1α. Immunostaining with antibodies against GlyR1α (clone mAb4a, see Methods; Table 2) yielded punctate labeling throughout the abducens nucleus (Fig. 7d), while such staining was entirely absent in the trochlear nucleus in agreement with a lack of glycinergic inputs to trochlear motoneurons (Fig. 7f; Table 3). In the abducens nucleus, all neuronal subtypes, expressed a stronger dendritic than somatic immunolabeling (Fig. 7d, black arrows; Fig. 7e, right). Moreover, numerous immunoreactive puncta were observed in the neuropil of the nucleus. Importantly, both MIF and SIF motoneurons revealed a somatic punctate GlyR1α-labeling, however, with varying abundance within the respective populations (Fig. 7e, red arrowheads and green arrows, respectively).

Potassium-chloride co-transporter (KCC2) has a similar expression pattern in the abducens and trochlear nuclei

The characterization of the inhibitory transmitter profile of MIF and SIF motoneurons was complemented by classifying the presence of the potassium-chloride symporter 2 subunit (KCC2). Accordingly, immunoperoxidase staining against KCC2 was combined with immunostaining for either ChAT or parvalbumin (PAV) as motoneuronal markers in both motor nuclei (Fig. 8). Because KCC2 co-localizes with both glycinergic and GABAergic receptors (Chamma et al. 2012), a potentially differential expression in abducens and trochlear neurons could provide further insight into the regulatory mechanisms provided by different types of inhibitory inputs. The immunostaining revealed that all three types of abducens neurons were labeled by the KCC2 antibody (Fig. 8a–c; Table 3). While the immunolabeling of the somatic membrane was weak, the labeling became gradually more intense towards the distal dendrites (Fig. 8b, c, right columns), strongly coinciding with the labeling pattern of the GlyR1α antibody (Fig. 7d, e, right column). In contrast, KCC2-immunolabeling was absent along the axons that form the abducens nerve root (Fig. 8a, NVI), in agreement with the reported properties of this protein (Chamma et al. 2012). In the trochlear nucleus, MIF and SIF motoneurons exhibited a KCC2-immunoreactivity that was comparable in extent with the similarly graded soma-dendritic increase in the intensity of abducens neurons (Fig. 8d, e). The labeling was much more intense at the outermost border of the trochlear nucleus, outside the dorsal cap that contains MIF motoneurons (Fig. 8d, e).

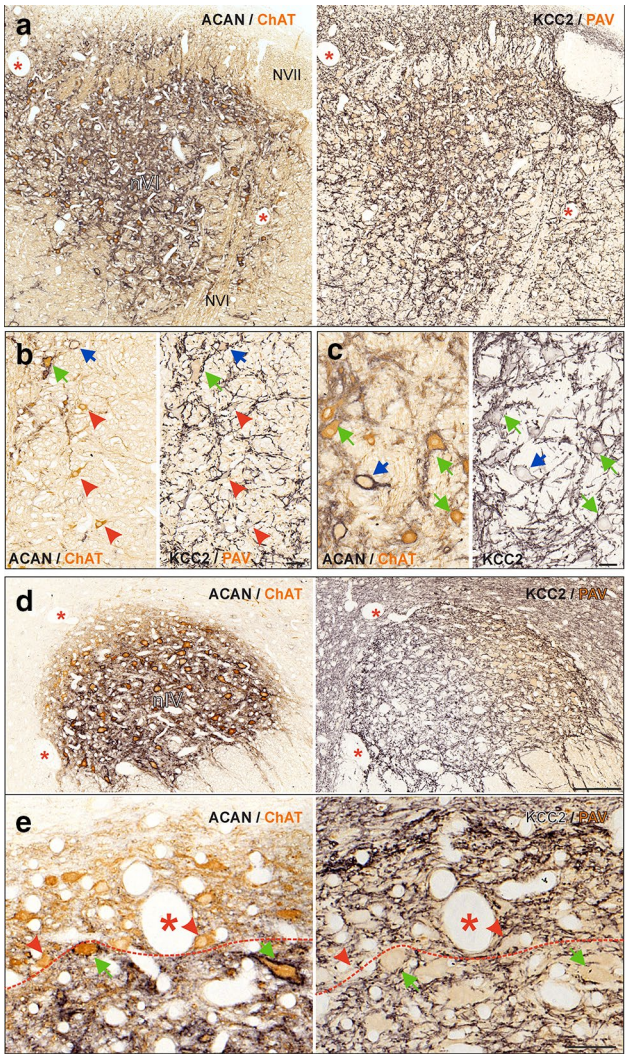

Fig. 8 Chloride-potassium co-transporter (KCC2) in abducens and trochlear neurons. **a–e** Consecutive paraffin sections through the abducens (nVI) (**a–c**) and trochlear nucleus (nIV) (**d, e**) immunostained for KCC2 (right) and combined aggrecan (ACAN)-based perineuronal nets (PN; black) and choline acetyltransferase (ChAT; brown, right). **b, c** Close-up of KCC2 (black) expression in MIF (red arrowheads) and SIF motoneurons (MNs) (green arrows) (**b**) and of INTs (blue arrow) (**c**). **e** Close-up of KCC2-immunolabeling in MIF MNs (red arrowheads) within the dorsal cap of nIV and SIF MNs (green arrows) within the core region of nIV. Note the intense labeling along the dorsal border of the trochlear nucleus in (**d**,**e**). Red dashed lines indicate the tentative position of the border delineating the dorsal cap of nIV. The details in **b, c, e** were obtained from different sections as those shown in **a,d**. Scale bar represents 200 µm in **a, d**, and 50 µm in **b, c,e**

MIF and SIF motoneurons differ in low voltage-activated calcium channel profiles

The expression of members of the voltage-gated calcium channel-3 family (low-voltage activated channels), which are generally involved in neuronal excitability, pace-making and repetitive firing (Zamponi et al. 2015) (Fig. 9; Table 3), were investigated with respective antibodies against all three members of the Cav3 family (Cav3.1–3.3). The expression pattern was assessed in the three sections adjacent to a section treated with antibodies against ChAT and PN, which again served as a reference for MIF and SIF motoneurons. At low magnification, we observed sparse immunolabeling for Cav3.1 subunit (Fig. 9a, first column), whereas Cav3.2 yielded weak somatic immunoreactivity (Fig. 9a, third column) in the abducens nucleus. We utilized Cav3.1- and Cav3.2-immunostaining in Purkinje cells as a direct internal control for the degree of positive staining (Fig. 9f). In contrast, Cav3.3-immunolabeling in abducens neurons was qualitatively comparable to that of the Purkinje cells (Fig. 9a, c, f, last columns).

Closer inspection of the labeling pattern of the three family members revealed that the somatic membrane of MIF abducens motoneurons contained the Cav3.1 subunit (Fig. 9b, red arrowheads), whereas no labeling was found in SIF motoneurons and INTs (Fig. 9b, left column, green and blue arrows, respectively). In contrast, somatic

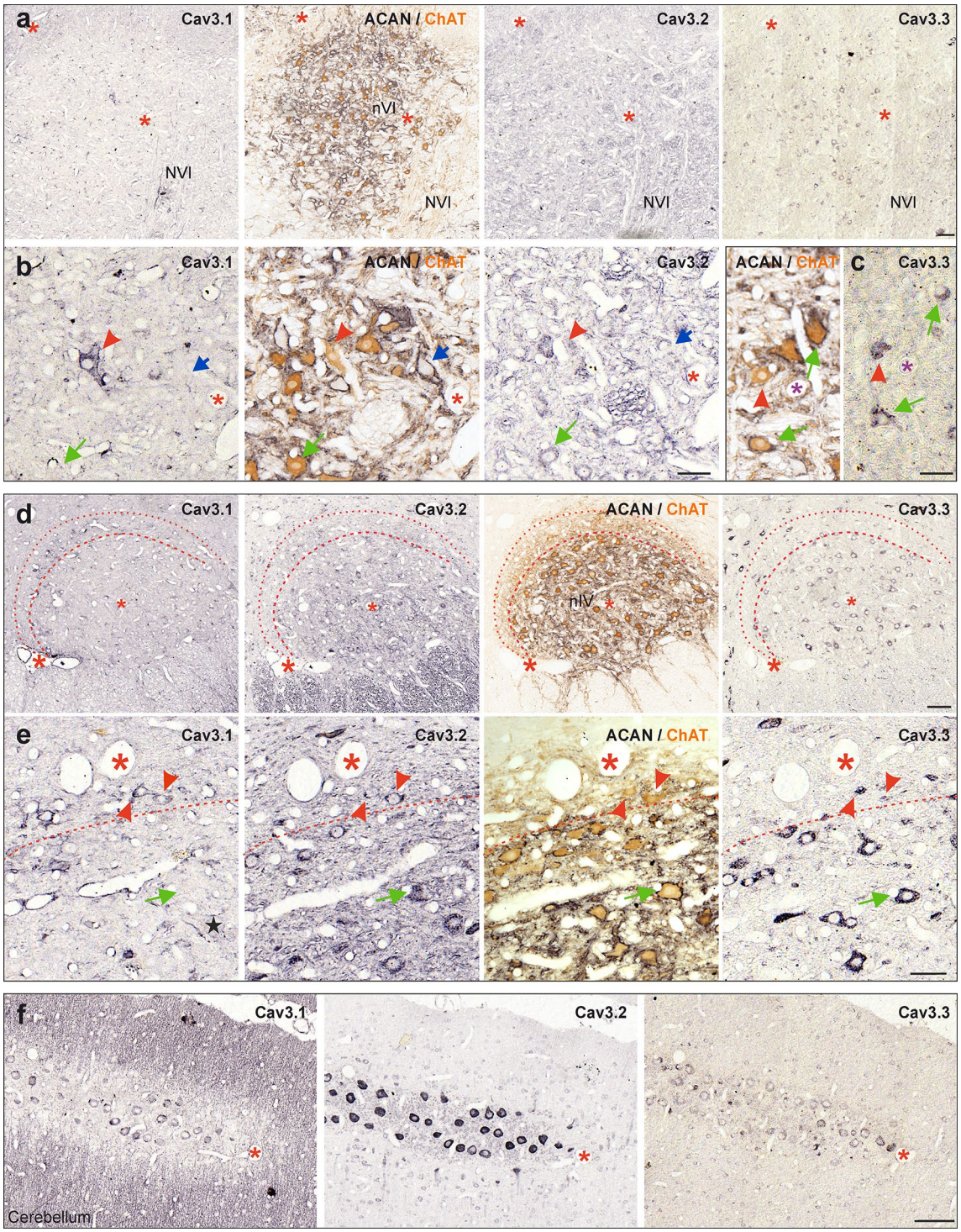

Cav3.2, as well as Cav3.3-immunolabeling, was encountered in all three abducens neuronal subtypes (Fig. 9b, c, INTs are not illustrated in Fig. 9c). The assessment of Cav3 channels in the trochlear nucleus yielded qualitatively similar results (Fig. 9d, e). Accordingly, intense Cav3.1-immunolabeling was encountered in trochlear MIF motoneurons, located within the dorsal cap of the nucleus (Fig. 9d, between red dashed lines, e, first columns, red arrowheads), while only a few SIF motoneurons within the core area of the nucleus expressed weak labeling along the somatic membrane (Fig. 9e, first column, green arrow, black star). In contrast, Cav3.2- and Cav3.3-immunolabeling were detected in both MIF and SIF trochlear motoneurons (Fig. 9d, e, second and last columns, red arrowheads

◂**Fig. 9** Low-voltage activated calcium channel family (Cav3) subunits in the abducens and trochlear nucleus. **a** Consecutive coronal paraffin sections through the abducens nucleus (nVI) (**a**) depicting the immunolabeling for Cav3.1 (first panel), Cav3.2 (third panel) and Cav3.3 (fourth panel) subunits with combined immunostaining for ChAT (brown) and ACAN (black) (second panel) as reference. **b, c** Close-up of Cav subunit expression in nVI MIF (red arrowheads) and SIF motoneurons (MNs) (green arrows) and INTs (blue arrow). **d** Consecutive coronal paraffin sections through the trochlear nucleus (nVI) depicting the immunolabeling for Cav3.1 (first panel), Cav3.2 (second panel) and Cav3.3 (fourth panel) subunits with combined immunostaining for ChAT (brown) and ACAN (black) (third panel) as reference. Thin dashed lines in **d** indicate the border of nIV and thick dashed lines indicate the boundary between the MIF and SIF MNs. **e** Close-up of Cav subunit expression in MIF (red arrowheads) and SIF MNs (green arrow) on different sections as those illustrated in **d**. Note the weak Cav3.1 expression along the membrane of some SIF MNs (left column, black star). Red dashed lines indicate the tentative position of the border delineating the dorsal cap of nIV. **f** Cerebellar Purkinje cells located on the same consecutive sections as nVI as controls for immunopositivity of the different Cav subunits. Scale bar indicates 100 µm in **a, d, f** and 50 µm in **b, c, e**

and green arrows, respectively). Collectively, these results suggest a differential contribution of the three subtypes of voltage-activated calcium channels to the excitation of neurons in both the abducens and trochlear nucleus.

Discussion

This study explored the basis for the functional properties of different groups of neurons in the abducens and trochlear nuclei in macaque monkey using immunohistochemistry with an emphasis on motoneurons of MIF and SIF muscle fibers, as shown in the summary figure (Fig. 10). Differences between MIF and SIF motoneurons with respect to voltage-gated potassium channel subunits Kv1.1 and Kv3.1b and low-voltage activated calcium channel subunit Cav3.1 were particularly prominent. This pattern suggests that MIF motoneuron membrane properties are preferentially suitable for the generation of low-dynamic motor commands. Moreover, different extents of synaptic inputs to cell bodies of MIF in comparison to SIF motoneurons were discovered for both excitatory and inhibitory inputs. This is in line with smaller numbers of synaptic contacts on somata and proximal dendrites of MIF-versus SIF-motoneurons of the medial rectus muscle (Erichsen et al. 2014). Together with differences in the glutamatergic receptor profile of MIF and SIF motoneurons (GluR2/3 and NMDAR1), the present findings suggest that the motor control of extraocular muscles is achieved through a combination of distinct intrinsic motoneuronal membrane properties and differentially organized synaptic inputs. Comparative observations for abducens internuclear neurons revealed that they display stronger immunolabeling for Kv3.1b, perineuronal nets and NMDAR1 as compared to SIF motoneurons, along with higher inhibitory synapse densities (see Table 3 and summary diagram in Fig. 10). Collectively, these findings may account for the previously observed enhanced excitability and earlier recruitment of abducens internuclear neurons.

Differences in connectivity and intrinsic membrane properties of MIF and SIF motoneurons

Different transmitter profiles of premotor inputs to MIF and SIF motoneurons in the abducens and trochlear nuclei

Glycinergic inputs to the abducens nucleus generally derive from multiple sources including inhibitory second-order vestibulo-ocular neurons in the ipsilateral medial vestibular nucleus (MVN), inhibitory burst neurons (IBNs) of the horizontal saccadic circuitry and possibly neurons in the contralateral nucleus prepositus hypoglossi (PPH) (Horn 2006; Spencer et al. 1989; Straka and Dieringer 1993). However, based on retrograde transsynaptic tracing studies, identified premotor neurons of abducens motoneurons, such as saccadic IBNs and second-order vestibulo-ocular neurons constitute a major source for glycinergic inputs to SIF, but not to MIF, motoneurons (Ugolini et al. 2006). Therefore, lower quantities of GlyT2-immunopositive puncta localized on MIF as compared to SIF abducens motoneurons can be explained by fewer glycinergic inputs from IBNs. However, the current study cannot rule out a differential organization of respective inputs to MIF and SIF abducens motoneurons from other sources. In the trochlear nucleus, the lack of GlyT2-positive puncta (not shown) confirms previous findings (Zeeh et al. 2015). This was expected, as inhibition from premotor neurons during saccades, VOR and gaze-holding is mediated by different transmitters for horizontal and vertical eye movements, not only in primates but also in other vertebrates including amphibians (Horn and Straka 2021; Soupiadou et al. 2018). According to this scheme, glycine is used in pathways for horizontal eye movements, and GABA is used in circuits comprising the vertical/oblique ocular motor system. This may be due to a differential anatomical origin of the presynaptic neurons and a differential distribution of these two transmitters along the longitudinal axis of the brainstem (Spencer and Baker 1992; Spencer et al. 1989; Straka et al. 2014).

GABAergic inputs to the abducens nucleus may originate from internuclear neurons in the oculomotor nucleus as demonstrated in cat (De la Cruz et al. 1992; Maciewicz et al. 1975). Stimulation and recording experiments in primates mainly revealed a crossed excitatory projection of oculomotor internuclear neurons to the abducens nucleus, consistent with a role in horizontal conjugate eye movements (Clendaniel and Mays 1994). The finding of a few ipsilaterally projecting oculomotor internuclear neurons that decrease their

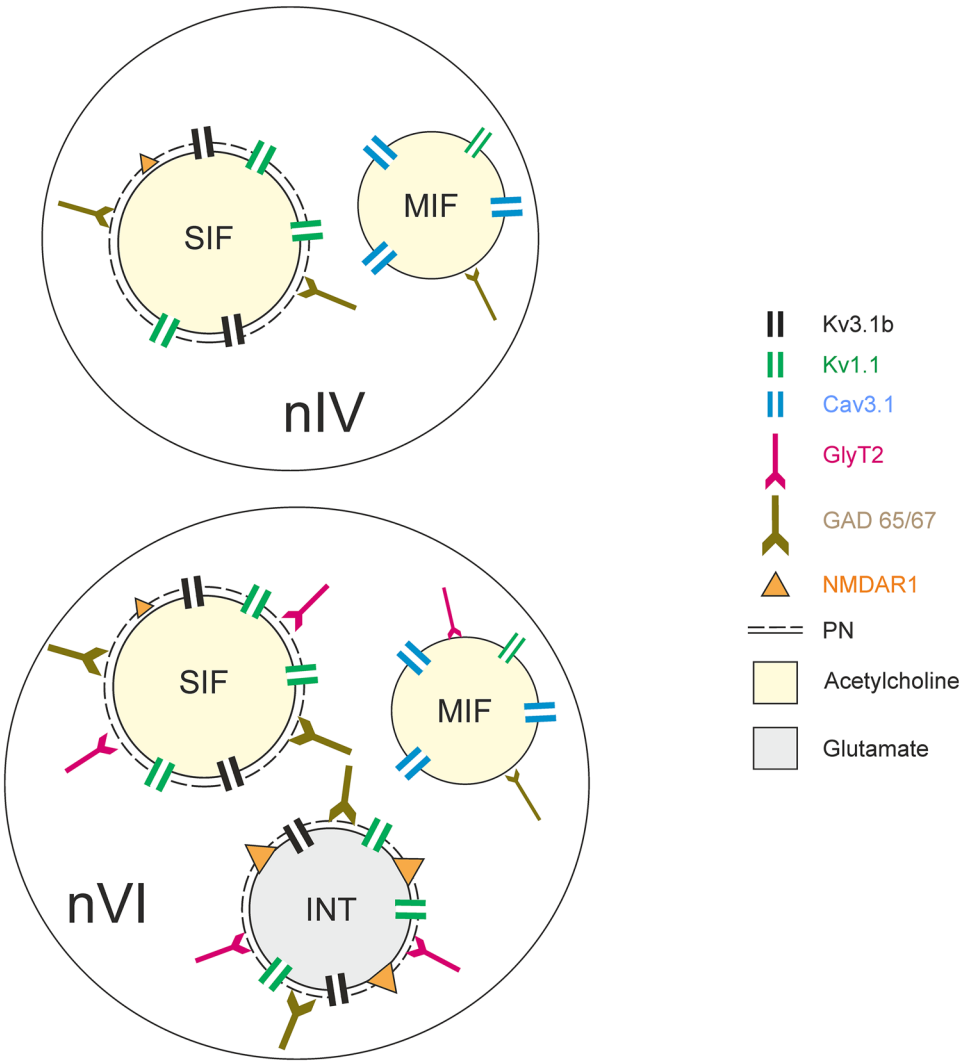

Fig. 10 Summary diagram depicting differential molecular signatures of trochlear and abducens neurons. Schematic representation delineating predominating ion channels, transmitters and transmitter receptors of the different sets of trochlear (upper) and abducens neurons (lower). The relative strength of the immunostaining is indicated by the size and number of the respective symbols

discharge during adduction of the ipsilateral eye indicates a likely auxiliary inhibitory projection to abducens neurons (Clendaniel and Mays 1994).

GABAergic afferents to the trochlear nucleus originate from second-order vestibulo-ocular neurons in the ipsilateral superior vestibular nucleus (SVN), which provide an inhibition following anterior semicircular canal stimulation (McElligott and Spencer 2000; Precht et al. 1973; Soupiadou et al. 2018) and primarily target SIF motoneurons (McCrea et al. 1987; Ugolini et al. 2006). Additional GABAergic inputs may arise from the ipsilateral dorsal Y-group, and provide an inhibition to superior oblique and inferior rectus motoneurons during upward smooth pursuit eye movements (Chubb and Fuchs 1982; Zeeh et al. 2020). GABAergic projections to the trochlear nucleus may also include inhibitory burst neurons for vertical saccades, located in the ipsilateral interstitial nucleus of Cajal (monkey: Horn et al. 2003) and in the rostral interstitial nucleus of the medial longitudinal fasciculus (RIMLF) (cat: Spencer and Wang 1996). In contrast to a previous report (Zeeh et al. 2015), a differential density of GAD-immunopositive terminals was encountered in the present study for MIF and SIF motoneurons (Fig. 6b). This discrepancy could simply be due to the use of thicker paraffin sections in the former study, which might have reduced the chance of evaluating overlapping puncta and/or reduced penetration of the antibodies. Nevertheless, the difference in GAD-immunopositive terminal density between SIF and MIF motoneurons was generally much lower for trochlear than for abducens motoneurons.

Glutamatergic inputs to abducens neurons, demonstrated by vGlut2-immunoreactive puncta, may arise from excitatory VOR neurons in the contralateral MVN, or ventral lateral vestibular nucleus (Delgado-García et al. 1986; McElligott and Spencer 2000), from excitatory premotor burst neurons located in the ipsilateral PPRF (Horn 2006; Ugolini

et al. 2006) and from non-cholinergic INTs located primarily in the contralateral oculomotor nucleus (Clendaniel and Mays 1994). As revealed by retrograde transsynaptic tracer studies, burst neurons in the PPRF and magnocellular neurons in the MVN project predominantly to SIF motoneurons (Ugolini et al. 2006; Wasicky et al. 2004). The results of the current study demonstrated the presence of about 50% more vGlut2-positive puncta per length of somatic membrane for SIF motoneurons compared to MIF motoneurons in the abducens nucleus (Fig. 6a, left). Whether or not additional projections from the PPRF are responsible for this difference was impossible to determine with the employed method. Moreover, it is also difficult to predict the functional consequences of the different extents of glutamatergic synapses for the overall excitability, and thus the excitability of MIF and SIF motoneurons, given the obvious morphological differences (Torres-Torrelo et al. 2012). The more intense immunolabeling of vGlut2 on motoneuronal dendrites as compared to the somatic membrane potentially has functional implications in terms of spatiotemporal integration of excitatory signals, assuming an electrotonic compartmentalization (Magee 2001; Rekling et al. 2000).

The trochlear nucleus receives monosynaptic inputs from excitatory premotor burst neurons in the ipsilateral RIMLF mediating downward saccades (Horn and Büttner-Ennever 1998; Moschovakis et al. 1991; Spencer and Wang 1996). In the cat, these projections use glutamate and/or aspartate as transmitter (Spencer and Wang 1996), and may therefore contribute to the vGlut2-immunopositive terminals observed on SIF motoneurons. In addition, part of the latter excitatory synapses likely derives from glutamatergic projections of second-order vestibular neurons located in the contralateral MVN and in the interstitial nucleus of Cajal, as suggested previously (Zeeh et al. 2015). Finally, weak ipsilateral excitatory projections to trochlear motoneurons originate in the PPH (Baker et al. 1977). Interestingly, vGlut2-immunopositive synaptic structures around the motoneurons were more intense in the trochlear than in the abducens nucleus, and the comparison between MIF and SIF motoneurons in the trochlear nucleus yielded smaller differences in immunopositive puncta per length of the somatic membrane (Fig. 6a, left). The more pronounced differentiation between MIF and SIF abducens motoneurons with respect to vGlut2-immunopositive synaptic structures might be related to the larger spectrum and dynamic diversity of horizontal (i.e., vergence, saccades) as compared to torsional eye movements encoded, at least in part in the trochlear nucleus.

Impact of transmitters on the neuronal excitability of MIF and SIF motoneurons

Glutamate, as the major excitatory neurotransmitter in the central nervous system has been shown to also depolarize oculomotor motoneurons (Durand et al. 1987; Torres-Torrelo et al. 2012). While the activation of glutamatergic AMPA receptors generates a fast-rising response, a relatively slower dynamic of the depolarization is achieved by NMDA receptors, as demonstrated for cat abducens motoneurons (Durand et al. 1987). Glutamate modulates the firing rate of extraocular motoneurons by decreasing the voltage threshold depending on cell size and eye position-related recruitment thresholds (Torres-Torrelo et al. 2012). Importantly, glutamate has a larger impact on the phasic as compared to the tonic component of the motoneuronal discharge (Torres-Torrelo et al. 2012) and thereby is capable of regulating the firing pattern and rate of motoneurons, which transmit strong phasic components. However, the phasic component/burst additionally requires intrinsic active membrane properties as a decisive factor for fast firing rate alterations, as demonstrated for spinal motoneurons (Iwagaki and Miles 2011; Torres-Torrelo et al. 2012). Therefore, the glutamatergic control of motoneuron discharge is probably achieved by a combination of respective transmitter receptor profiles and differential sodium/potassium channel expression patterns.

Glutamatergic synaptic transmission in the abducens and trochlear nuclei involves vGlut2, but not vGlut1, in agreement with the complementary expression of both transporter subtypes and predominant presence of vGlut2 in the brainstem (Fremeau et al. 2001, 2004). Although vGlut2 is associated with a higher transport probability and faster synaptic release in highly active circuits, as compared to vGlut1, vGlut2-mediated transmission does not necessarily imply higher firing rates in the target neuron (Fremeau et al. 2004). The lack of any terminals expressing vGlut1 in the abducens and trochlear nuclei confirms and extends previous observations that only the subpopulation of medial rectus MIF motoneurons in the oculomotor nucleus is targeted by vGlut1-positive terminals (Zeeh et al. 2015). The cell specificity of glutamatergic transmission may be due to the lower dynamic requirements of MIF motoneurons during convergence eye movements. In contrast, SIF motoneurons express significantly more vGlut2-immunopositive puncta per circumferential somatic membrane than MIF motoneurons, and this transporter subtype occurs at an even higher density on dendritic membranes. The recruitment of motoneurons depends on the input resistance, which as a rule of thumb is inversely correlated with the neuronal surface area. This suggests that similar amounts of excitatory synaptic elements depolarize the smaller MIF motoneurons more efficiently (Henneman et al. 1965; Magee 2001; Mendell 2005; Torres-Torrelo et al. 2012). However, fewer glutamatergic synapses on MIF motoneurons might cause less efficient membrane potential alterations given the smaller size of the glutamatergic synaptic structures (Fig. 6a). Alternatively, differential expression patterns of voltage-gated potassium channels could produce different neuronal outputs from MIF

and SIF motoneurons, collectively rendering a clear prediction of the findings on net firing rate changes at best difficult (see Perineuronal nets, potassium channels and fast-spiking section).

Control of neuronal excitability by intrinsic membrane properties of MIF and SIF motoneurons

Transmitter receptors and their functional impact on selective vulnerability in neurodegenerative diseases

Ionotropic glutamate receptors consist of AMPA/kainate and NMDA receptors. Increasing evidence indicates that NMDA receptors mediate slower and more prolonged responses, whereas AMPA receptors initiate more rapid and transient responses (Traynelis, 2010). Unlike AMPA receptors, which increase the permeability mainly for sodium and potassium, NMDA receptors are also permeable for Ca^{2+}, producing prolonged depolarizations (Dingledine et al. 1999). In the abducens nucleus of larval *Xenopus laevis*, motoneurons were subdivided into two functional subgroups with respect to the pharmacological profile of vestibular excitatory inputs (Dietrich et al. 2017). One population of motoneurons is mainly activated through AMPA receptors, while motoneurons of the second subgroup receive vestibular excitatory inputs predominantly through NMDA receptors (Dietrich et al. 2017). The present study revealed lower expression levels of GluR2/3- and a lack of NMDAR1-immunoreactivity in MIF motoneurons, whereas immunostaining for both receptors was present in SIF motoneurons. However, no indication for a potential distinction into subgroups with respect to ionotropic glutamate receptor expression was encountered in either of the two motor nuclei examined. This does, however, not exclude the possibility that histochemical analyses of other glutamate receptor subunits, including a more detailed quantification, would allow a dissociation into particular subcategories of SIF and MIF motoneurons.

Differential glutamatergic receptor expression in MIF and SIF motoneurons has important functional and clinical implications. First, fewer vGlut2-immunopositive terminals with fewer GluR2/3 and no NMDAR1 expression by MIF motoneurons provides suggestive evidence for lower synaptic sensitivity in response to glutamate, as compared to SIF motoneurons. Second, this could render MIF and SIF motoneurons differentially resistant to glutamate-induced excitotoxicity as found, for instance, in amyotrophic lateral sclerosis (ALS) (Brockington et al. 2013). The higher expression levels of AMPA-receptors containing the GluR2 subunit, which renders extraocular motoneurons less permeable to calcium, potentially represents one cause for the relative resistance of the ocular motor system to degeneration in ALS as compared to spinal motoneurons (Van Damme et al. 2005). However recent studies imply that the ocular motor system is not completely spared in ALS, but it may affect motoneurons differentially. Therefore, the comparably lower GluR2/3 expression in MIF motoneurons along with the absence of calcium-binding proteins (Eberhorn et al. 2005) could constitute one factor for the putatively higher vulnerability of MIF motoneurons as compared to SIF motoneurons, consistent with the observed degeneration of MIFs in ALS patients (Ahmadi et al. 2010; Tjust et al. 2017).

Control of motoneuronal excitability is also maintained by inhibitory transmitters through fast-acting ionotropic glycinergic and $GABA_A$ receptors, which are permeable for Cl^- upon ligand binding (Rekling et al. 2000). Glycine and $GABA_A$ receptors decrease excitability, depending on the intracellular Cl^- concentration, which is regulated in part by the activity of member 5 of KCC2 (Chamma et al. 2012). KCC2-immunolabeling of MIF and SIF motoneurons, therefore, complies with requirements for glycinergic and GABAergic neurotransmission. Similar motoneuron membrane localizations of GlyR1 and KCC2 suggest that they co-localize, with weak somatic labeling and stronger labeling of the dendrites (Figs. 7d, 8a–c). In addition, $GABA_A$ receptors have been demonstrated to also colocalize both with GlyR1 (Todd et al. 1996) and KCC2 (Huang et al. 2013). KCC2 determines the polarity and efficacy of $GABA_A$ and glycine receptors, and pathologies that derive from a KCC2 deficiency cause neural excitability-related disorders, such as epilepsy and Huntington's disease (Tang 2020).

Perineuronal nets, potassium channels and fast-spiking

Beyond a potential role in neuroprotection and regulating plasticity, PNs are associated with parvalbumin-immunopositive fast-spiking interneurons, where this structural element presumably acts as cation buffer by providing a negatively charged trap for sodium and potassium ions around the cell membrane (Härtig et al. 1999). Moreover, PNs are correlated with the expression of the voltage-gated potassium channel Kv3.1b, potentially enhancing firing characteristics of fast-spiking neurons via regulation of Kv3.1b and Kv1.1 expression and recruitment (Favuzzi, 2017; Härtig et al. 1999). Low voltage-activated members of the Kv1 family are known to regulate the resting membrane potential, spike threshold and neuronal excitability (Johnston et al. 2010). A recent study in mouse deep cerebellar nucleus neurons demonstrated that application of specific Kv1 channel blockers lowers action potential threshold, increases spontaneous firing rate (or introduces spontaneous tonic firing in previously silent neurons) and reduces the fast-spiking capacity (Feria Pliego and Pedroarena 2020). On the other hand, members of high-voltage activated Kv3 channels open during action potentials, thereby shortening spike duration by interfering with the repolarization (Johnston et al. 2010). Together, Kv1.1 and Kv3.1b enhance sustained and high-frequency

firing by minimizing Nav inactivation (Gu et al. 2018; Kaczmarek and Zhang 2017; Kodama et al. 2020).

Recent findings in cat indicated that both MIF and SIF motoneurons express phasic-tonic discharge patterns and contribute to all types of eye movements (Hernández et al. 2019). This appears to conflict with the fact that MIF motoneurons lack the Kv3.1 ion channel subunit, which is a reliable marker of fast-spiking neurons capable of bursts (Kodama et al. 2020), along with lower levels of Kv1.1-immunoreactivity. Additionally, the graded immunolabeling of Kv1.1 of abducens and trochlear neurons is interesting due to the role in regulating spike threshold, and therefore overall excitability. However, varying immunolabeling intensities cannot be translated directly into differential mRNA content or protein expression. Nonetheless, varying Kv1.1 expression levels comply with the observation that extraocular motoneurons appear to form a functionally continuous spectrum with regard to eye position and eye velocity-related recruitment thresholds (Hernández et al. 2019; Nieto-Gonzales et al. 2007). Therefore, Kv1.1 could be a contributor to the electrophysiological substrate required for regulating neuronal firing threshold and corresponding eye movement-related sensitivity. This suggestion places MIF and SIF motoneurons on opposite ends of a population spectrum with distinct histochemical profiles that correspond to neurons with relatively tonic or relatively phasic firing characteristics, respectively (Davis-López de Carrizosa et al. 2011; Horn and Straka 2021).

Fast-firing and associated ion channel expression profile

In a recent study conducted on MVN neurons with different firing characteristics in mice, Kodama et al. (2020) identified distinct co-expression patterns of genes, including (but not limited to) voltage-gated ion channel families, neurofilaments and calcium-binding proteins. An important discovery was the strong correlation of ion channel expression including Kv1.1, Kv3.1 and Nav1.6 in the fastest-spiking MVN neurons that constitute a major synaptic input to extraocular motoneurons (Kodama et al. 2020). These members of the 'fast spiking gene module' are potentially co-regulated and responsible for the persistence of a high excitability during repetitive firing (Kodama et al. 2020). Persistent high firing rates, such as found in ocular motor circuitries, require minimal Nav inactivation, which is facilitated by Kv1.1 and Kv3.1 subunits (Carter and Bean 2011; Foust et al. 2011; Kaczmarek and Zhang 2017). Our findings demonstrate that this correlation, required for sustained fast-spiking, is in fact implemented in SIF, but not in MIF motoneurons at the protein level (Figs. 1, 2, 3, 10). Although these findings may account for the reported lower threshold and reduced firing level of MIF motoneurons (Hernández et al. 2019), it cannot exclude a potential generation of bursts through the presence of other Kv subunits alongside Nav1.6 channels, as reported for Purkinje cells (Khavandgar et al. 2005; McKay and Turner 2004; Zagha et al. 2008). The hypothesis that the burst activity of MIF motoneurons is achieved through a set of different ion channel subunits complies with possibly distinct evolutionary origins of MIF and SIF motoneurons (Horn and Straka 2021; Walls 1962).

In addition, Kodama et al. (2020) reported a covarying expression of neurofilament proteins along with ion channels that are characteristic for the fast-spiking gene module. These features also correlate with axon caliber differences and even the regulation of dynamics and sustainability of transmitter release (Kodama et al. 2020). These findings also agree with the observation that MIF motoneurons lack non-phosphorylated neurofilaments (NP-NF) (Eberhorn et al. 2005). SIF motoneurons on the other hand co-express NP-NF (SMI-32), Kv1.1 and Kv3.1, and have larger axonal diameters indicative for sustained fast-spiking properties. Given that expression levels of neurofilaments covary with the axon caliber (Friede and Samorajski 1970; Lee and Cleveland 1996), a co-regulation of ion channel and neurofilament genes could account for a relationship between axon diameter as a proxy for high dynamics and fast-spiking capacity, as demonstrated for several other cell types (Perge et al. 2012).

Low voltage activated (T-type) calcium channels in MIF motoneurons and implications for muscle contractions

As members of a family of inward-permeating cation channels, low-voltage-activated (LVA) T-type calcium channels generally increase the excitability of cells (Weiss and Zamponi 2013). At resting membrane potential, these channels are typically inactive and therefore contribute only little to spike generation (Molineux, 2006; Weiss and Zamponi 2013). Upon release from a hyperpolarization, these channels depolarize the membrane to generate an LVA calcium spike and a rebound depolarization that drives a spike burst (post-inhibitory rebound burst) (Molineux et al. 2006). Therefore, T-type calcium channels are associated with regulating the excitability and pace-making at subthreshold voltage levels (Weiss and Zamponi 2013).

Selective expression of Cav3.1 channel, as observed in MIF motoneurons (Fig. 10), was shown to be sufficient for a rebound discharge (Molineux et al. 2006). On the other hand, cerebellar stellate and basket cells which express only Cav3.2 or Cav3.3 do not generate a rebound discharge under normal conditions, but only upon blockade of potassium channels (Molineux et al. 2006). The Cav3.3 subunit also contributes to a rebound discharge when co-expressed with potassium channels (Molineux et al. 2006). Taken together, post-inhibitory rebound depolarization generated by the

Cav3.1 channel could be responsible for the initial membrane depolarization and bursting in MIF motoneurons, with a different mechanism than that implemented in SIF motoneurons. Accordingly, the excitability and bursting behavior of SIF motoneurons are likely regulated by a combination of Kv channels and more efficient glutamatergic transmission. These differences in intrinsic membrane properties could explain why MIF motoneurons have lower recruitment thresholds and firing rates, while at the same time they are apparently able to generate spike bursts (Hernández et al. 2019). The lack of Kv3.1 and Kv1.1 channels, combined with Cav3.1 channel expression, suggests that the population of MIF motoneurons in this study corresponds to the early recruited motoneuron population with low sensitivity and extended tonic firing. In contrast SIF motoneurons exhibit brief bursts followed by a less persisting tonic firing (Davis-López de Carrizosa et al. 2011; Gonzalez-Forero et al. 2003).

T-type calcium channels, by causing action potential-independent sustained Ca^{2+} elevations near the resting membrane potential, control a multitude of cellular and physiological functions, such as (low-threshold) vesicular exocytosis (Weiss and Zamponi 2013). As a result, MIF motoneurons might release significant amounts of neurotransmitters from their axonal boutons around the resting membrane potential (Weiss and Zamponi 2013), especially with respect to the window current of T-type calcium channels (Perez-Reyes 2003). When activation and inactivation curves of T-type calcium channels overlap, a sustained influx of Ca^{2+} through the channels around the resting membrane potential is possible for up to minutes, where a significant proportion of channels is open, but not yet completely inactivated (Perez-Reyes 2003). This phenomenon, i.e., "window current", could facilitate low-threshold acetylcholine release onto multiply-innervated muscle fibers for an extended time. This is in contrast to singly-innervated fibers, where the discharge of SIF motoneurons is only brief, but at a considerably higher spike rate (Hernández et al. 2019), and therefore provokes a larger quantal transmitter release per time. Based on this interpretation, selective Cav3.1 channel expression in MIF motoneurons could account for a role in the activation of all eye movement types, albeit with lower sensitivity and with a predominant contribution to the maintenance of an elevated muscle tone (Hernández et al. 2019; Wasicky et al. 2004).

Presynaptic inputs and intrinsic membrane properties of internuclear neurons in comparison to SIF motoneurons

Internuclear neurons of the abducens nucleus, which use glutamate and/or aspartate as transmitter (Nguyen and Spencer 1999), receive patterns of synaptic inputs from premotor sources similar to adjacent abducens motoneurons (Spencer and Sterling 1977; Straka and Dieringer 1993). While motoneurons are cholinergic and project to the lateral rectus muscle, INTs project to the medial rectus subgroup of the contralateral oculomotor nucleus, enabling horizontal conjugate eye movements (Baker and Highstein 1975; Büttner-Ennever and Akert 1981; Ugolini et al. 2006). Following electrical stimulation of the vestibular nerve in the cat and frog, both abducens motoneurons and internuclear neurons display disynaptic EPSPs on the contralateral and IPSPs on the ipsilateral side (Baker and Highstein 1975; Straka and Dieringer 2004). Monosynaptic excitatory premotor commands for saccades arise from the ipsilateral pontine reticular formation (Highstein et al. 1976; Strassman et al. 1986). Interestingly, the sources of synaptic inputs received by INTs are similar to those of SIF motoneurons, but not to those of MIF motoneurons (Ugolini et al. 2006). This suggests that signals mediated onto MIF abducens motoneurons obviously find no correspondence in an internuclear pathway that interconnects the respective synergistic subtypes of lateral and medial rectus motoneurons.

Internuclear neurons facilitate the conjugacy of both eyes by mediating a signal copy to the oculomotor nucleus because this neuronal population exhibits the same burst-tonic firing pattern during horizontal eye movements (Fuchs et al. 1988). Moreover, INTs fire slightly before and with a somewhat higher intra-burst frequency than abducens motoneurons (Delgado-García et al. 1977), which facilitates precise phase relationships of lateral rectus and medial rectus muscle contractions (Davis-López de Carrizosa et al. 2011; Pastor and González-Forero 2003). The enhanced excitability and earlier recruitment of INTs potentially derives from morpho-physiological adaptations. Notably, the distinct behavior of INTs might be related to a higher density of synaptic inputs, as compared to SIF motoneurons (Highstein et al. 1982). Indeed, the present study has demonstrated a higher density of presumed inhibitory synaptic contacts onto the somata of INTs, compared to those on SIF motoneurons (Figs. 6b, c, 7b, c). However, only the density of GAD-immunopositive puncta was significantly higher, while the synaptic density of other transmitter types on SIF motoneurons and INTs were similar, in agreement with electron microscopic observations (Spencer and Sterling 1977). On the other hand, consistently stronger Kv3.1b- and PN-immunolabeling were found in INTs, as compared to SIF motoneurons (Figs. 1f, 2c), despite a higher density of glutamatergic synapses. This could explain an enhanced excitability and intra-burst frequency of INTs (Delgado-García et al. 1977).

A major difference between INTs and motoneurons emerging from the current study was the strong immunolabeling of NMDAR1 in the former cell type (Fig. 4f). Intense somatic and dendritic labeling of INTs with the NMDAR1

antibody assigns a distinct NMDAR-mediated excitation to these neurons in comparison to motoneurons. NMDA receptors mediate slower and more prolonged responses, whereas AMPA receptors provoke more rapid and transient responses (Traynelis et al. 2010). The intense NMDAR1 expression by INTs in comparison to motoneurons could assist in spike burst generation, as NMDA receptors were shown in cat abducens motoneurons to evoke a burst at threshold level followed by a stable repetitive firing (Durand et al. 1987).

Differential control of eye movements by extraocular motoneuron and muscle fiber types

Earlier work on extraocular muscles suggested the possibility that slow eye movements and gaze holding is achieved by slow-tonic (non-twitch) non-fatigable fibers, while fast eye movements such as saccades are produced by fast-twitch fatigable fibers, as observed in vertebrate skeletal muscles (Bormioli et al. 1980; Close and Hoh 1968; Henneman et al. 1965; Hoh 2020; Ugolini et al. 2006). However, the expression of numerous myosin heavy chain isoforms that define contraction characteristics in extraocular muscles suggests that the wide range of eye movements might be differentially controlled through the recruitment of several fiber types, rather than the often-emphasized bimodal distribution (Hoh 2020; Horn and Straka 2021). Indeed, apart from a classification according to the arrangement into an orbital and a global layer, extraocular muscle fibers can be subdivided into up to six types according to structural and histochemical properties such as fiber diameter, sarcoplasmic reticulum development, number of mitochondria and oxidative enzyme content (Shall and Goldberg 1992; Spencer and Porter 2006). In these analyses, global and orbital SIFs, as well as orbital MIFs, are arranged along a spectrum of fast/slow and fatigable/fatigue-resistant properties, whereas global MIFs are positioned at the non-twitch/slow-tonic end containing the slowest myosin heavy chain isoforms (Close and Hoh 1968; Hernández et al. 2019; Hoh 2020; Matyushkin 1964).

Conclusion

Distinct labeling patterns of ion channel and neurotransmission-related proteins were encountered for MIF and SIF motoneurons in the abducens and trochlear nuclei of macaque monkeys, in agreement with putative differences in physiological properties. These findings complement previous reports with regard to several functional aspects: (i) MIF motoneurons, histologically identified by ChAT-immunopositivity and lack of PNs likely correspond to global MIF motoneurons identified in cats by lower spike thresholds and firing rates. (ii) Although motoneurons along the entire spectrum of firing rates and activation thresholds are active during all eye movement types, the clear histological distinction including innervation pattern between SIF and MIF motoneurons suggests a differential distribution of electrophysiological properties. (iii) The wide range of motoneuronal activity might be achieved through a combination of varying density in transmitter phenotype, receptor expression pattern and ion channel composition. The immunohistochemical dissection performed in the current study thus represents a major step in linking morphological and biochemical features with known physiological and pharmacological properties, providing the basis for an assessment of corresponding aspects of homologous nuclei involved in human eye movement pathologies.

Acknowledgements The excellent technical assistance of Christine Unger and Ahmed Messoudi MPh as well as the contribution of Öykü Büyükşengün is acknowledged. The authors thank Drs. Alexander Thiele and Claudia Distler for providing fixated brainstem tissue of a macaque monkey (M5). Valuable suggestions from Dr. Miriam Barnerßoi are much appreciated. Finally, the authors thank Prof. Dr. med. Jens Waschke for his continuous support.

Funding Open Access funding enabled and organized by Projekt DEAL. This study was funded by the Deutsche Forschungsgemeinschaft (HO 1639/5-1 to AKEH; STR 478/3-1 to HS) and the Graduate School of Systemic Neurosciences (GSN)—LMU Munich (ÜSM), Munich Center for Neurosciences—Brain and Mind, Ludwig-Maximilians-Universität München, and National Institutes of Health EY06069, P51 OD010425, and an unrestricted departmental grant from Research to Prevent Blindness (MM, JF).

Availability of data and material The datasets generated during this study are available from the corresponding author on reasonable request.

Declarations

Conflict of interest The authors declare that they have no conflict of interest.

Ethics approval All experimental procedures conformed to the State and University Regulations on Laboratory Animal Care, including the Principles of Laboratory Animal Care (NIH Publication 85-23, Revised 1985), and were approved by the Animal Care Officers and Institutional Animal Care and Use Committees at the University of Washington, where all surgical interventions were performed.

References

Ahlfeld J, Mustari M, Horn AKE (2011) Sources of calretinin inputs to motoneurons of extraocular muscles involved in upgaze. Ann NY Acad Sci 1233:91–99. https://doi.org/10.1111/j.1749-6632.2011.06168.x

Ahmadi M, Liu J-X, Brännström T, Andersen PM, Stål P, Pedrosa-Domellöf F (2010) Human extraocular muscles in ALS. Invest Ophthalmol Vis Sci 51:3494–3501. https://doi.org/10.1167/iovs.09-5030

Baker R, Highstein SM (1975) Physiological identification of interneurons and motoneurons in the abducens nucleus. Brain Res 91:292–298. https://doi.org/10.1016/0006-8993(75)90551-x

Baker R, Berthoz A, Delgado-García J (1977) Monosynaptic excitation of trochlear motoneurons following electrical stimulation of the prepositus hypoglossi nucleus. Brain Res 121:157–161. https://doi.org/10.1016/0006-8993(77)90445-0

Bormioli SP, Sartore S, Vitadello M, Schiaffino S (1980) "Slow" myosins in vertebrate skeletal muscle. J Cell Biol 85:672–681. https://doi.org/10.1083/jcb.85.3.672

Brockington A, Ning K, Heath PR et al (2013) Unravelling the enigma of selective vulnerability in neurodegeneration: motor neurons resistant to degeneration in ALS show distinct gene expression characteristics and decreased susceptibility to excitotoxicity. Acta Neuropathol 125:95–109. https://doi.org/10.1007/s00401-012-1058-5

Bruce G, Wainer BH, Hersh LB (1985) Immunoaffinity purification of human choline acetyltransferase: comparison of the brain and placental enzymes. J Neurochem 45:611–620. https://doi.org/10.1111/j.1471-4159.1985.tb04030.x

Büttner-Ennever JA (1992) Paramedian tract cell groups: a review of connectivity and oculomotor function. In: Shimazu H, Shinoda Y (eds) Vestibular and brain stem control of eye, head and body movements. Japan Scientific Societies Press, Karger, Tokyo, Basel, pp 323–330. https://doi.org/10.1159/000421392

Büttner-Ennever JA (2006) The extraocular motor nuclei: organization and functional neuroanatomy. Prog Brain Res 151:95–125. https://doi.org/10.1016/S0079-6123(05)51004-5

Büttner-Ennever JA, Akert K (1981) Medial rectus subgroups of the oculomotor nucleus and their abducens internuclear input in the monkey. J Comp Neurol 197:17–27. https://doi.org/10.1002/cne.901970103

Büttner-Ennever JA, Horn AKE, Scherberger H, D'Ascanio P (2001) Motoneurons of twitch and nontwitch extraocular muscle fibers in the abducens, trochlear, and oculomotor nuclei of monkeys. J Comp Neurol 438:318–335. https://doi.org/10.1002/cne.1318

Carter BC, Bean BP (2011) Incomplete inactivation and rapid recovery of voltage-dependent sodium channels during high-frequency firing in cerebellar Purkinje neurons. J Neurophysiol 105:860–871. https://doi.org/10.1152/jn.01056.2010

Chamma I, Chevy Q, Poncer JC, Lévi S (2012) Role of the neuronal K-Cl co-transporter KCC2 in inhibitory and excitatory neurotransmission. Front Cell Neurosci 6:5. https://doi.org/10.3389/fncel.2012.00005

Chubb MC, Fuchs AF (1982) Contribution of y group of vestibular nuclei and dentate nucleus of cerebellum to generation of vertical smooth eye movements. J Neurophysiol 48:75–99. https://doi.org/10.1152/jn.1982.48.1.75

Clendaniel RA, Mays LE (1994) Characteristics of antidromically identified oculomotor internuclear neurons during vergence and versional eye movements. J Neurophysiol 71:1111–1127. https://doi.org/10.1152/jn.1994.71.3.1111

Close R, Hoh JF (1968) Effects of nerve cross-union on fast-twitch and slow-graded muscle fibres in the toad. J Physiol 198:103–125. https://doi.org/10.1113/jphysiol.1968.sp008596

Davis-López de Carrizosa MA, Morado-Díaz CJ, Miller JM, de la Cruz RR, Pastor AM (2011) Dual encoding of muscle tension and eye position by abducens motoneurons. J Neurosci 31:2271–2279. https://doi.org/10.1523/jneurosci.5416-10.2011

De la Cruz RR, Pastor AM, Martinez-Guijarro FJ, Lopez-Garcia C, Delgado-García JM (1992) Role of GABA in the extraocular motor nuclei of the cat: a postembedding immunocytochemical study. Neuroscience 51:911–929. https://doi.org/10.1016/0306-4522(92)90529-B

Dean P (1996) Motor unit recruitment in a distribution model of extraocular muscle. J Neurophysiol 76:727–742. https://doi.org/10.1152/jn.1996.76.2.727

Delgado-García JM, Baker R, Highstein S (1977) The activity of internuclear neurons identified within the abducens nucleus of the alert cat. In: Baker R, Berthoz A (eds) Control of gaze by brain stem neurons. Elsevier, Amsterdam, pp 291–300

Delgado-García JM, Del Pozo F, Baker R (1986) Behavior of neurons in the abducens nucleus of the alert cat. I. Motoneurons. Neuroscience 17:929–952. https://doi.org/10.1016/0306-4522(86)90073-4

Dieringer N, Precht W (1986) Functional organization of eye velocity and eye position signals in abducens motoneurons of the frog. J Comp Physiol 158:179–194. https://doi.org/10.1007/BF01338561

Dietrich H, Glasauer S, Straka H (2017) Functional organization of vestibulo-ocular responses in abducens motoneurons. J Neurosci 37:4032–4045. https://doi.org/10.1523/jneurosci.2626-16.2017

Dingledine R, Borges K, Bowie D, Traynelis SF (1999) The glutamate receptor ion channels. Pharmacol Rev 51:7–61

Durand J, Engberg I, Tyc-Dumont S (1987) l-Glutamate and N-methyl-d-aspartate actions on membrane potential and conductance of cat abducens motoneurones. Neurosci Lett 79:295–300. https://doi.org/10.1016/0304-3940(87)90447-2

Eberhorn AC, Ardelenanu P, Büttner-Ennever JA, Horn AKE (2005) Histochemical differences between motoneurons supplying multiply and singly innervated extraocular muscle fibers. J Comp Neurol 491:352–366. https://doi.org/10.1002/cne.20715

Eberhorn AC, Büttner-Ennever JA, Horn AKE (2006) Identification of motoneurons innervating multiply- or singly-innervated extraocular muscle fibres in the rat. Neuroscience 137:891–903. https://doi.org/10.1016/j.neuroscience.2005.10.038

Erichsen JT, Wright NF, May PJ (2014) Morphology and ultrastructure of medial rectus subgroup motoneurons in the macaque monkey. J Comp Neurol 522:626–641. https://doi.org/10.1002/cne.23437

Fairless R, Williams SK, Diem R (2019) Calcium-binding proteins as determinants of central nervous system neuronal vulnerability to disease. Int J Mol Sci 20:2146. https://doi.org/10.3390/ijms20092146

Favuzzi E, Marques-Smith A, Deogracias R, Winterflood CM, Sanchez-Aguilera A, Maeso P, Fernandes C, Ewers H, Rico B (2017) Activity-dependent gating of parvalbumin interneuron function by the perineuronal net protein brevican. Neuron 95:639–655.e10. https://doi.org/10.1016/j.neuron.2017.06.028

Feria Pliego JA, Pedroarena CM (2020) Kv1 potassium channels control action potential firing of putative GABAergic deep cerebellar nuclear neurons. Sci Rep 10:6954. https://doi.org/10.1038/s41598-020-63583-7

Foust AJ, Yu Y, Popovic M, Zecevic D, McCormick DA (2011) Somatic membrane potential and Kv1 channels control spike repolarization in cortical axon collaterals and presynaptic boutons. J Neurosci 31:15490–15498. https://doi.org/10.1523/jneurosci.2752-11.2011

Fremeau RT Jr, Troyer MD, Pahner I et al (2001) The expression of vesicular glutamate transporters defines two classes of excitatory

synapse. Neuron 31:247–260. https://doi.org/10.1016/s0896-6273(01)00344-0
Fremeau RT Jr, Voglmaier S, Seal RP, Edwards RH (2004) VGLUTs define subsets of excitatory neurons and suggest novel roles for glutamate. Trends Neurosci 27:98–103. https://doi.org/10.1016/j.tins.2003.11.005
Friede RL, Samorajski T (1970) Axon caliber related to neurofilaments and microtubules in sciatic nerve fibers of rats and mice. Anat Rec 167:379–387. https://doi.org/10.1002/ar.1091670402
Fuchs AF, Scudder CA, Kaneko CR (1988) Discharge patterns and recruitment order of identified motoneurons and internuclear neurons in the monkey abducens nucleus. J Neurophysiol 60:1874–1895. https://doi.org/10.1152/jn.1988.60.6.1874
Gonzalez-Forero D, De la Cruz RR, Delgado-García JM, Alvarez FJ, Pastor ÁM (2003) Functional alterations of cat abducens neurons after peripheral tetanus neurotoxin injection. J Neurophysiol 89:1878–1890. https://doi.org/10.1152/jn.01006.2002
Gu Y, Servello D, Han Z, Lalchandani RR, Ding JB, Huang K, Gu C (2018) Balanced activity between Kv3 and Nav channels determines fast-spiking in mammalian central neurons. iScience 9:120–137. https://doi.org/10.1016/j.isci.2018.10.014
Härtig W, Derouiche A, Welt K, Brauer K, Grosche J, Mäder M, Reichenbach A, Brückner G (1999) Cortical neurons immunoreactive for the potassium channel Kv3.1b subunit are predominantly surrounded by perineuronal nets presumed as a buffering system for cations. Brain Res 842:15–29. https://doi.org/10.1016/s0006-8993(99)01784-9
Henneman E, Somjen G, Carpenter DO (1965) Functional significance of cell size in spinal motoneurons. J Neurophysiol 28:560–580. https://doi.org/10.1152/jn.1965.28.3.560
Hernández GR, Blumer R, de la Cruz RR, Pastor AM (2019) Functional diversity of motoneurons in the oculomotor system. Proc Natl Acad Sci USA 116:3837–3846. https://doi.org/10.1073/pnas.1818524116
Highstein SM, Maekawa K, Steinacker A, Cohen B (1976) Synaptic input from the pontine reticular nuclei to abducens motoneurons and internuclear neurons in the cat. Brain Res 112:162–167. https://doi.org/10.1016/0006-8993(76)90344-9
Highstein SM, Karabelas A, Baker R, McCrea RA (1982) Comparison of the morphology of physiologically identified abducens motor and internuclear neurons in the cat: a light microscopic study employing the intracellular injection of horseradish peroxidase. J Comp Neurol 208:369–381. https://doi.org/10.1002/cne.902080407
Hoh JFY (2020) Myosin heavy chains in extraocular muscle fibres: distribution, regulation and function. Acta Physiol 231:e13535. https://doi.org/10.1111/apha.13535
Horn AKE (2006) The reticular formation. Prog Brain Res 151:127–155. https://doi.org/10.1016/s0079-6123(05)51005-7
Horn AKE, Büttner-Ennever JA (1998) Premotor neurons for vertical eye-movements in the rostral mesencephalon of monkey and man: the histological identification by parvalbumin immunostaining. J Comp Neurol 392:413–427. https://doi.org/10.1002/(Sici)1096-9861(19980323)392:4%3c413::aid-cne1%3e3.0.co;2-3
Horn AKE, Straka H (2021) Functional organization of extraocular motoneurons and eye muscles. Annu Rev Vis Sci 7 (in press). https://doi.org/10.1146/annurev-vision-100119-125043
Horn AKE, Helmchen C, Wahle P (2003) GABAergic neurons in the rostral mesencephalon of the Macaque monkey that control vertical eye movements. Ann NY Acad Sci 1004:19–28. https://doi.org/10.1196/annals.1303.003
Horn AK, Eberhorn A, Härtig W, Ardelenanu P, Messoudi A, Büttner-Ennever JA (2008) Perioculomotor cell groups in monkey and man defined by their histochemical and functional properties: reappraisal of the Edinger-Westphal nucleus. J Comp Neurol 507:1317–1335. https://doi.org/10.1002/cne.21598
Horn AKE, Horng A, Buresch N, Messoudi A, Hartig W (2018) Identification of functional cell groups in the abducens nucleus of monkey and human by perineuronal nets and choline acetyltransferase immunolabeling. Front Neuroanat 12:45. https://doi.org/10.3389/fnana.2018.00045
Huang Y, Wang JJ, Yung WH (2013) Coupling between GABA-A receptor and chloride transporter underlies ionic plasticity in cerebellar Purkinje neurons. Cerebellum 12:328–330. https://doi.org/10.1007/s12311-013-0453-3
Iwagaki N, Miles GB (2011) Activation of group I metabotropic glutamate receptors modulates locomotor-related motoneuron output in mice. J Neurophysiol 105:2108–2120. https://doi.org/10.1152/jn.01037.2010
Johnston J, Forsythe ID, Kopp-Scheinpflug C (2010) Going native: voltage-gated potassium channels controlling neuronal excitability. J Physiol 588:3187–3200. https://doi.org/10.1113/jphysiol.2010.191973
Kaczmarek LK, Zhang Y (2017) Kv3 channels: enablers of rapid firing, neurotransmitter release, and neuronal endurance. Physiol Rev 97:1431–1468. https://doi.org/10.1152/physrev.00002.2017
Khavandgar S, Walter JT, Sageser K, Khodakhah K (2005) Kv1 channels selectively prevent dendritic hyperexcitability in rat Purkinje cells. J Physiol 569:545–557. https://doi.org/10.1113/jphysiol.2005.098053
Kodama T, Gittis A, Shin M, Kelleher K, Kolkman K, McElvain L, Lam M, du Lac S (2020) Graded coexpression of ion channel, neurofilament, and synaptic genes in fast-spiking vestibular nucleus neurons. J Neurosci 40:496–508. https://doi.org/10.1523/jneurosci.1500-19.2019
Lee MK, Cleveland DW (1996) Neuronal intermediate filaments. Annu Rev Neurosci 19:187–217. https://doi.org/10.1146/annurev.ne.19.030196.001155
Leigh RJ, Zee DS (2015) The neurology of eye movements. Oxford University Press, Oxford
Lienbacher K, Horn AE (2012) Palisade endings and proprioception in extraocular muscles: a comparison with skeletal muscles. Biol Cybern 106:643–655. https://doi.org/10.1007/s00422-012-0519-1
Lienbacher K, Mustari M, Ying HS, Büttner-Ennever JA, Horn AKE (2011) Do palisade endings in extraocular muscles arise from neurons in the motor nuclei? Invest Ophthalmol Vis Sci 52:2510–2519. https://doi.org/10.1167/iovs.10-6008
Maciewicz RJ, Kaneko CRS, Highstein SM, Baker R (1975) Morphophysiological identification of interneurons in the oculomotor nucleus that project to the abducens nucleus in the cat. Brain Res 96:60–65. https://doi.org/10.1016/0006-8993(75)90571-5
Magee JC (2001) Dendritic integration of excitatory synaptic input. Nat Rev Neurosci 1:181–190. https://doi.org/10.1038/35044552
Matyushkin DP (1964) Varieties of tonic muscle fibers in the oculomotor apparatus of the rabbit. B Exp Biol Med 55:235–238. https://doi.org/10.1007/BF00799651
Mayadali ÜS, Lienbacher K, Mustari M, Strupp M, Horn AKE (2019) Potassium channels in omnipause neurons. Prog Brain Res 249:117–123. https://doi.org/10.1016/bs.pbr.2019.04.017
McCrea RA, Strassman A, Highstein SM (1987) Anatomical and physiological characteristics of vestibular neurons mediating the vertical vestibulo-ocular reflex of the squirrel monkey. J Comp Neurol 264:571–594. https://doi.org/10.1002/cne.902640409
McElligott J, Spencer R (2000) Neuropharmacological aspects of the vestibulo-ocular reflex. In: Beitz AJ, Anderson JH (eds) Neurochemistry of the vestibular system, vol 10. CRC Press, Boca Raton, pp 199–222

McKay BE, Turner RW (2004) Kv3 K^+ channels enable burst output in rat cerebellar Purkinje cells. Eur J Neurosci 20:729–739. https://doi.org/10.1111/j.1460-9568.2004.03539.x

Mendell LM (2005) The size principle: a rule describing the recruitment of motoneurons. J Neurophysiol 93:3024–3026. https://doi.org/10.1152/classicessays.00025.2005

Molineux ML et al (2006) Specific T-type calcium channel isoforms are associated with distinct burst phenotypes in deep cerebellar nuclear neurons. Proc Natl Acad Sci USA 103:5555–5560. https://doi.org/10.1073/pnas.0601261103

Moschovakis AK, Scudder CA, Highstein SM (1991) The structure of the primate oculomotor burst generator. I. Medium-lead burst neurons with upward on-directions. J Neurophysiol 65:203–217. https://doi.org/10.1152/jn.1991.65.2.203

Nabel AL, Callan AR, Gleiss SA, Kladisios N, Leibold C, Felmy F (2019) Distinct distribution patterns of potassium channel subunits in somato-dendritic compartments of neurons of the medial superior olive. Front Cell Neurosci 13:38–38. https://doi.org/10.3389/fncel.2019.00038

Nguyen LT, Spencer RF (1999) Abducens internuclear and ascending tract of Deiters inputs to medial rectus motoneurons in the cat oculomotor nucleus: Neurotransmitters. J Comp Neurol 411:73–86. https://doi.org/10.1002/(sici)1096-9861(19990816)411:1%3c73::aid-cne6%3e3.0.co;2-7

Nieto-Gonzales JL, Carrascal L, Nuñez-Abades P, Torres B (2007) Phasic and tonic firing properties in rat oculomotor nucleus motoneurons, studied *in vitro*. Eur J Neurosci 25:2682–2696. https://doi.org/10.1111/j.1460-9568.2007.05516.x

Pastor ÁM, González-Forero D (2003) Recruitment order of cat abducens motoneurons and internuclear neurons. J Neurophysiol 90:2240–2252. https://doi.org/10.1152/jn.00402.2003

Perez-Reyes E (2003) Molecular physiology of low-voltage-activated T-type calcium channels. Physiol Rev 83:117–161. https://doi.org/10.1152/physrev.00018.2002

Perge JA, Niven JE, Mugnaini E, Balasubramanian V, Sterling P (2012) Why do axons differ in caliber? J Neurosci 32:626–638. https://doi.org/10.1523/jneurosci.4254-11.2012

Precht W, Baker R, Okada Y (1973) Evidence for GABA as the synaptic transmitter of the inhibitory vestibulo-ocular pathway. Exp Brain Res 18:415–428. https://doi.org/10.1007/bf00239109

Rekling JC, Funk GD, Bayliss DA, Dong XW, Feldman JL (2000) Synaptic control of motoneuronal excitability. Physiol Rev 80:767–852. https://doi.org/10.1152/physrev.2000.80.2.767

Shall MS, Goldberg SJ (1992) Extraocular motor units—type classification and motoneuron stimulation frequency-muscle unit force relationships. Brain Res 587:291–300. https://doi.org/10.1016/0006-8993(92)91010-C

Soupiadou P, Branoner F, Straka H (2018) Pharmacological profile of vestibular inhibitory inputs to superior oblique motoneurons. J Neurol 265 (Suppl 1):18–25. https://doi.org/10.1007/s00415-018-8829-4

Spencer RF, Baker R (1992) GABA and glycine as inhibitory neurotransmitters in the vestibulo-ocular reflex. Ann N Y Acad Sci 656:602–611. https://doi.org/10.1111/j.1749-6632.1992.tb25239.x

Spencer RF, Porter JD (2006) Biological organization of the extraocular muscles. Prog Brain Res 151:43–80. https://doi.org/10.1016/S0079-6123(05)51002-1

Spencer RF, Sterling P (1977) An electron microscope study of motoneurones and interneurones in the cat abducens nucleus identified by retrograde intraaxonal transport of horseradish peroxidase. J Comp Neurol 176:65–85. https://doi.org/10.1002/cne.901760105

Spencer RF, Wang SF (1996) Immunohistochemical localization of neurotransmitters utilized by neurons in the rostral interstitial nucleus of the medial longitudinal fasciculus (riMLF) that project to the oculomotor and trochlear nuclei in the cat. J Comp Neurol 366:134–148. https://doi.org/10.1002/(sici)1096-9861(19960226)366:1%3c134::aid-cne9%3e3.0.co;2-4

Spencer RF, Wenthold RJ, Baker R (1989) Evidence for glycine as an inhibitory neurotransmitter of vestibular, reticular, and prepositus hypoglossi neurons that project to the cat abducens nucleus. J Neurosci 9:2718–2736. https://doi.org/10.1523/jneurosci.09-08-02718.1989

Straka H, Dieringer N (1993) Electrophysiological and pharmacological characterization of vestibular inputs to identified frog abducens motoneurons and internuclear neurons in vitro. Eur J Neurosci 5:251–260. https://doi.org/10.1111/j.1460-9568.1993.tb00491.x

Straka H, Dieringer N (2004) Basic organization principles of the VOR: lessons from frogs. Prog Neurobiol 73:259–309. https://doi.org/10.1016/j.pneurobio.2004.05.003

Straka H, Fritzsch B, Glover JC (2014) Connecting ears to eye muscles: evolution of a 'simple'' reflex arc.' Brain Behav Evolut 83:162–175. https://doi.org/10.1159/000357833

Strassman A, Highstein SM, McCrea RA (1986) Anatomy and physiology of saccadic burst neurons in the alert squirrel monkey. I. Excitatory burst neurons. J Comp Neurol 249:337–357. https://doi.org/10.1002/cne.902490303

Tang BL (2020) The expanding therapeutic potential of neuronal KCC2. Cells 9:240. https://doi.org/10.3390/cells9010240

Tjust AE, Danielsson A, Andersen PM, Brännström T, Domellöf P (2017) Impact of amyotrophic lateral sclerosis on slow tonic myofiber composition in human extraocular muscles. Invest Ophthalmol Vis Sci 58:3708–3715. https://doi.org/10.1167/iovs.17-22098

Todd AJ, Watt C, Spike RC, Sieghart W (1996) Colocalization of GABA, glycine, and their receptors at synapses in the rat spinal cord. J Neurosci 16:974–982. https://doi.org/10.1523/jneurosci.16-03-00974.1996

Torres-Torrelo J, Rodríguez-Rosell D, Nunez-Abades P, Carrascal L, Torres B (2012) Glutamate modulates the firing rate in oculomotor nucleus motoneurons as a function of the recruitment threshold current. J Physiol 590:3113–3127. https://doi.org/10.1113/jphysiol.2011.226985

Traynelis SF et al (2010) Glutamate receptor ion channels: structure, regulation, and function. Pharmacol Rev 62:405–496. https://doi.org/10.1124/pr.109.002451

Ugolini G, Klam F, Doldan Dans M, Dubayle D, Brandi A-M, Büttner-Ennever JA, Graf W (2006) Horizontal eye movement networks in primates as revealed by retrograde transneuronal transfer of rabies virus: differences in monosynaptic input to "slow" and "fast" abducens motoneurons. J Comp Neurol 498:762–785. https://doi.org/10.1002/cne.21092

Van Damme P, Braeken D, Callewaert G, Robberecht W, Van Den Bosch L (2005) GluR2 deficiency accelerates motor neuron degeneration in a mouse model of amyotrophic lateral sclerosis. J Neuropathol Exp Neurol 64:605–612. https://doi.org/10.1097/01.jnen.0000171647.09589.07

Walls GL (1962) The evolutionary history of eye movements. Vision Res 2:69–80. https://doi.org/10.1016/0042-6989(62)90064-0

Wasicky R, Horn AKE, Büttner-Ennever JA (2004) Twitch and non-twitch motoneuron subgroups of the medial rectus muscle in the oculomotor nucleus of monkeys receive different afferent projections. J Comp Neurol 479:117–129. https://doi.org/10.1002/cne.20296

Weiser M et al (1995) The potassium channel subunit KV3.1b is localized to somatic and axonal membranes of specific populations of CNS neurons. J Neurosci 15:4298–4314. https://doi.org/10.1523/jneurosci.15-06-04298.1995

Weiss N, Zamponi GW (2013) Control of low-threshold exocytosis by T-type calcium channels. BBA Rev Biomembr 1828:1579–1586. https://doi.org/10.1016/j.bbamem.2012.07.031

Wollmuth LP (2018) Ion permeation in ionotropic glutamate receptors: still dynamic after all these years. Curr Opin Physiol 2:36–41. https://doi.org/10.1016/j.cophys.2017.12.003

Zagha E, Lang EJ, Rudy B (2008) Kv3.3 channels at the Purkinje cell soma are necessary for generation of the classical complex spike waveform. J Neurosci 28:1291–1300. https://doi.org/10.1523/jneurosci.4358-07.2008

Zamponi GW, Striessnig J, Koschak A, Dolphin AC (2015) The physiology, pathology, and pharmacology of voltage-gated calcium channels and their future therapeutic potential. Pharmacol Rev 67:821–870. https://doi.org/10.1124/pr.114.009654

Zeeh C, Mustari MJ, Hess BJ, Horn AK (2015) Transmitter inputs to different motoneuron subgroups in the oculomotor and trochlear nucleus in monkey. Front Neuroanat 9:95. https://doi.org/10.3389/fnana.2015.00095

Zeeh C, Mayadali ÜS, Horn AKE (2020) Histochemical characterization of the vestibular Y-Group in monkey. Cerebellum. https://doi.org/10.1007/s12311-020-01200-z

Zimmermann L, Morado-Díaz CJ, Davis-López de Carrizosa MA, de la Cruz RR, May PJ, Streicher J, Pastor ÁM, Blumer R (2013) Axons giving rise to the palisade endings of feline extraocular muscles display motor features. J Neurosci 33:2784–2793. https://doi.org/10.1523/JNEUROSCI.4116-12.2013

3. Saccadic premotor burst neurons and histochemical correlates of their firing patterns in rhesus monkey

Mayadali ÜS, Lienbacher K, Shaikh AG, Horn AKE. Saccadic premotor burst neurons and histochemical correlates of their firing patterns in rhesus monkey. 2022. J. Neurol. Sci., 439, 120328. doi: 10.1016/j.jns.2022.120328

Open Access

GSN affiliated co-authors:

- Prof. Dr. Anja Horn-Bochtler; GSN associate faculty
  Chair of Vegetative Anatomy, Institute of Anatomy, Faculty of Medicine, LMU, Pettenkoferstr. 11 D-80336 Munich, Germany
  anja.bochtler@med.uni-muenchen.de
  +49 (0)89 / 2180-72667

Journal of the Neurological Sciences 439 (2022) 120328

Contents lists available at ScienceDirect

Journal of the Neurological Sciences

journal homepage: www.elsevier.com/locate/jns

Saccadic premotor burst neurons and histochemical correlates of their firing patterns in rhesus monkey

Ümit S. Mayadali [a,b], Karoline Lienbacher [a], Aasef G. Shaikh [c], Anja K.E. Horn [a,*]

[a] Chair of Vegetative Anatomy, Institute of Anatomy, Faculty of Medicine, LMU, Munich, Germany
[b] Graduate School of Systemic Neurosciences (GSN), LMU, Munich, Germany
[c] University Hospitals, and Cleveland VA Medical Center, Case Western Reserve University, Cleveland, OH, USA

ARTICLE INFO

Keywords:
Oculomotor
Ion channel
Potassium
Calcium
HCN
Post-inhibitory rebound

ABSTRACT

Bursting behavior of brainstem premotor burst neurons (BNs) is essential for initiation of saccades and calibrating their metrics. Several ion channel families such as voltage-gated potassium (Kv) channels, low-voltage-activated calcium (Cav3) channels and hyperpolarization-activated cyclic nucleotide–gated (HCN) channels are major regulators of the bursting in neurons. Therefore, it was speculated that ion channels with rapid kinematics are essential for characteristic firing patterns of the BNs and rapid saccade velocities. However, the expression patterns of ion channels are yet to be confirmed. Confirmation would not only support the neuromimetic model predictions for saccade generation in brainstem, but also contemporary views that channelopathies can cause saccade disorders in humans. As proof of concept, we examined excitatory BNs in the rostral interstitial nucleus of medial longitudinal fasciculus (RIMLF, vertical saccades) and inhibitory BNs in nucleus paragigantocellularis dorsalis (PGD, horizontal saccades) histochemically in macaque monkeys. We found strong expression of Kv channels, which enable rapid-firing, as well as HCN1&2 and Cav3.2&3.3, which enable post-inhibitory rebound bursting, in both BN populations. Moreover, PGD was found to host multiple neuron groups in terms of calretinin immunoreactivity. Our results provide histochemical evidence that supports models proposing post-inhibitory rebound facilitates bursting in BNs. Furthermore, our findings support the notion that deductions can be made about electrophysiological firing properties by histochemical examination of functional groups within the brainstem saccadic circuitry. This development is an important building block supporting the concept of channelopathies in saccadic disorders. Future histological studies in humans will confirm this approach for saccadic disorders.

1. Introduction

1.1. Premotor (burst) control of saccades (anatomical layout and connections)

Fast eye movements such as saccades or the quick phases of optokinetic reflexes, as well as vestibular forms of nystagmus, are achieved through the high-frequency bursting of motoneurons supplying extraocular muscles. As shown from anatomical tract-tracing and electrophysiological recording experiments in monkeys, the burst (phasic) component of motoneuron firing originates from input of premotor burst neurons located in the paramedian pontine reticular formation (PPRF) for horizontal eye movements [8,19,65] and in the rostral interstitial nucleus of medial longitudinal fascicle (RIMLF) for vertical/torsional eye movements [20,23,48]. While burst neurons (BNs) of the RIMLF lie throughout the wing-like shape of the nucleus, mid-sized BNs of PPRF are bilaterally intermingled with neurons of different sizes and shapes belonging to non-oculomotor systems, and are therefore often identified with the help of tract-tracing [23,65]. Both of these burst neuron populations are excitatory (EBNs) and utilize glutamate/aspartate as transmitters [62]. However, for conjugate saccadic eye movements, contralateral motor nuclei receive simultaneous inhibitory burst signals. The inhibitory premotor burst neurons (IBNs) are located in the nucleus paragigantocellularis dorsalis (PGD) for the horizontal eye movements [66,71] and presumably in the interstitial nucleus of Cajal for the vertical/torsional eye movements [29,67]. The interstitial nucleus of Cajal contains multiple neuronal populations alongside IBNs, which require further delineation and identification [22,67]. IBNs of the horizontal

* Corresponding author at: Institute of Anatomy and Cell Biology I, Ludwig-Maximilians-Universität, Pettenkoferstr. 11, 80336 Munich, Germany.
E-mail address: Anja.Bochtler@med.uni-muenchen.de (A.K.E. Horn).

https://doi.org/10.1016/j.jns.2022.120328
Received 16 February 2022; Received in revised form 14 June 2022; Accepted 15 June 2022
Available online 20 June 2022

system utilize glycine, whereas IBNs of the vertical system are thought to utilize GABA as their transmitter [29,63]. Monosynaptic and simultaneous innervation of extraocular motoneurons by premotor EBNs and IBNs is essential for synchronous and precise initiation and generation of saccadic eye movements.

1.2. Physiological and histochemical properties of burst (and other premotor) neurons

Premotor burst neurons receive saccadic parameters (i.e speed, duration) via synaptic inputs originating mainly from glutamatergic superior colliculus neurons [61], glycinergic omnipause neurons (OPNs) [26] and likely indirectly from GABAergic oculomotor cerebellar nuclei neurons [36]. The superior colliculus provides translated spatio-temporally mapped information. The premotor neurons translate this input into a burst determining the speed, direction and distance of the saccade. OPNs mark saccade initiations by ceasing their tonic inhibition of burst neurons and remaining inactive during saccades. They may also play a minor role in saccade termination by reactivating and thereby inhibiting the burst neurons [49]. Upon excitation by the superior colliculus and disinhibition by OPNs, the burst neurons initiate spiking at rates up to 1000 Hz, which determines both saccadic velocity and the short saccade duration [61]. The eye position signal is calculated by the neural integrators in the interstitial nucleus of Cajal (INC) and prepositus hypoglossi nucleus (PPH), which receive monosynaptic bursting information from EBNs. The integrators subsequently send the speed-to-location integrated information as eye position signal to motoneurons to form the tonic component of their firing pattern [5,15,61]. The high speed and precision of data transmission produced by the interplay of OPNs, BNs and motoneurons is crucial for generating fast and accurate eye movements.

The EBNs in the RIMLF, the IBNs in PGD, as well as OPNs located in the nucleus raphe interpositus are identified at a cellular level by histochemical labeling with parvalbumin (PAV) and by the perineuronal nets enveloping them [22,28]. Moreover, RIMLF-EBNs are further divided into two main subpopulations with respect to their calretinin (CR) immunoreactivity. It has been demonstrated through their anatomical connections to motoneurons of vertically pulling eye muscles that CR-positive EBNs in the RIMLF represent up-burst neurons, whereas CR-negative EBNs represent down-burst neurons [1,2,72].

1.3. Pathological cases related to burst generator dysfunction

High-frequency discharges from saccadic premotor burst neurons are utilized by motoneurons of the eye muscles to overcome the physical forces limiting eye bulb movement such as inertia and surface resistance in order to initiate saccades [24,61]. Therefore, neurologically identified slowing or complete loss of saccadic eye movements has mainly been correlated with alterations or loss of burst neuron function [17,39,50]. This phenomenon is often found in various eye movement disorders of diverse etiology, such as progressive supranuclear palsy (PSP) [3,59], Niemann-Pick disease Type C (NPC) [4], or saccade slowing after cardiac surgery [11]. The observation of symptoms from these diseases demonstrates that the presentation of saccade slowing can vary enormously. For instance, PSP and NPC initially affect vertical saccades rather than horizontal saccades [7,51,52,64], while some studies report that downward rather than upward saccades are affected in NPC [51] suggesting differential neuronal susceptibility to neurodegeneration. Moreover, the observation that the loss or slowing of saccadic eye movements are not necessarily indicators of burst neuron loss, but rather that alterations in the cellular environment (and thus, indirectly, cellular function) form the basis of hypotheses for proper burst neuron function and predictions in pathologies.

1.4. Predictions and hypotheses related to pathophysiology of burst generators

A neuromimetic model for saccade generation describing membrane kinematics of EBNs and IBNs [45,57] successfully broke down the irregular trajectory or slowed saccades observed in PSP cases [59]. The study explained reduced saccadic speed and irregular trajectory as being a result of reduced EBN activity and imprecisely timed IBN activity [59]. Moreover, these models can predict what kind of biophysiological properties these neurons should possess, and the type of ion channels that should be expressed on their membranes to produce these phenomena. One such a phenomenon is the post-inhibitory rebound (PIR) behavior of premotor burst neurons [12]. PIR occurs due to a low membrane threshold voltage, and as a result, a single neuron is capable of firing at high rates automatically and without excitation when released from inhibition [12]. Hence, it has been suggested that EBNs and IBNs should express HCN channels and Cav3 family, both of which are low-voltage-activated channel families, for the healthy generation of saccades. They also suggested that saccadic slowing would occur if these channels are downregulated or impaired [59]. The models further predicted that HCN and Cav3 channel subtypes with rapid membrane kinematics, such as HCN1 and HCN2, would create suitable infrastructure for required burst neuron characteristics facilitating saccade dynamics.

1.5. Aim of the study

This work aims to characterize the histochemical signature of saccadic premotor burst neurons with the specific goal to investigate biophysiological markers that govern the burst-firing characteristics of these neurons in macaque monkey. Bursting in neurons is intrinsically regulated by ion channel families such as voltage-gated potassium (Kv) channels, low-voltage-activated calcium (Cav3) channels and hyperpolarization-activated cyclic nucleotide–gated (HCN) channels. To test whether transmitter content or eye movement direction translates into different neuronal characteristics with respect to ion channel expression, we investigated the excitatory burst neurons of vertical saccadic circuitry and the inhibitory burst neurons of horizontal saccadic circuitry. The choice of these cells was primarily driven by the ease of delineating them without additional tract-tracing. Overall, this inquiry shall provide histochemical evidence in support of, or against, the neuromimetic model for saccade generation based on clinical data from saccadic disorders. Furthermore, the identification of additional markers related to healthy burst generation paves the way for post-mortem histochemical identification of possible channelopathies in human cases with saccadic disorders.

2. Results

2.1. Combination of perineuronal net and non-phosphorylated neurofilament immunoreactivity as a marker of premotor saccadic burst neurons

2.1.1. PN/SMI32 co-immunolabeling of burst neurons in the RIMLF

As previously shown [2], cholera toxin B (CTB) injection into the oculomotor nucleus (nIII) resulted in retrogradely labeled, medium-sized premotor burst neurons (BNs) located in the rostral interstitial nucleus of medial longitudinal fasciculus (RIMLF), bilaterally. These neurons are histochemically characterized by the calcium-binding protein parvalbumin (PAV) and also by the presence of perineuronal nets (PNs) [28]. Combined immunofluorescence detection of CTB, PAV and non-phosphorylated neurofilament (NP-NF; shown by SMI-32 antibody) revealed that all CTB labeled PAV-immunopositive neurons in the RIMLF were simultaneously SMI-32-immunopositive, as well (Fig. 1a). Furthermore, PAV-positive puncta, likely representing synaptic terminals, were observed on the cell membrane of CTB labeled neurons (Fig. 1a, red in composite). Moreover, combined immunofluorescence

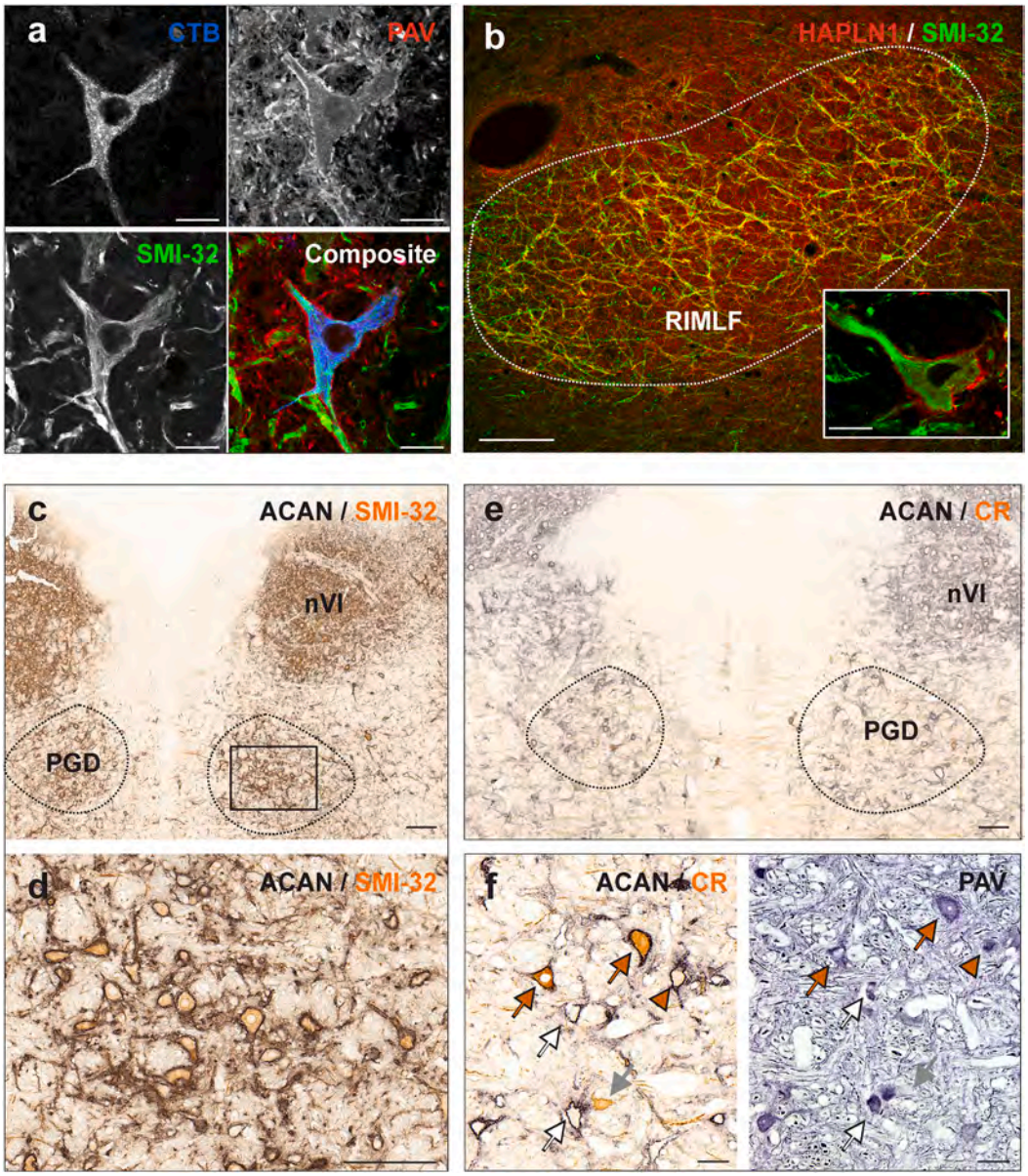

Fig. 1. Histochemical markers of burst neurons in the rostral interstitial nucleus of medial longitudinal fasciculus (RIMLF) and nucleus paragigantocellularis dorsalis (PGD). **a** Retrogradely labeled medium-sized premotor burst neurons (BNs) in the RIMLF (blue; upper left) following cholera toxin B (CTB) injection into the oculomotor nucleus (nIII) co-express parvalbumin (PAV, red; upper right) and SMI-32 (green; lower left). PAV-immunostaining also yields punctate staining on somatic and dendritic membrane of BNs (red, lower right) possibly labeling presynaptic terminals from sources such as omnipause neurons. Colours of the antibody labels correspond to immunolabeling colour depicted in the composite image. **b** A combination of perineuronal nets (PN, HAPLN1, red) and SMI-32-immunostaining (green) highlights medium-sized premotor BNs of the RIMLF. Close-up of a BN within the RIMLF from the same staining series but different section is shown in the inset. **c** Combined immunohistochemistry of PN (ACAN, black)/SMI-32 (brown) labels medium-sized neuronal population in PGD, presumed to be inhibitory burst neurons of horizontal saccadic circuitry. **d** Close-up of PGD as indicated by the rectangle in **c**, co-immunostained for ACAN and SMI-32, containing various medium-sized neurons. **e** Combination of PN marker ACAN with calcium binding protein calretinin (CR) yields multiple neuronal populations with regards to CR-immunoreactivity. **f** Neurons labeled with PAV (right, black) and PNs (ACAN, left, black) either express CR (orange arrows), or lack CR-immunolabeling (white arrows). Several neurons with PNs expressed weak CR-immunolabeling (orange arrowhead). Lastly, a number of CR-positive neurons lacking PNs were found (gray arrow). These neurons were PAV-immunonegative. Scale bar represents 20 μm in **a** and inset in **b**; 200 μm in **b-e** and 50 μm in **f.** (For interpretation of the references to colour in this figure legend, the reader is referred to the web version of this article.)

for PNs (HAPLN1) and SMI-32 labeled all the neurons, which are likely to be BNs of the RIMLF (Fig. 1b).

2.1.2. *PN/SMI32 co-immunolabeling of burst neurons in PGD*

The validity of this co-immunolabeling as a marker for all BNs was further investigated by combined immunoperoxidase-based staining of inhibitory BNs in nucleus paragigantocellularis dorsalis (PGD) by PN marker aggrecan (ACAN) and NP-NF marker SMI-32, using previously established anatomical definitions [22,27]. All the neurons that are labeled by the PN marker in PGD were also immunolabeled by SMI-32 antibody (Fig. 1c,d). These findings enabled the utilization of SMI-32/PN combination as a viable BN marker, regardless of whether the cell belonged to the horizontal or vertical saccadic circuitry, or whether it carried out an excitatory or inhibitory role in the saccadic eye movement system.

2.1.3. Calretinin labeling of burst neurons in the PGD

Another histochemical marker used to further delineate the neuronal populations in the RIMLF is calretinin (CR) [2]. CR-immunostaining in pontomedullary sections at the level of PGD revealed multiple neuronal populations in the IBN area (Fig. 1e,f). The neurons immunolabeled for ACAN and parvalbumin (PAV), which are putative IBNs, contained CR-positive (Fig. 1f; orange arrows) and CR-negative (Fig. 1f; white arrows) subpopulations, including several neurons that expressed weak CR-immunolabeling (Fig. 1f, Fig. 3c; orange arrowheads). These ACAN-positive neurons with differential CR-immunoreactivity showed no morphological differences, such as neuronal size and shape (Fig. 1e,f). However, an additional CR-positive neuronal population was found that lacked ACAN-immunolabeling (Fig. 1f, Fig. 3c; gray arrow). Furthermore, these small to medium-sized neurons expressed no PAV (Fig. 1f, Fig. 3c; gray arrow). Based on their differing histochemical signature, this last population of cells is not considered as IBNs.

2.2. Voltage-gated potassium channels in premotor saccadic burst neurons

2.2.1. Excitatory burst neurons in the RIMLF co-express Kv1.1, Kv3.1b and KCC2

Next, we investigated the expression of voltage-gated potassium channels that are responsible for fast-firing in saccadic premotor burst neurons with high metabolic activity (Fig. 2). Excitatory burst neurons for vertical saccades in the RIMLF (EBN_V) identified with PN marker ACAN and neurofilament marker SMI-32 were tested for Kv1.1-, Kv3.1b- and KCC2-immunoreactivity. We found that ACAN- and SMI-32-immunopositive putative EBN_V were co-labeled with all three potassium channel antibodies (Fig. 2c). Moreover, the investigation of qualitative differences in immunoreactivity for up- ($n = 19$) and down-gaze ($n = 23$) burst neurons yielded no difference in Kv1.1 or Kv3.1b profiles (Fig. 2a,b). Up-gaze neurons (orange arrows) were labeled with a combination of calretinin (CR, brown) and PN (black) markers whereas down-gaze neurons (white arrows) were identified with PN-labeling (black) and no CR-labeling (Fig. 2a,b), as established previously [2]. The Kv1.1-labeling intensity of neurons varied within the RIMLF, however no qualitative correlation between Kv.1.1-labeling intensity and the expression of CR was observed (Fig. 2a,b, left). On the other hand, no clear variation in intensity or appearance of immunolabeling was found for Kv3.1b and KCC2 (Fig. 2a-c, right).

2.2.2. Horizontal inhibitory burst neurons do not differ in expression of Kv1.1, Kv3.1b and KCC2

Next, we investigated whether or not inhibitory burst neurons in the horizontal saccadic circuitry (IBN_H) with glycinergic transmitter content would differ in voltage-gated potassium channel profiles from excitatory burst neurons of the RIMLF with glutamate as transmitters [62] (Fig. 3). Immunohistochemical staining of IBN_H area in PGD revealed that middle-sized ACAN- and SMI-32-co-immunolabeled neurons also showed Kv1.1-, Kv3.1b- and KCC2-immunoreactivity (Fig. 3a,b; arrow, $n = 42$), which was a qualitatively similar profile to EBN_V of the RIMLF (Fig. 2). While Kv3.1b-labeling was uniform across all IBN_H in the nucleus, Kv1.1-labeling intensity was variable, with some neurons having stronger somatic labeling than other neurons of similar size (Fig. 3a,b, second column). However, among ACAN-positive putative IBN_H, Kv1.1-immunolabeling did not exhibit qualitatively different patterns between calretinin (CR)-positive (Fig. 3c; orange arrows and arrowheads) and CR-negative (Fig. 3c; white arrows) neurons. The CR-positive neurons

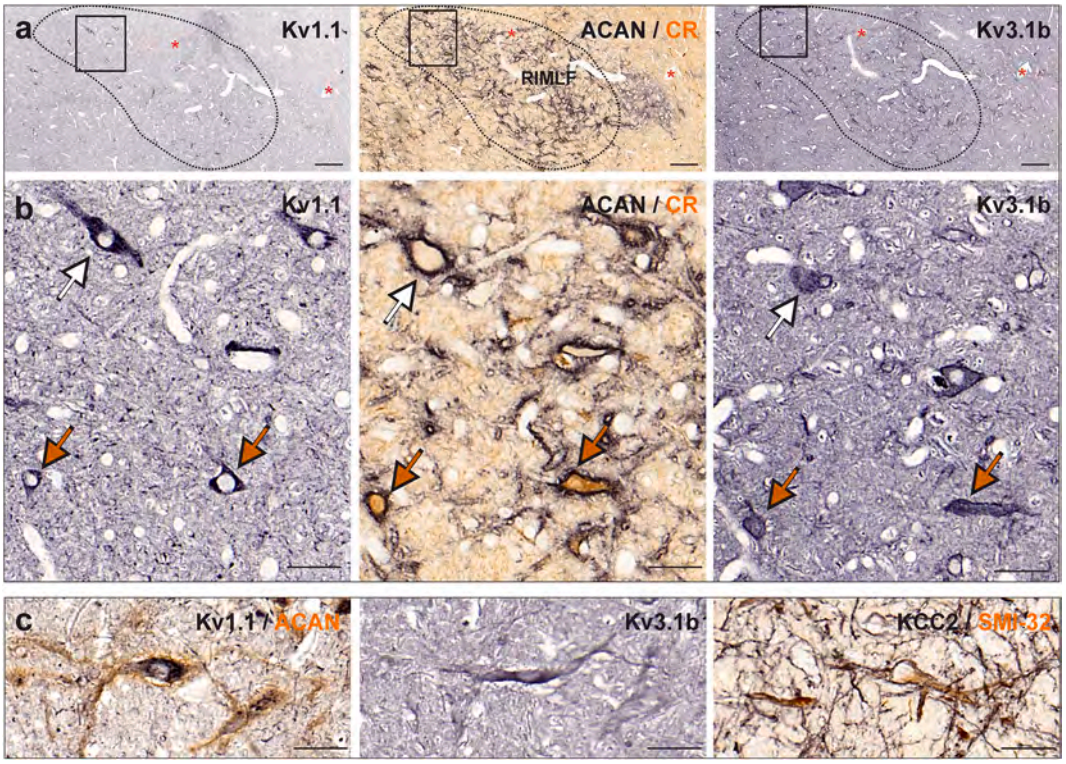

Fig. 2. Immunoperoxidase labeling of Kv1.1, Kv3.1b and KCC2 proteins in excitatory burst neurons of the rostral interstitial nucleus of medial longitudinal fasciculus (RIMLF). **a** Consecutive coronal paraffin sections through the RIMLF immunostained for Kv1.1 (left), Kv3.1b (right), combined aggrecan (ACAN)-based perineuronal nets (black) and calretinin (CR; brown, middle), respectively. ACAN/CR combination serves the identification of up- (CR-positive) and down- (CR-negative) burst neurons. **b** Close-up from areas indicated by rectangles comparing Kv1.1 (left) and Kv3.1b (right) expression in up- and down-burst neurons. Neither Kv1.1- nor Kv3.1b-immunolabeling differs qualitatively between CR-positive (orange arrows, $n = 19$) and CR-negative (white arrows, $n = 23$) subpopulations. **c** Consecutive 7 μm thick paraffin sections depicting a medium-sized excitatory burst neuron that co-expresses potassium channel proteins Kv1.1 (left, black), Kv3.1b (middle) and KCC2 (right, black). Scale bar represents 200 μm in **a** and 50 μm in **b-c**. (For interpretation of the references to colour in this figure legend, the reader is referred to the web version of this article.)

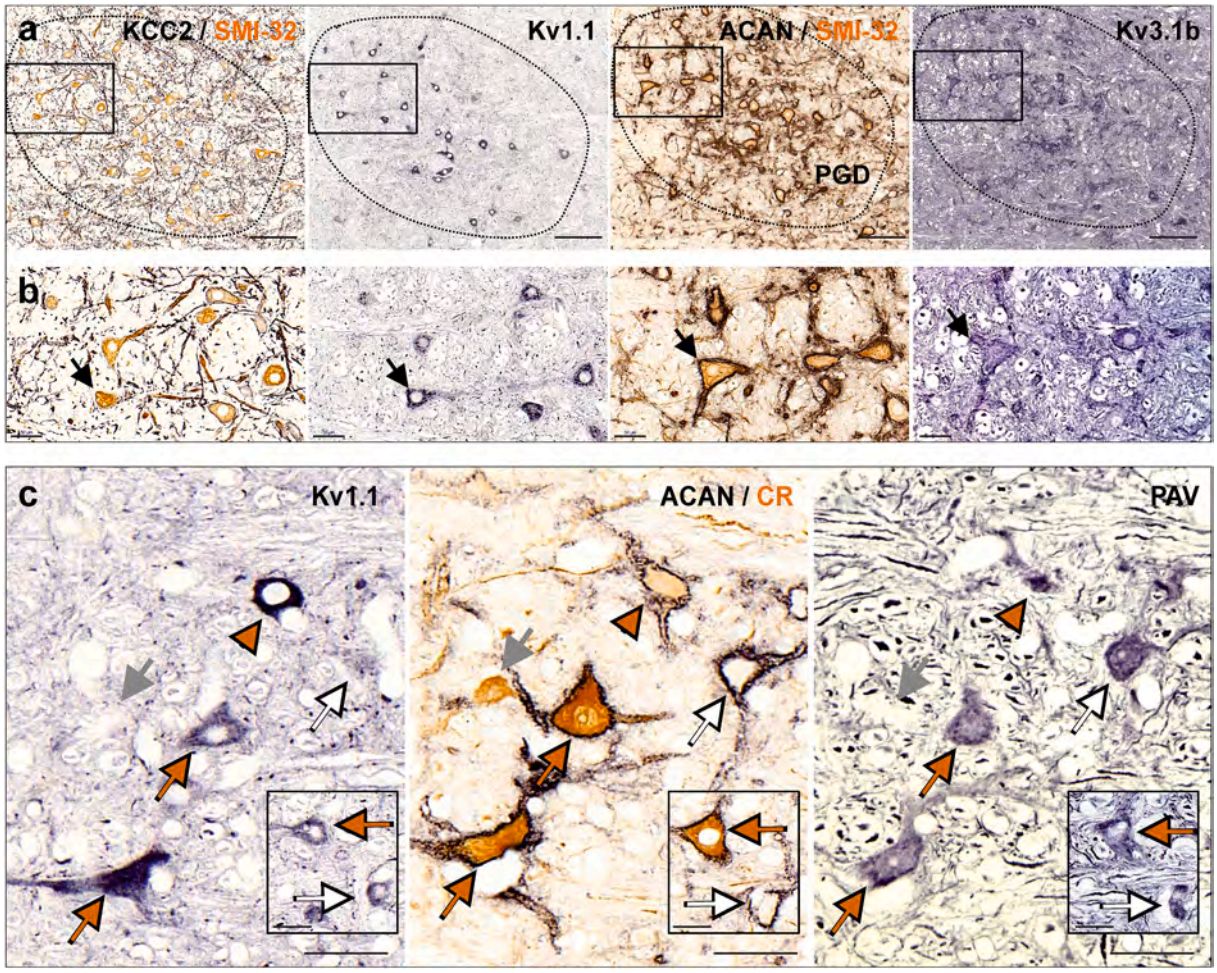

Fig. 3. Immunoperoxidase labeling of Kv1.1, Kv3.1b and KCC2 proteins in inhibitory burst neurons of the right nucleus paragigantocellularis dorsalis (PGD). **a** Four consecutive coronal paraffin sections through the pontomedullary junction at the level of PGD immunostained for KCC2 (first column, black), Kv1.1 (second column), Kv3.1b (last column), combined aggrecan (ACAN)-based perineuronal nets (black) and SMI-32 (brown, third column). Note that intensity of Kv1.1-immunolabeling varied within the nucleus (second column). Neurons labeled with ACAN/SMI-32 ($n = 42$) co-expressed all three potassium channel subunits. **b** Detailed view of potassium channel immunolabeling, as seen in the rectangle indicated in **a**. The same neuron (arrow) can be seen to co-express all three potassium channel proteins. KCC2-labeling was weak in the somatic membrane but strong in dendrites. Kv1.1-labeling focused on cell body, whereas Kv3.1b-labeling was localized more towards somatic and dendritic membrane. **c** Investigation of whether or not varied Kv1.1-labeling intensity had a correlation with varied calretinin (CR)-expression within PGD in three 5 μm thick consecutive paraffin sections stained for Kv1.1 (left), parvalbumin (PAV, right), combined ACAN-based perineuronal nets (black) and CR (brown, middle). ACAN-positive neurons (CR-positive, orange arrows; weak CR positive; orange arrowheads; CR-negative, white arrows) expressed Kv1.1 at varying levels. Kv1.1-immunolabeling intensity had no correlation with the CR-expression in neurons with ACAN-positive perineuronal nets, as seen in insets. Smaller CR-immunopositive neurons which lacked ACAN and PAV (gray arrows) did not display Kv1.1-immunolabeling. Scale bar represents 200 μm in **a,** 50 μm in **b-c** and 30 μm for the insets in **c**. (For interpretation of the references to colour in this figure legend, the reader is referred to the web version of this article.)

that lacked PAV and ACAN-positive PNs lacked Kv1.1- labeling (Fig. 3c; gray arrow).

In summary, saccadic premotor burst neurons were found to express co-immunoreactivity for Kv1.1, Kv3.1b and KCC2 regardless of belonging to the vertical or horizontal system, and regardless of having excitatory or inhibitory transmitters.

2.3. Low-voltage-activated HCN and Cav3 channels in premotor saccadic burst neurons

A hypothesis based on current clinical and modeling data predicts PIR in premotor BNs in the saccadic system, and this requires the expression of low-voltage-activated ion channels [45,57,59]. Therefore, we investigated the presence of immunoreactivity for hyperpolarization-activated cyclic nucleotide–gated (HCN) channel subunits HCN1, HCN2 (Fig. 4, Fig. 5); and low-voltage-activated T-type calcium channel subunits Cav3.1, Cav3.2 and Cav3.3 (Fig. 6) in EBN_V and IBN_H of rhesus monkeys.

2.3.1. HCN1 and HCN2 subunits in the burst neurons of the RIMLF and PGD

In the RIMLF, HCN1 and HCN2 subunit-immunolabeling was found along the somatic and dendritic membrane of EBN_V ($n = 45$) in punctate form, presumably labeling the post-synaptic membranes of afferent inhibitory synapses (Fig. 4a,b; arrow). The labeling pattern or intensity did not differ between up- ($n = 22$) and down-gaze ($n = 23$) burst neurons designated by positive (orange arrows) and negative (white arrows) CR-immunolabeling, respectively (Fig. 4c). The labeling pattern and intensity of HCN1 and HCN2 had obvious qualitative differences. For example, strong membrane and neuropil labeling was found in the portions of the thalamus (not shown), adjacent to the midbrain in these sections. Additionally, labeling on the membranes of EBN_V in the RIMLF was less intense than that of motoneurons of singly-innervated muscle fibers (SIF) of the abducens (Fig. 4d; green arrows) and trochlear nuclei (Fig. 4e; green arrows), where labeling manifested as a continuous line along the length of somatic membrane. In contrast, motoneurons of multiply-innervated muscle fibers (MIF) lacked HCN1- and HCN2-

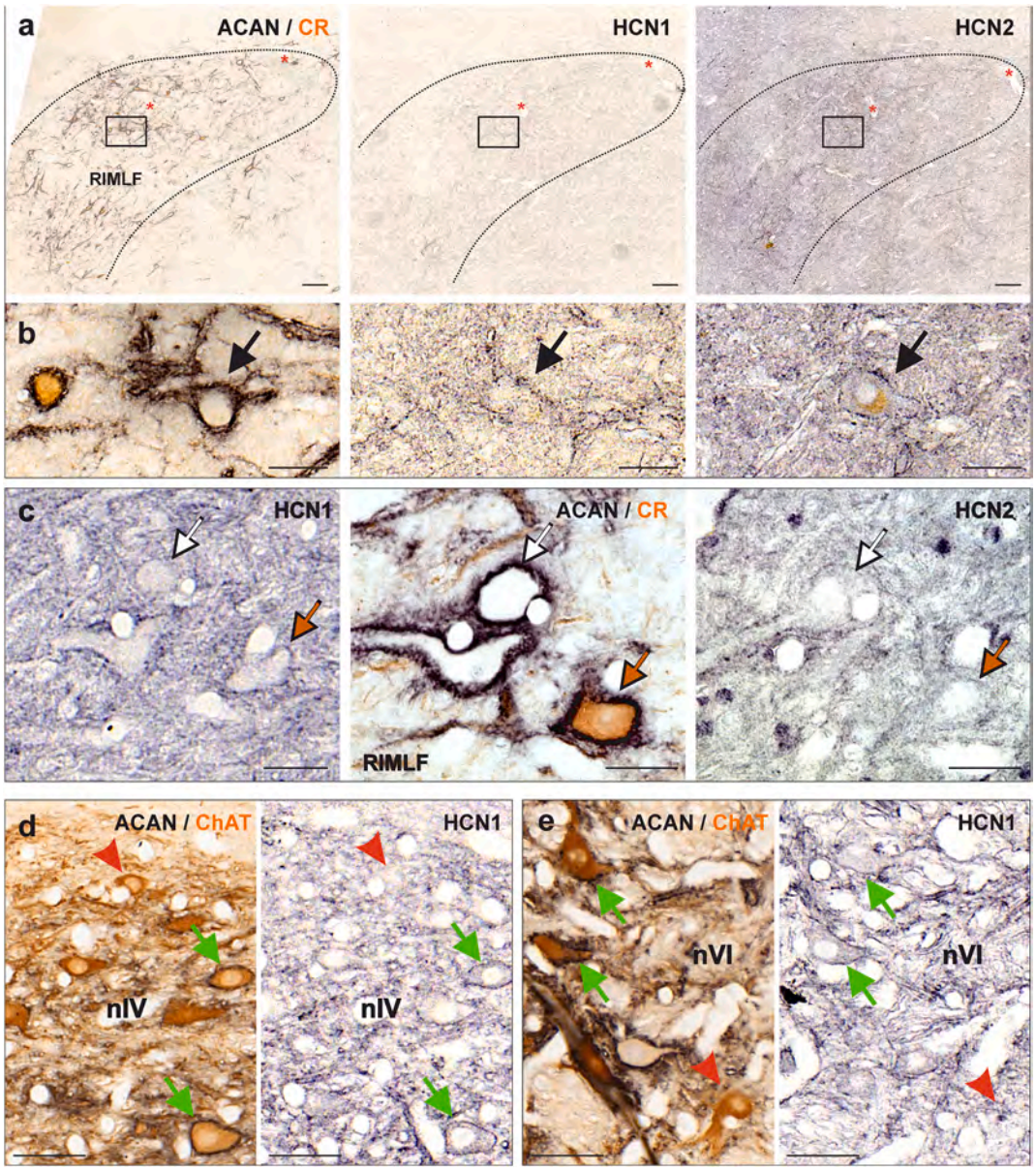

Fig. 4. Immunoperoxidase labeling of HCN1 and HCN2 channels in excitatory burst neurons of the rostral interstitial nucleus of medial longitudinal fasciculus (RIMLF) and motoneurons of trochlear (nIV) and abducens nuclei (nVI). **a** Consecutive 7 μm thick coronal paraffin sections through the midbrain at the level of the RIMLF immunostained for HCN1 (middle), HCN2 (right), combined aggrecan (ACAN)-based perineuronal nets (black) and calretinin (CR; brown, left), respectively. Punctate staining of cell bodies and processes for both HCN subunits are visible throughout the RIMLF. As a landmark, the same blood vessels are indicated by red asterisks. **b** Detailed view of HCN1- and HCN2-labeling pattern seen in the RIMLF designated by a rectangle. The same neurons ($n = 45$) express HCN1- and HCN2-immunopositive puncta on their membranes, which presumably labels the post-synaptic membranes of inhibitory synapses. **c** Close-up from 5 μm thick consecutive coronal paraffin sections demonstrating HCN1- and HCN2-immunostaining in up- and down-burst neurons of the RIMLF shows no qualitative difference between CR-positive (up, orange arrows, $n = 22$) or CR-negative (down, white arrows, $n = 23$) burst neurons. **d,e** Consecutive 5 μm thick sections demonstrating HCN1-labeling in the motoneurons of the trochlear (**d**) and abducens (**e**) nucleus. Combined aggrecan (ACAN)-based perineuronal nets (black) and choline acetyltransferase (ChAT; brown, left)-immunostaining is used to identify motoneurons of multiply-innervated muscle fibers (MIF) (red arrowheads) and of singly-innervated muscle fibers (SIF) (green arrows). Intense HCN1-immunolabeling (**d**,**e**, right) was found as a continuous line along the length of somatic membrane of SIF motoneurons (green arrows), whereas no labeling was observed on membranes of MIF motoneurons (red arrowheads). Scale bar represents 200 μm in **a,** 30 μm in **c** and 50 μm in **b,d-e**. (For interpretation of the references to colour in this figure legend, the reader is referred to the web version of this article.)

immunolabeling on their membranes (Fig. 4d,e; red arrows).

On the other hand, ACAN-immunopositive putative IBN_H in PGD exhibited qualitatively similar HCN1- and HCN2-labeling pattern and intensity to EBN_V with somatic membrane immunoreactivity (Fig. 5a,b). These neurons (n = 45) co-expressed HCN1- and HCN2-immunolabeling (Fig. 5b, arrows). Moreover, the labeling pattern and intensity did not differ between ACAN-immunopositive neurons with positive (orange arrows, $n = 10$) and negative (white arrows, $n = 14$) CR-immunolabeling (Fig. 5c). Lastly, for comparison, HCN1 and HCN2 expression on the OPNs membranes were examined within raphe interpositus (Fig. 5d). While OPNs expressed weaker HCN1-immunolabeling on their membrane compared to BNs and SIF MNs, the labeling pattern was similar to that of SIF MNs, in that it manifested as a continuous line along the length of somatic and dendritic membrane (Fig. 5d, left). HCN2-immunolabeling in OPNs was sparse and in punctate form in comparison to BNs and SIF motoneurons (Fig. 5d, right). The specificity and

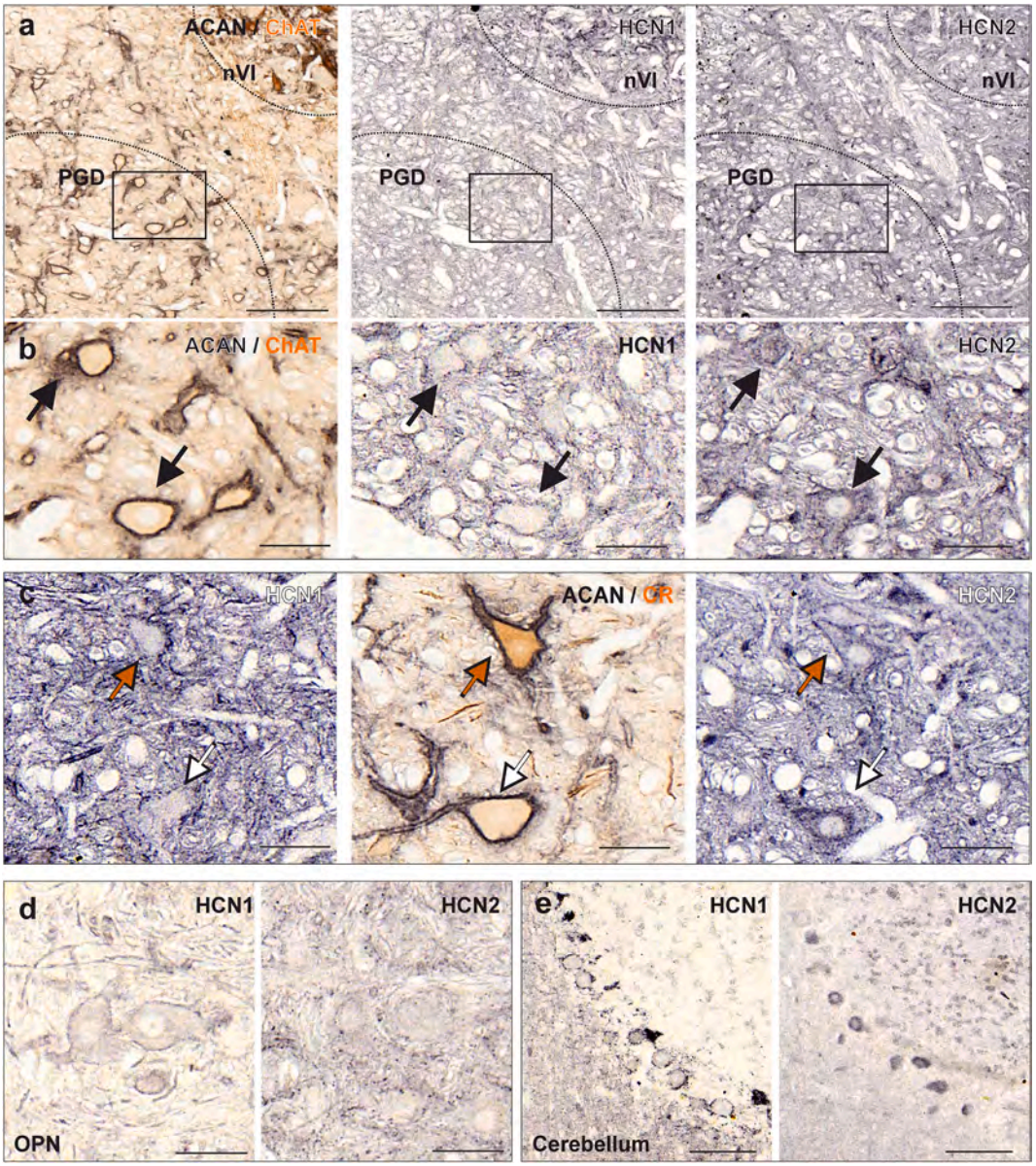

Fig. 5. Immunoperoxidase labeling of HCN1 and HCN2 channels in inhibitory burst neurons of nucleus paragigantocellularis dorsalis (PGD) and omnipause neurons (OPN). **a** Consecutive 5 μm thick coronal paraffin sections through the pons at the level of PGD immunostained for HCN1 (middle), HCN2 (right), combined aggrecan (ACAN)-based perineuronal nets (black) choline acetyltransferase (ChAT; brown, left). Note that the HCN1-labeling pattern and intensity differed between abducens nucleus (nVI) and PGD (middle). **b** Detailed view from PGD area (rectangle in **a**) showing that same neurons enveloped by ACAN (n = 45) are immunolabeled by both HCN1 (middle, arrows) and HCN2 (left, arrows). Punctate HCN1- and HCN2-labeling was found on the membranes of putative IBNs similar to EBNs of the RIMLF. **C** Close-up from consecutive 5 μm thick coronal paraffin sections demonstrating both calretinin (CR)-positive (orange arrows) and CR-negative (white arrows) are immunolabeled by HCN1 (left) and HCN2 (right) antibodies in a qualitatively similar fashion. **d** HCN1- and HCN2-immunolabeling in OPNs is weaker in comparison to BNs or SIF motoneurons. However, dense membrane labeling displaying a continuous line is qualitatively similar to SIF motoneurons. **e** Cerebellar staining on the same sections as PGD acts as a control for the specificity and sensitivity of the HCN1 (left) and HCN2 (right) antibodies. HCN1-labeling on Purkinje cells was mainly found on the cell membrane and basket cell pinceau structures (left), whereas HCN2 was found in the soma of Purkinje cells (right). Scale bar represents 200 μm in **a,** 100 μm in **e** and 50 μm in **b-d**. (For interpretation of the references to colour in this figure legend, the reader is referred to the web version of this article.)

sensitivity of HCN1 and HCN2 antibodies were further confirmed by cerebellar staining on the same sections as IBN_H (Fig. 5e), which were immunostained simultaneously with midbrain sections containing EBN_V. HCN1-labeling on Purkinje cells was mainly found on the cell membrane and also basket cell pinceau structures (Fig. 5e; left), as previously observed [74], while HCN2-immunolabeling was found in the soma of Purkinje cells (Fig. 5e, right).

2.3.2. *Cav3 subunits in the burst neurons of the RIMLF and PGD*

Lastly, expression of Cav3 subunits (Cav3.1–3.3) was investigated in the EBNs of the RIMLF and IBNs of PGD on consecutive 5 μm thick paraffin sections (Fig. 6). Cav3.1 somatic membrane labeling was mainly absent in both burst neuron populations (RIMLF: Fig. 6a, upper left; 6b, first column). Only a few ACAN-positive neurons with weak somatic Cav3.1-labeling were observed in PGD (Fig. 6d, red arrows). In general, staining for Cav3.2 and Cav3.3 antibodies yielded moderate to strong somatic labeling in both burst neuron populations (Fig. 6a,b; black arrows). Interestingly, especially in PGD, Cav3.2-labeling varied, with strong intensities in some ACAN-positive neurons and only weak labeling in others (Fig. 6c,d; second and third column; gray arrows). A possible correlation between this variation and CR expression was not investigated in this study.

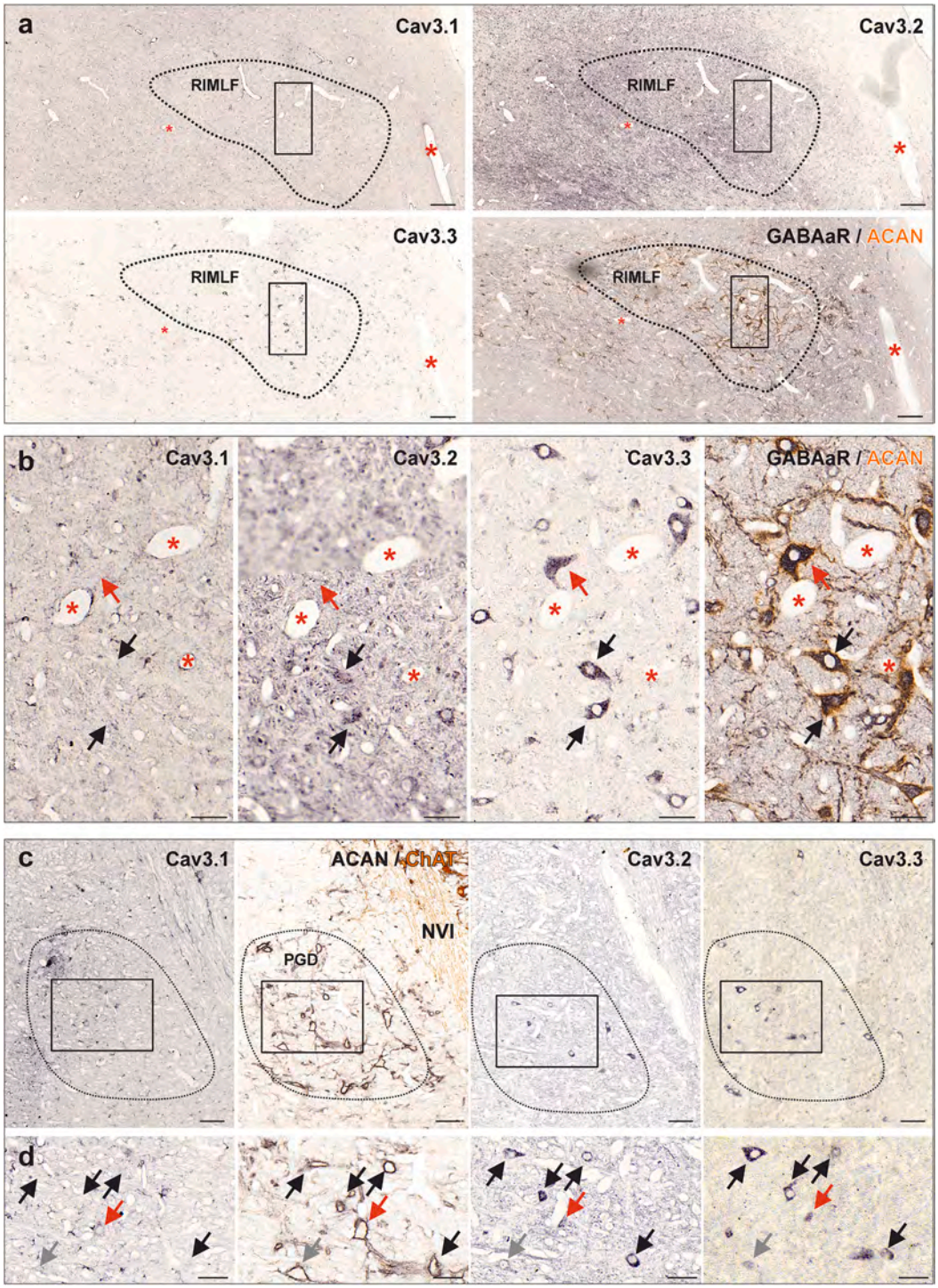

Fig. 6. Immunoperoxidase labeling of Cav3 subunits in excitatory burst neurons (EBNs) of the rostral interstitial nucleus of medial longitudinal fasciculus (RIMLF) and inhibitory burst neurons of nucleus paragigantocellularis dorsalis (PGD). **a** Four consecutive coronal paraffin sections through the rostral midbrain at the level of the RIMLF immunostained for Cav3.1 (top left), Cav3.2 (top right), Cav3.3 (bottom left), and finally combined aggrecan (ACAN)-based perineuronal nets (brown) and GABAa receptor (GABAaR) (black, bottom right). **b** Detailed view from sections in **a** (rectangle) displaying moderate to strong Cav3.2 (second column) and Cav3.3 (third column) subunit-immunoreactivity for medium-sized EBNs. However, no clear somatic or membrane labeling for Cav3.1 subunit in these neurons was detected (left). Several neurons with positive Cav3.3-immunoreactivity lacked both Cav3.1- and Cav3.2-labeling (red arrows). **c** Four consecutive coronal paraffin sections through the PGD immunostained for Cav3.1 (first column), Cav3.2 (third column), Cav3.3 (last column) subunits, and finally combined aggrecan (ACAN)-based perineuronal nets (black) and choline acetyltransferase (ChAT; brown, second column). Medium-sized PN-immunopositive neurons located in PGD also displayed moderate to strong Cav3.2 (third column) and Cav3.3 (last column) subunit-immunoreactivity. Note the varied intensity of Cav3.2-immunolabeling within PGD. **d** Close-ups from **c** (rectangle) detailing staining patterns for Cav3 subunits in neurons indicated with black arrows. ACAN-immunopositive neurons lack Cav3.1 (first column), however a few neurons were found to display weak Cav3.1-labeling (red arrows). An ACAN-immunopositive neuron with weak Cav3.2 can also be seen (gray arrows, second and third columns). Scale bar represents 200 μm in **a,c** and 50 μm in **b,d**. (For interpretation of the references to colour in this figure legend, the reader is referred to the web version of this article.)

3. Discussion

This study investigated the histochemical signature of the premotor burst neurons (BNs) in macaque monkey, related to their intrinsic membrane properties that facilitate bursting at high firing rates. Ion channel profiles of two premotor BN populations (EBNs of the RIMLF and IBNs of PGD) with different anatomical connections and transmitter content were explored in order to eliminate any specific biases regarding their physiological profiles. Neither of the BN populations differed in their ion channel expression profiles, within the constraints of this study. Regardless of their excitatory or inhibitory effect, or whether they belong to horizontal or vertical components of the saccadic circuitry, all BNs expressed Kv1.1 and Kv3.1, a combination required for fast-firing, and they expressed low-voltage-activated ion channels. This supports the PIR hypothesis of BNs [45,50,57]. Moreover, discovery of the expression profiles of these ion channel proteins in BNs of the saccadic system of macaque monkey paves the way for post-mortem investigation of altered phenotypes in human pathology cases with eye movement disorders.

3.1. Markers of burst neurons and multiple subpopulations of inhibitory burst neurons

In this study, we posited that the combination of perineuronal nets (PNs) and non-phosphorylated neurofilament (NPNF, SMI32) represented a superior marker of burst neurons (BNs) in comparison to parvalbumin (PAV), based on high-resolution confocal microscopy images (Fig. 1). In thick sections (>20 μm), PAV-immunostaining was often found to yield strong neuropil labeling, which is inconvenient for simultaneously examining immunohistochemical staining. Moreover, the abundance of PAV-positive boutons within the RIMLF is an added reason for this intense signal (Fig. 1a), possibly representing, at least in part, pre-synaptic terminals of PAV-positive OPNs [26]. Therefore, SMI-32 was chosen as a superior marker due to its reliable coverage of the EBN population (Fig. 1b), and also due to its clear labeling of both somata and neuronal processes. Furthermore, this approach allows prospective analysis and accurate quantification of synaptic inputs to the EBNs.

A surprising finding in this study was the discovery of subpopulations within the IBN area with regards to calretinin (CR)-immunostaining (Fig. 1e,f), similar to previous findings on EBNs within the RIMLF [2,28]. The neurons that are co-labeled by PNs and PAV in PGD, which were originally identified as the IBNs by combined tract-tracing [22,27], contained examples with strong, weak or even no CR-immunolabeling (Fig. 1f, Fig. 3c). This variation in CR expression could have physiological significance, as CR might play a role in modulating neuronal excitability [16]. The fact that most identified neurons within IBN area showed similar histochemical signature with regards to known BN markers (PAV, PN and SMI32) and also ion channel immunolabeling regardless of their CR expression, strongly suggests the existence of more than one population with bursting/fast-firing activity [9,54,71]. Recording studies in squirrel monkey revealed that only 50% of neurons within the IBN area are saccadic burst neurons, and these are divided into short-lead and long-lead burst neurons based on the timing of the initiation of the burst with respect to the beginning of the saccade [54]. A considerable population (25%) of tonic neurons that show eye position sensitivity only, but no correlation with saccades, were also recorded [54]. Short-lead burst neurons are considered to represent the saccadic IBNs that provide monosynaptic inhibition of motoneurons and internuclear neurons in the contralateral abducens nucleus, as well as of contralateral IBNs and EBN_{H}s [54,66,71]. In contrast, the projection targets and action of long-lead burst neurons are less clear. One hypothesis suggests they act as local excitatory interneurons receiving input from the superior colliculus and activating the short-lead IBNs [54]. In light of these observations, the PAV- and ACAN-positive neurons within the IBN area may represent long-lead and short-lead burst neurons, and display the histochemical signature of fast-firing properties. However, whether or not the CR-labeling corresponds to a subpopulation of IBNs with a difference in anatomical connections [66], such as found in BNs of the RIMLF, needs to be further investigated. In the RIMLF, due to their differential connections to different motoneuron subgroups in the oculomotor nucleus, CR-positive premotor BNs were found to control upward eye movements, whereas CR-negative BNs were found to be responsible for downward eye movements [2,72]. Despite their different expression of calcium-binding proteins, there was no significant difference in the ion channel expression profile of up- (CR-positive) and down- (CR-negative) BN subpopulations in the RIMLF. This is in line with the similar saccadic parameters they show while generating upward or downward saccades in primates [46,47].

The additional CR-positive neurons of PGD with no PN, PAV or Kv expression do not conform to the BN histochemical profile (Fig. 3c; gray arrows), and may therefore represent the tonic neurons with eye position sensitivity described in squirrel monkey [54]. This assumption would be in line with the recently observed differential histochemical characteristics of MIF and SIF motoneurons [43]. The former population lacks PN and Kv3.1, and expresses reduced Kv1.1, compared to PN-positive SIF motoneurons with strong Kv1.1 and Kv3.1b expression. It is likely that this reflects the different firing characteristics expressed by these motoneuron populations [6,21,43]. Additionally, expression of CR in itself could be related to excitability [16,40,53]. Overall, anatomical and/or physiological significance of calretinin within IBN area requires further investigation.

3.2. Potassium channels, perineuronal nets, and fast-spiking

A recent study in mice identified the pre-oculomotor vestibular neuron subpopulation as the one with the fastest firing capacity within medial vestibular nucleus [37]. Furthermore, via gene-profiling, the authors identified a strong correlation between fast-firing and Kv1.1, Kv3.1 (and Nav1.6) co-expression [37]. This co-expression profile was already observed in the neurons of oculomotor circuitry, such as omnipause neurons (OPNs) [42], pre-oculomotor (dorsal) Y-group neurons [73], and SIF motoneurons within the abducens and trochlear nuclei, as well as the internuclear neurons of the abducens nucleus [43]. Therefore, with the addition of results regarding premotor burst neurons presented in this study, there's significant evidence that the tightly controlled and rapid eye movement types require simultaneous expression of Kv1.1 and Kv3.1 at multiple levels in the oculomotor circuitry.

Perineuronal nets (PNs), which were found ensheathing BNs in the present study, as well as OPNs [22], SIF motoneurons, abducens internuclear neurons [30] and pre-oculomotor Y-group neurons [73], are presumed to have physiological roles that tie them to voltage-gated potassium channel function [18]. PNs have been demonstrated to regulate Kv3.1b and Kv1.1 expression and recruitment, which suggests that they serve to enhance the firing characteristics of fast-spiking neurons [13,18]. Therefore, loss of PNs surrounding OPNs and/or EBNv could cause Kv1.1 and/or Kv3.1 dysregulation, indirectly contributing to saccadic dysfunction. PN loss, but no obvious neuronal loss, as observed in saccadic palsy after cardiac surgery [10], supports an indirect physiological role of PNs for healthy saccade generation.

Our recent work has found significant differences between the ion channel profiles of MIF and SIF motoneurons in the abducens and trochlear nuclei [43]. MIF motoneurons, which are considered to be responsible for low-dynamic motor commands, had reduced Kv1.1 levels, and no membrane bound Kv3.1, in comparison to SIF motoneurons, which strongly expressed Kv1.1 and Kv3.1 subunit immunoreactivity [43]. However, within the motonuclei, the Kv1.1-labeling intensity among SIF motoneurons varied, which was considered to correspond to variations in the resting membrane potentials and firing thresholds of these cells. These properties are in turn thought to be important for recruitment of ocular motor units, as required for the fine

tuning of the eye movements [25,43]. Interestingly, within both premotor BN populations, we observed a similar pattern of varied Kv1.1-immunolabeling (Fig. 2a, Fig. 3a). With the assumption of varied protein expression from varied immunolabeling intensity, this observation suggests that BN population could consist of a range of activation thresholds [44]. These observations render premotor burst neurons qualitatively closer to SIF motoneurons (or abducens internuclear neurons) compared to MIF motoneurons, in terms of fast-firing capacity [43]. This makes sense, as SIF motoneurons receive their burst signal from the BNs and should be able to reproduce the burst signal on their membrane with high fidelity, whereas MIF motoneurons receive no direct input from BNs [69].

3.3. Low voltage-activated cation channels and post-inhibitory rebound bursting (PIR) in burst neurons

Low voltage-activated calcium channels (T type, Cav3) and hyperpolarization-activated and cyclic nucleotide–gated (HCN) channels are inward-permeating cation channels that open at sub-threshold and hyperpolarized voltages [34,55]. By allowing cation influx at low voltages, these channels likely play a decisive role in the firing pattern of the burst neurons after disinhibition. To elucidate, a neuron can elicit regular (tonic) firing when depolarized from resting membrane potential (~ −55 mV), or high frequency burst firing when depolarized from a potential below −70 mV. The latter is found during sustained hyperpolarization, which BNs receive from OPNs. The neuromimetic model demonstrates that up- or down-regulation of these channels' activity could result in diminished or increased strength in post-inhibitory rebound (PIR) burst, respectively, as a response to similar inhibitory stimulus [56].

The EBNs of the vertical and the IBNs of the horizontal saccadic circuitry exhibited similar HCN1-HCN2- and Cav3.2–3.3- immunoreactivity (Figs. 4-6), which indicates they have the capacity for PIR bursting, given that the prerequisite for this phenomenon is provided by the sustained tonic inhibition from OPNs [35,41]. Punctate HCN1-andHCN2- labeling on the BN somatic and dendritic membranes could correspond to the synaptic terminals of glycinergic input from the OPNs, where PIR phenomenon would take place on the post-synaptic membrane of BNs. The PIR phenomenon would require a preferential expression of the "faster" subunits, i.e. HCN1 or HCN2 rather than HCN4 in neurons. Weak HCN4 subunit immunolabeling was also found in putative burst neurons of the RIMLF and PGD (not shown). However, a quantitative comparison cannot be made within the scope of immunohistochemical methodology, so we cannot conclusively show a skewed expression towards the subunits with faster kinetics.

The lack of Cav3.1 subunit immunolabeling is interesting in the light of recent findings in MIF and SIF motoneurons, which apparently use different components of low voltage-activated cation channels for their burst generation [43]. MIF motoneurons strongly express Cav3.1 subunit in abducens and trochlear nuclei almost exclusively [43], while lacking HCN1 and HCN2 subunits (Fig. 4c,d). In contrast, SIF motoneurons mostly lack Cav3.1 subunit [43], while expressing strong HCN1- andHCN2-immunolabeling (Fig. 4c,d), which was more intense than seen in BNs (Figs. 4a,b & 5a,b). The stronger and continuous HCN1-immunolabeling along the length of SIF motoneuron somatic membrane, in contrast to punctate labeling in (presumably) post-synaptic membranes of OPN terminals contacting BNs, could indicate their additional capacity for eye position-related tonic firing after the initial burst. Similar HCN1-immunolabeling along the length of somatic and proximal dendrite, albeit weaker in comparison to SIF motoneurons, was found in OPNs (Fig. 5c), which supports the hypothesis that post-synaptic labeling pattern of HCN channels could correspond to the differences in post-inhibitory outcome of tonic or burst firing patterns.

3.4. Hypotheses on pathological cases as a result of channelopathy

The results shown in this study provide histochemical evidence that premotor burst neurons (BNs) are equipped with the necessary apparatus for post-inhibitory rebound bursting, and that this high frequency bursting is maintained through activity (at least in part) of Kv3 and Kv1 subunits. In light of this evidence, several hypotheses derived from the neuromimetic model based on clinical data may be considered even more viable, as these provide likely explanations of saccadic disorders in structurally intact oculomotor system [56,58]. Predictions of the model include up-regulation of HCN or Cav3 activity in BNs as an etiology for saccadic oscillations, and down-regulation possibly leading to slowed or curved saccades (such as seen in PSP) through weaker post-inhibitory bursts of BNs [58,59].

Another example of where saccadic irregularities could not be explained by neuronal loss in oculomotor system was observed in a saccadic palsy after cardiac surgery [11]. In this case, perineuronal nets (PNs) were damaged or lost in OPNs and excitatory BNs, indicating a secondary dysfunction related to health of the extracellular matrix proteins is likely sufficient for emergence of saccadic symptoms [10]. Such a dysfunction could be related to calcium binding protein expression and/or potassium channel (for example Kv3.1) function and recruitment to neuronal membrane, where PN ensheathment is essential, and without which proper biophysiological properties for fast-firing could not be maintained [13,18]. Moreover, all three potassium channels tested in this study are related to regulating neuronal firing patterns and excitability, and therefore bear clinical implications, as circuit wide instabilities and oscillations may arise from dysfunction of these ion channels [32,60,70]. Although saccadic disorders are not classified as channelopathies, there is accumulating evidence suggesting the involvement of ion channel deficits in neurodegenerative diseases that cause saccadic disorders. For example, it is possible that some cases of spinocerebellar ataxia (e.g. SCA1, SCA2, SCA6, SCA24 and SCA30), which produce abnormal saccades, are thought to be caused by channelopathies [14,68]. Especially in SCA1–3, saccadic slowing is a clinical hallmark. which may precede any other ataxia symptoms and eventually devolve into complete gaze palsy [31]. On the other hand, opsoclonus, which is defined as back-to-back saccades without an intersaccadic interval, might be related to channelopathies, although mechanisms underlying this pathophysiology is unclear [68]. Other evidence can be the intervention with ion channel blockers that mitigate saccadic symptoms [33,56].

Within the scope of this study, no ion channel signature difference was found between premotor burst neurons of up- or down-gaze, or between horizontal or vertical circuitry, in terms of Kv1, Kv3, Cav3 or HCN1–2 expression. Any potential difference in ion channel (or transmitter) content could potentially connect the onset of selective symptoms (i.e. vertical gaze palsy in PSP) and selective vulnerability of specific neurons to neurodegeneration and neurotoxicity [38]. Therefore, the search for established potential markers of neural vulnerability in the premotor burst neurons of saccadic circuitry will follow in future studies.

Overall, the data presented in this study enables post-mortem investigation of key proteins related to biophysiology of burst neurons in homologue human tissue and pathophysiology in cases with saccadic disorders.

4. Conclusion

This study investigated the histochemical signature of the premotor burst neurons (BNs) in macaque monkey related to intrinsic membrane properties that facilitate bursting at high firing rates. The proof of concept was explored by looking for the ion channel profiles of two premotor burst neuron populations (EBNs of the RIMLF and IBNs of PGD) with different anatomical connections and transmitter content (Fig. 7). The main findings were, that (1) BNs can be delineated by

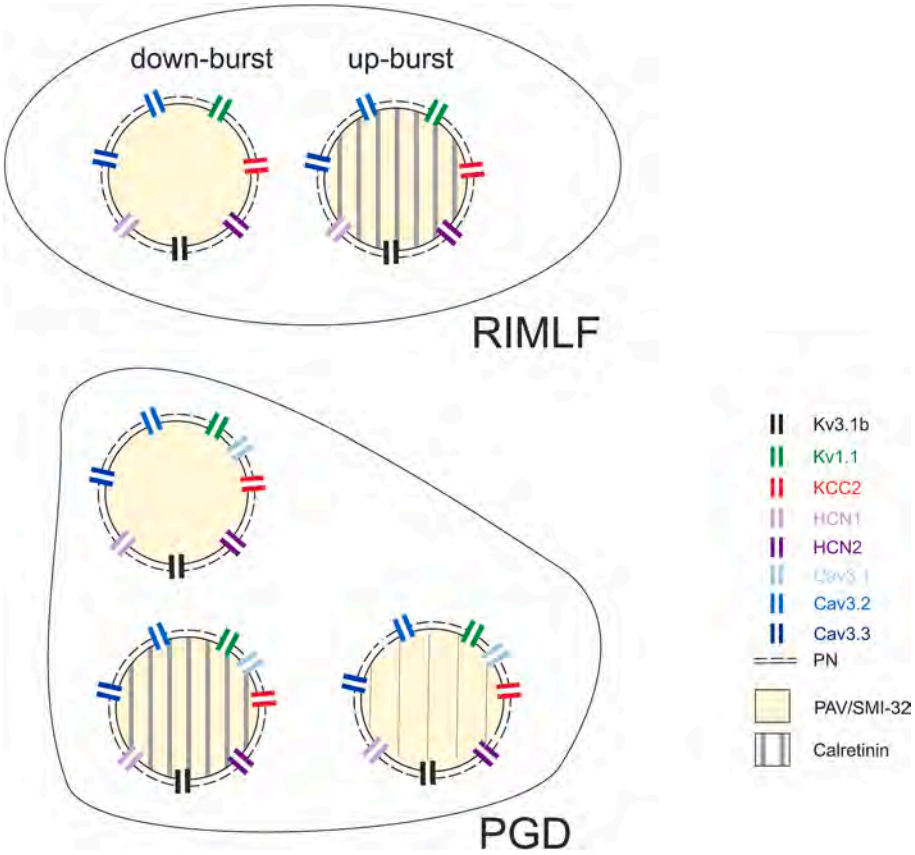

Fig. 7. Summary diagram depicting molecular signatures of excitatory burst neurons in the rostral interstitial nucleus of medial longitudinal fasciculus (RIMLF) and putative inhibitory burst neurons located in nucleus paragigantocellularis dorsalis (PGD). Schematic representation illustrates qualitatively similar ion channel profiles for burst neurons in the RIMLF (upper) and PGD (lower).

combined immunohistochemistry of perineuronal nets (PN; ACAN, HAPLN1 etc.) and non-phosphorylated neuro-filaments (NP-NF; SMI32); (2) the IBN area located in PGD contains more than one neuronal population, and they can be delineated with calretinin-immunostaining; and finally (3) both BN populations express the voltage-gated potassium channels that comply with their fast-firing characteristics. Furthermore, they express HCN1 and HCN2 and Cav3.2–3.3 channels, which supports the PIR-bursting hypothesis of BNs. Overall, these results collectively provide histochemical evidence, and indirectly, information on physiological properties of BNs. This evidence can be used to test hypotheses originating from clinical data from which mathematical models were derived. Furthermore, this study represents a significant step in investigation of BN channelopathy as a cause for symptoms of eye movements in disorders such as PSP, opsoclonus and NPC in pathological post-mortem human brainstem tissue.

5. Methods

5.1. Brain tissue

Brainstem tissue specimens from five rhesus monkeys (*Macaca mulatta*) fixed by transcardial perfusion with 4% paraformaldehyde in 0.1 M phosphate buffer and stored either in a mixture of glycerol and phosphate buffer at −20 °C or embedded in paraffin was used for histochemical tests and evaluation performed within this work. The brain sections from a case used in a previous study [73], which had received a central tracer injection with 1% cholera toxin subunit B (CTB, Sigma/Biological laboratories) into the right oculomotor nucleus (nIII) was used for retrograde labeling of excitatory burst neurons (EBNs) in the rostral interstitial nucleus of medial longitudinal fasciculus (RIMLF). Tracer injection was carried out under isoflurane-induced (1.25%–2.5%) anesthesia and aseptic conditions. After three days survival time, this animal was sacrificed with an overdose of sodium pentobarbital (>90 mg/kg, I.V.) and then transcardially perfused with 0.9% saline followed by 4% paraformaldehyde in 0.1 M phosphate buffer (PBS; pH 7.4) [2]. Frozen, free-floating sections (40 μm) of this case was used for double- or triple-immunofluorescence staining. Paraffin embedded sections of varying thickness (5–10 μm) from the remaining three cases were used for immunoperoxidase based detection, referred to in a previous study as M4-M6 [43], as well as an additional case.

All experimental procedures involving tracer injections had conformed to the state and university regulations on Laboratory Animal Care, including the Principles of Laboratory Animal Care (NIH Publication 85–23, Revised 1985), and were approved by the Animal Care Officers and Institutional Animal Care and Use Committees at Emory University and University of Washington, where all surgical interventions and perfusions were made [2].

5.2. Staining protocol

Putative burst neurons were identified by combined immunostaining for PN (ACAN or HAPLN1), non-phosphorylated neurofilaments (SMI-32) and parvalbumin (PAV). The ion channel profile of these neurons was investigated by immunostaining with antibodies against specific ion channels (see Table 1) in neighboring sections on identified neurons. In the RIMLF, staining for calretinin (CR) in addition to PN marker served to distinguish between up- and down-burst neurons, and in the IBN area, CR was used to delineate neuronal populations. For the sections containing motoneurons, combination of PN marker ACAN (aggrecan) and choline acetyltransferase (ChAT) was used to identify motoneuron

Table 1
Summary of primary antibodies and dilutions for the immunolabeling. IF: immunofluorescence. IHC: immunohistochemistry (peroxidase).

Antibody	Host	Antigen	Manufacturer	RRID	Dilution
CTB	Goat/Polyclonal	Cholera Toxin B	List Biological Lab., CA, USA	AB_10013220	1:5000 (IF)
PAV	Rabbit/Polyclonal	Parvalbumin	Swant, Marly, Fribourg, Switzerland	AB_10000344	1:1000 (IF)
PAV	Mouse/Monoclonal	Parvalbumin	Swant, Marly, Fribourg, Switzerland	AB_10000343	1:2500 (IHC)
SMI-32	Mouse/Monoclonal	Nonphosphorylated Neurofilament marker H	SM1353, Acris Antibodies	AB_2715852	1:2500 (IF & IHC)
HAPLN1	Goat/Polyclonal	Hyaluronan and proteoglycan link protein 1	R&D Systems, MN, USA	AB_2116135	1:100 (IF)
ACAN	Mouse/Monoclonal	Aggrecan	Acris Antibodies GmbH, Herford, Germany	AB_972582	1:75 (IHC)
CR	Rabbit/Polyclonal	Calretinin	Swant, Marly, Fribourg, Switzerland	AB_10000321	1:2500 (IHC)
ChAT	Goat/Polyclonal	Choline Acetyltransferase	Chemicon, Temecula, CA, USA	AB_2079751	1:50 (IHC)
GABAaR	Guinea Pig/ Polyclonal	γ-Aminobutyric acid receptor type A subunit α1	Alomone Labs Jerusalem BioPark (JBP)	AB_2756618	1:1000 (IHC)
Kv1.1	Rabbit/Polyclonal	Voltage-Gated Potassium Channel 1.1	Alomone Labs Jerusalem BioPark (JBP)	AB_2040144	1:750 (IHC)
Kv3.1b	Rabbit/Polyclonal	Voltage-Gated Potassium Channel 3.1b	Härtig (Weiser et al. 1995)[75]	(AB_2040166)	1:6000 (IHC)
KCC2	Rabbit/Polyclonal	Potassium-Chloride Cotransporter 2	Chemicon, Temecula, CA, USA	AB_310611	1:4000 (IHC)
HCN1	Rabbit/Polyclonal	Hyperpolarization-activated cyclic nucleotide-gated channel 1	Thermo Fischer Scientific, MA, USA	AB_2735891	1:400 (IHC)
HCN2	Rabbit/Polyclonal	Hyperpolarization-activated cyclic nucleotide-gated channel 2	Thermo Fischer Scientific, MA, USA	AB_2735892	1:1500 (IHC)
Cav3.1	Rabbit/Polyclonal	T-Type Voltage-Gated Calcium Channel 3.1	Alomone Labs Jerusalem BioPark (JBP)	AB_2039779	1:1000 (IHC)
Cav3.2	Rabbit/Polyclonal	T-Type Voltage-Gated Calcium Channel 3.2	Alomone Labs Jerusalem BioPark (JBP)	AB_2039781	1:1000 (IHC)
Cav3.3	Rabbit/Polyclonal	T-Type Voltage-Gated Calcium Channel 3.3	Alomone Labs Jerusalem BioPark (JBP)	AB_2039783	1:1000 (IHC)

types. Motoneurons of multiply-innervated fibers (MIF) were identified by positive ChAT-, but negative PN-immunolabeling, whereas motoneurons of singly-innervated fibers (SIF) were identified by positive ChAT- and PN-immunolabeling, as previously established [30].

Visualization of the tracer, immunofluorescence or immunoperoxidase staining of free-floating or paraffin embedded tissue, respectively, and analysis and processing of stained sections was performed exactly as described in detail in our recent study [43]. A list of antibodies used in this study is provided in Table 1.

Funding

This study was funded by the Deutsche Forschungsgemeinschaft (HO 1639/5-1 to AKEH) and the Graduate School of Systemic Neurosciences (GSN)—LMU Munich (ÜSM), Munich Center for Neurosciences—Brain and Mind, Ludwig-Maximilians-Universität München.

Acknowledgements

The excellent technical assistance of Christine Unger and Ahmed Messoudi MPh is acknowledged. The authors thank Drs. Alexander Thiele and Claudia Distler for providing fixed brainstem tissue of two macaque monkeys. Finally, the authors thank Prof. Dr. med. Jens Waschke for his continuous support.

References

[1] C. Adamczyk, M. Strupp, K. Jahn, A.K.E. Horn, Calretinin as a marker for premotor neurons involved in upgaze in human brainstem, Front. Neuroanat. 9 (2015) 153, https://doi.org/10.3389/fnana.2015.00153.
[2] J. Ahlfeld, M. Mustari, A.K.E. Horn, Sources of calretinin inputs to motoneurons of extraocular muscles involved in upgaze, Ann. N. Y. Acad. Sci. 1233 (2011) 91–99, https://doi.org/10.1111/j.1749-6632.2011.06168.x (Basic and Clinical Ocular Motor and Vestibular Research).
[3] R. Bhidayasiri, D.E. Riley, J.T. Somers, A.J. Lerner, J.A. Büttner-Ennever, R. J. Leigh, Pathophysiology of slow vertical saccades in progressive supranuclear palsy, Neurology 57 (2001) 2070–2077, https://doi.org/10.1212/wnl.57.11.2070.
[4] T. Bremova-Ertl, L. Abel, M. Walterfang, E. Salsano, A. Ardissone, V. Malinová, M. Kolníková, J. Gascón Bayarri, A. Reza Tavasoli, M. Reza Ashrafi, Y. Amraoui, E. Mengel, S.A. Kolb, A. Brecht, S. Bardins, M. Strupp, A cross-sectional, prospective ocular motor study in 72 patients with Niemann-Pick disease type C, Eur. J. Neurol. 28 (9) (2021) 3040–3050, https://doi.org/10.1111/ene.14955.
[5] S.C. Cannon, D.A. Robinson, Loss of the neural integrator of the oculomotor system from brain stem lesions in monkey, J. Neurophysiol. 57 (1987) 1383–1409, https://doi.org/10.1152/jn.1987.57.5.1383.
[6] G. Carrero-Rojas, R. Hernández, R. Blumer, R.R. de la Cruz, A. Pastor, MIF versus SIF motoneurons, what are their respective contribution in the oculomotor medial rectus pool? J. Neurosci. 41 (47) (2021) 9782–9793, https://doi.org/10.1523/JNEUROSCI.1480-21.2021.
[7] A.L. Chen, D.E. Riley, S.A. King, A.C. Joshi, A. Serra, K. Liao, M.L. Cohen, J. Otero-Millan, S. Martinez-Conde, M. Strupp, R.J. Leigh, The disturbance of gaze in progressive supranuclear palsy (PSP): implications for pathogenesis, Front. Neurol. 1 (2010), https://doi.org/10.3389/fneur.2010.00147.
[8] B. Cohen, A. Komatsuzaki, Eye movements induced by stimulation of the pontine reticular formation: evidence for integration in oculomotor pathways, Exp. Neurol. 36 (1) (1972) 101–117, https://doi.org/10.1016/0014-4886(72)90139-2.
[9] K.E. Cullen, D. Guitton, C.G. Rey, W. Jiang, Gaze-related activity of putative inhibitory burst neurons in the head-free cat, J. Neurophysiol. 70 (1993) 2678–2683, https://doi.org/10.1152/jn.1993.70.6.2678.
[10] S.D.Z. Eggers, A.K.E. Horn, S. Roeber, W. Härtig, G. Nair, D.S. Reich, R. John Leigh, Saccadic palsy following cardiac surgery: a review and new hypothesis, Ann. N. Y. Acad. Sci. 1343 (1) (2015) 113–119, https://doi.org/10.1111/nyas.12666.
[11] S.D.Z. Eggers, A.K.E. Horn, S. Roeber, W. Härtig, G. Nair, D.S. Reich, R.J. Leigh, Saccadic palsy following cardiac surgery: possible role of perineuronal nets, PLoS One 10 (7) (2015), e0132075, https://doi.org/10.1371/journal.pone.0132075.
[12] J.D. Enderle, E.J. Engelken, Simulation of oculomotor post-inhibitory rebound burst firing using a Hodgkin-Huxley model of a neuron, Biomed. Sci. Instrum. 31 (1995) 53–58. https://pubmed.ncbi.nlm.nih.gov/11121510/.
[13] E. Favuzzi, A. Marques-Smith, R. Deogracias, C.M. Winterflood, A. Sánchez-Aguilera, L. Mantoan, P. Maeso, C. Fernandes, H. Ewers, B. Rico, Activity-dependent gating of Parvalbumin interneuron function by the perineuronal net protein Brevican, Neuron 95 (3) (2017) 639–655.e610, https://doi.org/10.1016/j.neuron.2017.06.028.
[14] M. Frontali, Spinocerebellar ataxia type 6: channelopathy or glutamine repeat disorder? Brain Res. Bull. 56 (3–4) (2001) 227–231, https://doi.org/10.1016/s0361-9230(01)00574-3, 2001 Oct-Nov 1.
[15] K. Fukushima, C.R. Kaneko, Vestibular integrators in the oculomotor system, Neurosci. Res. 22 (1995) 249–258, https://doi.org/10.1016/0168-0102(95)00904-8.
[16] D. Gall, C. Roussel, T. Nieus, G. Cheron, L. Servais, E. D'Angelo, S.N. Schiffmann, Role of calcium binding proteins in the control of cerebellar granule cell neuronal excitability: experimental and modeling studies, Progr. Brain Res. Z. De and Cicirata, Elsevier. 148 (2005) 321–328, https://doi.org/10.1016/S0079-6123(04)48025-X.
[17] M.R. Hanson, M.A. Hamid, R.L. Tomsak, S.S. Chou, R.J. Leigh, Selective saccadic palsy caused by pontine lesions: clinical, physiological, and pathological correlations, Ann. Neurol. 20 (2) (1986) 209–217, https://doi.org/10.1002/ana.410200206.

[18] W. Härtig, A. Derouiche, K. Welt, K. Brauer, J. Grosche, M. Mäder, A. Reichenbach, G. Brückner, Cortical neurons immunoreactive for the potassium channel Kv3.1b subunit are predominantly surrounded by perineuronal nets presumed as a buffering system for cations, Brain Res. 842 (1999) 15–29, https://doi.org/10.1016/s0006-8993(99)01784-9.

[19] K. Hepp, V. Henn, Spatio-temporal recoding of rapid eye movement signals in the monkey paramedian pontine reticular formation (PPRF), Exp. Brain Res. 52 (1983) 105–120, https://doi.org/10.1007/BF00237155.

[20] K. Hepp, T. Vilis, V. Henn, On the generation of rapid eye movements in three dimensions, Ann. N. Y. Acad. Sci. 545 (1988) 140–153, https://doi.org/10.1111/j.1749-6632.1988.tb19560.x.

[21] G.R. Hernandez, R. Blumer, R.R. de la Cruz, A.M. Pastor, Functional diversity of motoneurons in the oculomotor system, Proc. Natl. Acad. Sci. U. S. A. 116 (9) (2019) 3837–3846, https://doi.org/10.1073/pnas.1818524116.

[22] A.K.E. Horn, The reticular formation, Prog. Brain Res. 151 (2006) 127–155, https://doi.org/10.1016/S0079-6123(05)51005-7.

[23] A.K.E. Horn, J.A. Büttner-Ennever, Premotor neurons for vertical eye-movements in the rostral mesencephalon of monkey and man: the histological identification by parvalbumin immunostaining, J. Comp. Neurol. 392 (1998) 413–427, https://doi.org/10.1002/(sici)1096-9861(19980323)392:4<413::aid-cne1>3.0.co;2-3.

[24] A.K.E. Horn, R.J. Leigh, The anatomy and physiology of the ocular motor system, Handb. Clin. Neurol. 102 (2011) 21–69, https://doi.org/10.1016/B978-0-444-52903-9.00008-X.

[25] A.K.E. Horn, H. Straka, Functional organization of extraocular motoneurons and eye muscles, Ann. Rev. Vision Sci. 7 (2021) 793–825, https://doi.org/10.1146/annurev-vision-100119-125043.

[26] A.K.E. Horn, J.A. Büttner-Ennever, P. Wahle, I. Reichenberger, Neurotransmitter profile of saccadic omnipause neurons in nucleus raphe interpositus, J. Neurosci. 14 (1994) 2032–2046, https://doi.org/10.1523/JNEUROSCI.14-04-02032.1994.

[27] A.K.E. Horn, J.A. Büttner-Ennever, Y. Suzuki, V. Henn, Histological identification of premotor neurons for horizontal saccades in monkey and man by parvalbumin immunostaining, J. Comp. Neurol. 359 (2) (1995) 350–363, https://doi.org/10.1002/cne.903590212.

[28] A.K.E. Horn, G. Brückner, W. Härtig, A. Messoudi, Saccadic omnipause and burst neurons in monkey and human are ensheathed by perineuronal nets but differ in their expression of calcium-binding proteins, J. Comp. Neurol. 455 (2003) 341–352, https://doi.org/10.1002/cne.10495.

[29] A.K.E. Horn, C. Helmchen, P. Wahle, GABAergic neurons in the rostral mesencephalon of the Macaque monkey that control vertical eye movements, Ann. N. Y. Acad. Sci. 1004 (2003) 19–28, https://doi.org/10.1196/annals.1303.003.

[30] A.K.E. Horn, A. Horng, N. Buresch, A. Messoudi, W. Hartig, Identification of functional cell groups in the abducens nucleus of monkey and human by perineuronal nets and choline acetyltransferase immunolabeling, Front. Neuroanat. 12 (2018) 45, https://doi.org/10.3389/fnana.2018.00045.

[31] K. Jensen, S.B. Beylergil, A.G. Shaikh, Slow saccades in cerebellar disease, Cerebellum Ataxias 6 (2019) 1, https://doi.org/10.1186/s40673-018-0095-9. Jan 17.

[32] L.K. Kaczmarek, Y. Zhang, Kv3 channels: enablers of rapid firing, neurotransmitter release, and neuronal endurance, Physiol. Rev. 97 (4) (2017) 1431–1468, https://doi.org/10.1152/physrev.00002.2017.

[33] R. Kalla, S. Glasauer, U. Büttner, T. Brandt, M. Strupp, 4-Aminopyridine restores vertical and horizontal neural integrator function in downbeat nystagmus, Sep 130 (Pt 9) (2007) 2441–2451, https://doi.org/10.1093/brain/awm172.

[34] D. Kase, K. Imoto, The role of HCN channels on membrane excitability in the nervous system, J. Signal Transduct. 2012 (2012), 619747, https://doi.org/10.1155/2012/619747.

[35] E.L. Keller, Participation of medial pontine reticular formation in eye movement generation in monkey, J. Neurophysiol. 37 (2) (1974) 316–332, https://doi.org/10.1152/jn.1974.37.2.316.

[36] A. Kheradmand, D. Zee, Cerebellum and ocular motor control, Front. Neurol. 2 (53) (2011), https://doi.org/10.3389/fneur.2011.00053.

[37] T. Kodama, A.H. Gittis, M. Shin, K. Kelleher, K.E. Kolkman, L. McElvain, M. Lam, S. du Lac, Graded coexpression of ion channel, neurofilament, and synaptic genes in fast-spiking vestibular nucleus neurons, J. Neurosci. 40 (3) (2020) 496–508, https://doi.org/10.1523/JNEUROSCI.1500-19.2019.

[38] P. Kumar, D. Kumar, S.K. Jha, N.K. Jha, R.K. Ambasta, Chapter three - Ion channels in neurological disorders, in: Advances in Protein Chemistry and Structural Biology. R. Donev 103, Academic Press, 2016, pp. 97–136, https://doi.org/10.1016/bs.apcsb.2015.10.006.

[39] R.J. Leigh, D.S. Zee. The Neurology of Eye Movements., 5th, Oxford University Press, Oxford, New York, 2015.

[40] K. Lienbacher, S. Ono, J. Fleuriet, M. Mustari, A.K.E. Horn, A subset of palisade endings only in the medial and inferior rectus muscle in monkey contain calretinin, Invest. Ophthalmol. Vis. Sci. 59 (7) (2018) 2944–2954, https://doi.org/10.1167/iovs.18-24322.

[41] E.S. Luschei, A.F. Fuchs, Activity of brain stem neurons during eye movements of alert monkeys, J. Neurophysiol. 35 (4) (1972) 445–461, https://doi.org/10.1152/jn.1972.35.4.445.

[42] Ü.S. Mayadali, K. Lienbacher, M. Mustari, M. Strupp, A.K.E. Horn, Potassium channels in omnipause neurons, Prog. Brain Res. 249 (2019) 117–123, https://doi.org/10.1016/bs.pbr.2019.04.017.

[43] Ü.S. Mayadali, J. Fleuriet, M. Mustari, H. Straka, A.K.E. Horn, Transmitter and ion channel profiles of neurons in the primate abducens and trochlear nuclei, Brain Struct. Funct. 226 (7) (2021) 2125–2151, https://doi.org/10.1007/s00429-021-02315-7.

[44] M.S. Missal, De Brouwer, P. Lefévre, E. Olivier, Activity of mesencephalic vertical burst neurons during saccades and smooth pursuit, J. Neurophysiol. 83 (2000) 2080–2092, https://doi.org/10.1152/jn.2000.83.4.2080.

[45] K. Miura, L.M. Optican, Membrane channel properties of premotor excitatory burst neurons may underlie saccade slowing after lesions of omnipause neurons, J. Comput. Neurosci. 20 (2006) 25–41, https://doi.org/10.1007/s10827-006-4258-y.

[46] A.K. Moschovakis, C.A. Scudder, S.M. Highstein, The structure of the primate oculomotor burst generator. I. Medium-lead burst neurons with upward on-directions, J. Neurophysiol. 65 (1991) 203–217, https://doi.org/10.1152/jn.1991.65.2.203.

[47] A.K. Moschovakis, C.A. Scudder, S.M. Highstein, J.D. Warren, The structure of the primate oculomotor burst generator. II. Medium-lead burst neurons with downward on-directions, J. Neurophysiol. 65 (1991) 218–229, https://doi.org/10.1152/jn.1991.65.2.218.

[48] A.K. Moschovakis, C.A. Scudder, S.M. Highstein, The microscopic anatomy and physiology of the mammalian saccadic system, Prog. Neurobiol. 50 (2–3) (1996) 133–254, https://doi.org/10.1016/S0301-0082(96)00034-2.

[49] L.M. Optican, E. Pretegiani, What stops a saccade? Philos. Trans. Roy. Soc. B: Biol.. Sci. 372 (1718) (2017) 20160194, https://doi.org/10.1098/rstb.2016.0194.

[50] S.R. Ramat, D. Zee Leigh, L. Optican, What clinical disorders tell us about the neural control of saccadic eye movements, Brain J. Neurol. 130 (2007) 10–35, https://doi.org/10.1093/brain/awl309.

[51] K.G. Rottach, R.D. Von Maydell, V.E. Das, A.Z. Zivotofsky, A.O. DiScenna, J. L. Gordon, D.M.D. Landis, R.J. Leigh, Evidence for independent feedback control of horizontal and vertical saccades from Niemann-Pick type C disease, Vis. Res. 37 (24) (1997) 3627–3638, https://doi.org/10.1016/S0042-6989(96)00066-1.

[52] E.C. Salsano, A. Umeh, D. Pareyson Rufa, D.S. Zee, Vertical supranuclear gaze palsy in Niemann-Pick type C disease, Neurol. Sci. 33 (6) (2012) 1225–1232, https://doi.org/10.1007/s10072-012-1155-1.

[53] B. Schwaller, Calretinin: from a "simple" Ca^{2+} buffer to a multifunctional protein implicated in many biological processes, Front. Neuroanat. 8 (2014), https://doi.org/10.3389/fnana.2014.00003.

[54] C.A. Scudder, A.F. Fuchs, T.P. Langer, Characteristics and functional identification of saccadic inhibitory burst neurons in the alert monkey, J. Neurophysiol. 59 (1988) 1430–1454, https://doi.org/10.1152/jn.1988.59.5.1430.

[55] A. Senatore, J.D. Spafford, Physiology and pathology of voltage-gated T-type calcium channels, in: S.W. Schaffer, M. Li (Eds.), T-type Calcium Channels in Basic and Clinical Science, Springer Vienna, Vienna, 2015, pp. 3–17, https://doi.org/10.1007/978-3-7091-1413-1_1.

[56] A.G. Shaikh, Saccadic oscillations – membrane, model, and medicine, Expert Rev. Ophthalmol. 7 (5) (2012) 481–486, https://doi.org/10.1586/eop.12.55.

[57] A.G. Shaikh, K. Miura, L.M. Optican, S. Ramat, R.J. Leigh, D.S. Zee, A new familial disease of saccadic oscillations and limb tremor provides clues to mechanisms of common tremor disorders, Brain 130 (Pt 11) (2007) 3020–3031, https://doi.org/10.1093/brain/awm240.

[58] A.G. Shaikh, D.S. Zee, L.M. Optican, K. Miura, S. Ramat, R.J. Leigh, The effects of ion channel blockers validate the conductance-based model of saccadic oscillations, Ann. N. Y. Acad. Sci. 1233 (2011) 58–63, https://doi.org/10.1111/j.1749-6632.2011.06130.x.

[59] A.G. Shaikh, S.A. Factor, J. Juncos, Saccades in progressive supranuclear palsy - maladapted, irregular, curved, and slow, Mov. Disorders Clin. Practice 4 (5) (2017) 671–681, https://doi.org/10.1002/mdc3.12491.

[60] C.C. Shieh, M. Coghlan, J.P. Sullivan, M. Gopalakrishnan, Potassium channels: molecular defects, diseases, and therapeutic opportunities, Pharmacol. Rev. 52 (4) (2000) 557–594.

[61] D.L. Sparks, The brainstem control of saccadic eye movements, Nat. Rev. Neurosci. 3 (12) (2002) 952–964, https://doi.org/10.1038/nrn986.

[62] R.F. Spencer, S.F. Wang, Immunohistochemical localization of neurotransmitters utilized by neurons in the rostral interstitial nucleus of the medial longitudinal fasciculus (riMLF) that project to the oculomotor and trochlear nuclei in the cat, J. Comp. Neurol. 366 (1996) 134–148, https://doi.org/10.1002/(SICI)1096-9861(19960226)366:1<134::AID-CNE9>3.0.CO;2-4.

[63] R.F. Spencer, R.J. Wenthold, R. Baker, Evidence for glycine as an inhibitory neurotransmitter of vestibular, reticular, and prepositus hypoglossi neurons that project to the cat abducens nucleus, J. Neurosci. 9 (1989) 2718–2736, https://doi.org/10.1523/JNEUROSCI.09-08-02718.1989.

[64] J. Steele, J.C. Richardson, J. Olszewski, Progressive supranuclear palsy. A heterogeneous system degeneration involving brain stem, basal ganglia and cerebellum with vertical gaze and pseudobulbar palsy, nuchal dystonia and dementia, Arch. Neurol. 10 (1964) 333–359, https://doi.org/10.1001/archneur.1964.00460160003001.

[65] A. Strassman, S.M. Highstein, R.A. McCrea, Anatomy and physiology of saccadic burst neurons in the alert squirrel monkey. I. Excitatory burst neurons, J. Comp. Neurol. 249 (1986) 337–357, https://doi.org/10.1002/cne.902490303.

[66] A. Strassman, S.M. Highstein, R.A. McCrea, Anatomy and physiology of saccadic burst neurons in the alert squirrel monkey. II. Inhibitory burst neurons, J. Comp. Neurol. 249 (1986) 358–380, https://doi.org/10.1002/cne.902490304.

[67] Y. Sugiuchi, M. Takahashi, Y. Shinoda, Input-output organization of inhibitory neurons in the interstitial nucleus of Cajal projecting to the contralateral trochlear and oculomotor nucleus, J. Neurophysiol. 110 (3) (2013) 640–657, https://doi.org/10.1152/jn.01045.2012.

[68] M.J. Thurtell, R.L. Tomsak, R.J. Leigh, Disorders of saccades, Curr. Neurol. Neurosci. Rep. Sep 7 (5) (2007) 407–416, https://doi.org/10.1007/s11910-007-0063-x.

[69] G. Ugolini, F. Klam, M. Doldan Dans, D. Dubayle, A.-M. Brandi, J.A. Büttner-Ennever, W. Graf, Horizontal eye movement networks in primates as revealed by retrograde transneuronal transfer of rabies virus: differences in monosynaptic input to “slow” and “fast” abducens motoneurons, J. Comp. Neurol. 498 (2006) 762–785, https://doi.org/10.1002/cne.21092.

[70] L. Vinay, C. Jean-Xavier, Plasticity of spinal cord locomotor networks and contribution of cation-chloride cotransporters, Brain Res. Rev. 57 (1) (2008) 103–110, https://doi.org/10.1016/j.brainresrev.2007.09.003.

[71] K. Yoshida, R.A. McCrea, A. Berthoz, P.P. Vidal, Morphological and physiological characteristics of inhibitory burst neurons controlling horizontal rapid eye movements in the alert cat, J. Neurophysiol. 48 (1982) 761–784, https://doi.org/10.1152/jn.1982.48.3.761.

[72] C. Zeeh, B.J. Hess, A.K.E. Horn, Calretinin inputs are confined to motoneurons for upward eye movements in monkey, J. Comp. Neurol. 521 (14) (2013) 3154–3166, https://doi.org/10.1002/cne.23337.

[73] C. Zeeh, Ü.S. Mayadali, A.K.E. Horn, Histochemical characterization of the vestibular Y-group in monkey, Cerebellum 20 (2020) 701–716, https://doi.org/10.1007/s12311-020-01200-z.

[74] J. Zhou, A. Brown, E. Lackey, M. Arancillo, T. Lin, R. Sillitoe, Purkinje cell neurotransmission patterns cerebellar basket cells into zonal modules defined by distinct pinceau sizes, Elife 9 (2020), e55569, https://doi.org/10.7554/eLife.55569.sa2.

[75] M. Weiser, E. Bueno, C. Sekirnjak, M. Martone E., H. Baker, D. Hillman, S. Chen, W. Thornhill, M. Ellisman, B Rudy, The potassium channel subunit Kv3.1b is localized to somatic and axonal membranes of specific populations of CNS neurons, J. Neurosci. 15 (6) (1995) 4298–4314, https://doi.org/10.1523/JNEUROSCI.15-06-04298.1995.

4. Histochemical characterization of the vestibular y-group in monkey

Zeeh C, **Mayadali ÜS**, Horn AKE. 2021. Histochemical characterization of the vestibular y-group in monkey. Cerebellum 20, 701–716 (2021). doi: 10.1007/s12311-020-01200-z

Open Access

GSN affiliated co-authors:

- Prof. Dr. Anja Horn-Bochtler; GSN associate faculty
  Chair of Vegetative Anatomy, Institute of Anatomy, Faculty of Medicine, LMU, Pettenkoferstr. 11 D-80336 Munich, Germany
  anja.bochtler@med.uni-muenchen.de
  +49 (0)89 / 2180-726

The Cerebellum (2021) 20:701–716
https://doi.org/10.1007/s12311-020-01200-z

ORIGINAL PAPER

Histochemical Characterization of the Vestibular Y-Group in Monkey

Christina Zeeh[1] · Ümit S. Mayadali[1,2] · Anja K.E. Horn[1]

Accepted: 4 October 2020 / Published online: 20 October 2020

Abstract

The Y-group plays an important role in the generation of upward smooth pursuit eye movements and contributes to the adaptive properties of the vertical vestibulo-ocular reflex. Malfunction of this circuitry may cause eye movement disorders, such as downbeat nystagmus. To characterize the neuron populations in the Y-group, we performed immunostainings for cellular proteins related to firing characteristics and transmitters (calretinin, GABA-related proteins and ion channels) in brainstem sections of macaque monkeys that had received tracer injections into the oculomotor nucleus. Two histochemically different populations of premotor neurons were identified: The calretinin-positive population represents the excitatory projection to contralateral upgaze motoneurons, whereas the GABAergic population represents the inhibitory projection to ipsilateral downgaze motoneurons. Both populations receive a strong supply by GABAergic nerve endings most likely originating from floccular Purkinje cells. All premotor neurons express nonphosphorylated neurofilaments and are ensheathed by strong perineuronal nets. In addition, they contain the voltage-gated potassium channels Kv1.1 and Kv3.1b which suggests biophysical similarities to high-activity premotor neurons of vestibular and oculomotor systems. The premotor neurons of Y-group form a homogenous population with histochemical characteristics compatible with fast-firing projection neurons that can also undergo plasticity and contribute to motor learning as found for the adaptation of the vestibulo-ocular reflex in response to visual-vestibular mismatch stimulation. The histochemical characterization of premotor neurons in the Y-group allows the identification of the homologue cell groups in human, including their transmitter inputs and will serve as basis for correlated anatomical-neuropathological studies of clinical cases with downbeat nystagmus.

Keywords Vestibulo-ocular reflex · Floccular-target neurons · Smooth pursuit · Voltage-gated potassium channels · Calretinin · Glutamate decarboxylase

Introduction

The Y-group plays an important role in the generation of smooth pursuit (upward) eye movements [1], but is also involved in the adaptive properties of the vertical vestibulo-ocular reflex (VOR) for example in response to mismatch of visual and vestibular input by wearing optical devices, or in VOR suppression during combined eye-head tracking [2, 3]. Recording studies in monkey revealed a rather uniform neuron population in the Y-group that modulated in phase with eye velocity during visual following, modulated in phase with head velocity during VOR suppression, but did not modulate during the VOR in darkness [4]. Accordingly, the Y-group is part of a circuitry that uses vestibular and visual signals mediated by the cerebellar flocculus to control eye movements. Malfunction of this circuitry may cause eye movement disorders, such as downbeat nystagmus seen after floccular lesions [5].

The Y-group is a well-defined nucleus in the cerebellar white matter at the level of the cerebellomedullary junction described in several mammalian species [6]. Cytoarchitecturally, it consists of a dorsal larger-celled Y-group (Yd) corresponding to the infracerebellar nucleus [7] and a small-celled ventral Y-group (Yv) [8, 9]. Only the Yv receives direct input from saccular afferents [10–12], has commissural connections to the contralateral vestibular nuclei and Yv [13–16] and projects to the

Christina Zeeh and Ümit S. Mayadali contributed equally to this work.

✉ Anja K.E. Horn
Anja.Bochtler@med.uni-muenchen.de

[1] Institute of Anatomy and Cell Biology, Dept. I, Ludwig-Maximilians University, Pettenkoferstrasse 11, Munich 80366, Germany

[2] Graduate School of Systemic Neurosciences, Großhaderner Str. 2, Planegg 82152, Germany

flocculus [17, 18]. The Yd receives a disynaptic excitatory input from the ipsilateral anterior and posterior semicircular canals via neurons in the anterior-lateral corner of the superior vestibular nucleus (SVN) and caudal medial vestibular nucleus (MVN) carrying head velocity-only signals [19]. Neurons in the Yd further receive a strong inhibitory input from Purkinje cells of the flocculus (vertical optokinetic and visual-related zones F1 and F3) and ventral paraflocculus; they are therefore termed floccular-target neurons (FTN) [17, 20–22]. The Yd contains a large population of premotor neurons, which includes excitatory neurons targeting motoneurons for upgaze in the contralateral oculomotor nucleus (nIII), as well as neurons with ipsilateral projections to motoneurons in nIII and trochlear nucleus (nIV) involved in downgaze, which presumably have an inhibitory function [7, 14, 23–25]. Our previous studies indicated that the excitatory projections of Yd to nIII are associated with the calcium-binding protein calretinin (CR) [26, 27]. In the present study, we aimed to delineate contralaterally and ipsilaterally projecting neurons by their histochemical properties and by investigating the presence of different cellular proteins, which are related to firing characteristics and transmitters (calretinin, GABA-related proteins and ion channels).

Material and Methods

The tissue of seven rhesus monkeys (*Macaca mulatta*) from previous studies stored either in a mixture of glycerol and phosphate buffer at − 20 °C or embedded in paraffin was used for staining in the present investigation.

All experimental procedures involving tracer injections had conformed to the state and university regulations on Laboratory Animal Care, including the Principles of Laboratory Animal Care (NIH Publication 85-23, Revised 1985), and were approved by the Animal Care Officers and Institutional Animal Care and Use Committees at Emory University and University of Washington, where all surgical interventions and perfusions were made for previous studies [27–29]. The brains of all cases were fixed by transcardial perfusion with 4% paraformaldehyde (PFA) in 0.1 M phosphate buffer except one case, which was fixed with 2% PFA and 0.5% glutaraldehyde (see Table 1).

The brain sections of two rhesus monkeys (*Macaca mulatta*) from a previous study, who had received a central tracer injection with either 1% cholera toxin subunit B (CTB, Sigma/Biological laboratories, TC1) into the right oculomotor nucleus (nIII) or with 5% wheat-germ agglutinin (WGA; EY Lab, San Mateo, CA; TC2) into the left nIII were used (for details see [27, 28]). Frozen free-floating sections (40 μm) of one additional case was used for double-immunofluorescence staining (M3), and immunoperoxidase staining for different markers was performed in neighbouring thin sections (5 μm) of three paraffin embedded cases (PF1, PF2, PF3). Immunostained sections from previous two cases (M1, M4) treated with a polyclonal sheep glutamate decarboxylase (GAD) and rabbit GABA antiserum were analysed for GABAergic neurons in Yd for validation. A section from a case with a large WGA-HRP injection into nIII (M5) served to illustrate the complete population of premotor neurons in Yd (see Table 1).

Table 1

Case	Injection	Fixation	Sections	IF	IHC
TC1	1% CTB in right nIII	4%PFA	Frozen	gCTB+mCR+rGAD gCTB+rCR+mGAD gCTB+rCR, gCTB+rGAD	
TC2	5% WGA in left nIII	4% PFA	Frozen	gWGA+mNPNF, gWGA+mACAN, gWGA+rGAD, gWGA+rCR	WGA
PF1		4% PFA	Paraffin		CSPG, NPNF, rCR+mACAN, mCR+rGAD, Kv3.1b, Kv1.1
PF2		4% PFA	Paraffin		rCR+mACAN, mCR+rGAD, Kv3.1b, Kv1.1
PF3		4% PFA	Paraffin		rCR+mACAN, mCR+rGAD, Kv3.1b, Kv1.1
M1		4% PFA	Frozen		sGAD+Nissl
M2		4% PFA	Frozen		rCR+Nissl,
M3		4% PFA	Frozen	rGAD+mCR, mCB+rCR	gChAT
M4		2% PFA, 0,5% GA	Vibratome		rGABA
M5	2,5% WGA-HRP	4% PFA	Frozen		*

An overview of injection, fixation and immunohistochemistry details for each case. *WGA-HRP was visualized by tetramethylbenzidine reaction

Visualization of the Tracer Combined with Different Markers

In selected sections of the two tracer cases (TC1, TC2) combined immunofluorescence labelling was performed for the simultaneous detection of WGA or CTB and different markers as described previously [27]: Free floating sections were incubated in a cocktail containing either goat antiWGA (1:250, AB_2315611) or goat antiCTb (1:5000, AB_10013220) and one or two of the following antibodies for 48 h at 4 °C: rabbit (1:500, AB_90715) or mouse anti-glutamate decarboxylase (GAD65/67) (1:500, AB_10710523) to reveal GABAergic profiles, mouse anti-nonphosphorylated neurofilaments (NPNF) (1:2500, AB_2715852), mouse anti-aggrecan (ACAN) (1:25, AB_972582) to stain perineuronal nets (PN) and rabbit or mouse anti-calretinin (CR) (1:1000, AB_10000320; 1:2000). After washing, the sections were treated with a mixture of Alexa 488 tagged donkey anti-goat (1:200; AB_2534102) and Cy3-tagged donkey anti-rabbit (1:200, AB_2307443) or Cy3-tagged donkey anti-mouse (1:200, AB_2687868) for 2 h at room temperature. For triple immunofluorescence, either CTB or CR was detected with DyLight™ 405 tagged secondary antibodies (donkey anti-goat IgG, AB_2340426 or donkey anti-rabbit IgG, AB_2340616).

Immunofluorescence Staining for Different Markers

To validate the findings of tracer-labelled neurons, we investigated, whether CR-positive neurons coexpressing GAD-immunoreactivity are present. For that cryosections of case M2 were incubated in a cocktail with mouse anti-CR (1:2000, AB_10000320) and rabbit antiGAD65/67 (1:500, AB_90715). The antigenic sites were detected by treating sections with a mixture of Alexa 488 tagged donkey anti-mouse (1:200; AB_2341099) and Cy3-tagged donkey anti-rabbit (1:200, AB_2307443) as described previously [26]. Additional sections were incubated in a cocktail with mouse anti-GAD (1:500, AB_10710523), rabbit anti-calbindin (CB) (1:1000, AB_10000340) and goat anti-hyaluronan and proteoglycan link protein 1 (HPLN) (1:100, AB_2116135) revealing PNs to study coexpression of both markers in synaptic boutons attached to neurons in the dentate nucleus and premotor neurons in Yd.

Immunoperoxidase Staining of Paraffin Sections

Sets of neighbouring 5 μm thick paraffin sections of 3 monkey cases (PF1, PF2, PF3) were stained with immunoperoxidase methods either for the detection of CR and GAD, CR and ACAN, or potassium channels Kv1.1 or Kv3.1b, chondroitin-sulphate proteoglycans (CSPG) or NPNF. After dewaxing and rehydration sections were rinsed in distilled water and reacted in 0.01 M sodium citrate buffer (pH 6.0) at 1160 w in microwave (AEG, Micromat) three times for 3 min. After cooling down to room temperature sections were rinsed in distilled water and transferred to Tris buffered saline (TBS; pH 7.6) for subsequent immunostaining. Single immunoperoxidase detection of the potassium channels was achieved by incubating the sections in either rabbit anti-Kv1.1 (1:750, AB_2040144) or rabbit anti-Kv3.1b (1:6000, AB_2040166) for 48 h at 4 °C. Neighbouring sections were immunostained for either the combined detection of CR and PN or CR and GAD. This was achieved by processing sections with rabbit anti-GAD (rGAD; 1:2000, AB_90715) or mouse anti-ACAN (1:75; AB_972582), with subsequent incubation in biotinylated secondary anti-rabbit IgG (1:200; AB_2336201) or anti-mouse IgG (1:200, AB_2313581) and extravidin peroxidase (EAP) (1:1000; Sigma, St. Louis, MO) visualized with diaminobenzidine-(DAB)-Ni to yield a black reaction product. For the subsequent detection of CR, sections were incubated in either mouse anti-CR (1:2000; AB_10000320) or rabbit antiCR (1:2500, AB_10000321). The antigenic sites were visualized with incubations in biotinylated horse anti-mouse or anti-rabbit (1:200; AB_2313581 or AB_2336201) followed by EAP and a final DAB reaction to yield a brown reaction product. Other dewaxed sections were treated with either mouse anti-chondroitin sulphate proteoglycan (CSPG; 1:500, AB_2219944) or mouse anti-NPNF (1:5000, AB_2715852), followed by an incubation in biotinylated anti-rabbit (1:200; AB_2336201) and EAP with subsequent DAB-Ni reaction. In additional sections cholinergic neurons were detected by immunostaining for choline acetyltransferase (ChAT) as described previously [30]. To confirm the presence of GABAergic neurons in the Y-group, sections that had been immunostained with sheep anti-GAD [31] or mouse anti-[7]GABA [32] from previous studies were evaluated [33, 34].

Analysis of Stained Sections

The slides were examined and analysed with a Leica microscope DMRB (Bensheim, Germany). Photographs were taken with a digital camera (PixeraPro 600ES; Klughammer, Markt Indersdorf, Germany) mounted on the microscope. The images were captured on a computer with PixeraViewfinder software (Klughammer) and processed with Photoshop 7.0 (Adobe Systems, Mountain View, CA, USA). In each complete image, the sharpness, contrast and brightness were adjusted using the 'unsharp mask' and 'levels adjustment tool' of Photoshop until the appearance of the labelling seen through the microscope was achieved. The images were arranged and labelled with CorelDraw (version18.0; Corel Corporation, SCR_014235).

Images from selected immunofluorescence preparations were taken with a laser-scanning confocal microscope (Leica SP5, Mannheim, Germany) at × 20 or × 63 magnification. Dual and triple imaging of Alexa 488, Cy3 and Dylight was

sequentially recorded at 488 or 543 or 405 nm excitation wavelength, respectively. *Z*-series were collected every 0.5 μm (at × 63) or 1 μm (at × 20) through each section. Image stacks were processed with Fiji/ImageJ software (https://imagej.net/Fiji, SCR_003070). Contrast and brightness of the final composite images were adjusted to reflect the appearance of the labelling, seen through the microscope by using Fiji software.

Immunoperoxidase staining of paraffin sections was imaged using a slide scanner (Mirax MIDI, Zeiss) equipped with a Plan-Apochromat objective (Zeiss, × 20). The digitized images were viewed and photographed with the free software Panoramic Viewer (3DHistech; 1.152.3) and Case Viewer (3DHistech; v2.2). The corresponding detailed views of equally arranged and magnified images of neighbouring sections were analysed on the computer screen. The same neurons were identified by their location with the help of anatomical landmarks, e.g. capillaries.

The cell size profile of the GABAergic and CR-positive neurons within the complete Y-group neuron population was revealed with Fiji/ImageJ software by outlining the somata in Nissl- and immunostained sections at the focus plane of the cell nucleus. The cell sizes were calculated as mean diameter (dmin+dmax/2) and histograms were created with Excel (2016; Microsoft).

Results

In Nissl-stained sections, see Fig. 1a, the two subdivisions of the Y-group are clearly outlined by their cytoarchitecture. The dorsal Y-group (Yd) is composed of loosely packed mainly medium-sized multipolar neurons with mean diameters between 20 and 40 μm, with less small neurons (mean diameter between 10 and 20 μm; see Fig. 4), whereas the ventral Y-group (Yv) consists of tightly packed smaller neurons overlying the inferior cerebellar peduncle (ICP) [35]. At planes of the cerebello-medullary junction the Yd is bordered dorsally by the dentate nucleus (DEN), and lateral by the fibres of the floccular peduncles, which contain the scattered neurons of the basal interstitial nucleus of the cerebellum (BIN) (Fig. 1a) [36].

Properties of Projection Neurons to Oculomotor Nuclei

The population and location of premotor neurons in Yd is illustrated in Fig. 1b resulting from a large bilateral WGA-HRP injection covering the oculomotor (nIII) and trochlear nuclei (nIV) (case M5). Two tracer cases with smaller injections were chosen for the present study (Fig. 2). Whereas the WGA-injection of case TC2 showed some spread to the contralateral side (Fig. 2c, light grey), the CTB-injection in case TC1 was confined to one side involving nIV and lateral and dorsal portions of nIII (Fig. 2a–d, dark grey). The halo of the injection site also covered parts of the medial longitudinal fascicle (MLF), and for both cases involvement of the caudal interstitial nucleus of Cajal (INC) cannot be ruled out. In both cases, tracer injections resulted in retrograde labelling of a large population of medium-sized neurons in the Yd of both sides with a slight contralateral predominance as described in previous studies [24, 37]. In addition, numerous retrogradely labelled neurons were present in the magnocellular part of the medial vestibular nucleus (MVN) mainly contralateral and the superior vestibular nucleus (SVN) on both sides representing secondary vestibulo-ocular neurons (Fig. 2e–i) [6]. The labelling of internuclear neurons only in the contralateral abducens nucleus (nVI) confirmed the strict unilateral injection of case TC1 (Fig. 2e).

Double-immunofluorescence staining showed that all tracer-labelled neurons in Yd are ensheathed by prominent aggrecan (ACAN)–based perineuronal nets (PN) (Fig. 1c, red). In parallel sections immunoreactivity for non-phosphorylated neurofilaments (NPNF) was found in most tracer-labelled neurons (Fig. 1d, e, large arrows), but some retrogradely neurons lacked NPNF (Fig. 1d, e small arrows). In line with these observations, the analysis of neighbouring 5 μm sections containing Yd revealed that all NPNF-positive neurons are ensheathed by PN, here visualized by detection of chondroitin-sulphate proteoglycans (CSPG) (Fig. 1f, g; arrows). Strongly stained PN were also present around small neurons within the Yv, which expressed only weak NPNF-immunoreactivity, if at all (Fig. 1f,g; thin arrow in Yv).

The careful analysis of tracer-labelled neurons in both cases revealed that approximately 90% (91% in TC1; 87% in TC2) in the contralateral Yd contain the calcium-binding protein calretinin (CR) (Fig. 2f, h green dots; Fig. 3a, b, d thin arrows) and only few lack CR (Fig. 2f, h, open green dots; Fig. 3a, b, d solid arrow). None was found on the ipsilateral side. Tracer-labelled neurons on the ipsilateral side expressed GAD-immunoreactivity within their somata, but no CR (Fig. 2g, i, red dots; Fig. 3e–h, arrows). Open circles on the ipsilateral side in Fig. 2g, i indicate neurons whose somata could not clearly be judged. Triple-immunofluorescence staining revealed that tracer-labelled CR-positive neurons in the contralateral Yd did not express somatic GAD-immunofluorescence (Fig. 3i–l), as tracer-labelled GAD-positive neurons in the ipsilateral Yd did not express CR (Fig. 3m–p). Few tracer-labelled neurons were found, that neither contained CR nor GAD (Fig. 3q–t, arrow). Strongly GAD-positive puncta were distributed in the neuropil throughout the complete Yd, with numerous of them attached to the somata and proximal dendrites of the tracer-labelled neurons (Fig. 3i–p, arrows). The morphometric analysis revealed that CR- and GAD-positive neurons formed similar large populations (CR: 41%; GAD 49%) covering almost the whole spectrum of cell sizes in

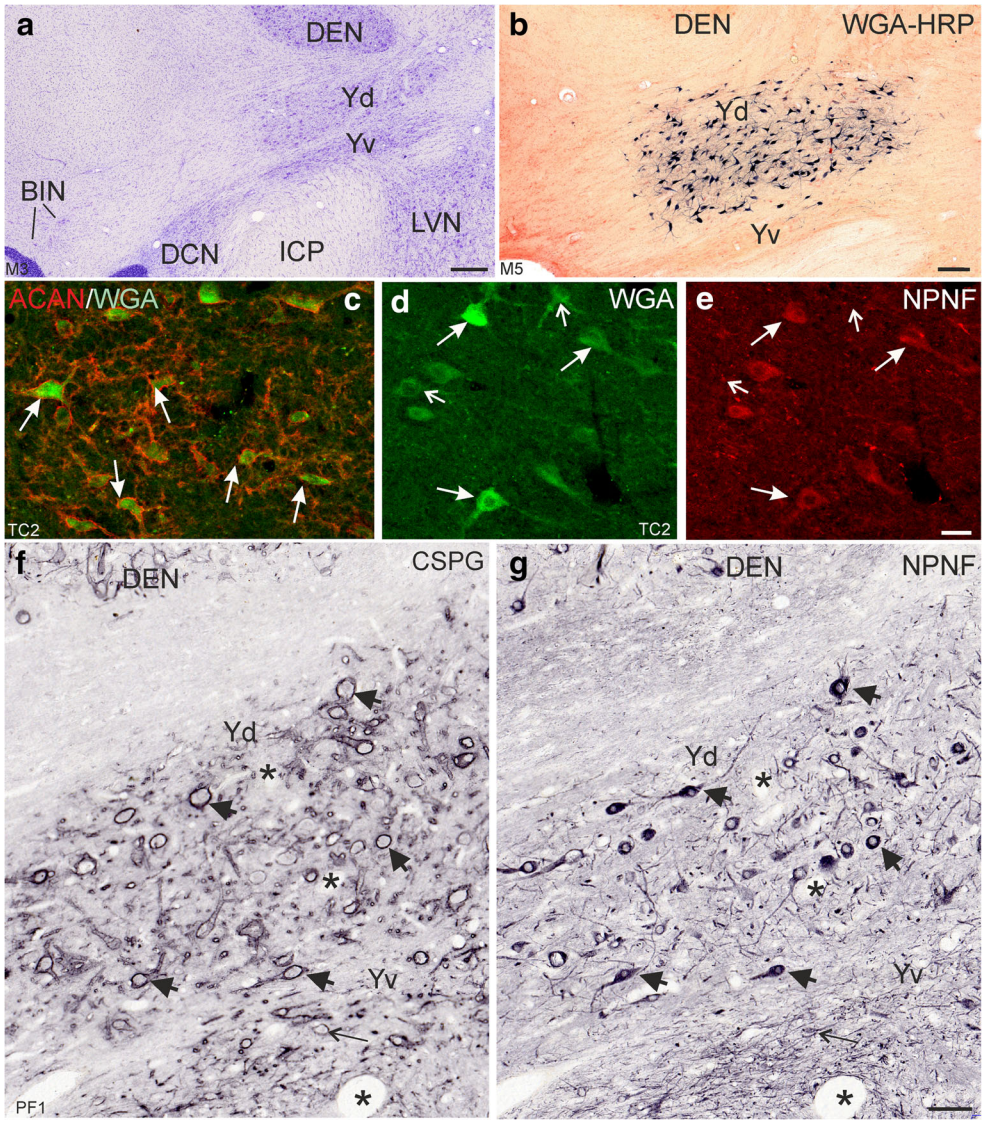

Fig. 1 **a** Transverse section through the brainstem of monkey to demonstrate the location of the Y-group with its ventral (Yv) and dorsal (Yd) subdivisions. **b** Overview of transverse section showing retrogradely labelled neurons only in the Yd after WGA-HRP injection into the oculomotor nucleus. **c** Double immunofluorescence staining for WGA (green) and aggrecan (ACAN)-based perineuronal nets (red) demonstrates that all tracer-labelled cells are ensheathed by perineuronal nets (white arrows). **d**, **e** Similarly, except few (small arrows) tracer-labelled neurons (**d**) express immunoreactivity for nonphosphorylated neurofilaments (NPNF) (**e**, long arrows). **f**, **g** Neighbouring 5 μm thin frontal sections of the Y-group immunostained for chondroitin-sulphate proteoglycans (CSPG) (**f**) or NP-NF (**g**) demonstrates that both markers are coexpressed in medium-sized neurons in the dorsal Y-group (Yd) (**f,g**, large arrows). Smaller neurons in the ventral Y-group (Yv) are ensheathed by perineuronal nets as well , but express only weak NPNF-immunoreactivity (**f, g**, thin arrow). The asterisks label the same blood vessels in both sections as a landmark. BIN, basal interstitial nucleus of the cerebellum; CTB, cholera toxin subunit B; DCN, dorsal cochlear nucleus; DEN, dentate nucleus; LVN, lateral vestibular nucleus; WGA, wheat germ agglutinin; Yd, Y-group dorsal part, Yv, Y-group ventral part; ICP, inferior cerebellar peduncle. Scale bar = 500 μm in **a**, 200 μm in **b**, 50 μm in **e** (applies to **c**–**e**), 100 μm in **g** (applies to **f**–**g**)

Yd except small cell bodies with less than 16 μm mean diameter (Fig. 4a, b). The analysis of tracer-labelled CR- and GAD-positive neurons revealed a more focussed population of medium-sized neurons with mean diameters between 20 and 32 μm (Fig. 4c).

Since the GAD-immunoreactivity was only weakly expressed in cell bodies (Fig. 3o), we confirmed the presence of GABAergic neurons in the Yd by analyses of sections from previous immunoperoxidase staining with different antibodies directed against either GAD [31] or GABA [32]. Both antibodies revealed a consistent moderate GAD- or GABA-immunoreactivity in some small (less than 20 μm) and numerous medium-sized neurons in Yd (Fig. 5a, b), which were contacted by numerous immunopositive puncta most likely representing synaptic terminals (Fig. 5a, b arrows).

To validate the observation that neurons do not coexpress GAD and CR from triple-immunofluorescence, where

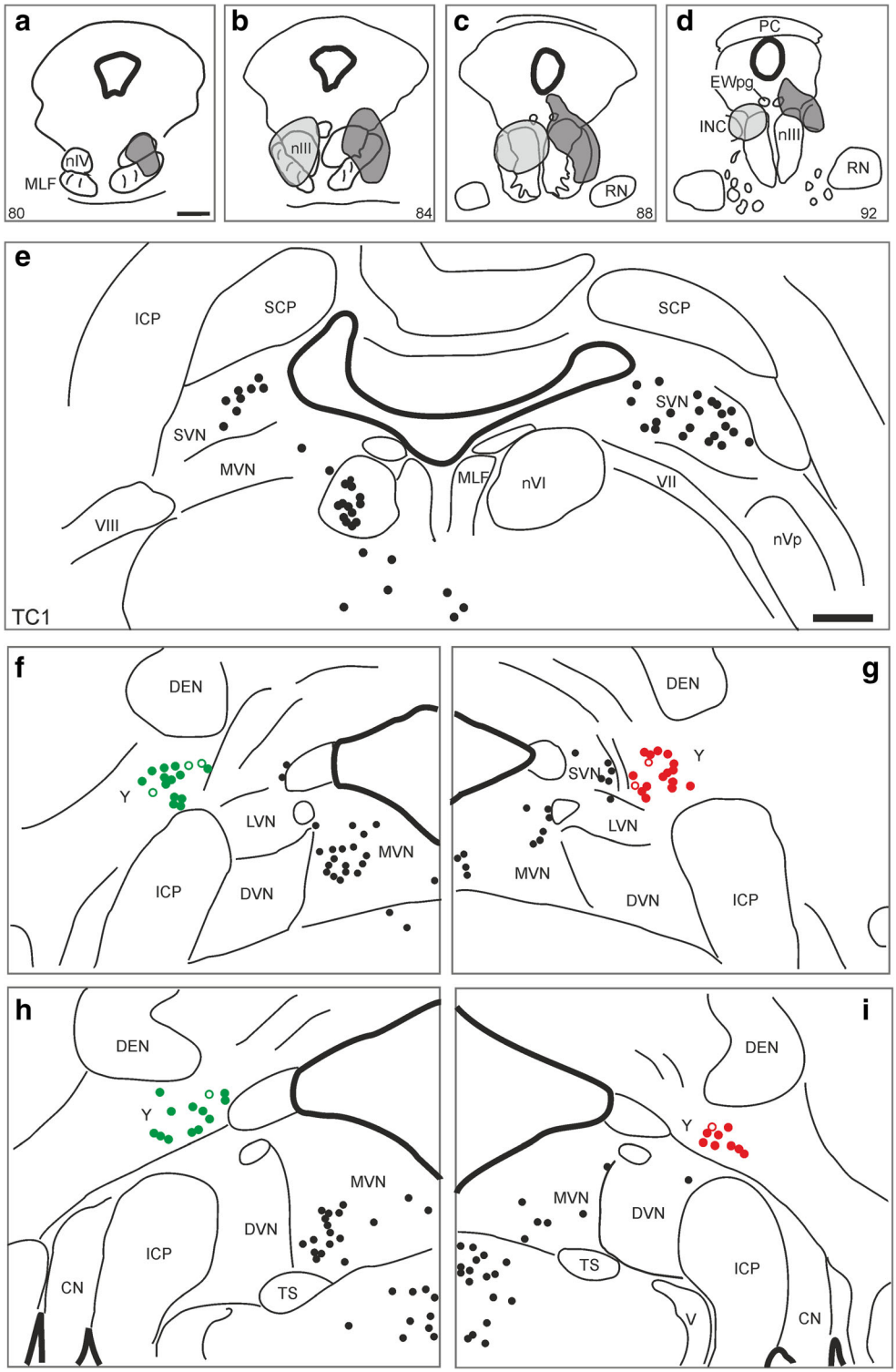

compromises were made in choice of primary antibodies in combination with the secondary antibodies (with blue giving the poorest signal), dual immunofluorescence was performed using rabbit GAD and mouse CR antibodies only. These were detected with green and red fluorescing secondary antibodies (Fig. 5d–l). Both, CR- and GAD-positive neurons are intermingled in Yd (Fig. 5d–f; thin and solid arrows, respectively) and both populations receive a similar dense supply by GAD-positive boutons (Fig. 5h–l). Few neurons did not express any of the markers (Fig. 5k, l, asterisk) and may represent a different neuron population. One further small population of cholinergic neurons was found with ChAT-

◀ **Fig. 2** Demonstration of the tracer injection sites for two cases drawn in one series of sections through the oculomotor nucleus (nIII) region, on the left side for WGA (TC2, light grey), on the right side for CTB (TC1, dark grey) (**a**–**d**). A series of frontal sections through the medulla demonstrates the analysis of the retrogradely labelled neurons in the Y-group (Y) of the case with the unilateral CTB-injection into the right nIII. The green closed circles indicate calretinin (CR)-positive tracer–labelled neurons, the open circles CR-negative ones in Y. The red closed circles represent glutamate decarboxylase (GAD)—positive neurons, the open circles could not be judged (**f**–**i**). The black dots in all sections of **e-i** indicate tracer-labelled neurons not analysed for CR or GAD-immunoreactivity. CN, cochlear nucleus; DEN, dentate nucleus; DVN, descending vestibular nucleus; EWpg, preganglionic Edinger-Westphal nucleus; ICP, inferior cerebellar peduncle; INC, interstitial nucleus of Cajal; LVN, lateral vestibular nucleus; MVN, medial vestibular nucleus; MLF, medial longitudinal fascicle; nIV, trochlear nucleus; nVI, abducens nucleus; nVp, principal trigeminal nucleus; PC, posterior commissure; RN, red nucleus; SVN, superior vestibular nucleus; SCP, superior cerebellar peduncle; TS, nucleus of the solitary tract; V, trigeminal nerve; VII, facial nerve; VIII, vestibular nerve; Scale bar = 1 mm in **a** (applies to **a**–**d**), 1 mm in **e** (applies to **e**–**i**)

immunostaining (Fig. 5c). These small ChAT-positive neurons had mean diameters of 15 μm, clearly different from the larger-sized premotor neurons (see Fig. 4). In addition, numerous ChAT-positive varicosities were found in close contact to medium-sized neurons in Yd (Fig. 5c, asterisk, arrows). A comparative triple-immunofluorescence staining revealed a strong coexpression of calbindin (CB) in GAD-positive boutons around neurons in the dentate nucleus (Fig. 5r–u, arrows), which was less pronounced in GAD-positive terminals attached to putative premotor neurons in Yd identified by PNs (revealed with HPLN antibodies) (Fig. 5m–q, arrows).

Expression of Potassium Channels

In order to investigate the different neuronal populations in Yd for the expression of the potassium channels Kv1.1 and Kv3.1b, neighbouring thin 5 μm sections stained for either CR and ACAN, GAD and CR or Kv1.1 or Kv3.1b were analysed. Virtually, all CR-positive and GAD-positive neurons ensheathed by ACAN-based PNs expressed moderate to strong Kv1.1 immunoreactivity appearing as granular staining within the cytoplasm of the soma and proximal dendrites (Fig. 6a, b, c, arrows, e). Several neurons were visible in all neighbouring sections and allowed the additional analysis for Kv3.1b expression, which was present in all CR- and GAD-positive neurons with PNs (Fig. 6a, c, d, arrows). Unlike Kv1.1, the Kv3.1b immunoreactivity appeared as faint staining of the somata but was concentrated in the cell membrane as seen before (Fig. 6e, f) [38]. No obvious differences in the staining intensity for Kv1.1 or Kv3.1b was observed between CR-positive and GAD-positive neurons ensheathed by PN (compare Fig. 6 a with b and d). Similarly, neighbouring sections of putative secondary vestibulo-ocular neurons in the magnocellular portion of the medial vestibular nucleus (MVN) identified by PN and NPNF-expression were analysed [29]. As for Yd, all putative secondary vestibulo-ocular neurons showed immunostaining for Kv1.1 and Kv3.1b (Fig. 6g–i, arrows). The reliability of Kv immunostaining was validated in the cerebellum. GABAergic Purkinje cells show moderate Kv1.1-staining of the cell bodies, but strong staining of the pinceau, a meshwork of GABAergic terminals of basket cells associated with the axonal initial segment of Purkinje cells [39] (Fig. 6k, arrow). Only very weak Kv3.1b staining was present in the Purkinje cell, but strong immunoreactivity was expressed in the granular and molecular layers as reported before (Fig. 6l) [40]. In addition, strong Kv1.1 staining was observed in small cells, which were also distributed in the fibre tracts passing to the cerebellum, most likely representing glial cells (Fig. 6b, arrowhead).

Discussion

The present study provides a histochemical characterization of neurons within the Yd that project to motoneurons of vertically pulling extraocular muscles with following main findings: The Yd contains two sets of projection neurons, excitatory CR-positive neurons projecting contralaterally, and an inhibitory GABAergic, but CR-negative population projecting ipsilaterally. Otherwise both populations show similar characteristics, including a strong GABAergic input, expression of nonphosphorylated neurofilaments (NPNF), wrapping with perineuronal nets, and a strong immunoreactivity for the voltage-gated potassium channels Kv1.1 and Kv3.1b. Similar histochemical profiles were found for secondary vestibulo-ocular neurons.

Identified Cell Populations in Yd

CR- and GAD-Positive Premotor Neurons

A strong projection from the Yd to the oculomotor nucleus (nIII) is known from tract-tracing experiments in different species [7, 14, 23–25]. In deviation to previous findings, the present study revealed a CR-positive projection exclusively to the contralateral side [27]. The small fraction of tracer-labelled CR-positive neurons also in the ipsilateral Yd side in the previous study is attributed to tracer spread across the midline at the injection site, which did not occur in cases of the present work. A new finding was the demonstration of an ipsilateral GABAergic projection to the motonuclei. The lack of CR and GAD coexpression in the cell bodies of Yd goes along with the lack of coexpression of both proteins in synaptic terminals targeting upgaze motoneurons [26]. Accordingly, CR- and GAD-positive neurons form two

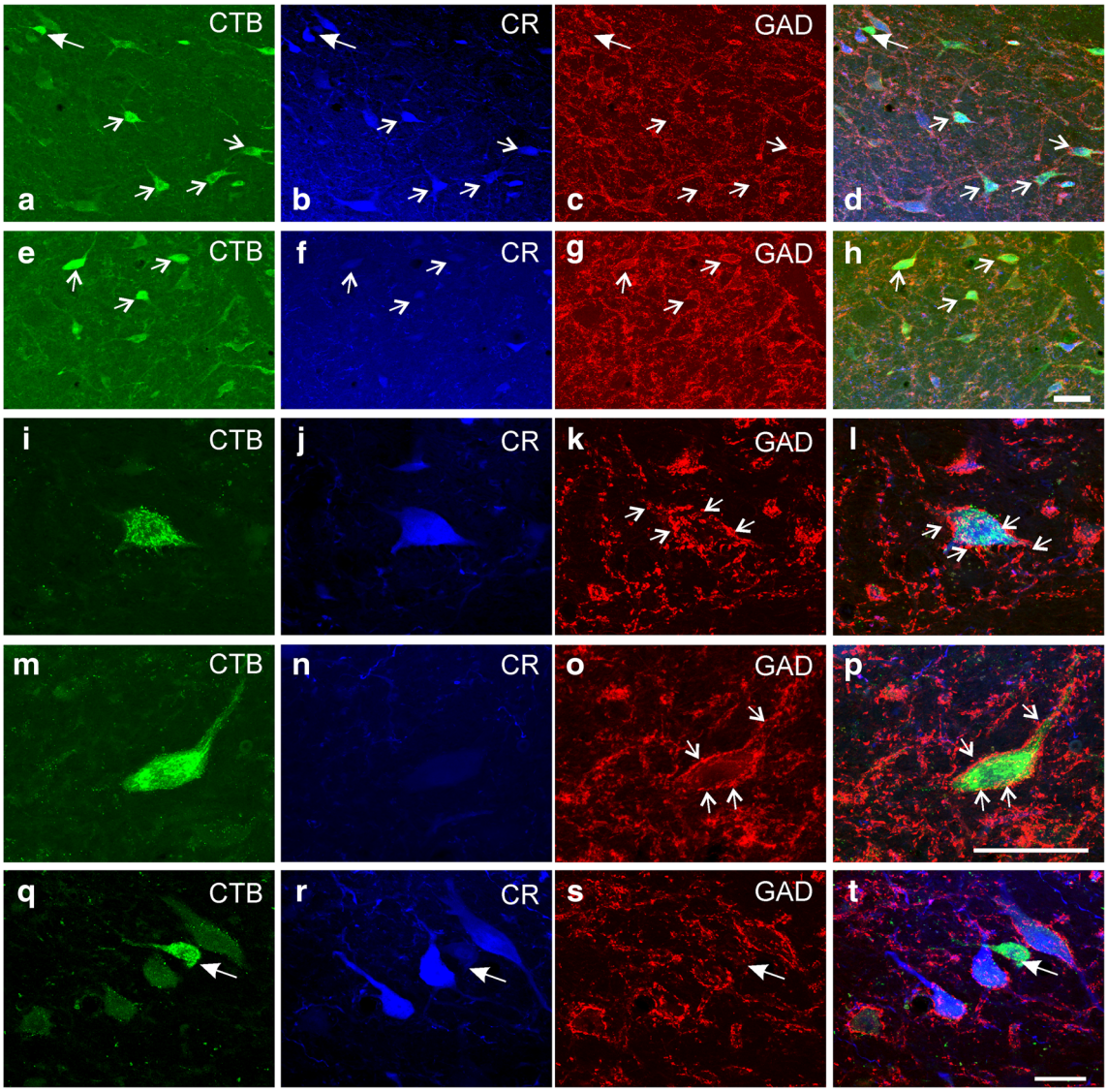

Fig. 3 **a**–**h** Overview confocal images of double-immunofluorescence staining for cholera toxin subunit B (CTB) combined with the detection of calretinin (CR) and glutamate decarboxylase (GAD) in frontal sections through the dorsal Y-group of a monkey (TC1) who had received a unilateral tracer injection into the right oculomotor nucleus. **a**–**d** shows the staining for the contralateral side, **e**–**h** for the ipsilateral side. Note that almost all retrogradely labelled neurons (**a**, green) contain CR (**b**, blue), but not somatal GAD immunostaining (**c**, red). The arrows indicate examples of CR-positive and GAD-negative tracer-labelled neurons appearing cyan in the overlay (**d**) (**a**–**c**, small arrows). A small number of tracer-labelled neurons were found that did neither express CR nor GAD (solid arrow in **a**–**d**). On the contrary, none of tracer-labelled neurons in the ipsilateral Yd express CR (**e**, **f**, **h** arrows) but show somatal GAD-immunostaining (**g**, arrows). Detailed view of a CR-positive tracer-labelled neuron (from **a**) in the contralateral Yd, which does not express GAD in the cell body, but numerous GAD-boutons outlining the cell body (**i**–**l,** arrows). Detailed view of a CR-negative tracer-labelled neuron (from **e**) in the ipsilateral Yd with moderate GAD-immunoreactivity of the cell body also outlined by GAD-positive boutons (**m**–**p**, arrows). Detail of a tracer-labelled neuron in the contralateral Yd (from **a**) that does neither express CR nor GAD within the cell body (arrow, **q**–**t**). Scale bar = 100 μm in **h** (applies to **a**–**h**), 50 μm in **p** (applies to **i**–**p**), 50 μm in **t** (applies to **q**–**t**)

independent populations in Yd, and the following assumption can be made: CR-positive neurons in Yd represent excitatory premotor neurons that may use glutamate as transmitter [8] and project through the crossing ventral tegmental tract (CVTT) to target the twitch and non-twitch motoneurons of the inferior oblique (IO) and superior rectus muscles (SR) in the contralateral nIII [14, 27, 41] and S-group [42]. This is consistent with stimulation experiments of the Y-group resulting in slow upward movements of both eyes [1] and with EPSPs in SR and IO motoneurons in contralateral nIII [43]. Similarly, recording in Yd showed an increase in firing rates during upward eye movements, with the neurons discharging in relation to upward head and eye velocity [1].

Accordingly, the GAD-positive tracer–labelled neurons must be considered as GABAergic premotor neurons, whose

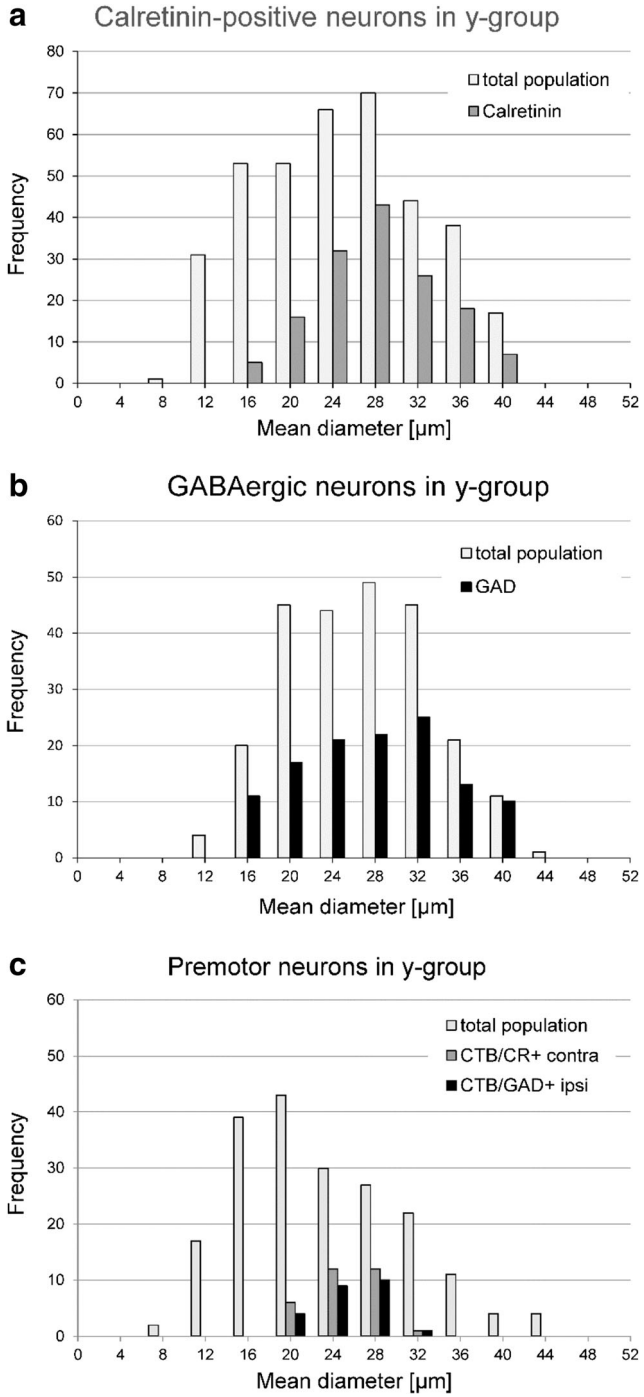

Fig. 4 Cell size histogram of the calretinin (CR)- (**a**) and GAD-positive neurons (**b**) within the total neuron population in the dorsal Y-group (Yd) revealed from Nissl-stained sections. There is no clear indication for a bimodal population, but cell sizes range from small mean diameters of 10 µm to large cells with mean diameters of more than 40 µm. CR- and GAD-positive neurons cover almost the complete spectrum except neurons smaller than 16 µm. The lower panel shows the cell sizes of tracer-labelled CR- and GAD-positive neurons in Yd, which involve similar populations of medium-sized neurons.

axons travel in the brachium conjunctivum (BC) to inhibit the motoneurons of the inferior rectus (IR) and superior oblique muscle (SO) motoneurons on the ipsilateral side during upgaze. The presence of GABA- or GAD-positive neurons in Yd was demonstrated before but was not correlated with premotor neurons [8, 44, 45]. Thereby the present study provides the anatomical basis for the findings of recording and stimulation experiments in Yd [1] and demonstrates a similar organization of crossing excitatory projections and ipsilateral inhibitory projections to respective motoneuronal groups as for the vestibulo-ocular projections of the anterior semicircular canals [8].

Nonpremotor Neurons in Yd

Smaller tracer-negative GAD–positive neurons in Yd may include projection neurons to the rostral dorsal cap and ventrolateral outgrowth of the contralateral inferior olive shown in rabbit with combined tracer labelling and EM analysis [46]. This projection does not arise from oculomotor projecting neurons as shown by double tracer injections in rat and rabbit, but both populations are intermingled within Yd [47] (Fig. 7).

Our finding of few primarily small ChAT-positive neurons in the Yd is consistent with other reports [48]. These cholinergic neurons differ clearly in size and morphology from those in the adjacent BIN, which coexpress GABAergic markers and send projections to the flocculus [36, 48]. It is not clear, whether ChAT-positive neurons within the Yd represent local interneurons giving rise to the abundant network of ChAT-positive nerve fibres and varicosities found in the Yd neuropil (see Fig. 5c), or whether they are projection neurons.

GABAergic Input to Y-Group Neurons

Anterograde tract tracing, stimulation and recording studies in monkey and cat had shown a strong projection from floccular Purkinje cells to Yd [21, 22, 49]. The covering of all tracer-labelled neurons in Yd with GAD-positive terminals, which show strong coexpression of calbindin (Fig. 5m–q, insert) expressed by Purkinje cells [50], is consistent with the expected strong GABAergic input from floccular Purkinje cells. This confirms that all premotor neurons in Yd are ‘floccular target neurons’ (FTN) consistent with electrophysiological studies in cat, which demonstrated that all identified FTNs in Yd could be antidromically activated from stimulation of the contralateral nIII [49]. But unlike FTNs in the SVN, which represent secondary vestibulo-oculomotor neurons, FTNs of the Yd are not directly targeted by primary vestibular afferents. They rather receive an indirect input via interneurons in the SVN and MVN that are activated from afferents of the anterior and posterior semicircular canals (see Fig.7) [19]. Lesions of

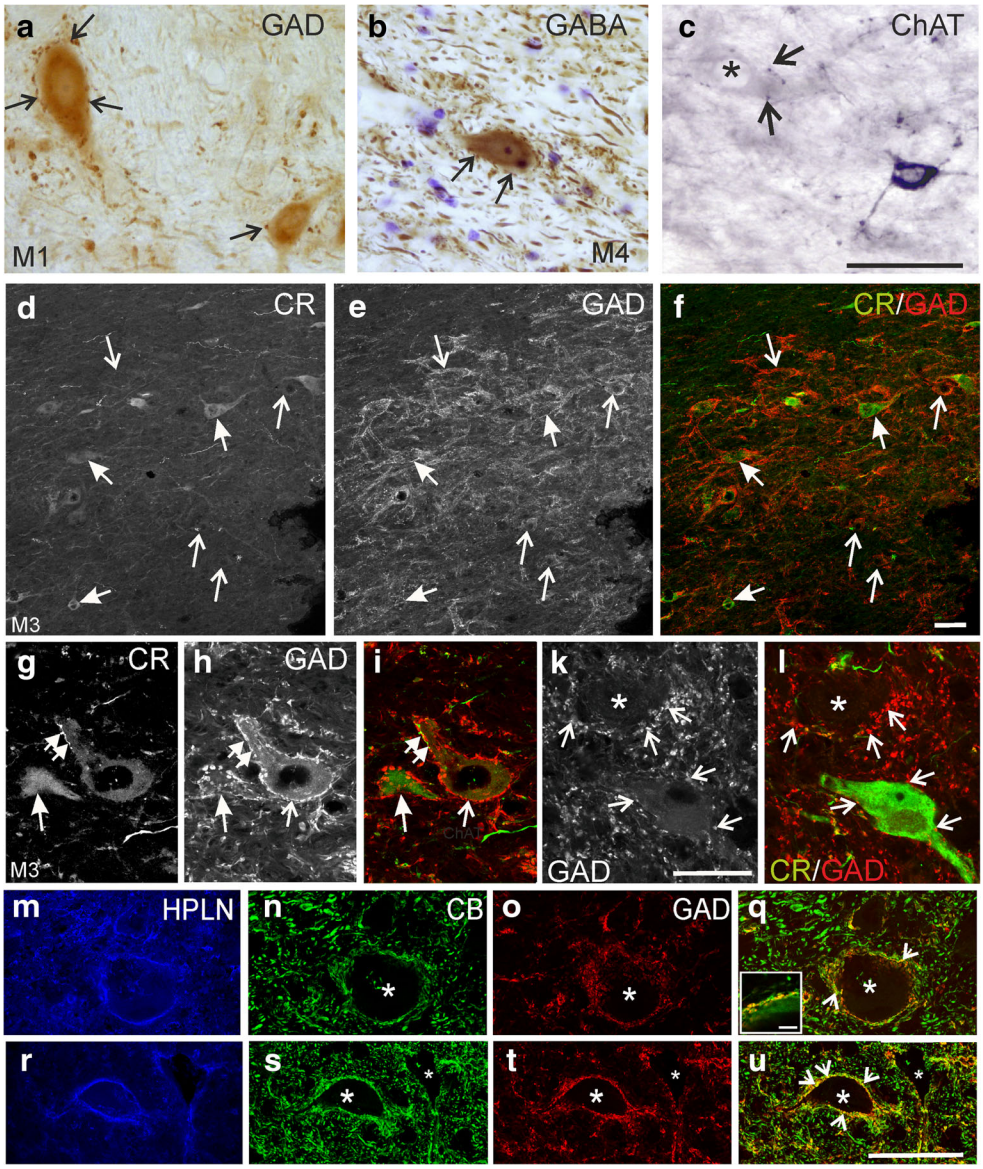

Fig. 5 Detailed view of the dorsal Y-group (Yd) with medium-sized glutamate decarboxylase (GAD)-positive neurons (**a**, arrows) detected with a sheep antibody in thick sections. Detailed view of a medium-sized GABA-positive neuron in Yd that is contacted by GABA-positive punctate profiles (**b**, arrows). The section is counterstained with cresyl violet. Detailed view of a small ChAT-positive neuron in the Yd (**c**). Note the numerous stained axons with varicosities (arrows), some of them in close contact with ChAT-negative medium-sized neurons (asterisk). **d**–**l** Double immunostaining with rabbit CR and mouse GAD antibodies in the Yd of case M3. **d**–**f** CR-positive (solid arrows) and GAD-positive (open arrows) represent independent neuron populations without coexpression of both antigens. **g**–**h** Confocal images of detailed views reveal that CR-positive (**g**; solid arrow) as well as GAD-positive neurons (**h**; thin arrow) are associated with numerous GAD-positive boutons (**h**, **i**; small arrows). Note that all GAD-positive boutons do not coexpress CR (**g**–**i**, double arrows). **k**, **l** Some small neurons within Yd outlined by GAD-positive puncta (arrows) lack CR and GAD in their somata (**k**, **l**; asterisk). **m-q** Confocal images of putative premotor neurons in Yd ensheathed by perineuronal nets stained with antibodies against hyaluronan and proteoglycan link protein 1 (HPLN) in Yd (**m**) combined with calbindin (CB) (**n**) and GAD (**o**). **r-u** In comparison, a neuron of the dentate nucleus is shown with similar staining. Note that neurons in both nuclei (asteriks) receive a strong supply by GAD-positive boutons many coexpressing CB, appearing in yellow in the overlays (**o**, **u**, arrows) as seen in bottom left box (**q**) detail picture of membrane. These boutons most probably originate from CB-positive Purkinje cells. The coexpression is stronger in the dentate nucleus. Scale bar = 50 μm in **c** (applies to **a**–**c**); 50 μm in **f** (applies to **d**–**f**), 50 μm in **l** (applies to **g**–**l**); 50 μm in **u** (applies to **m**–**u**), 5 μm in insert of **q**

the cerebellar loop through the flocculus may cause spontaneous upward drifts and compensating fast downward phases seen in downbeat nystagmus [3, 5]. Since 90% of floccular Purkinje cells have downward on directions, but almost none upward [21], the removal or malfunction of floccular Purkinje cells may induce an increased activity of FTNs in the Yd and SVN, which results in upward drifts of the eyes [5].

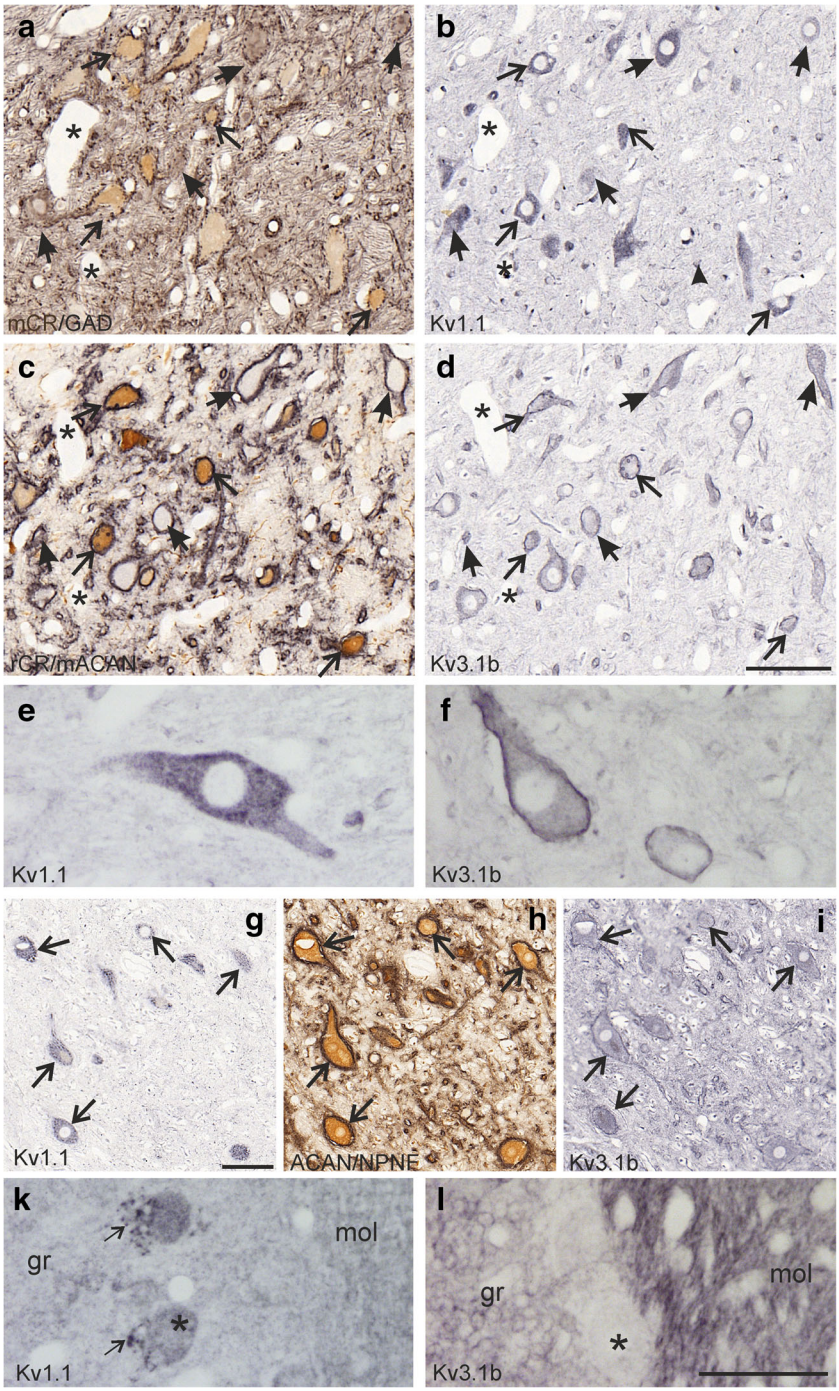

Fig. 6 **a**–**d** Detailed views of four neighbouring paraffin sections (5 μm) through the Y-group (Yd) stained with immunoperoxidase methods for the simultaneous detection of calretinin (CR) in brown and glutamate decarboxylase (GAD) in black (**a**) or CR (brown) and aggrecan (ACAN, black) (**c**), or for the potassium channels Kv1.1 (**b**) or Kv3.1b (**d**) of case PF3. All CR- (**a**, **c**, thin arrows) and GAD-positive (**a**, solid arrows) neurons are ensheathed by ACAN-based perineuronal nets (**c**, black, thin and solid arrows), and they expressed moderate to strong Kv1.1- (**b**, arrows) and Kv3.1b-immunoreactivity (**d**, arrows). In **a**–**d** thin arrows indicate CR-positive neurons, short solid arrows putative GABAergic neurons. **e** Detail of a Kv1.1- positive neurons within Yd showing the more granular staining of the soma and proximal dendrites. **f** Detail of a Kv3.1b-positive neurons demonstrating the faint soma labelling but strong labelling of the outer cell membrane. **g**–**i** Detailed views of neighbouring paraffin sections of the magnocellular medial vestibular nucleus with putative secondary vestibulo-ocular neurons identified by their expression of nonphosphorylated neurofilament (NPNF) and perineuronal nets (ACAN) in black (**h**) (case PF2). Note that all putative vestibulo-ocular neurons express Kv1.1 and Kv3.1b (**g-i-**, arrows) as the premotor neurons in Yd **(b-d**, arrows). **k** Detailed view of the cerebellar cortex stained for Kv1.1 and Kv3.1b. Note the strong Kv1.1. expression in the pinceau (arrow) at Kv1.1-positive Purkinje cells (asterisk). **l** Detail of cerebellar cortex stained for Kv3.1b. Weak Kv3.1b-immunoreactivity is present in Purkinje cells (asterisk), but strong labelling is found in the molecular (mol) and granular layer (gr). Scale bar = 100 μm in **d** applies to **a**–**d**; 50 μm in **l** (applies to **e**, **f**, **k**, **l**); 100 μm in **g** (applies to **g**–**i**)

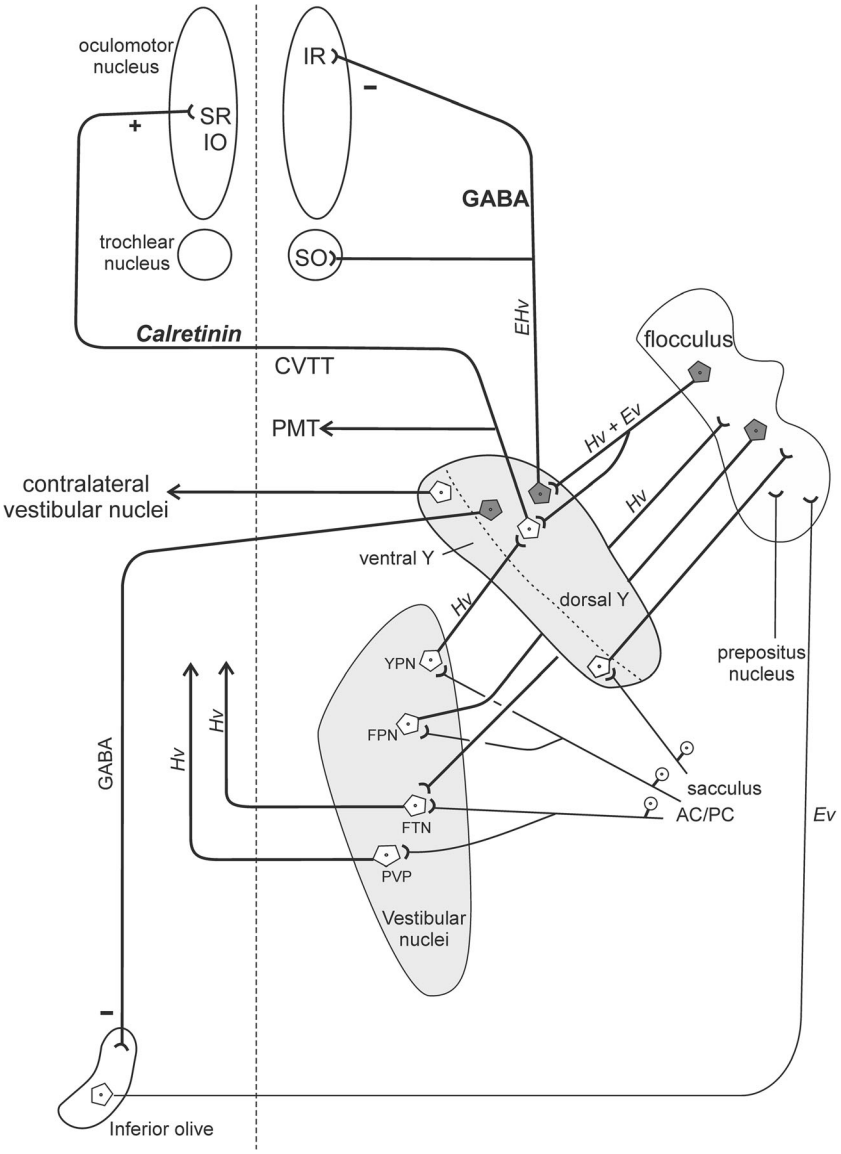

Fig. 7 Summary diagram demonstrating the major connections of the Y-group: The dorsal Y-group (Yd) contains excitatory calretinin-positive neurons that target upgaze motoneurons in the contralateral oculomotor nucleus and GABAergic inhibitory neurons that project to downgaze motoneurons ipsilateral that may sent off projections to the paramedian tract neurons (PMT) - only drawn for the excitatory path. Both populations receive a strong GABAergic input from the flocculus. Via 'Y-projecting interneurons' (YPN) in the superior vestibular nucleus, the premotor neurons receive an input from the vertical semicircular canals. Floccular-projecting neurons (FPN) form another separate population that gives off collaterals to the Y-group or YPNs. In the vestibular nuclei floccular-target neurons (FTN) and position-vestibular-pause neurons (PVP) transmit head velocity signals to the motonuclei via the vestibulo-ocular reflex. Visual input is relayed to the flocculus by climbing fibres from the inferior olive and mossy fibres from the prepositus nucleus and nucleus reticularis tegmenti pontis. CVTT, crossing ventral tegmental tract, Ev eye velocity; Hv, head velocity; IR, inferior rectus muscle; IO, inferior oblique muscle; SO, superior oblique muscle; SR, superior rectus muscle

Significance of Histochemical Properties of Yd Neurons

Neurofilaments

As secondary vestibulo-oculomotor neurons in the MVN and SVN the premotor neurons in Yd contain nonphosphorylated neurofilaments (NPNF) [27, 57, 29], which shape the somatic and dendritic cytoskeleton [51]. It is present in specific neuronal populations including highly active neurons of the eye movement system, e.g. omnipause neurons, saccadic burst neurons and eye muscle motoneurons [38, 52]. Due to the lack of NPNF in local interneurons, it was assumed that NPNF may contribute to long-distance projections [53]. More recent findings suggest a correlation with the amount of axonal myelination [54] rather than axonal length only.

Perineuronal Nets

As other functional neurons of the oculomotor system excitatory CR- and inhibitory GAD–positive neurons in Yd are wrapped by well-developed PNs also previously found in human [30, 55, 56]. PNs are lattice-like aggregates of extracellular matrix molecules with holes at synaptic contact sites [57], which ensheath distinct highly active neurons, which often contain the calcium-binding protein parvalbumin and the voltage-gated potassium channel Kv3.1b. One assumed function of PNs is a role as cation buffer [55, 58]. The expression of well-developed PNs with concomitant Kv3.1b expression in FTNs is in accordance with high spontaneous firing rates of 80–110 spikes/s recorded in squirrel monkey that are upregulated during upgaze [59]. As additional and intriguing hypothesis, PN may contribute to motor learning/adaptation of the VOR (by gain changes after wearing minimizing or magnifying googles), which is compatible with the adaptive properties of FTNs in Yd [4, 60, 61]. There is accumulating evidence that the formation of PNs does not only restrict plasticity at the end of the critical periods during postnatal development [62–64], but may also participate in the control of regained plasticity of neurons involved in adaptive processes like vestibular compensation [65]. After unilateral labyrinthectomy in adult mice, the frequency of PNs and staining intensity was strongly diminished in the lateral vestibular nuclei (mostly involved in posture), in parallel with an increase of excitatory and inhibitory synapses in the lateral vestibular nuclei of both sides. After recovery from vestibular deficits, PNs were completely restored, and in mice with genetically defective PN, vestibular compensation was accelerated [65]. The chemorepulsive protein Sema3A found as an integral component in a subset of PNs including those around neurons in the vestibular nuclei neurons may contribute to the PN mediated plasticity [66].

Voltage-Gated Potassium Channels Kv3.1b and Kv1.1

Alongside their role in regulating plasticity, PNs are thought to facilitate firing characteristics of fast-firing neurons via regulating expression of voltage-gated potassium channels and their localization to cell membrane [67]. Accordingly, Kv1.1 and Kv3.1b subunits form complexes with PN proteins [67]. Whereas low voltage-activated Kv1 channels regulate the resting membrane potential, threshold potential and neuronal excitability [68], high voltage activated Kv3 channels open during action potentials, actively shortening the spike duration and enabling maintained and high firing rates [69]. Together, Kv1 and Kv3 channels cooperate with Nav channels for action potential generation in highly active fast spiking neurons such as in auditory, vestibular and oculomotor systems in brainstem [38, 70]. Kv1.1 and Kv3.1b channels were similarly expressed in both, excitatory and inhibitory premotor FTNs in Yd as in secondary vestibulo-ocular neurons in the MVN. This observation suggests similar and fast firing properties for GAD-positive and CR-positive subpopulations and is in line with uniform firing patterns of Yd neurons [4]. Located between floccular Purkinje cells and oculomotor nucleus, FTNs in Yd exhibit histochemical and biophysical similarities to vestibulo-ocular neurons in vestibular nuclei—rather than to Purkinje cells (Fig. 6k, l) [38, 70].

Proposed Circuitry

In the absence of a desired gaze shift (and Yd modulation of gaze), the eye and head movements are driven by the vestibulo-ocular reflex (VOR). A simplified model for the brainstem control of eye movements includes the direct 3-neuron VOR pathway from the vestibular afferents running in the 8th nerve, the secondary vestibular neurons in the vestibular nuclei and the motoneurons of extraocular muscles in the motonuclei (Fig. 7) [71]. Parallel indirect pathways loop through the flocculus, which include floccular-projecting neurons (FPN) in the vestibular nuclei and the ventral Y-group, both receiving direct primary afferents from vertical semicircular canals and sacculus, respectively, and projections back from the flocculus to ‘floccular target neurons’ (FTN) in the SVN and Yd. FTNs in Yd receive disynaptic excitatory signals (head velocity) from the ipsilateral vertical semicircular canals via interneurons in the anterior-lateral corner of the SVN (and MVN) [19], which are transmitted via crossing direct excitatory CR-positive and ipsilateral GABAergic projections to upgaze and downgaze motoneurons, respectively. Head-velocity signals from anterior and posterior semicircular canals reach the FTN in Yd via interneurons in the SVN (and MVN) [19]. Eye-velocity signals to Yd neurons are transmitted through the flocculus, which receives visual input via climbing fibres from the inferior olive (input from the nucleus of the optic tract) and mossy fibres (from the nucleus prepositus hypoglossi) [21, 72]. Thereby, the FTNs in the Yd transmit eye and head velocity signals to the extraocular muscles inducing upward ocular following movements. Accordingly, during pursuit Purkinje cells (mainly of the paraflocculus) provide the eye movement signal to premotor neurons, and during VOR cancellation (from flocculus) the head velocity signal via the FTNs in Yd necessary to cancel the VOR drive to motoneurons. Lesions of these circuits can result in nystagmus [3, 5].

Conclusion

Two histochemically different populations of premotor neurons projecting to the nIII were identified in Yd: The CR-positive population represents the excitatory projection to contralateral upgaze motoneurons, whereas the GAD-positive

population represents the inhibitory projection to ipsilateral downgaze motoneurons. Both populations receive a strong GABAergic input from floccular Purkinje cells indicating that all premotor neurons in Yd represent FTNs. Aside from their differing content of CR and transmitters, both premotor cell groups form a homogenous population with similar histochemical characteristics compatible with fast-firing properties, e.g. PNs and Kv channels, which were also found for secondary vestibulo-ocular neurons. The presence of well-developed PNs may also contribute to the mechanism of their adaptive capacity. The histochemical signature of premotor neurons in Yd allows the identification of the homologue cell groups in human including their inputs and will serve as basis for correlated anatomical-neuropathological studies of clinical cases with downbeat nystagmus, which is often associated with lesions of the vestibulocerebellum [3, 73]. Accordingly, the CR-positive neurons ensheathed by PN in the human Y-group most likely represent the excitatory premotor neurons targeting upgaze motoneurons in nIII [56, 74], but the pattern of GABAergic neurons and terminals as well as the ion channel expression pattern has to be studied in the future.

Acknowledgments The authors thank Prof. Jens Waschke for his continuous support. The excellent technical assistance of Christine Unger and Ahmed Messoudi is acknowledged.

Funding Open Access funding enabled and organized by Projekt DEAL. This study was funded by a grant from the Deutsche Forschungsgemeinschaft (Ho 1639/5-1), the BMBF (IFB/LMU-01E0901), and The Graduate School of Systemic Neurosciences (GSN-LMU) - LMU Munich.

Compliance with Ethical Standards

Conflict of Interest The authors declare that they have no conflict of interest.

References

1. Chubb MC, Fuchs AF. Contribution of y group of vestibular nuclei and dentate nucleus of cerebellum to generation of vertical smooth eye movements. J Neurophysiol. 1982;48:75–99.
2. Blazquez PM, Davis-Lopez de Carrizosa M, Heiney SA, Highstein SM. Neuronal substrates of motor learning in the velocity storage generated during optokinetic stimulation in the squirrel monkey. J Neurophysiol. 2007;97:1114–26. https://doi.org/10.1152/jn.00983.2006.
3. Leigh RJ, Zee DS. The neurology of eye movements. Oxford. Oxford University Press; 2015.
4. Partsalis AM, Zhang Y, Highstein SM. Dorsal Y group in the squirrel monkey. I. Neuronal responses during rapid and long-term modifications of the vertical VOR. J Neurophysiol. 1995;73:615–31.
5. Marti S, Straumann D, Büttner U. Glasauer S. A model-based theory on the origin of downbeat nystagmus. Exp Brain Res. 2008;188:613–31.
6. Goldberg JM, Wilson VJ, Cullen KE, Angelaki DE, Broussard DM, Büttner-Ennever JA, et al. The vestibular system. A sixth sense. Oxford: Oxford University Press; 2012.
7. Gacek RR. Location of brain stem neurons projecting to the oculomotor nucleus in the cat. Exp Neurol. 1977;57:725–49.
8. Highstein SM, Holstein GR. The anatomy of the vestibular nuclei. Prog Brain Res. 2006;151:157–203.
9. Büttner-Ennever JA, Horn AKE. Olszewski and Baxter's cytoarchitecture of the human brainstem. Basel, Freiburg: Karger; 2014.
10. Gacek RR. The course and central termination of first order neurons supplying vestibular end organs in the cat. Acta Otolaryngol. 1969;254:1–66.
11. Kevetter GA, Perachio AA. Distribution of vestibular afferents that innervate the sacculus and posterior canal in gerbil. J Comp Neurol. 1986;254:410–24.
12. Carleton SC, Carpenter MB. Distribution of primary vesibular fibers in the brainstem and cerebellum of the monkey. Brain Res. 1984;294:281–98.
13. Gacek RR. Location of commissural neurons in the vestibular nuclei of the cat. Exp Neurol. 1978;59:479–91.
14. Carpenter MB, Cowie RJ. Connections and oculomotor projections of the superior vestibular nucleus and cell group 'y'. Brain Res. 1985;336:265–87.
15. Pompeiano O, Mergner T, Corvaja N. Commissural, perihypoglossal and reticular afferent projections to the vestibular nuclei in the cat: an experimental anatomical study with horseradish peroxidase. Arch Ital Biol. 1978;116:130–72.
16. Horn AKE. Neuroanatomy of central vestibular connections. In: The Senses. Amsterdam: Elsevier; 2020. https://doi.org/10.1016/B978-0-12-805408-6.23911-0.
17. Nagao S, Kitamura T, Nakamura N, Hiramatsu T, Yamada J. Differences of the primate flocculus and ventral paraflocculus in the mossy and climbing fiber input organization. J Comp Neurol. 1997;382:480–98.
18. Langer TP, Fuchs AF, Scudder CA, Chubb MC. Afferents to the flocculus of the cerebellum in the rhesus macaque as revealed by retrograde transport of horseradish peroxidase. J Comp Neurol. 1985;235:1–25.
19. Blazquez P, Partsalis A, Gerrits NM, Highstein SM. Input of anterior and posterior semicircular canal interneurons encoding head-velocity to the dorsal Y group of the vestibular nuclei. J Neurophysiol. 2000;83:2891–904.
20. Blanks RHI, Precht W, Torigoe Y. Afferent projections to the cerebellar flocculus in the pigmented rat demonstrated by retrograde transport of horseradish peroxidase. Exp Brain Res. 1983;52:293–306.
21. Partsalis AM, Zhang Y, Highstein SM. Dorsal Y group in the squirrel monkey. II. Contribution of the cerebellar flocculus to neuronal responses in normal and adapted animals. J Neurophysiol. 1995;73:632–50.
22. Langer TP, Fuchs AF, Chubb MC, Scudder CA, Lisberger SG. Floccular efferents in the rhesus macaque as revealed by

autoradiography and horseradish peroxidase. J Comp Neurol. 1985;235:26–37.
23. Graybiel AM, Hartwieg EA. Some afferent connections of the oculomotor complex in the cat: an experimental study with tracer techniques. Brain Res. 1974;81:543–51.
24. Steiger HJ, Büttner-Ennever JA. Oculomotor nucleus afferents in the monkey demonstrated with horseradish peroxidase. Brain Res. 1979;160:1–15.
25. Sato Y, Kawasaki T. Organization of maculo-ocular pathways via y-group nucleus and its relevance to cerebellar flocculus in cats. Physiologist. 1987;30:S77–80.
26. Zeeh C, Hess BJ, Horn AKE. Calretinin inputs are confined to motoneurons for upward eye movements in monkey. J Comp Neurol. 2013;521:3154–66.
27. Ahlfeld J, Mustari M, Horn AKE. Sources of calretinin inputs to motoneurons of extraocular muscles involved in upgaze. Ann N Y Acad Sci. 2011;1233:91–9.
28. Lienbacher K, Mustari M, Ying HS, Büttner-Ennever JA, Horn AKE. Do palisade endings in extraocular muscles arise from neurons in the motor nuclei? Invest Ophthalmol Vis Sci. 2011;52:2510–19.
29. McMillan A, Mustari M, Horn A. Identification of secondary vestibulo-ocular neurons in human based on their histochemical characteristics found in monkey. J Neurol. 2017;264:1–3. https://doi.org/10.1007/s00415-017-8397-z.
30. Horn AKE, Horng A, Buresch N, Messoudi A, Härtig W. Identification of functional cell groups in the abducens nucleus of monkey and human by perineuronal nets and choline acetyltransferase immunolabeling. Front Neuroanat. 2018;12:45. https://doi.org/10.3389/fnana.2018.00045.
31. Oertel WH, Schmechel DE, Mugnaini E, Tappaz ML, Kopin IJ. Immunocytochemical localization of glutamate decarboxylase in rat cerebellum with a new antiserum. Neuroscience. 1981;6:2715–35. https://doi.org/10.1016/0306-4522(81)90115-9.
32. Holstein GR, Martinelli GP, Degen JW, Cohen B. GABAergic neurons in the primate vestibular nuclei. Ann N Y Acad Sci. 1996;781:443–57.
33. Horn AKE, Helmchen C, Wahle P. GABAergic neurons in the rostral mesencephalon of the macaque monkey that control vertical eye movements. Ann N Y Acad Sci. 2003;1004:19–28.
34. Zeeh C, Mustari MJ, Hess BJM, Horn AKE. Transmitter inputs to different motoneuron subgroups in the oculomotor and trochlear nucleus in monkey. Front Neuroanat. 2015;9:95. https://doi.org/10.3389/fnana.2015.00095.
35. Holstein GR. The vestibular system. In: Mai JK, Paxinos G, editors. The human nervous system. Amsterdam: Elsevier; 2012. p. 1239–69.
36. Langer TP. Basal interstitial nucleus of the cerebellum: cerebellar nucleus related to the flocculus. J Comp Neurol. 1985;235:38–47.
37. Büttner-Ennever JA, Grob P, Akert K, Bizzini B. Transsynaptic retrograde labeling in the oculomotor system of the monkey with [125I] tetanus toxin BIIb fragment. Neurosci Lett. 1981;26:233–8.
38. Mayadali ÜS, Lienbacher K, Mustari M, Strupp M, Horn A. Potassium channels in omnipause neurons. Prog Brain Res. 2019;249:117–23.
39. Wang H, Kunkel DD, Martin TM, Schwartzkroin PA, Tempel BL. Heteromultimeric K+ channels in terminal and juxtaparanodal regions of neurons. Nature. 1993;365:75–9. https://doi.org/10.1038/365075a0.
40. Weiser M, Bueno E, Sekirnjak C, Martone M, Baker H, Hillman D, et al. The potassium channel subunit KV3.1b is localized to somatic and axonal membranes of specific populations of CNS neurons. J Neurosci. 1995;15:4298–314. https://doi.org/10.1523/jneurosci.15-06-04298.1995.
41. Stanton GB. Afferents to oculomotor nuclei from area "Y" in Macaca mulatta: an anterograde degeneration study. J Comp Neurol. 1980;192:377–85.
42. Wasicky R, Horn AKE, Büttner-Ennever JA. Twitch and non-twitch motoneuron subgroups of the medial rectus muscle in the oculomotor nucleus of monkeys receive different afferent projections. J Comp Neurol. 2004;479:117–29.
43. Highstein SM. Organization of the inhibitory and excitatory vestibulo-ocular reflex pathways to the third and fourth nuclei in rabbit. Brain Res. 1971;32:218–24.
44. Mugnani E, Oertel WH. An atlas of the distribution of GABAergic neurons and terminals in the rat CNS as revealed by GAD immunocytochemistry. In: Handbook of Chemical Neuroanatomy, vol. 4; 1985. p. 436–608.
45. Carpenter MB, Huang Y, Pereia AB, Hersh LB. Immunocytochemical features of the vestibular nuclei in the monkey and the cat. J Hirnforsch. 1990;31:585–99.
46. De Zeeuw CI, Gerrits NM, Voogd J, Leonard CS, Simpson JI. The rostral dorsal cap and ventrolateral outgrowth of the rabbit inferior olive receive a GABAergic input from dorsal group Y and the ventral dentate nucleus. J Comp Neurol. 1994;341:420–32.
47. Wentzel PR, Wylie DRW, Ruigrok TJH, de Zeeuw CI. Olivary projecting neurons in the nucleus prepositus hypoglossi, group y and ventral dentate nucleus do not project to the oculomotor complex in the rabbit and the rat. Neurosci Lett. 1995;190:45–8.
48. Jaarsma D, Blot FGC, Wu B, Venkatesan S, Voogd J, Meijer D, et al. The basal interstitial nucleus (BIN) of the cerebellum provides diffuse ascending inhibitory input to the floccular granule cell layer. J Comp Neurol. 2018;526:2231–56. https://doi.org/10.1002/cne.24479.
49. Sato Y, Kawasaki T. Target neurons of floccular caudal zone inhibition in Y-group nucleus of vestibular nuclear complex. J Neurophysiol. 1987;57:460–80.
50. Fortin M, Marchand R, Parent A. Calcium-binding proteins in primate cerebellum. Neurosci Res. 1998;30:155–68.
51. Sternberger LA, Sternberger NH. Monoclonal antibodies distinguish phorphorylated and non-phosphorylated forms of neurofilaments in situ. Proc Natl Acad Sci. 1983;80:6126–30.
52. Horn AKE, Adamcyzk C. Reticular formation - eye movements. Gaze and blinks. In: Mai JK, Paxinos G, editors. The human nervous system. Amsterdam: Elsevier; 2011.
53. Campbell MJ, Morrison JH. Monoclonal antibody to neurofilament protein (SMI-32) labels a subpopulation of pyramidal neurons in the human and monkey neocortex. J Comp Neurol. 1989;282:191–205. https://doi.org/10.1002/cne.902820204.
54. Kirkcaldie MTK, Dickson TC, King CE, Grasby D, Riederer BM, Vickers JC. Neurofilament triplet proteins are restricted to a subset of neurons in the rat neocortex. J Chem Neuroanat. 2002;24:163–71. https://doi.org/10.1016/S0891-0618(02)00043-1.
55. Horn AKE, Brückner G, Härtig W, Messoudi A. Saccadic omnipause and burst neurons in monkey and human are ensheathed by perineuronal nets but differ in their expression of calcium-binding proteins. J Comp Neurol. 2003;455:341–52.
56. Adamczyk C, Strupp M, Jahn K, Horn AKE. Calretinin as a marker for premotor neurons involved in upgaze in human brainstem. Front Neuroanat. 2015;9. https://doi.org/10.3389/fnana.2015.00153.
57. Celio MR, Blümcke I. Perineuronal nets - a specialized form of extracellular matrix in the adult nervous system. Brain Res Rev. 1994;19:1128–45.
58. Härtig W, Derouiche A, Welt K, Brauer K, Grosche J, Mäder M, et al. Cortical neurons immunoreactive for the potassium channel Kv3.1b subunit are predominantly surrounded by perineuronal nets presumed as a buffering system for cations. Brain Res. 1999;842:15–29.
59. Blazquez PM, Hirata Y, Highstein SM. Chronic changes in inputs to dorsal Y neurons accompany VOR motor learning. J

Neurophysiol. 2006;95:1812–25. https://doi.org/10.1152/jn.01061.2005.
60. Dulac S, Raymond JL, Sejnowski TJ, Lisberger SG. Learning and memory in the vestibulo-ocular reflex. Annu Rev Neurosci. 1995;441:18409–41.
61. Sekirnjak C, Vissel B, Bollinger J, Faulstich M, du Lac S. Purkinje cell synapses target physiologically unique brainstem neurons. J Neurosci. 2003;23:6392–8. https://doi.org/10.1523/JNEUROSCI.23-15-06392.2003.
62. Pizzorusso T, Medini P, Berardi N, Chierzi S, Fawcett JW, Maffei L. Reactivation of ocular dominance plasticity in the adult visual cortex. Science. 2002;298:1248–51. https://doi.org/10.1126/science.1072699.
63. Sorg BA, Berretta S, Blacktop JM, Fawcett JW, Kitagawa H, Kwok JCF, et al. Casting a wide net: role of perineuronal nets in neural plasticity. J Neurosci. 2016;36:11459–68. https://doi.org/10.1523/jneurosci.2351-16.2016.
64. van't Spijker HM, Kwok JCF. A sweet talk: the molecular systems of perineuronal nets in controlling neuronal communication. Front Integr Neurosci. 2017;11:33. https://doi.org/10.3389/fnint.2017.00033.
65. Faralli A, Dagna F, Albera A, Bekku Y, Oohashi T, Albera R, et al. Modifications of perineuronal nets and remodelling of excitatory and inhibitory afferents during vestibular compensation in the adult mouse. Brain Struct Funct. 2016;221:3193–209. https://doi.org/10.1007/s00429-015-1095-7.
66. de Winter F, Kwok JCF, Fawcett JW, Vo TT, Carulli D, Verhaagen J. The chemorepulsive protein Semaphorin 3A and perineuronal net-mediated plasticity. Neural Plast. 2016;2016:3679545. https://doi.org/10.1155/2016/3679545.
67. Favuzzi E, Marques-Smith A, Deogracias R, Winterflood CM, Sánchez-Aguilera A, Mantoan L, et al. Activity-dependent gating of parvalbumin interneuron function by the perineuronal net protein. Brevican Neuron. 2017;95:639–55.e10. https://doi.org/10.1016/j.neuron.2017.06.028.
68. Ovsepian SV, LeBerre M, Steuber V, O'Leary VB, Leibold C, Oliver DJ. Distinctive role of KV1.1 subunit in the biology and functions of low threshold K+ channels with implications for neurological disease. Pharmacol Therapeut. 2016;159:93–101. https://doi.org/10.1016/j.pharmthera.2016.01.005.
69. Johnston J, Forsythe ID. Kopp-Scheinpflug C. Going native: voltage-gated potassium channels controlling neuronal excitability. J Physiol. 2010;588:3187–200.
70. Kodama T, Gittis AH, Shin M, Kelleher K, Kolkman KE, McElvain L, et al. Graded coexpression of ion channel, neurofilament, and synaptic genes in fast-spiking vestibular nucleus neurons. J Neurosci. 2020;40:496–508. https://doi.org/10.1523/jneurosci.1500-19.2019.
71. Blázquez PM, Pastor AM. Cerebellar control of eye movements. In: Manto M, Schmahmann JD, Rossi F, Gruol DL, Koibuchi N, editors. Handbook of the cerebellum and cerebellar disorders. Dordrecht: Springer Netherlands; 2013. p. 1155–73.
72. Rambold H, Churchland A, Selig Y, Jasmin L, Lisberger SG. Partial ablations of the flocculus and ventral paraflocculus in monkeys cause linked deficits in smooth pursuit eye movements and adaptive modification of the VOR. J Neurophysiol. 2002;87:912–24. https://doi.org/10.1152/jn.00768.2000.
73. Bronstein AM, Miller DH, Rudge P, Kendall BE. Down beating nystagmus: magnetic resonance imaging and neuro-otological findings. J Neurol Sci. 1987;81:173–84.
74. Che Ngwa E, Zeeh C, Messoudi A, Büttner-Ennever JA, Horn AK. Delineation of motoneuron subgroups supplying individual eye muscles in the human oculomotor nucleus. Front Neuroanat. 2014;8:2. https://doi.org/10.3389/fnana.2014.00002.

Discussion

The work presented here introduces ion channel and transmitter-related profiling to various neuronal groups with different functions in the oculomotor system of monkey concerning their diverse firing patterns. Although these initial findings cannot yet be considered as a full-fledged library of ion channel and transmitter profiling that illuminates the differentiators of the firing patterns in neurons within the oculomotor system, differences already found on the motor or premotor levels proved promising (Figure 12; Table 1).

Numerous studies in the literature aim at profiling the required machinery determining different firing patterns between various nuclei, and even between subpopulations within one nucleus (Kodama *et al.*, 2020). These studies take advantage of model organisms that allow for multiple research methodologies such as electrophysiology, protein and mRNA quantification and anatomical classification. These techniques can be utilized simultaneously in order to causally bind certain combinations of cellular expression patterns and transmitter content to the observed functional outcome. Although the conclusions drawn from these approaches serve as an important foundation for the research conducted here, there are limitations regarding the translation of the observations from mouse/rat to rhesus monkey and ultimately to human tissue specimen. These issues are mainly two-fold: Firstly, monkey as an experimental organism practically does not allow for an easy combinatorial use of these methods. Despite valuable research describing electrophysiological properties of different neuron types of the oculomotor circuitry in living animals, the combination of these approaches with pharmacology, gene profiling and single unit recording is simply unattainable. Secondly, as the direction of this research aims toward the characterization of alterations in ion channel and transmitter profiles as a potential cause of many eye movement disorders in human pathologies, these approaches would ultimately prove fruitless. Therefore, this thesis aimed at providing an approach that could connect histochemical profiling of neurons in the oculomotor system with their function in post-mortem fixed human brainstem tissue.

The work presented in this thesis achieved building an initial bridge between the histochemistry and electrophysiology of different neuron types of the oculomotor circuitry by demonstrating different ion channel and transmitter content of the functionally different subpopulations of motoneurons. This was demonstrated in the publication “Transmitter and ion channel profiles of neurons in the primate abducens and trochlear nuclei” by showcasing significant histochemical differences with respect to ion channel expression related to fast-firing of neurons between the motoneurons of multiply-innervated muscle fibers (MIF) and singly-innervated muscle fibers (SIF). Previously established anatomical, histochemical and physiological differences between MIF and SIF motoneurons and known properties of these ion channels enabled the identification of their physiological properties indirectly through histochemical methods. Furthermore, the histochemical characterization of premotor neurons was utilized to test hypotheses originating from the clinical data from which mathematical models were derived. In the publication “Saccadic premotor burst neurons and histochemical correlates of their firing patterns in

rhesus monkey", predictions of a neuromimetic model of saccade generation were confirmed regarding the ion channel profile of premotor burst neurons (BNs). These findings not only expanded the histochemical signature library of the neurons in the oculomotor system, but also demonstrated that the top-down mathematical modelling approach could be met with a bottom-up histochemical method to illuminate phenomena observed in clinical settings. Finally, I introduced ion channel profiling to a variety of neurons in the oculomotor system with different firing patterns. These neurons included the tonic firing omnipause neurons (OPNs) and Y-group neurons, burst/tonic firing motoneurons of the abducens and trochlear nuclei, bursting premotor neurons, and cerebellar Purkinje cells with their complex firing patterns. This was achieved as the long-term outcome of this thesis, covered by all of the presented publications; and overall, it paved the way to understanding the expression and immunolabeling patterns of ion channels in relation to distinct physiological characteristics of these neurons in the oculomotor system. Moreover, the transmitter-related data presented in Paper 2 was complementary to the ion channel profiles in the investigation of possible physiological regulation by transmitter inputs and receptors. With these novel findings, identification of the neural regulators in the healthy generation of eye movements, as well as in pathologies, is within reach.

1. Voltage-gated potassium channels in the functional groups of the oculomotor system

Two classes of delayed-rectifier voltage-gated potassium channel subunits (Kv1.1 and Kv3.1) were focused on in various neurons of the oculomotor system within this dissertation. These subunits play a substantial role in determining neuronal excitability and fast-firing capabilities, respectively (Johnston *et al.*, 2010). No definitive qualitative difference was observed in Kv1.1 or Kv3.1b expression in the tonic or burst firing neurons, as OPNs (Paper 1), Y-group neurons (Paper 4) and premotor BNs of the RIMLF and PGD (Paper 3) all expressed strong immunoreactivity for both Kv1.1 and Kv3.1b. Therefore, the utility of these markers as differentiators of firing patterns may be inapplicable, which is in line with their physiological roles. In contrast to slow-firing modulatory neurons (Hobohm *et al.*, 1998), OPNs with firing rates up to ~200 Hz and BNs with firing rates up to ~1KHz display strong Kv3.1 subunit immunoreactivity. This could mean that the 200 Hz spike frequency is well above a putative threshold of firing rate that specifically requires Kv3.1 subunit expression to achieve fast-firing in the oculomotor circuitry (Gandhi & Keller, 1999; Sparks, 2002). It is also important to note that, in our observations, Kv1.1 expression was present even in the absence of Kv3 subunit in slow-firing or modulatory neurons, related to the oculomotor circuitry or otherwise, such as neurons of the inferior olive (not shown). However, not all fast-firing neuron types expressed Kv1.1 (or Kv3.1b) subunits, as observed in Purkinje cells, which are capable of firing at rates up to ~150 Hz with complex patterns (McKay & Turner, 2004; Fernandez *et al.*, 2007; Zeeh *et al.*, 2021). This is due to the fact that Purkinje cells express other subunits to facilitate their specific firing patterns, such as Kv1.5 (Chung *et al.*, 2001) and Kv3.3-Kv3.4 (Weiser *et al.*, 1994; Zagha *et al.*, 2008). Finding distinct profiles of Kv expression within the functional groups

of the oculomotor system for fast-firing remains to be plausible; however, as the voltage-gated potassium channel family has twelve subunit families, this endeavor is not warranted without compelling evidence from other studies (such as the established perineuronal net-Kv3.1b connection used in this thesis).

A substantial deviation from this often-observed Kv1.1 and Kv3.1b co-expression pattern was found in the MIF motoneurons of the abducens and trochlear nuclei (Paper 2). In a clear contrast to SIF motoneurons and INTs, MIF motoneurons lacked the Kv3.1b subunit immunolabeling, and expressed weaker Kv1.1 subunit staining (Paper 2). This finding was interesting as a first indication of the physiological delineation through histochemical means. More importantly, valuable work performed in other organisms with other methods could be utilized as complementary information to interpret the present histochemical data. Such an example can be found in Paper 2, coming from Hernández et al., where the electrophysiological recordings of MIF and SIF motoneurons performed in cat outlined significant differences between the firing properties of MIF and SIF motoneurons (Hernández *et al.*, 2019). Although both motoneuron populations employ a phasic and a tonic component in firing, and are active during all types of eye movements contrary to previous conceptualizations (Büttner-Ennever & Horn, 2002a; Hernández *et al.*, 2019; Horn & Straka, 2021), MIF motoneurons have lower thresholds, lower eye movement-related sensitivities and reduced firing levels (Hernández *et al.*, 2019). As a reduced Kv1.1 expression would manifest as lower action potential thresholds and a higher rate of spontaneous firing, our findings related to the reduced Kv1.1 expression in MIF motoneurons could explain and enhance the findings of Hernández and colleagues. Similarly, reduced firing levels of MIF motoneurons could be explained by the absence of Kv3.1b, as found in this study. However, it must be noted that this does not rule out the possibility of employing other subunit combinations in MIF compared to SIF motoneurons. Similarly, in terms of the quantity of these channels expressed and anchored to the membrane, even SIF motoneurons likely form a spectrum to account for the differential responses to similar post-synaptic potentials. This would be in accordance with the proposed modern understanding of functional segregation of MIF and SIF motoneurons within motor nuclei as a response to distinct transmitter input types they receive (Fig. 10) (Horn & Straka, 2021). Another caveat is the limitation of histochemical methods, as they do not rule out all protein expression or mRNA content without confirmation by molecular techniques. Without the assistance of a molecular approach, it is also not possible to infer any “graded” gene expression regarding the fast-firing profiles, as done in the medial vestibular nuclei (MVN) of rat (Kodama *et al.*, 2020). Therefore, the speculation on the varied Kv1.1 immunolabeling strength was limited to a possible differential expression within the SIF motoneurons that could correspond to the manifestation of a range of activation thresholds, as observed in cat (Hernández *et al.*, 2019).

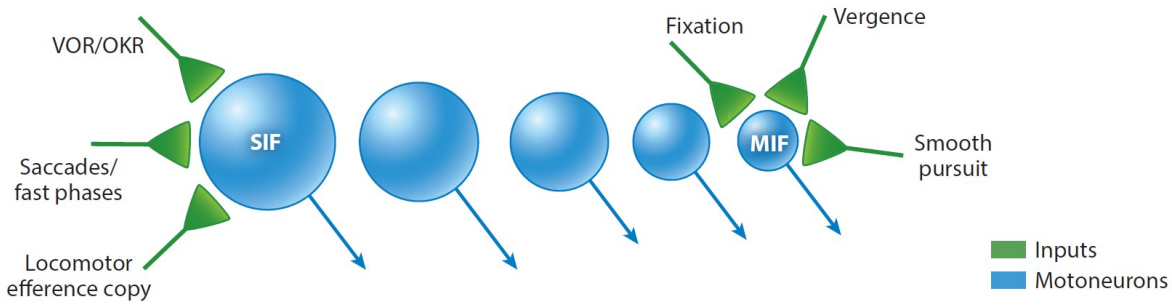

Figure 10: A modern view of differential synaptic inputs to the motoneurons depending on distinct eye movement types. This view defines motoneurons on a functional continuum rather than a clear segregation into different dynamic properties. This continuum places SIF and MIF motoneuron definitions at the extreme ends of a spectrum Figure taken with permission from (Horn & Straka, 2021).

Overall, the requirements for the fast-firing capacity of neurons within a tightly controlled circuitry, as observed in the pre-oculomotor subpopulations of MVN (Kodama *et al.*, 2020), are met by the majority of neurons in the oculomotor system. With the exception of MIF motoneurons, the correlation between Kv1.1 and Kv3.1 is displayed in all neurons presented in this work, and associated Nav1.6 co-expression is demonstrated in the motoneurons of the abducens and trochlear nuclei (Paper 2). This exception, along with observed differences in the transmitter-related proteins of MIF motoneurons, could be explained by possible distinct evolutionary origins across multiple species (see *Chapter 5*).

2. Low-voltage activated ion channels in the functional groups of the oculomotor system

The bursting behavior of neurons in the central nervous system not only depends on the fast-firing capacity (provided by the interplay between Nav and Kv channels), but also requires the expression of low-voltage activated cation channels that govern effective recovery from hyperpolarized voltages. In a tightly controlled circuitry such as the oculomotor system, it has been proposed that the premotor BNs should express T-type calcium channels (Cav3) and HCN channels (Ramat *et al.*, 2005; Shaikh *et al.*, 2008; Daye *et al.*, 2013). Mathematical models based on clinical data successfully explain the cause of irregular saccades in several disorders as dysregulation of bursts by the alterations in the expression of these channels (Shaikh *et al.*, 2007; Shaikh, 2012; Shaikh *et al.*, 2017).

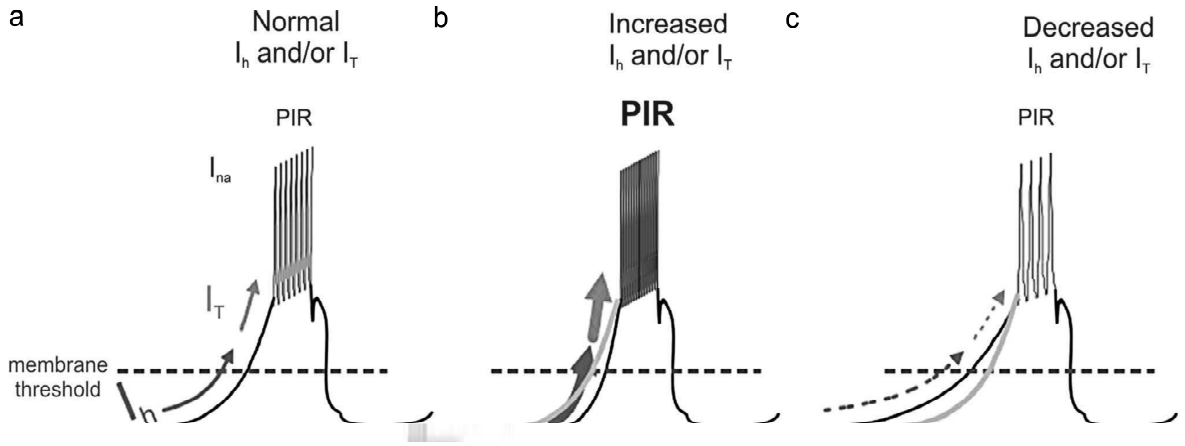

Figure 11: Activation windows of HCN (I_h) and T-type calcium (I_T) channels in the post-inhibitory burst generation and potential effects of their over-expression (**b**) and under-expression (**c**) in the burst generation. Figure taken with permission from (Shaikh *et al.*, 2008).

Findings reported in Paper 2 and 3 regarding the roles of these channels in motoneurons of the abducens and trochlear nuclei suggest that the MIF and SIF motoneurons employ distinct kinetics of post-inhibitory burst generation. While HCN1 channels are not found on the membranes of MIF motoneurons, Cav3.1 immunolabeling was distinctly stronger than that of SIF motoneurons. Conversely, SIF motoneurons displayed strong and continuous HCN1 immunolabeling along the length of their membranes, only sparse labeling was found for Cav3.1. These findings suggest that the post-inhibitory recovery of MIF motoneuron activity is regulated more readily and at more positive voltages, whereas the SIF motoneuron activity requires recovery more selectively and from more negative voltages (Figs. 8&11). Along this line of thinking, these results can be interpreted as evidence of MIF motoneurons displaying more spontaneous activity during all eye movement types, albeit with low dynamic commands; whereas SIF motoneurons employ a variety in their activation range, and are, in general, more selectively activated (Fig. 10) (Hernández *et al.*, 2019; Carrero-Rojas *et al.*, 2021; Horn & Straka, 2021).

Another significant contribution of the work presented in Paper 3 was the histochemical confirmation of low-voltage-gated ion channel expression in the BNs, in support of the post-inhibitory rebound (PIR) hypothesis of these neurons (Miura & Optican, 2006; Ramat *et al.*, 2007; Shaikh *et al.*, 2007). In order for PIR bursting to occur, two conditions must be met: Firstly, the neurons displaying PIR behavior should be under sustained inhibition, which lowers and maintains their membrane potential at a hyperpolarized state. Secondly, the physiological machinery must exist within these cells in order to accelerate the membrane potential towards positive values rapidly upon their disinhibition (Enderle & Engelken, 1995). The first condition is met for all premotor BNs of the oculomotor system, as they all receive sustained tonic monosynaptic inhibition from the OPNs during intersaccadic intervals (Cohen & Henn, 1972; Luschei & Fuchs, 1972; Keller, 1974; Evinger *et al.*, 1982). The second condition is also met, as it was demonstrated here (Paper 3) that both the EBNs of the vertical and the IBNs of the

horizontal saccadic circuitry express multitudes of HCN and Cav3 channels on their membrane. Despite not demonstrating the staining patterns in the IBNs of the vertical and the EBNs of the horizontal saccadic circuitry within this thesis, it is plausible to consider all premotor BNs exhibiting similar characteristics regarding the expression of low-voltage gated cation channels due to the necessity of synchronous eye movements. (Strassman *et al.*, 1986a; b; Moschovakis *et al.*, 1991a; Moschovakis *et al.*, 1991b).

Due to the punctate appearance of especially HCN1 and HCN2 channel immunoreactivity on the BN membranes, it is plausible to attribute the expression of these channels predominantly to the post-synaptic sites for the theoretical implications. Moreover, it would make sense that these channels are concentrated at the inhibitory post-synaptic sites of terminals received from the OPNs, as they theoretically could initiate membrane depolarization upon the cessation of glycinergic OPN inhibition instantly. However, a confirmation for the co-localization of synaptic sites with HCN, or specifically glycinergic synaptic sites with HCN immunolabeling is yet to be demonstrated. Furthermore, it must be noted that HCN channels could be also located on the presynaptic sites for the regulation of transmitter release (Huang & Trussell, 2014; Hegle *et al.*, 2017). Therefore, a closer inspection of the localization of these channels in each cell type would prove beneficial.

Interestingly, the HCN1 staining pattern in other neurons, such as the OPNs and SIF motoneurons, differed from that of BNs. Qualitative evaluation and comparison of the labeling patterns were performed within the same staining and the same case to mitigate potential variations due to the section thickness, tissue quality and test errors. This approach yielded distinct labeling patterns and staining intensities in the BNs, OPNs and SIF motoneurons. The continuous labeling along the length of membranes observed in the OPNs and SIF motoneurons was in clear contrast to the punctate labeling on the BN membranes. Moreover, although similar in localization, membrane labeling for HCN1 in the OPNs appeared weaker compared to the SIF motoneurons. These differences are quite interesting, as localization and expressed (and employed) protein amount could alter the firing characteristics significantly. Although quite premature to make grand inferences, it is promising to connect the differences in immunolabeling patterns with differences in firing characteristics, as OPNs do not burst, and the premotor BNs do not exhibit sustained tonic firing. More data is required (see Table 1) to gain a deeper insight into the functional implications of such differences, as it also sheds light on possible complications in (saccadic) disorders when these patterns change.

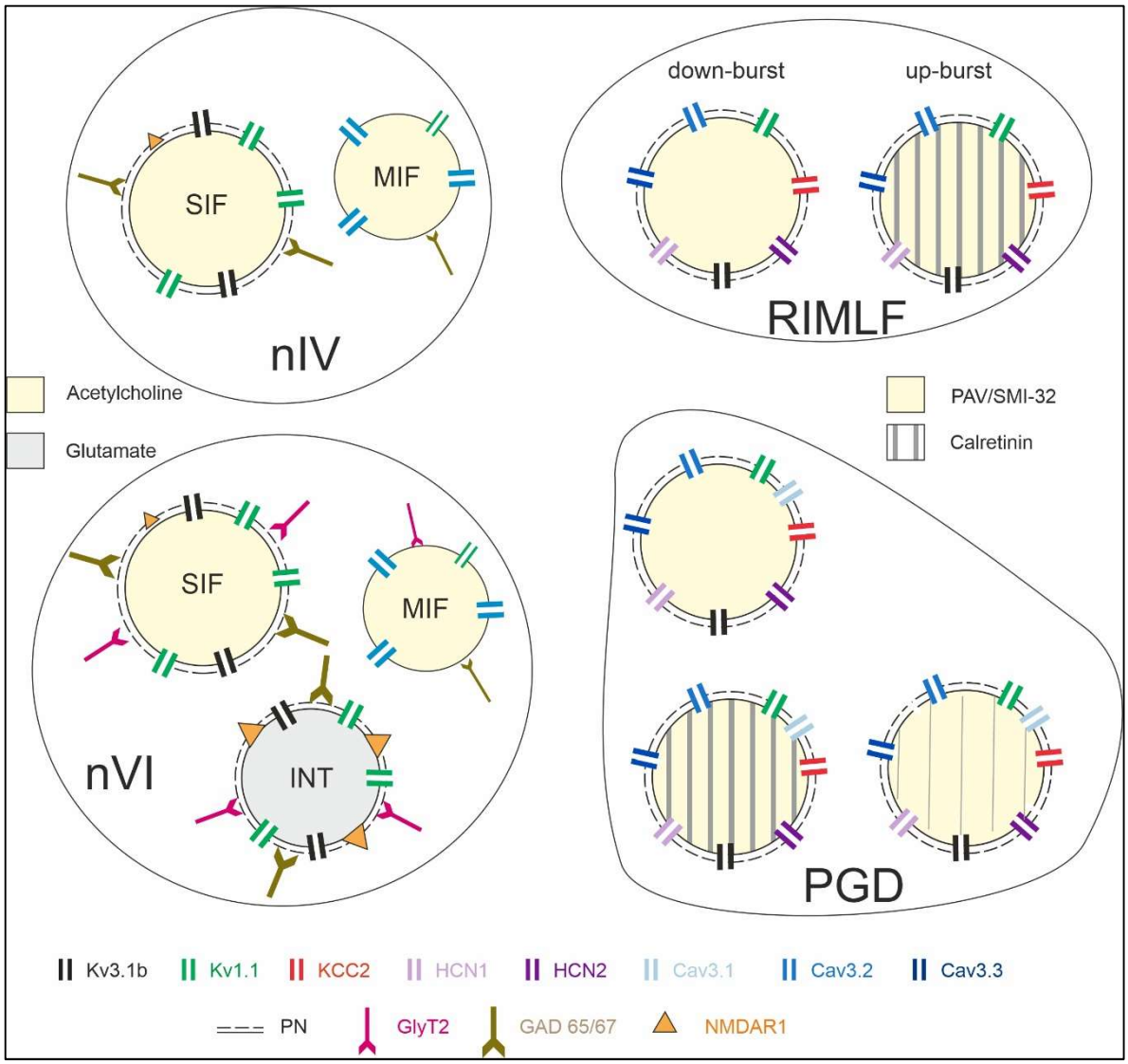

Figure 12: Collective summary diagram depicting differential molecular signatures of various motor (left) and premotor neurons (right) in the oculomotor system, as reported in Paper 2 and 3. Figure adapted from (Mayadali *et al.*, 2021; Mayadali *et al.*, 2022; distributed under the Creative Commons Attribution License CC BY 4.0). nIV: trochlear nucleus; nVI: abducens nucleus; RIMLF: rostral interstitial nucleus of medial longitudinal fascicle; PGD: nucleus paragigantocellularis dorsalis; MIF: motoneurons of multiply-innervated fibers; SIF: motoneurons of singly-innervated fibers; INTs: internuclear neurons; PAV: parvalbumin

	N. Abducens			N. Trochlearis						
	MIF MNs	SIF MNs	INTs	MIF MNs	SIF MNs	RIMLF EBNs	PGD IBNs	OPNs	Yd Group
Kv1.1	+	+++	+++	+	+++	+++	+++	+++	+++
Kv3.1b	-	++	+++	-	++	+++	+++	+++	+++
Nav1.6	+	+	+	+	+				
KCC2	+	+	+	+	+	+	+	?	?
Cav3.1	+++	-	-	+++	-/+	-	-/+	?	?
Cav3.2	+	++	++	+	++	+/++	+/++	?	?
Cav3.3	+	+	+	+	+	+	+	?	?
HCN1	-	+++	+++	-	+++	++	++	++	?
HCN2	?	?	?	?	?	++	++	+	?
vGlut1	-	-	-	-	-				
vGlut2	++	+++	+++	++	+++				
GlyT2	+	++	++	-	-				
GAD65/67	+	++	++	+	+				
GluR2/3	+	++	++	+	++				
NMDAR1	-	+	+++	-	+				
GlyR1a	+	+	+	-	-				

Table 1: Qualitative summary of the ion channel and transmitter-related protein immunolabeling in the neurons of the abducens and trochlear nuclei, premotor burst neurons and omnipause neurons, as reported in the research papers within this thesis (Mayadali *et al.*, 2019; Zeeh *et al.*, 2021; Mayadali *et al.*, 2021; Mayadali *et al.*, 2022). Symbols denote − no labeling, + weak, + + moderate, + + + strong labeling, and "?" denotes not yet reported information. MIF MNs: motoneurons of multiply-innervated fibers; SIF MNs: motoneurons of singly-innervated fibers; INTs: internuclear neurons; RIMLF EBNs: excitatory burst neurons of rostral interstitial nucleus of medial longitudinal fascicle; PGD IBNs: putative inhibitory burst neurons of the nucleus paragigantocellularis dorsalis; OPNs: omnipause neurons; Yd: dorsal Y-group neurons.

3. Physiological significance of the calcium-binding proteins and extracellular matrix

3.1. Calcium-binding proteins: more than anatomical markers

Calcium-binding proteins such as parvalbumin (PAV) and calretinin (CR) have been important anatomical markers to delineate the neurons of the saccadic circuitry, as well as subpopulations in the motor or premotor groups (Paper 4) (Horn *et al.*, 1995; de la Cruz *et al.*, 1998; Ahlfeld *et al.*, 2011; Zeeh *et al.*, 2013). Two observations suggest that investigation of their physiological roles might be valuable for the study of physiological properties in neurons of the oculomotor circuitry: Firstly, the association of PAV with perineuronal nets (PNs) and voltage-gated potassium channel subunit Kv3.1 in the GABAergic cortical neurons (Härtig *et al.*, 1999). The established widespread expression of PAV in neurons of the oculomotor system except MIF motoneurons suggests that PAV could be considered a facilitating factor of fast-firing (Eberhorn *et al.*, 2005). It may also function as a potential factor for the resistance of ocular motoneurons to the neurodegeneration observed in ALS (Elliott & Snider, 1995). Another calcium-binding protein, calexcitin, was similarly demonstrated to modulate neuronal excitability, as it inhibits potassium channels and enhances membrane excitability (Nelson *et al.*, 1996). Secondly, at various stages of the research work for this thesis, we have encountered a variance in CR

immunolabeling strength, as pointed out in Paper 3. Although primarily used to identify subpopulations into the CR-positive and CR-negative groups in Paper 4, personal observations indicated that this is a widespread phenomenon in neurons of the oculomotor system. With the caveat that "varied immunolabeling does not conclusively indicate varied protein expression" in mind, the persistent occurrence of this phenomenon is worthy of note. This could imply that CR could be employed as a modulator of the neurons' biophysiological properties and firing regulation, as previously suggested (Camp & Wijesinghe, 2009). Furthermore, the observation that CR is found exclusively in the excitatory neurons within the oculomotor circuitry so far heavily implies functional significance (Ahlfeld *et al.*, 2011; Adamczyk *et al.*, 2015; Zeeh *et al.*, 2021).

In light of these observations, the findings in Paper 3 concerning the presence of a CR-positive subpopulation within the presumed "IBN area" located in the PGD are intriguing. Because, this either suggests existence of an inhibitory CR-positive population, or an excitatory sub-population interspersed among the IBNs of the horizontal saccadic circuitry. Moreover, the qualitative segregation of strong CR-positive, weak CR-positive and CR-negative within this nucleus is still visible. The INTs of the abducens nucleus present as weak CR-positive neurons, as reported in Paper 2; however, the article did not elaborate on this point. In contrast to PAV, the physiological role of CR is not apparently correlated to certain neuronal types with high activity (Ahlfeld *et al.*, 2011). However, some reports propose CR to be a modulator of neuronal excitability (Camp & Wijesinghe, 2009). Nevertheless, it is clear that CR expression is still not a good marker to delineate a subpopulation in terms of physiological properties. The CR-negative and positive populations found in the RIMLF, Y-group and now in the IBN population of PGD suggest that CR expression might not differentiate the function these neurons serve (Horn *et al.*, 2003a; Zeeh *et al.*, 2021). Clearly, further investigation into the CR expression in a wide range of neurons within the oculomotor system is required in order to correlate these morphological features with their physiological properties.

3.2. Extracellular matrix, physiological and clinical implications

Similar to the utilization of calcium-binding proteins as anatomical markers, extracellular matrix proteins forming PNs have proven useful to identify the OPNs, BNs, Y-group neurons and SIF motoneurons (Horn *et al.*, 2003a; Eberhorn *et al.*, 2005; Horn *et al.*, 2018; Zeeh *et al.*, 2021).

The association of PNs with the expression of Kv3.1b subunit implies the role of this condensed extracellular matrix structure in the regulation of neuronal excitability. It is postulated that PNs act as cation buffers by providing a negatively charged trap for the sodium and potassium ions around the cell membrane (Härtig *et al.*, 1999). This presumably enables a more rapid exchange of ions in close proximity to the cell membrane, where the ion channel proteins are embedded, assisting in the reduction of the inter-spike interval (Härtig *et al.*, 1999). Moreover, PNs are thought to facilitate the firing characteristics of fast-spiking neurons via regulating the expression of Kv3.1b and Kv1.1 and their

recruitment to the cell membrane (Härtig *et al.*, 1999; Favuzzi *et al.*, 2017). Additionally, PNs could have indirect effects on the expression of certain proteins and channels, as demonstrated by Yamada et al., where digestion of PNs resulted in the reduction of parvalbumin levels (Yamada *et al.*, 2015). On the other hand, the reverse is also possible, as blockade of L-type Ca^{2+} voltage-gated channels and AMPA receptors reduces PN accumulation while increasing membrane excitability (Dityatev *et al.*, 2007).

Clinically, PN loss is associated with epilepsy (Rogers *et al.*, 2018), seizures (Vedunova *et al.*, 2013), and hypoxia-ischemia (Fowke *et al.*, 2018), probably such as in the case with gaze palsy following cardiac surgery (*see Chapter 6.1*) (Eggers *et al.*, 2015). However, the mechanism by which PN loss can cause neuronal (and circuit-level) dysfunction requires further analysis. One study undertaken in alert macaque monkeys found that the enzymatic degradation of PNs in the fastigial nucleus does not change saccadic adaptation parameters (Mueller *et al.*, 2014). PN loss in saccadic disorders as a potential mechanism of pathogenesis is still to be thoroughly investigated.

4. Physiological regulation of the firing characteristics via transmitter-related proteins

Bulk of novel data regarding the differential transmitter-related protein expression and its possible effects on physiological function is provided in Paper 2. It was demonstrated that the MIF motoneurons not only had distinct ion channel expression profiles in comparison to the SIF motoneurons, but also received fewer glutamatergic, GABAergic and glycinergic synaptic terminals, and employed reduced AMPA or NMDA receptors on their membrane. Although it is difficult to speculate on how the density of these synaptic terminals translates into their excitability due to their differences in neuronal size, a reasonable assumption would be that the SIF motoneurons display a larger reliance on transmitter inputs from the premotor areas than MIF motoneurons, in terms of regulating their firing characteristics. This is supported by weaker ionotropic GLUR2/3 and absent ionotropic NMDAR1 labeling in MIF motoneurons, which could be interpreted as a looser firing control imposed by the premotor areas in comparison to SIF motoneurons, which receive burst spikes from the saccadic premotor regions, and therefore need to be tightly controlled in their spiking (Ugolini *et al.*, 2006).

There were interesting findings regarding the transmitter profile of INTs in comparison to the motoneurons of the abducens nucleus (Paper 2). These included significantly higher NMDAR1 labeling, a slightly higher density of the inhibitory synapses on their somata, and a stronger immunolabeling for the PNs and Kv3.1b subunit, compared to SIF motoneurons. In order to speculate on the physiological implications of these differences, the role and characteristics of the INTs should be reminded. INTs are responsible for maintaining the conjugacy of both eyes by effectively sending an efference copy to the motoneurons of the medial rectus in the oculomotor nucleus; and this is achieved by displaying the same burst/tonic firing pattern during the horizontal eye movements (Fuchs *et al.*, 1988). Synchronous lateral rectus and medial rectus contraction is facilitated by the fact that INTs discharge slightly before and with a higher intra-burst frequency than the abducens motoneurons, as well as having a higher density of

synaptic terminals on their membranes (Delgado-Garcia *et al.*, 1977; Highstein *et al.*, 1982). Interestingly, the recorded enhanced excitability of INTs was not reflected by a clear difference in their Kv1.1 labeling, as seen between the labeling of MIF and SIF motoneurons in the abducens nucleus. However, shorter intra-spike duration in comparison to that of SIF motoneurons could be attributed to the stronger Kv3.1b (and indirectly to PN) expression. Lastly, significantly higher NMDAR1 labeling of INTs in comparison to SIF motoneurons is quite interesting, as NMDA receptors mediate slower and more prolonged responses in contrast to the AMPA receptors (Traynelis *et al.*, 2010). However, distinct NMDA receptor-mediated excitation of INTs has several implications. Primarily, NMDAR1 could assist in the enhanced burst generation in comparison to the SIF motoneurons, as NMDA receptors were shown to trigger a burst at threshold level followed by tonic firing in the cat abducens motoneurons (Durand *et al.*, 1987). Furthermore, the additional Ca^{2+} influx, which NMDA receptors are permeable to in contrast to the AMPA receptors, not only prolongs the excitatory response of neurons, but also implies differential cellular responses and mechanisms. This hypothesis was further substantiated by the observation that INTs may express weak calretinin (CR) immunoreactivity, which was not detected previously in monkey (Zeeh *et al.*, 2013), but only in the cat abducens nucleus (de la Cruz *et al.*, 1998). NMDAR1 subunit was previously demonstrated to be associated with CR in the cat retina, suggesting a biochemical and/or functional association (Araki & Hamassaki-Britto, 2000); and the intense NMDAR1 immunolabeling in INTs might be correlated to the observed CR-immunoreactivity. This point has not been discussed in the research article (Paper 2), as it was beyond the scope of the specific investigation; however, it is a noteworthy observation that could unravel further physiological discoveries.

Transmitter-related proteins and their expression patterns in the premotor areas were not reported within the scope of this thesis. However, it is of critical importance to examine various neuronal groups in the brainstem and the oculomotor cerebellar areas for multiple reasons: Firstly, the transmitter receptor type and the density of synaptic inputs could prove to be a major correlate of the distinct firing patterns within the oculomotor circuitry. The comparison of the motoneurons and INTs with the premotor BNs or tonic firing OPNs, as well as the neural integrators, could be a valuable complement to the distinct ion channel profiles. Secondly, potential differences in employed transmitters at various neuronal groups of the oculomotor circuitry could shed light on several biophysiological differences resulting in the variation of the eye movements. For instance, utilization of glycine in the neurons of the oculomotor system is limited to pontine or medullary nuclei, whereas GABAergic inhibition is prominent towards the midbrain regions (Spencer & Baker, 1992; Spencer *et al.*, 1992; Wentzel *et al.*, 1993). The biomechanical implications of employing different neurotransmitters in a highly synergistic circuit could be the key to explaining mechanical differences between the horizontal and vertical components of eye movements. Examples can be given on the differences in parameters between the horizontal and vertical saccades, such as the velocity or the differential deterioration of the horizontal vs. vertical saccades with age (Irving & Lillakas, 2018), or the underlying evolutionary development of these components (Straka *et al.*, 2014; Horn & Straka, 2021). Thirdly, the qualitative and quantitative evaluation of transmitter-related proteins

in various oculomotor neurons could help to explain the differential vulnerability of a subset of oculomotor neurons due to excitotoxicity. This set of characterizations, in turn, would enable the development of a targeted pharmacological intervention for susceptible neuronal groups.

5. Interspecies concerns and considerations

The overarching goal of this thesis remains the proper identification of causes and potential interventions for eye movement disorders in human. In this endeavor, methodological limitations significantly increase in the direction of human tissue evaluation. The wide range of tools available, and the power of combining multiple approaches in Xenopus larvae or mice studies dwindle, as one studies primates and ultimately humans. For instance, the electrophysiology recordings that could be obtained from rhesus monkeys cannot be used in humans; or the combined molecular profiling and electrophysiology that can be utilized in mice and rats is not feasible in cats. However, the further researchers need to trace the model organisms back in the evolutionary tree to employ a wider range of applications, the less applicable the anatomical or functional similarities become in the oculomotor circuitry. To illustrate, animals with eyes located on the side of their heads such as birds, or animals with little or no vertical saccadic capacities such as rats or mice (Sakatani & Isa, 2007; Wallace *et al.*, 2013) could be of limited use in the full understanding of the oculomotor circuitry in primates. Therefore, special care needs to be taken to transfer the knowledge obtained in multiple research areas to the non-human primate oculomotor research, as this thesis aims to do, or ultimately to humans.

This thesis lays the foundation for the histochemical correlates of physiological function in the monkey oculomotor system to be able to evaluate human tissue specimen. As rhesus monkeys are among the closest to humans in the evolutionary tree, the anatomy and building blocks of physiological makeup in the oculomotor system can be considered highly transferable. Therefore, establishing the profile of the transmitter and intrinsic membrane properties defining the physiology in neurons of the monkey oculomotor system is the critical first step prior to studying human characteristics. Better control in the experimental procedures, tissue preparation (such as transcardial perfusion fixation) and preservation in monkey tissue specimen are valuable advantages that allow for the sensitive tests necessary to establish the transmitter and ion channel profiles that will serve as the basis for human research. However, in human tissue, it is important to take into consideration that the study of ion channel expression via histochemistry presents an additional layer of challenge. This is due to additional factors such as the post-mortem delay, sub-optimal tissue fixation protocols, compounding unspecific neurodegeneration due to the age of donors in both control and pathological cases, and finally the increased requirements of sensitivity for ion channel labeling detection. These challenges require specific optimization processes for the express purpose of reliable ion channel labeling detection with a high signal-to-noise ratio. With the mitigation of these concerns, the transmitter and ion channel proteins that were demonstrated to be of significant importance will be assessed further in human tissue specimen. This library, as established

for the neurons of the oculomotor circuitry in human, will provide the necessary control for the alterations in cases with oculomotor symptoms.

In order to accomplish its goal, this dissertation drew from results obtained in multitudes of research approaches and model organisms. These include molecular profiling in rat MVN neurons to establish a fast-firing gene module, electrophysiological and anatomical characterization of various neurons in the oculomotor systems of cat, Xenopus larvae and monkey, clinical data collected in disorders of saccades and other eye movements, and finally mathematical models and their predictions regarding membrane profiles in the oculomotor system based on the clinical experimentation. Several considerations must be kept in mind regarding the limitations introduced by the transference of knowledge obtained in less complex organisms. To expand on this point in order, firstly, it is feasible to apply the fast-firing gene module information obtained in rats to monkeys. The findings regarding co-varied ion channel expression outlined several subunits such as Kv1.1, Kv3.1 and Nav1.6, which are basic building blocks of the action potential generation and regulation across species (Jan & Jan, 2012; Moran *et al.*, 2015) and are highly conserved through the evolutionary tree. However, it cannot be concluded that no further subunits contribute to the regulation of firing characteristics in monkey and human. Secondly, especially the study on motoneurons (Paper 2) relied on the electrophysiology data collected in cat, as well as Xenopus larvae; it must be noted that there are several key differences already reported in the organization of the oculomotor system between cats and rhesus monkeys. These include CR-positive INTs of the abducens nucleus in cat, or the inhibitory saccadic BNs located within RIMLF in cat, but located within INC in primates (Spencer & Wang, 1996; de la Cruz *et al.*, 1998). However, in terms of the definition of the firing characteristics for MIF and SIF motoneurons, the study provided valuable information regarding subverting expectations of a strict functional segregation approach as interpreted from anatomical and histochemical segregation of these motoneurons (Hernández *et al.*, 2019). This could be expanded on the findings from Xenopus larvae, where motoneurons can be segregated into two main groups in terms of the transmitter receptors they express (i.e. AMPA or NMDA) (Dietrich *et al.*, 2017), and not simply "slow" firing MIF and "fast" firing SIF motoneurons. Finally, regarding the top-down approach of mathematical models and their predictions regarding the intrinsic membrane properties of the saccadic BNs, it should be noted that a quantifiable comparison in ratios or in the absolute amount of expressed protein is not possible by our approach. Therefore, the conclusions in Paper 3 were limited to the qualitative histochemical confirmation of the protein expression for ion channels, and not a strict comparative skewed subunit expression towards one member of the ion channel family. Overall, it is of utmost importance that both bottom-up and top-down approaches are taken into consideration for an accurate understanding of the big picture of biophysiological function in neurons of the oculomotor system.

6. Prospective clinical and pharmacological considerations

6.1. Saccadic disorders and the physiological substrates of brainstem saccadic circuit dysfunction

Aside from lesion studies, substantial insight into the brainstem premotor saccadic circuit is provided by the clinical examinations of saccadic disorders or neurodegenerative diseases with saccadic symptoms. These include, but are not limited to, progressive supranuclear palsy (PSP), Niemann Pick Disease Type C (NPC) opsoclonus, and syndrome of saccadic palsy following cardiac or aortic surgery.

Progressive supranuclear palsy (PSP)

PSP is a sporadic neurodegenerative disorder presenting with neurofibrillary tangles as aggregates of tau proteins, neuropil threads and tufted astrocytes in the brain (Litvan *et al.*, 1997; Dickson *et al.*, 2007). Alongside the often-observed symptoms of parkinsonism, the distinguishing feature of PSP in its classical form is the slowing of vertical (initially upward) saccades, which may eventually result in vertical gaze palsy (Steele *et al.*, 1964; Wenning *et al.*, 1997; Chen *et al.*, 2010). In the advanced stages of the disease, an additional impairment of the horizontal saccades is observed and may ultimately progress towards a complete ophthalmoplegia. So far, only a few studies have correlated the eye movement deficits of PSP with the degeneration of the brainstem regions involved in saccade generation (Steele *et al.*, 1964; Daniel *et al.*, 1995). A significant cell loss of the OPNs was found in a morphometric post-mortem analysis of PSP cases, but the loss of EBNs in the RIMLF as the substrate for vertical saccades is not yet evaluated (Revesz *et al.*, 1996). In PSP, both the amplitude and the velocity of a saccade are abnormal, leading to highly irregular and curved saccades (Shaikh *et al.*, 2017). This consolidates the hypotheses involving the contribution of BN dysfunction as the underlying cause. Potentially, downregulation of the Kv channels or the PIR phenomenon (downregulated Cav or HCN channels) could contribute to the progression of saccadic slowing. Additionally, interruption of saccades is observed, which could be due to a spontaneous pathological premature firing of the fastigial nucleus, as it stimulates the OPNs and IBNs to end a saccade, or of OPNs themselves (Shaikh *et al.*, 2017). These observations suggest that the alterations of the neuronal microenvironment and ion channel content of the BNs are likely contributors to the degeneration, rather than pure cell loss. With the established ion channel profiles of BNs in RIMLF and pontine reticular formation, cases with selective vertical gaze palsy shall be important in observing any changes regarding the bursting capacity of these neurons.

Niemann-Pick disease type C (NPC)

NPC is a rare genetic lysosomal storage disorder characterized by an inability of the body to transport cholesterol and other lipids in the cells (Chang *et al.*, 2005). NPC presents with several oculomotor symptoms such as impaired saccades (initially down-gaze), smooth pursuit, and optokinetic nystagmus in the vertical direction, with relatively normal eye movements in the horizontal direction (Salsano *et al.*, 2012; Gupta *et al.*, 2018). Similar to PSP, the degeneration occurs initially for vertical saccades and later

for horizontal saccades (Blundell *et al.*, 2018). The underlying pathophysiology selectively affecting one aspect of the saccadic circuitry is not yet clear. However, initial findings rule out the contribution of INC and motoneurons (Abel *et al.*, 2012), pointing to BN dysfunction in the saccadic circuitry (Solomon *et al.*, 2005). The possible implications of a distinct pathology yielding similar eye movement disturbances (i.e. PSP and NPC) include alterations of the BN membrane proteins as a cause of pathophysiology.

Opsoclonus

Opsoclonus consists of uncontrolled, rapid and multidirectional conjugate eye movements without intersaccadic intervals (Wong *et al.*, 2001; Wong, 2007). It frequently occurs along with myoclonus and ataxia in opsoclonus myoclonus syndrome, a rare autoimmune disease (Pike, 2013). A lesion in the cerebellar vermis is suggested as an underlying cause of the observed symptoms, as it leads to the disinhibition of the fastigial nucleus that projects to the BNs in the brainstem (Noda *et al.*, 1990). Dysfunction in the brainstem saccadic circuitry, such as the malfunction of the OPNs and/or BNs, is another suggested explanation for the observed oscillations in all directions, even though a post-mortem examination of two opsoclonus cases did not reveal any structural OPN lesion (Ridley *et al.*, 1987). As previously explained (see *Introduction: Chapter 5.1*), failure of the PIR phenomenon due to changing membrane characteristics in the OPNs and BNs could be an underlying reason for these symptoms. As this thesis established in the monkey brainstem that the BNs (and partly OPNs) are equipped with the necessary cellular machinery for the generation of PIR bursting (i.e. HCN and Cav3 channels as well as Kv1&Kv3.1), these neuron groups shall be tested for the alterations of these proteins in opsoclonus cases. An upregulation in Cav or HCN channels in BNs could contribute to the instability and oscillations observed in opsoclonus or ocular flutter.

As suggested by the hypotheses regarding the etiology of opsoclonus, specific neurons such as the OPNs, BNs or Purkinje cells in the cerebellar vermis and FOR could be evaluated for any alterations in the already-established ion channel and transmitter profiles. However, limitations of the histochemical methodology must be carefully observed in testing some of these hypotheses. For instance, one explanation of the eye oscillations, such as those found in opsoclonus, is the increased $GABA_A$ receptor sensitivity (Optican & Pretegiani, 2017a). This phenomenon can occur without any alterations in the protein expression patterns, and therefore impossible to test with the immunohistochemical methods. However, there could be indirect targets, such as particular α subunits, of which prominence and possible effects could be tested with adequately sensitive antibodies. Alternatively, possible alterations in protein expression reportedly up- or down-regulated as a result of the increased $GABA_A$ receptor sensitivity could be targeted.

Saccadic palsy following cardiac surgery

In rare cases, patients who undergo cardiac or aortic surgery may wake up with a saccadic palsy similar to what is observed in PSP, but with otherwise normal eye movements (Bernat & Lukovits, 2004;

Solomon *et al.*, 2008). As presumed in PSP, dysfunction of the saccadic burst generator in the reticular formation is expected, despite no confirmation of brainstem infarcts was found with MRI (Solomon *et al.*, 2008). Neuropathological post-mortem assessment revealed neuronal necrosis, axonal loss and astrogliosis in the pontine reticular formation, without specific evaluation of the saccadic neurons (Hanson *et al.*, 1986). The possible effects of an ischemic cerebral insult on the cellular microenvironment could be an underlying mechanism; however, the pathomechanism for this syndrome is yet unclear. Initial analysis revealed the breaking up of the PNs around OPNs and BNs, despite no neuronal loss or apparent changes in the transmitter content of these neurons (Eggers *et al.*, 2015). This phenomenon provides another example of alterations in the neurophysiology and microenvironment causing eye movement symptoms without actual neuronal loss. With the findings reported in this thesis, it is presumable to attribute the dysfunction of BNs and/or OPNs to the indirect effects of PN loss. This could involve alterations in Kv3 or Kv1 expression as their modulation is associated with healthy extracellular matrix proteins in the form of PNs (Härtig *et al.*, 1999; Favuzzi *et al.*, 2017). Naturally, one of the next steps in this research shall be the investigation of established ion channel proteins in the neurons of the saccadic circuit, in particular the OPNs and BNs.

6.2. Potential for the pharmacological intervention to distinct populations of the oculomotor system

As seen in amyotrophic lateral sclerosis (ALS), the selective vulnerability of different motoneurons might be due to the different transmitter and ion channel content of their membranes (Elliott & Snider, 1995; Laslo *et al.*, 2001). Although initial reports did not find differences in the GluR2/3 expression between differentially vulnerable motoneurons in ALS (Laslo *et al.*, 2001), multitudes of distinct ion channels were found in this thesis to be differentially equipped by the MIF and SIF motoneurons (Paper 2&3). These findings open up the possibility of a selective pharmacological intervention for the treatment of eye movement-related symptoms in multiple neurodegenerative disorders affecting motor function. With the established histochemical signatures of MIF and SIF motoneurons in monkey, it is now made feasible to assess its homologue counterpart in human, as well as potential alterations between the pathological brainstem tissue and matched controls.

Several studies demonstrated that specific ion channel blockers can be prescribed to treat eye movement disorders. One prominent example is the use of low-dose 4-aminopyridine (4-AP), a voltage-gated potassium channel blocker used in the treatment of downbeat nystagmus, supposedly by restoring the vertical and horizontal neural integrator function (Kalla *et al.*, 2007; Strupp *et al.*, 2008). This pharmacological treatment is also considered for upbeat nystagmus, episodic ataxias and multiple sclerosis (Strupp *et al.*, 2008). Despite the findings in this thesis report differential expression of Kv1 and Kv3 subunits most prominently between the MIF and SIF motoneurons, delineation of different oculomotor populations with different Kv channel expressions might explain, and further allow fine-tuning of the pharmacological intervention possibilities for the treatment of various oculomotor symptoms.

The differential expression of HCN channels found in MIF and SIF motoneurons, as well as differences in their expression pattern and intensity, enables selective pharmacological targeting of these channels in functional neuronal groups exclusively. HCN channel blockers, such as ivabradine hydrochloride could prove to be beneficial in the regulation of the HCN channel activity in SIF motoneurons, as well as BNs. Furthermore, developments in isoform-selective HCN channel blockers could further enhance the possible therapeutical applications in oculomotor disorders.

Conclusion

The main achievements of this thesis are:

1- A bridge was built between the histochemistry and electrophysiology in various neurons of the oculomotor circuitry by demonstrating different ion channel and transmitter content of functionally different motoneuron subpopulations in monkey. This was achieved in the publication "Transmitter and ion channel profiles of neurons in the primate abducens and trochlear nuclei" by showcasing significant histochemical differences with respect to the ion channel expression related to the fast-firing of neurons between motoneurons of multiply innervated fibers (MIF) and of singly innervated fibers (SIF). Previously established anatomical, histochemical and physiological differences between the MIF and SIF motoneurons and known properties of these ion channels enabled an identification of the physiological properties indirectly through the histochemical methods. This milestone in oculomotor research, therefore, will be a valuable tool for further identification of physiologically different (sub-) populations in the oculomotor circuitry (for example in the interstitial nucleus of Cajal) through histochemical methods.

2- Histochemical characterization of the premotor neurons was utilized to test computational hypotheses originating from clinical data, from which mathematical models were derived. In the publication "Saccadic premotor burst neurons and histochemical correlates of their firing patterns in rhesus monkey", predictions of a neuromimetic model of saccadic generation were confirmed regarding the ion channel profile of premotor burst neurons. Our findings not only expanded the histochemical signature library of neurons of the oculomotor system regarding the ion channel expression profiles, but also demonstrated that the top-down mathematical modelling approach could be met with a bottom-up histochemical method to illuminate the phenomena observed in clinical settings.

3- Ion channel profiling was introduced to various functional neurons of the oculomotor system in monkey with diverse firing patterns, i.e. tonic firing omnipause neurons and Y-group neurons, motoneurons of the abducens and trochlear nuclei, as well as Purkinje cells of cerebellum with their burst-tonic firing patterns; and finally bursting premotor neurons of saccadic circuitry. Although initial findings cannot yet be considered as a full-fledged library of ion channel and transmitter profiling that determines the differentiation of the firing patterns in neurons of the oculomotor system, differences already found on various levels (motor or premotor) are promising. Furthermore, these will serve as a

stepping stone towards identifying a combination of protein expressions that not only determines the differences in firing patterns but also point to certain candidate proteins that could readily be a source of vulnerability to cellular insult for a particular type of neuron.

4- Meaningful differences were demonstrated in transmitter-related profiles of motoneurons (i.e. MIF and SIF motoneurons) and internuclear neurons of the abducens nucleus with distinct physiological and histochemical signatures in monkey. These differences not only shed light on the physiological distinctions observed between these neuron types, but also reserve the potential to explain the differential susceptibility to excitotoxicity or aggregate proteins observed in various neurodegenerative diseases in human.

References

Abel, L.A., Bowman, E.A., Velakoulis, D., Fahey, M.C., Desmond, P., Macfarlane, M.D., Looi, J.C., Adamson, C.L. & Walterfang, M. (2012) Saccadic eye movement characteristics in adult Niemann-Pick Type C disease: relationships with disease severity and brain structural measures. *PloS One*, **7**, e50947.

Adamczyk, C., Strupp, M., Jahn, K. & Horn, A.K.E. (2015) Calretinin as a marker for premotor neurons involved in upgaze in human brainstem. *Front. Neuroanat.*, **9**, 153.

Ahlfeld, J., Mustari, M. & Horn, A.K.E. (2011) Sources of calretinin inputs to motoneurons of extraocular muscles involved in upgaze. *Ann. N. Y. Acad. Sci.*, **1233**, 91 - 99.

Anderson, T.J. & MacAskill, M.R. (2013) Eye movements in patients with neurodegenerative disorders. *Nat. Rev. Neurol.*, **9**, 74.

Angstadt, J.D., Grassmann, J.L., Theriault, K.M. & Levasseur, S.M. (2005) Mechanisms of postinhibitory rebound and its modulation by serotonin in excitatory swim motor neurons of the medicinal leech. *J. Comp. Physiol. A.*, **191**, 715-732.

Araki, C.M. & Hamassaki-Britto, D.E. (2000) Calretinin co-localizes with the NMDA receptor subunit NR1 in cholinergic amacrine cells of the rat retina. *Brain Res.*, **869**, 220-224.

Ariano, M.A., Cepeda, C., Calvert, C.R., Flores-Hernández, J., Hernández-Echeagaray, E., Klapstein, G.J., Chandler, S.H., Aronin, N., DiFiglia, M. & Levine, M.S. (2005) Striatal potassium channel dysfunction in huntington's disease transgenic mice. *J. Neurophysiol.*, **93**, 2565-2574.

Baker, R. & Highstein, S.M. (1975) Physiological identification of interneurons and motoneurons in the abducens nucleus. *Brain Res.*, **91**, 292-298.

Balmer, T.S. (2016) Perineuronal nets enhance the excitability of fast-spiking neurons. *eNeuro*, **3**, ENEURO.0112-0116.2016.

Baruscotti, M., Bucchi, A. & DiFrancesco, D. (2005) Physiology and pharmacology of the cardiac pacemaker ("funny") current. *Pharmacol. Therapeut.*, **107**, 59-79.

Basso, M.A. & May, P.J. (2017) Circuits for action and cognition: a view from the superior colliculus. *Annu. Rev. Vis. Sc.*, **3**, 197-226.

Ben-Ari, Y., Woodin, M., Sernagor, E., Cancedda, L., Vinay, L., Rivera, C., Legendre, P., Luhmann, H., Bordey, A., Wenner, P., Fukuda, A., van den Pol, A., Gaiarsa, J.-L. & Cherubini, E. (2012) Refuting the challenges of the developmental shift of polarity of GABA actions: GABA more exciting than ever! *Front. Cell Neurosci.*, **6,** 35.

Benarroch, E.E. (2011) Glycine and its synaptic interactions: functional and clinical implications. *Neurology*, **77**, 677-683.

Benarroch, E.E. (2013) HCN channels: function and clinical implications. *Neurology*, **80**, 304-310.

Bernat, J.L. & Lukovits, T.G. (2004) Syndrome resembling PSP after surgical repair of ascending aorta dissection or aneurysm. *Neurology*, **63**, 1141-1142.

Betz, H., Langosch, D., Hoch, W., Prior, P., Pribilla, I., Kuhse, J., Schmieden, V., Malosio, M.L., Matzenbach, B., Holzinger, F., Kuryatov, A., Schmitt, B., Maulet, Y. & Becker, C.M. (1991) Structure and expression of inhibitory glycine receptors. *Adv. Exp. Med. Biol.*, **287**, 421-430.

Blazquez, P., Partsalis, A., Gerrits, N.M. & Highstein, S.M. (2000) Input of anterior and posterior semicircular canal interneurons encoding head-velocity to the dorsal Y group of the vestibular nuclei. *J. Neurophysiol.*, **83**, 2891-2904.

Blundell, J., Frisson, S., Chakrapani, A., Gissen, P., Hendriksz, C., Vijay, S. & Olson, A. (2018) Oculomotor abnormalities in children with Niemann-Pick Type C. *Mol. Genet. Metab.*, **123**, 159-168.

Bohlen, M.O., Bui, K., Stahl, J.S., May, P.J. & Warren, S. (2019) Mouse extraocular muscles and the musculotopic organization of their innervation. *Anat. Rec.*, **302**, 1865-1885.

Bohlen, M.O., Warren, S., Mustari, M.J. & May, P.J. (2017) Examination of feline extraocular motoneuron pools as a function of muscle fiber innervation type and muscle layer. *J. Comp. Neurol.,* **525**, 919-935.

Bowery, N.G. & Smart, T.G. (2006) GABA and glycine as neurotransmitters: a brief history. *Brit. J. Pharmacol.*, **147 Suppl 1**, S109-119.

Braitenberg, V. & Schüz, A. (1998) *Cortex: statistics and geometry of neuronal connectivity (Second edition)*. Springer.

Brandenburg, C., Smith, L.A., Kilander, M.B.C., Bridi, M.S., Lin, Y.-C., Huang, S. & Blatt, G.J. (2021) Parvalbumin subtypes of cerebellar Purkinje cells contribute to differential intrinsic firing properties. *Mol. Cell. Neurosci.*, **115**, 103650.

Brew, H.M. & Forsythe, I.D. (1995) Two voltage-dependent K^+ conductances with complementary functions in postsynaptic integration at a central auditory synapse. *J. Neurosci.,* **15**, 8011-8022.

Büttner-Ennever, J.A. (2006) The extraocular motor nuclei: organization and functional neuroanatomy. *Prog. Brain Res.*, **151**, 95-125.

Büttner-Ennever, J.A. & Akert, K. (1981) Medial rectus subgroups of the oculomotor nucleus and their abducens internuclear input in the monkey. *J. Comp. Neurol.* , **197**, 17-27.

Büttner-Ennever, J.A., Cohen, B., Horn, A.K.E. & Reisine, H. (1996) Pretectal projections to the oculomotor complex of the monkey and their role in eye movements. *J. Comp. Neurol.*, **366**, 348-359.

Büttner-Ennever, J.A., Cohen, B., Pause, M. & Fries, W. (1988) Raphe nucleus of the pons containing omnipause neurons of the oculomotor system in the monkey, and its homologue in man. *J. Comp. Neurol.*, **267**, 307-321.

Büttner-Ennever, J.A. & Horn, A.K.E. (2002a) The neuroanatomical basis of oculomotor disorders: the dual motor control of extraocular muscles and its possible role in proprioception. *Curr. Opin. Neurol.*, **15**, 35-43.

Büttner-Ennever, J.A. & Horn, A.K.E. (2002b) Oculomotor system: a dual innervation of the eye muscles from the abducens, trochlear, and oculomotor nuclei. *Movement Disord.*, **17**, 2-3.

Büttner-Ennever, J.A., Horn, A.K.E., Henn, V. & Cohen, B. (1999) Projections from the superior colliculus motor map to omnipause neurons in monkey. *J. Comp. Neurol.*, **413**, 55-67.

Büttner-Ennever, J.A., Horn, A.K.E., Scherberger, H. & D'Ascanio, P. (2001) Motoneurons of twitch and nontwitch extraocular muscle fibers in the abducens, trochlear, and oculomotor nuclei of monkeys. *J. Comp. Neurol.*, **438**, 318-335.

Büttner, U., Büttner-Ennever, J.A. & Henn, V. (1977) Vertical eye movement related unit activity in the rostral mesencephalic reticular formation of the alert monkey. *Brain Res.*, **130**, 239-252.

Camp, A.J. & Wijesinghe, R. (2009) Calretinin: modulator of neuronal excitability. *Int. J. Biochem. Cell Biol.*, **41**, 2118-2121.

Campolongo, P., Ratano, P., Ciotti, M.T., Florenzano, F., Nori, S.L., Marolda, R., Palmery, M., Rinaldi, A.M., Zona, C., Possenti, R., Calissano, P. & Severini, C. (2013) Systemic administration of substance P recovers beta amyloid-induced cognitive deficits in rat: involvement of Kv potassium channels. *PLoS One*, **8**, e78036.

Cannon, S.C., Robinson, D.A. & Shamma, S. (1983) A proposed neural network for the integrator of the oculomotor system. *Biol. Cybern.*, **49**, 127-136.

Carpenter, M.B. & Cowie, R.J. (1985) Connections and oculomotor projections of the superior vestibular nucleus and cell group 'y'. *Brain Res.*, **336**, 265-287.

Carrero-Rojas, G., Hernández, R., Blumer, R., R de la Cruz, R. & Pastor, A. (2021) MIF versus SIF motoneurons, what are their respective contribution in the oculomotor medial rectus pool? *J. Neurosci.*, **41**, 9782-9793.

Carunchio, I., Mollinari, C., Pieri, M., Merlo, D. & Zona, C. (2008) GAB(A) receptors present higher affinity and modified subunit composition in spinal motor neurons from a genetic model of amyotrophic lateral sclerosis. *Eur. J. Neurosci.*, **28**, 1275-1285.

Catterall, W.A. (1984) The molecular basis of neuronal excitability. *Science*, **223**, 653-661.

Chamma, I., Chevy, Q., Poncer, J.C. & Lévi, S. (2012) Role of the neuronal K-Cl co-transporter KCC2 in inhibitory and excitatory neurotransmission. *Front. Cell. Neurosci.*, **6**, 5.

Chang, T.-Y., Reid, P.C., Sugii, S., Ohgami, N., Cruz, J.C. & Chang, C.C.Y. (2005) Niemann-Pick Type C disease and intracellular cholesterol trafficking. *J. Biol. Chem.*, **280**, 20917-20920.

Chen, A.L., Riley, D.E., King, S.A., Joshi, A.C., Serra, A., Liao, K., Cohen, M.L., Otero-Millan, J., Martinez-Conde, S., Strupp, M. & Leigh, R.J. (2010) The disturbance of gaze in progressive supranuclear palsy (PSP): Implications for Pathogenesis. *Front. Neurol.*, **1**, 147.

Chen, T., Gai, W.P. & Abbott, C.A. (2014) Dipeptidyl peptidase 10 (DPP10(789)): a voltage gated potassium channel associated protein is abnormally expressed in Alzheimer's and other neurodegenerative diseases. *BioMed Res. Int.*, **2014**, 209398.

Chopra, R., Bushart, D.D. & Shakkottai, V.G. (2018) Dendritic potassium channel dysfunction may contribute to dendrite degeneration in spinocerebellar ataxia type 1. *PLoS One*, **13**, e0198040.

Chung, Y.H., Shin, C.-M., Kim, M.J., Lee, B.K. & Cha, C.I. (2001) Immunohistochemical study on the distribution of six members of the Kv1 channel subunits in the rat cerebellum. *Brain Res.*, **895**, 173-177.

Cogan, D.G. (1954) Ocular dysmetria; flutterlike oscillations of the eyes, and opsoclonus. *AMA Arch. Ophthalmol.*, **51**, 318-335.

Cohen, B. & Henn, V. (1972) Unit activity in the pontine reticular formation associated with eye movements. *Brain Res.*, **46**, 403-410.

Cohen, B., Komatsuzaki, A. & Bender, M.B. (1968) Electrooculographic syndrome in monkeys after pontine reticular formation lesions. *Arch. Neurol.*, **18**, 78-92.

Crunelli, V., Tóth, T.I., Cope, D.W., Blethyn, K. & Hughes, S.W. (2005) The 'window' T-type calcium current in brain dynamics of different behavioural states. *J. Physiol.*, **562**, 121-129.

Cummings, K.A. & Popescu, G.K. (2015) Glycine-dependent activation of NMDA receptors. *J. Gener. Physiol.*, **145**, 513-527.

Daniel, S.E., DeBruin, V.M.S. & Lees, A.J. (1995) The clinical and pathological spectrum of the Steele-Richardson-Olszewski syndrome (progressive supranuclear palsy): a reappraisal. *Brain*, **118**, 759-770.

Daye, P.M., Optican, L.M., Roze, E., Gaymard, B. & Pouget, P. (2013) Neuromimetic model of saccades for localizing deficits in an atypical eye-movement pathology. *J. Transl. Med.*, **11**, 125.

de la Cruz, R.R., Pastor, A.M., Martinez-Guijarro, F.J., Lopez-Garcia, C. & Delgado-Garcia, J.M. (1998) Localization of parvalbumin, calretinin, and calbindin D-28k in identified extraocular motoneurons and internuclear neurons of the cat. *J. Comp. Neurol.*, **390**, 377-391.

de Winter, F., Kwok, J.C.F., Fawcett, J.W., Vo, T.T., Carulli, D. & Verhaagen, J. (2016) The chemorepulsive protein semaphorin 3A and perineuronal net-mediated plasticity. *Neural Plast.*, **2016**, 3679545-3679545.

Delgado-Garcia, J., Baker, R. & Highstein, S. (1977) The activity of internuclear neurons identified within the abducens nucleus of the alert cat. *Control of Gaze by Brain Stem Neurons*, *Developments in Neuroscience*, **1,** 291-300.

Dickson, D.W., Rademakers, R. & Hutton, M.L. (2007) Progressive supranuclear palsy: pathology and genetics. *Brain Pathol.*, **17**, 74-82.

Dietrich, H., Glasauer, S. & Straka, H. (2017) Functional organization of vestibulo-ocular responses in abducens motoneurons. *J. Neurosci.*, **37**, 4032-4045.

Dingledine, R., Borges, K., Bowie, D. & Traynelis, S.F. (1999) The glutamate receptor ion channels. *Pharmacol. Rev.*, **51**, 7-62.

Dityatev, A., Brückner, G., Dityateva, G., Grosche, J., Kleene, R. & Schachner, M. (2007) Activity-dependent formation and functions of chondroitin sulfate-rich extracellular matrix of perineuronal nets. *Develop. Neurobiol.*, **67**, 570-588.

Durand, J., Engberg, I. & Tyc-Dumont, S. (1987) l-Glutamate and N-methyl-d-aspartate actions on membrane potential and conductance of cat abducens motoneurones. *Neurosci. Lett.*, **79**, 295-300.

Eberhorn, A.C., Ardelenanu, P., Büttner-Ennever, J.A. & Horn, A.K.E. (2005) Histochemical differences between motoneurons supplying multiply and singly innervated extraocular muscle fibers. *J. Comp. Neurol.*, **491**, 352-366.

Eberhorn, A.C., Büttner-Ennever, J.A. & Horn, A.K.E. (2006) Identification of motoneurons supplying multiply- or singly-innervated extraocular muscle fibers in the rat. *Neuroscience*, **137**, 891-903.

Eggers, S.D.Z., Horn, A.K.E., Roeber, S., Härtig, W., Nair, G., Reich, D.S. & Leigh, R.J. (2015) Saccadic palsy following cardiac surgery: possible role of perineuronal nets. *PLoS One*, **10**, e0132075.

Elliott, J.L. & Snider, W.D. (1995) Parvalbumin is a marker of ALS-resistant motor neurons. *Neuroreport*, **6**, 449-452.

Enderle, J.D. & Engelken, E.J. (1995) Simulation of oculomotor post-inhibitory rebound burst firing using a Hodgkin-Huxley model of a neuron. *Biomed. Sci. Instrum.*, **31**, 53-58.

Erichsen, J.T., Wright, N.F. & May, P.J. (2014) Morphology and ultrastructure of medial rectus subgroup motoneurons in the macaque monkey. *J. Comp. Neurol.*, **522**, 626-641.

Everling, S., Paré, M., Dorris, M.C. & Munoz, D.P. (1998) Comparison of the discharge characteristics of brain stem omnipause neurons and superior colliculus fixation neurons in monkey: Implications for control of fixation and saccade behavior. *J. Neurophysiol.*, **79**, 511-528.

Evinger, C., Kaneko, C.R. & Fuchs, A.F. (1982) Activity of omnipause neurons in alert cats during saccadic eye movements and visual stimili. *J. Neurophysiol.*, **47**, 827-843.

Fairless, R., Williams, S.K. & Diem, R. (2019) Calcium-binding proteins as determinants of central nervous system neuronal vulnerability to disease. *Int. J. Mol. Sci.*, **20**.

Favuzzi, E., Marques-Smith, A., Deogracias, R., Winterflood, C.M., Sánchez-Aguilera, A., Mantoan, L., Maeso, P., Fernandes, C., Ewers, H. & Rico, B. (2017) Activity-dependent gating of parvalbumin interneuron function by the perineuronal net protein brevican. *Neuron*, **95**, 639-655.e610.

Fernandez, F.R., Engbers, J.D.T. & Turner, R.W. (2007) Firing dynamics of cerebellar Purkinje cells. *J. Neurophysiol.*, **98**, 278-294.

Fowke, T.M., Galinsky, R., Davidson, J.O., Wassink, G., Karunasinghe, R.N., Prasad, J.D., Bennet, L., Gunn, A.J. & Dean, J.M. (2018) Loss of interneurons and disruption of perineuronal nets in the cerebral cortex following hypoxia-ischaemia in near-term fetal sheep. *Sci. Rep.*, **8**, 17686.

Fremeau, R.T., Jr., Kam, K., Qureshi, T., Johnson, J., Copenhagen, D.R., Storm-Mathisen, J., Chaudhry, F.A., Nicoll, R.A. & Edwards, R.H. (2004) Vesicular glutamate transporters 1 and 2 target to functionally distinct synaptic release sites. *Science*, **304**, 1815-1819.

Fuchs, A.F., Robinson, F.R. & Straube, A. (1993) Role of the caudal fastigial nucleus in saccade generation. 1. neuronal discharge patterns. *J. Neurophysiol.*, **70**, 1723-1740.

Fuchs, A.F., Scudder, C.A. & Kaneko, C.R. (1988) Discharge patterns and recruitment order of identified motoneurons and internuclear neurons in the monkey abducens nucleus. *J. Neurophysiol.*, **60**, 1874-1895.

Gacek, R.R. (1977) Location of brain stem neurons projecting to the oculomotor nucleus in the cat. *Exp. Neurol.*, **57**, 725-749.

Gandhi, N.J. & Katnani, H.A. (2011) Motor functions of the superior colliculus. *Ann. Rev. Neurosci.*, **34**, 205-231.

Gandhi, N.J. & Keller, E.L. (1999) Comparison of saccades perturbed by stimulation of the rostral superior colliculus, the caudal superior colliculus, and the omnipause neuron region. *J. Neurophysiol.*, **82**, 3236-3253.

Garcia-Segura, L.M., Baetens, D., Roth, J., Norman, A.W. & Orci, L. (1984) Immunohistochemical mapping of calcium-binding protein immunoreactivity in the rat central nervous system. *Brain Res.*, **296**, 75-86.

Gittelman, J.X. & Tempel, B.L. (2006) Kv1.1-containing channels are critical for temporal precision during spike initiation. *J. Neurophysiol.*, **96**, 1203-1214.

Giuliodori, M.J. & Zuccolilli, G. (2004) Postsynaptic potential summation and action potential initiation: function following form. *Adv. Physiol. Educ.*, **28**, 79-80.

Goetz, T., Wulff, P. & Wisden, W. (2009) GABAA receptors: molecular biology, cell biology, and pharmacology. *Encyclopedia of Neuroscience*. Academic Press, Oxford, 463-470.

Goldberg, J., Wilson, V., Cullen, K., Angelaki, D., Broussard, D., Buttner-Ennever, J., Fukushima, K. & Minor, L. (2012) *The Vestibular System: A Sixth Sense*, **1**, 1-560.

Grzybowska, E.A. (2018) Calcium-binding proteins with disordered structure and their role in secretion, storage, and cellular signaling. *Biomolecules*, **8**.

Gupta, D.K., Blanco-Palmero, V.A., Chung, W.K. & Kuo, S.H. (2018) Abnormal vertical eye movements as a clue for diagnosis of Niemann-Pick Type C. *Tremor Other Hyperkinet. Mov.*, **8**, 560.

Hanson, M.R., Hamid, M.A., Tomsak, R.L., Chou, S.S. & Leigh, R.J. (1986) Selective saccadic palsy caused by pontine lesions: clinical, physiological, and pathological correlations. *Ann. Neurol.*, **20**, 209-217.

Härtig, W., Brauer, K., Bigl, V. & Brückner, G. (1994) Chondroitin sulfate proteoglycan-immunoreactivity of lectin-labeled perineuronal nets around parvalbumin-containing neurons. *Brain Res.*, **635**, 307-311.

Härtig, W., Brauer, K. & Brückner, G. (1992) Wisteria floribunda agglutinin-labelled nets surround parvalbumin-containing neurons. *Neuroreport*, **3**, 869-872.

Härtig, W., Derouiche, A., Welt, K., Brauer, K., Grosche, J., Mäder, M., Reichenbach, A. & Brückner, G. (1999) Cortical neurons immunoreactive for the potassium channel Kv3.1b subunit are predominantly surrounded by perineuronal nets presumed as a buffering system for cations. *Brain Res.*, **842**, 15-29.

Harvey, R.J., Carta, E., Pearce, B.R., Chung, S.K., Supplisson, S., Rees, M.I. & Harvey, K. (2008) A critical role for glycine transporters in hyperexcitability disorders. *Front. Mol. Neurosci.*, **1**, 1.

Hegle, A.P., Frank, C.A., Berndt, A., Klose, M., Allan, D.W. & Accili, E.A. (2017) The Ih channel gene promotes synaptic transmission and coordinated movement in drosophila melanogaster. *Front. Mol. Neurosci.*, **10**, 41.

Henn, V., Lang, W., Hepp, K. & Reisine, H. (1984) Experimental gaze palsies in monkeys and their relation to human pathology. *Brain*, **107**, 619-636.

Hernández, G.R., Blumer, R., de la Cruz, R.R. & Pastor, A.M. (2019) Functional diversity of motoneurons in the oculomotor system. *Proc. Natl. Acad. Sci. U S A*, **116**, 3837-3846.

Highstein, S.M., Karabelas, A., Baker, R. & McCrea, R.A. (1982) Comparison of the morphology of physiologically identified abducens motor and internuclear neurons in the cat: a light microscopic study employing the intracellular injection of horseradish peroxidase. *J. Comp. Neurol.*, **208**, 369-381.

Hobohm, C., Härtig, W., Brauer, K. & Brückner, G. (1998) Low expression of extracellular matrix components in rat brain stem regions containing modulatory aminergic neurons. *J. Chem. Neuroanat.*, **15**, 135-142.

Hodgkin, A.L. & Huxley, A.F. (1952a) Currents carried by sodium and potassium ions through the membrane of the giant axon of Loligo. *J. Physiol.*, **116**, 449-472.

Hodgkin, A.L. & Huxley, A.F. (1952b) A quantitative description of membrane current and its application to conduction and excitation in nerve. *J. Physiol.*, **117**, 500-544.

Hoh, J.F.Y. (2020) Myosin heavy chains in extraocular muscle fibres: distribution, regulation and function. *Acta Physiol.*, **231(2)**, e13535.

Horn, A. & Straka, H. (2021) Functional organization of extraocular motoneurons and eye muscles. *Ann. Rev. Vis. Sci.*, **7**, 793-825.

Horn, A.K., Büttner-Ennever, J.A., Suzuki, Y. & Henn, V. (1995) Histological identification of premotor neurons for horizontal saccades in monkey and man by parvalbumin immunostaining. *J. Comp. Neurol.*, **359**, 350-363.

Horn, A.K., Eberhorn, A., Härtig, W., Ardelenanu, P., Messoudi, A. & Büttner-Ennever, J.A. (2008) Perioculomotor cell groups in monkey and man defined by their histochemical and functional properties: reappraisal of the Edinger-Westphal nucleus. *J. Comp. Neurol.*, **507**, 1317-1335.

Horn, A.K.E. (2006) The reticular formation. *Prog. Brain Res.*, **151**, 127-155.

Horn, A.K.E. & Adamcyzk, C. (2011) Reticular formation - eye movements, gaze and blinks. Mai, J.K & Paxinos G. (eds). *The human nervous system (Third edition)*, Academic Press. 328-366.

Horn, A.K.E., Brückner, G., Härtig, W. & Messoudi, A. (2003a) Saccadic omnipause and burst neurons in monkey and human are ensheathed by perineuronal nets but differ in their expression of calcium-binding proteins. *J. Comp. Neurol.*, **455**, 341-352.

Horn, A.K.E. & Büttner-Ennever, J.A. (1998) Premotor neurons for vertical eye-movements in the rostral mesencephalon of monkey and man: the histological identification by parvalbumin immunostaining. *J. Comp. Neurol.*, **392**, 413-427.

Horn, A.K.E., Büttner-Ennever, J.A. & Büttner, U. (1996) Saccadic premotor neurons in the brainstem: functional neuroanatomy and clinical implications. *Neuro-Ophthalm.*, **16**, 229-240.

Horn, A.K.E., Büttner-Ennever, J.A., Wahle, P. & Reichenberger, I. (1994) Neurotransmitter profile of saccadic omnipause neurons in nucleus raphe interpositus. *J. Neurosci.*, **14**, 2032-2046.

Horn, A.K.E., Helmchen, C. & Wahle, P. (2003b) GABAergic neurons in the rostral mesencephalon of the Macaque monkey that control vertical eye movements. *Ann. N.Y. Acad. Sci.*, **1004**, 19-28.

Horn, A.K.E., Horng, A., Buresch, N., Messoudi, A. & Hartig, W. (2018) Identification of functional cell groups in the abducens nucleus of monkey and human by perineuronal nets and choline acetyltransferase immunolabeling. *Front. Neuroanat.*, **12**, 45.

Huang, H. & Trussell, Laurence O. (2014) Presynaptic HCN channels regulate vesicular glutamate transport. *Neuron*, **84**, 340-346.

Ikeshima, H., Yuasa, S., Matsuo, K., Kawamura, K., Hata, J. & Takano, T. (1993) Expression of three nonallelic genes coding calmodulin exhibits similar localization on the central nervous system of adult rats. *J. Neurosci. Res.*, **36**, 111-119.

Irving, E.L. & Lillakas, L. (2018) Difference between vertical and horizontal saccades across the human lifespan. *Exp. Eye Res*., **183**, 38-45.

Isa, T. & Sasaki, S. (2002) Brainstem control of head movements during orienting; organization of the premotor circuits. *Prog. Neurobiol.*, **66**, 205-241.

Iwagaki, N. & Miles, G.B. (2011) Activation of group I metabotropic glutamate receptors modulates locomotor-related motoneuron output in mice. *J. Neurophysiol.*, **105**, 2108-2120.

Jan, L.Y. & Jan, Y.N. (2012) Voltage-gated potassium channels and the diversity of electrical signalling. *J. Neurophysiol.*, **590**, 2591-2599.

Jeub, M., Herbst, M., Spauschus, A., Fleischer, H., Klockgether, T., Wuellner, U. & Evert, B.O. (2006) Potassium channel dysfunction and depolarized resting membrane potential in a cell model of SCA3. *Exp. Neurol.*, **201**, 182-192.

Johnston, J., Forsythe, I.D. & Kopp-Scheinpflug, C. (2010) Going native: voltage-gated potassium channels controlling neuronal excitability. *J. Neurophysiol.*, **588**, 3187-3200.

Kalla, R., Glasauer, S., Büttner, U., Brandt, T. & Strupp, M. (2007) 4-Aminopyridine restores vertical and horizontal neural integrator function in downbeat nystagmus. *Brain*, **130**, 2441-2451.

Kandel, E.R., Schwartz, J.H., Jessel, T.M., Siegelbaum, S.A. & Hudspeth, A.J. (2013) *Principles of neural science. McGraw-Hill Companies*, **5**, 1030-1032.

Kaneko, C.R.S. (1996) Effect of ibotenic acid lesions of the omnipause neurons on saccadic eye movements in Rhesus macaques. *J. Neurophysiol.*, **75**, 2229-2242.

Keller, E.L. (1974) Participation of medial pontine reticular formation in eye movement generation in monkey. *J. Neurophysiol.*, **37**, 316-332.

Kheradmand, A. & Zee, D. (2011) Cerebellum and ocular motor control. *Front. Neurol.*, **2**, 53.

Khurana, S., Liu, Z., Lewis, A.S., Rosa, K., Chetkovich, D. & Golding, N.L. (2012) An essential role for modulation of hyperpolarization-activated current in the development of binaural temporal precision. *J. Neurosci.*, **32**, 2814-2823.

Kim, S.-H., Zee, D.S., du Lac, S., Kim, H.J. & Kim, J.-S. (2016) Nucleus prepositus hypoglossi lesions produce a unique ocular motor syndrome. *Neurology*, **87**, 2026–2033

Klug, A. & Trussell, L.O. (2006) Activation and deactivation of voltage-dependent K^+ channels during synaptically driven action potentials in the MNTB. *J. Neurophysiol.*, **96**, 1547-1555.

Kodama, T., Gittis, A.H., Shin, M., Kelleher, K., Kolkman, K.E., McElvain, L., Lam, M. & du Lac, S. (2020) Graded coexpression of ion channel, neurofilament, and synaptic denes in fast-spiking vestibular nucleus neurons. *J. Neurosci.*, **40**, 496-508.

Kourie, J.I. & Henry, C.L. (2001) Protein aggregation and deposition: implications for ion channel formation and membrane damage. *Croat. Med. J.*, **42**, 359-374.

Laslo, P., Lipski, J., Nicholson, F.B., Miles, G.B. & Funk, G.D. (2000) Calcium binding proteins in motoneurons at low and high risk for degeneration in ALS. *Neuroreport*, **11**, 3305-3308.

Laslo, P., Lipski, J., Nicholson, L.F., Miles, G.B. & Funk, G.D. (2001) GluR2 AMPA receptor subunit expression in motoneurons at low and high risk for degeneration in amyotrophic lateral sclerosis. *Exp. Neurol.*, **169**, 461-471.

Latal, A.T., Kremer, T., Gomeza, J., Eulenburg, V. & Hülsmann, S. (2010) Development of synaptic inhibition in glycine transporter 2 deficient mice. *Mol. Cell. Neurosci.*, **44**, 342-352.

Lau, C.G., Takeuchi, K., Rodenas-Ruano, A., Takayasu, Y., Murphy, J., Bennett, M.V. & Zukin, R.S. (2009) Regulation of NMDA receptor Ca^{2+} signalling and synaptic plasticity. *Biochem. Soc. Trans.*, **37**, 1369-1374.

Lee, H.H., Deeb, T.Z., Walker, J.A., Davies, P.A. & Moss, S.J. (2011) NMDA receptor activity downregulates KCC2 resulting in depolarizing GABAA receptor-mediated currents. *Nat. Neurosci.*, **14**, 736-743.

Leigh, R.J. & Zee, D.S. (2015) *The Neurology of Eye Movements (Fifth edition)*. Oxford University Press.

Litvan, I., Campell, G., Mangone, C.A., Verny, M., McKee, A., Ray Chaudhuri, K., Jellinger, K., Pearce, R.K.B. & D'Olhaberriague, L. (1997) Which clinical features differentiate progressive suprenuclear palsy (Steele-Richrdson-Olszewski syndrome) from related disorders? A clinicopathological study. *Brain*, **120**, 65-74.

Liu, H., Wang, D., Wong, K.S., Gong, Y. & Xia, L. (2016) An improved spherical coordinate system applied in oculomotor system-the possibility for rapid strabismus diagnosis. 12th International conference on natural computation, fuzzy systems and knowledge discovery (ICNC-FSKD). 729-733.

Login, I.S. (1982) Progressive supranuclear palsy. *Neurology*, **32**, 918-919.

Loup, F., Wieser, H.G., Yonekawa, Y., Aguzzi, A. & Fritschy, J.M. (2000) Selective alterations in GABAA receptor subtypes in human temporal lobe epilepsy. *J. Neurosci.,* **20**, 5401-5419.

Luschei, E.S. & Fuchs, A.F. (1972) Activity of brain stem neurons during eye movements of alert monkeys. *J. Neurophysiol.*, **35**, 445-461.

Lynch, J.C. & Tian, J.-R. (2006) Cortico-cortical networks and cortico-subcortical loops for the higher control of eye movements. *Prog. Brain. Res.*, **151**, 461-501.

Marti, S., Straumann, D., Büttner, U. & Glasauer, S. (2008) A model-based theory on the origin of downbeat nystagmus. *Exp. Brain Res*., **188**, 613-31.

Matsumoto, M., Inoue, K.-i. & Takada, M. (2018) Causal role of neural signals transmitted from the frontal eye field to the superior colliculus in saccade generation. *Front. Neural Circuits*, **12**, 69.

Mayadali, Ü.S., Fleuriet, J., Mustari, M., Straka, H. & Horn, A.K.E. (2021) Transmitter and ion channel profiles of neurons in the primate abducens and trochlear nuclei. *Brain Struct. Funct*., **226**, 2125-2151.

Mayadali, Ü.S., Lienbacher, K., Mustari, M., Strupp, M. & Horn, A.K.E. (2019) Potassium channels in omnipause neurons. *Prog. Brain. Res.*, **249**, 117-123.

Mayadali, Ü.S., Lienbacher, K., Shaikh, A.G. & Horn, A.K.E. (2022) Saccadic premotor burst neurons and histochemical correlates of their firing patterns in rhesus monkey. *J. Neurol. Sci.*, **439**, 120328.

McCormick, D.A. (2013) Chapter 5 - Membrane potential and action potential. In Squire, L.R., Berg, D., Bloom, F.E., du Lac, S., Ghosh, A., Spitzer, N.C. *Fundamental Neuroscience (Fourth edition)*. Academic Press, San Diego, 93-116.

McElligott, J. & Spencer, R. (2000) Neuropharmacological aspects of the vestibulo-ocular reflex. In Beitz, A.J., Anderson, J.H. CRC Press, Boca Raton; London; New York; Washington, D.C., 199-222.

McKay, B.E. & Turner, R.W. (2004) Kv3 K^+ channels enable burst output in rat cerebellar Purkinje cells. *Eur. J. Neurosci.*, **20**, 729-739.

McLean, C.A., Cherny, R.A., Fraser, F.W., Fuller, S.J., Smith, M.J., Beyreuther, K., Bush, A.I. & Masters, C.L. (1999) Soluble pool of Abeta amyloid as a determinant of severity of neurodegeneration in Alzheimer's disease. *Ann. Neurol.*, **46**, 860-866.

Miles, G.B., Lipski, J., Lorier, A.R., Laslo, P. & Funk, G.D. (2004) Differential expression of voltage-activated calcium channels in III and XII motoneurones during development in the rat. *Eur. J. Neurosci.*, **20**, 903-913.

Miura, K. & Optican, L.M. (2006) Membrane channel properties of premotor excitatory burst neurons may underlie saccade slowing after lesions of omnipause neurons. *J. Comput. Neurosci.*, **20**, 25-41.

Molineux, M.L., McRory, J.E., McKay, B.E., Hamid, J., Mehaffey, W.H., Rehak, R., Snutch, T.P., Zamponi, G.W. & Turner, R.W. (2006) Specific T-type calcium channel isoforms are associated with distinct burst phenotypes in deep cerebellar nuclear neurons. *Proc. Natl. Acad. Sci. U S A*, **103**, 5555-5560.

Moran, Y., Barzilai, M.G., Liebeskind, B.J. & Zakon, H.H. (2015) Evolution of voltage-gated ion channels at the emergence of Metazoa. *J. Exp. Biol.*, **218**, 515-525.

Morris, N.P. & Henderson, Z. (2000) Perineuronal nets ensheath fast spiking, parvalbumin-immunoreactive neurons in the medial septum/diagonal band complex. *Eur. J. Neurosci.*, **12**, 828-838.

Moschovakis, A.K. (1997) The neural integrators of the mammalian saccadic system. *Front. Biosci.*, **2**, d552-577.

Moschovakis, A.K., Scudder, C.A. & Highstein, S.M. (1991a) The structure of the primate oculomotor burst generator. I. Medium-lead burst neurons with upward on-directions. *J. Neurophysiol.*, **65**, 203-217.

Moschovakis, A.K., Scudder, C.A. & Highstein, S.M. (1996) The microscopic anatomy and physiology of the mammalian saccadic system. *Prog. Neurobiol.*, **50**, 133-133.

Moschovakis, A.K., Scudder, C.A., Highstein, S.M. & Warren, J.D. (1991b) The structure of the primate oculomotor burst generator. II. Medium-lead burst neurons with downward on-directions. *J. Neurophysiol.*, **65**, 218-229.

Mueller, A., Davis, A., Carlson, S.S. & Robinson, F.R. (2014) N-acetylgalactosamine positive perineuronal nets in the saccade-related-part of the cerebellar fastigial nucleus do not maintain saccade gain. *PLoS One*, **9**, e86154.

Munoz, D.P. & Wurtz, R.H. (1992) Role of the rostral superior colliculus in active visual fixation and execution of express saccades. *J. Neurophysiol.*, **67**, 1000-1002.

Munoz, D.P. & Wurtz, R.H. (1993) Fixation cells in monkey superior colliculus. I. Characteristics of cell discharge. *J. Neurophysiol.*, **70**, 559-575.

Nelson, T.J., Cavallaro, S., Yi, C.-L., McPhie, D., Schreurs, B.G., Gusev, P.A., Favit, A., Zohar, O., Kim, J., Beushausen, S., Ascoli, G., Olds, J., Neve, R. & Alkon, D.L. (1996) Calexcitin: a signaling protein that binds calcium and GTP, inhibits potassium channels, and enhances membrane excitability. *Proc. Natl. Acad. Sci. U S A*, **93**, 13808-13813.

Nichols, K., Hanan, J. & Ranasinghe, M. (2013) Transforming the Social Practices of Learning with Representations: A Study of Disciplinary Discourse. *Res. Sci. Educ.*, **43**, 179–208

Noda, H., Sugita, S. & Ikeda, Y. (1990) Afferent and efferent connections of the oculomotor region of the fastigial nucleus in the macaque monkey. *J. Comp. Neurol.*, **302**, 330-348.

O'Brien, J.A. & Berger, A.J. (1999) Cotransmission of GABA and glycine to brain stem motoneurons. *J. Neurophysiol.*, **82**, 1638-1641.

Optican, L.M. (2008) The role of omnipause neurons: why glycine? *Prog. Brain Res.* Elsevier, **171**, 115-121.

Optican, L.M. & Pretegiani, E. (2017a) A GABAergic dysfunction in the olivary-cerebellar-brainstem network may cause eye oscillations and body tremor. II. model simulations of saccadic eye oscillations. *Front. Neurol.*, **8**, 372.

Optican, L.M. & Pretegiani, E. (2017b) What stops a saccade? *Philos. Trans. R. Soc. Lond. B. Biol. Sci.*, **372**, 20160194.

Partsalis, A.M., Zhang, Y. & Highstein, S.M. (1995) Dorsal Y group in the squirrel monkey. II. Contribution of the cerebellar flocculus to neuronal responses in normal and adapted animals. *J. Neurophysiol.*, **73**, 632-650.

Perez-Reyes E. (2003) Molecular physiology of low-voltage-activated T-type calcium channels. *Physiol. Rev.*, **83**, 117–161.

Pierrot-Deseilligny, C., Ploner, C.J., Muri, R.M., Gaymard, B. & Rivaud-Pechoux, S. (2002) Effects of cortical lesions on saccadic: eye movements in humans. *Ann. N. Y. Acad. Sci.*, **956**, 216-229.

Pike, M. (2013) Opsoclonus-myoclonus syndrome. *Handb. Clin. Neurol.*, **112**, 1209-1211.

Pun, S., Santos, A.F., Saxena, S., Xu, L. & Caroni, P. (2006) Selective vulnerability and pruning of phasic motoneuron axons in motoneuron disease alleviated by CNTF. *Nat. Neurosci.*, **9**, 408.

Puri, S. & Shaikh, A.G. (2017) Basic and translational neuro-ophthalmology of visually guided saccades: disorders of velocity. *Expert. Rev. Ophthalmol.*, **12**, 457-473.

Rajendra, S., Lynch, J.W. & Schofield, P.R. (1997) The glycine receptor. *Pharmacol. Ther.*, **73**, 121-146.

Ramat, S., Leigh, J.R., Zee, D.S. & Optican, L.M. (2005) Ocular oscillations generated by coupling of brainstem excitatory and inhibitory saccadic burst neurons. *Exp. Brain Res.*, **160**, 89-106.

Ramat, S., Leigh, R., Zee, D. & Optican, L. (2007) What clinical disorders tell us about the neural control of saccadic eye movements. *Brain*, **130**, 10-35.

Revesz, T., Sangha, H. & Daniel, S.E. (1996) The nucleus raphe interpositus in the Steele-Richardson-Olszewski syndrome (progressive supranuclear palsy). *Brain*, **119**, 1137-1143.

Ridley, A., Kennard, C., Scholtz, C.L., Büttner-Ennever, J.A., Summers, B. & Turnbull, A. (1987) Omnipause neurons in two cases of opsoclonus associated with oat cell carcinoma of the lung. *Brain*, **110**, 1699-1709.

Rivera, C., Voipio, J., Payne, J.A., Ruusuvuori, E., Lahtinen, H., Lamsa, K., Pirvola, U., Saarma, M. & Kaila, K. (1999) The K^+/Cl^- co-transporter KCC2 renders GABA hyperpolarizing during neuronal maturation. *Nature*, **397**, 251-255.

Robinson, F.R. & Fuchs, A.F. (2001) The role of the cerebellum in voluntary eye movements. *Annu. Rev. Neurosci.*, **24**, 981-1004.

Rogers, S.L., Rankin-Gee, E., Risbud, R.M., Porter, B.E. & Marsh, E.D. (2018) Normal development of the perineuronal net in humans; in patients with and without epilepsy. *Neuroscience*, **384**, 350-360.

Roselli, F. & Caroni, P. (2015) From intrinsic firing properties to selective neuronal vulnerability in neurodegenerative diseases. *Neuron*, **85**, 901-910.

Ross, C.A. & Poirier, M.A. (2004) Protein aggregation and neurodegenerative disease. *Nat. Med.*, **10**, S10-S17.

Rossier, M.F. (2016) T-type calcium channel: a privileged gate for calcium entry and control of adrenal steroidogenesis. *Front. Endocrinol.*, **7**, 43.

Russier, M., Kopysova, I.L., Ankri, N., Ferrand, N. & Debanne, D. (2002) GABA and glycine co-release optimizes functional inhibition in rat brainstem motoneurons in vitro. *J. Neurophysiol.*, **541**, 123-137.

Saito, Y. & Sugimura, T. (2020) Different activation mechanisms of excitatory networks in the rat oculomotor integrators for vertical and horizontal gaze holding. *eneuro*, **7**, ENEURO.0364-0319.2019.

Sakatani, T. & Isa, T. (2007) Quantitative analysis of spontaneous saccade-like rapid eye movements in C57BL/6 mice. *Neurosci. Res.*, **58**, 324-331.

Salsano, E., Umeh, C., Rufa, A., Pareyson, D. & Zee, D.S. (2012) Vertical supranuclear gaze palsy in Niemann-Pick Type C disease. *Neurol. Sci.*, **33**, 1225-1232.

Sanchez, K. & Rowe, F.J. (2018) Role of neural integrators in oculomotor systems: a systematic narrative literature review. *Acta Ophthalmol.*, **96**, e111-e118.

Saxena, S. & Caroni, P. (2011) Selective neuronal vulnerability in neurodegenerative diseases: from stressor thresholds to degeneration. *Neuron*, **71**, 35-48.

Saxena, S., Roselli, F., Singh, K., Leptien, K., Julien, J.P., Gros-Louis, F. & Caroni, P. (2013) Neuroprotection through excitability and mTOR required in ALS motoneurons to delay disease and extend survival. *Neuron*, **80**, 80-96.

Senatore, A. & Spafford, J.D. (2015) Physiology and pathology of voltage-Gated T-type calcium channels. *T-type Calcium Channels in Basic and Clinical Science*. Springer Vienna, Vienna, 3-17.

Shaikh, A.G. (2012) Saccadic oscillations – membrane, model, and medicine. *Expert Rev. Ophthalmol.*, **7**, 481-486.

Shaikh, A.G., Factor, S.A. & Juncos, J. (2017) Saccades in progressive supranuclear palsy - maladapted, irregular, curved, and slow. *Mov. Disord. Clin. Pract.*, **4**, 671-681.

Shaikh, A.G., Miura, K., Optican, L.M., Ramat, S., Leigh, R.J. & Zee, D.S. (2007) A new familial disease of saccadic oscillations and limb tremor provides clues to mechanisms of common tremor disorders. *Brain*, **130**, 3020-3031.

Shaikh, A.G., Ramat, S., Optican, L.M., Miura, K., Leigh, R.J. & Zee, D.S. (2008) Saccadic burst cell membrane dysfunction is responsible for saccadic oscillations. *J. Neuroophthalmol.*, **28**, 329-336.

Shinoda, Y., Sugiuchi, Y., Takahashi, M. & Izawa, Y. (2011) Neural substrate for suppression of omnipause neurons at the onset of saccades. *Ann. N. Y. Acad. Sci.*, **1233**, 100-106.

Soetedjo, R., Kaneko, C.R.S. & Fuchs, A.F. (2002) Evidence that the superior colliculus participates in the feedback control of saccadic eye movements. *J. Neurophysiol.*, **87**, 679-695.

Solomon, D., Ramat, S., Tomsak, R.L., Reich, S.G., Shin, R.K., Zee, D.S. & Leigh, R.J. (2008) Saccadic palsy after cardiac surgery: characteristics and pathogenesis. *Ann. Neurol.*, **63**, 355-365.

Solomon, D., Winkelman, C., Zee, D.S., Gray, L. & Büttner-Ennever, J.A. (2005) Niemann-Pick Type C disease in two affected sisters: ocular motor recordings and brainstem neuropathology. *Ann. N. Y. Acad. Sci*., **1039**, 436-45.

Sparks, D., Rohrer, W.H. & Zhang, Y. (2000) The role of the superior colliculus in saccade initiation: a study of express saccades and the gap effect. *Vision Res.*, **40**, 2763-2777.

Sparks, D.L. (2002) The brainstem control of saccadic eye movements. *Nat. Rev. Neurosci.*, **3**, 952-964.

Spencer, R.F. & Baker, R. (1992) GABA and glycine as inhibitory neurotransmitters in the vestibulo-ocular reflex. *Ann. N. Y. Acad. Sci.*, **656**, 602-611.

Spencer, R.F. & Porter, J.D. (2006) Biological organization of the extraocular muscles. *Prog. Brain. Res.*, **151**, 43-80.

Spencer, R.F. & Wang, S.F. (1996) Immunohistochemical localization of neurotransmitters utilized by neurons in the rostral interstitial nucleus of the medial longitudinal fasciculus (riMLF) that project to the oculomotor and trochlear nuclei in the cat. *J. Comp. Neurol.*, **366**, 134-148.

Spencer, R.F., Wang, S.F. & Baker, R. (1992) The pathways and functions of GABA in the oculomotor system. *Prog. Brain. Res.*, **90**, 307-331.

Spencer, R.F., Wenthold, R.J. & Baker, R. (1989) Evidence for glycine as an inhibitory neurotransmitter of vestibular, reticular, and prepositus hypoglossi neurons that project to the cat abducens nucleus. *J. Neurosci.*, **9**, 2718-2736.

Steele, J., Richardson, J.C. & Olszewski, J. (1964) Progressive supranuclear palsy. A heterogeneous system degeneration involving brain stem, basal ganglia and cerebellum with vertical gaze and pseudobulbar palsy, nuchal dystonia and dementia. *Arch. Neurol.*, **10**, 333-359.

Straka, H., Fritzsch, B. & Glover, J.C. (2014) Connecting ears to eye muscles: evolution of a 'simple' reflex arc. *Brain, Behav. and Evol.*, **83**, 162-175.

Strassman, A., Highstein, S.M. & McCrea, R.A. (1986a) Anatomy and physiology of saccadic burst neurons in the alert squirrel monkey. I. Excitatory burst neurons. *J. Comp. Neurol.*, **249**, 337-357.

Strassman, A., Highstein, S.M. & McCrea, R.A. (1986b) Anatomy and physiology of saccadic burst neurons in the alert squirrel monkey. II. Inhibitory burst neurons. *J. Comp. Neurol.*, **249**, 358-380.

Straube, A., Deubel, H., Ditterich, J. & Eggert, T. (2001) Cerebellar lesions impair rapid saccade amplitude adaptation. *Neurology*, **57**, 2105-2108.

Strupp, M., Kalla, R., Glasauer, S., Wagner, J., Hüfner, K., Jahn, K. & Brandt, T. (2008) Aminopyridines for the treatment of cerebellar and ocular motor disorders. *Prog. Brain. Res.*, **171**, 535-541.

Sugiuchi, Y., Takahashi, M. & Shinoda, Y. (2013) Input-output organization of inhibitory neurons in the interstitial nucleus of Cajal projecting to the contralateral trochlear and oculomotor nucleus. *J. Neurophysiol.*, **110**, 640-657.

Suzuki, D.A., Yamada, T. & Hoedema, R. (1999) Smooth-pursuit eye-movement deficits with chemical lesions in macaque nucleus reticularis tegmenti pontis. *J. Neurophysiol.*, **82**, 1178-1186.

Suzuki, Y., Büttner-Ennever, J.A., Straumann, D., Hepp, K., Hess, B.J.M. & Henn, V. (1995) Deficits in torsional and vertical rapid eye movements and shift of Listing's plane after uni- and bilateral lesions of the rostral interstitial nucleus of the medial longitudinal fasciculus. *Exp. Brain. Res.*, **106**, 215-232.

Tang, X., Büttner-Ennever, J.A., Mustari, M.J. & Horn, A.K.E. (2015) Internal organization of medial rectus and inferior rectus muscle neurons in the C-group of the oculomotor nucleus in monkey. *J. Comp. Neurol.*, **523**, 1809–1823.

Thurtell, M.J., Tomsak, R.L. & Leigh, R.J. (2007) Disorders of saccades. *Curr. Neurol. Neurosci. Rep.*, **7**, 407-416.

Timic Stamenic, T. & Todorovic, S.M. (2022) Thalamic T-type calcium channels as targets for hypnotics and general anesthetics. *Int. J. Mol. Sci.*, **23**, 2349.

Torres-Torrelo, J., Rodríguez-Rosell, D., Nunez-Abades, P., Carrascal, L. & Torres, B. (2012) Glutamate modulates the firing rate in oculomotor nucleus motoneurons as a function of the recruitment threshold current. *J. Physiol.*, **590**, 3113-3127.

Traynelis, S.F., Wollmuth, L.P., McBain, C.J., Menniti, F.S., Vance, K.M., Ogden, K.K., Hansen, K.B., Yuan, H., Myers, S.J. & Dingledine, R. (2010) Glutamate receptor ion channels: structure, regulation, and function. *Pharmacol. Rev.*, **62**, 405-496.

Tsien, R.Y. (2013) Very long-term memories may be stored in the pattern of holes in the perineuronal net. *Proc. Natl. Acad. Sci. U S A*, **110**, 12456-12461.

Ugolini, G., Büttner-Ennever, J.A., Doldan, M. & al., e. (2001) Horizontal eye movement networks in primates: differences in monosynaptic input to slow and fast abducens motoneurons. *Abstr. Soc. Neurosci.*, **27**, 403-413.

Ugolini, G., Klam, F., Doldan Dans, M., Dubayle, D., Brandi, A.-M., Büttner-Ennever, J.A. & Graf, W. (2006) Horizontal eye movement networks in primates as revealed by retrograde transneuronal transfer of rabies virus: differences in monosynaptic input to "slow" and "fast" abducens motoneurons. *J. Comp. Neurol.*, **498**, 762-785.

Vedunova, M., Sakharnova, T., Mitroshina, E., Perminova, M., Zakharov, Y., Pimashkin, A., Dityatev, A. & Mukhina, I. (2013) Seizure-like activity in hyaluronidase-treated dissociated hippocampal cultures. *Front. Cell. Neurosci.*, **7**, 149.

Venugopal, S., Ghulam-Jhelani, Z., Simmons, D. & Chandler, S.H. (2021) Diminished GAD67 terminals and ambient GABA inhibition associated with reduced motor neuron recruitment threshold in the SOD1/G93A ALS mouse. *bioRxiv*, 2021.2012.2016.473041.

Vigneault, É., Poirel, O., Riad, M., Prud'homme, J., Dumas, S., Turecki, G., Fasano, C., Mechawar, N. & El Mestikawy, S. (2015) Distribution of vesicular glutamate transporters in the human brain. *Front. Neuroanat.*, **9**, 23.

Wallace, D.J., Greenberg, D.S., Sawinski, J., Rulla, S., Notaro, G. & Kerr, J.N.D. (2013) Rats maintain an overhead binocular field at the expense of constant fusion. *Nature*, **498**, 65-69.

Wang, L.Y., Gan, L., Forsythe, I.D. & Kaczmarek, L.K. (1998) Contribution of the Kv3.1 potassium channel to high-frequency firing in mouse auditory neurones. *J. Physiol.*, **509 (Pt 1)**, 183-194.

Wang, N., Perkins, E., Zhou, L., Warren, S. & May, P.J. (2013) Anatomical evidence that the superior colliculus controls saccades through central mesencephalic reticular formation gating of omnipause neuron activity. *J. Neurosci.*, **33**, 16285-16296.

Wang, N., Perkins, E., Zhou, L., Warren, S. & May, P.J. (2017) Reticular formation connections underlying horizontal gaze: the central mesencephalic reticular formation (cMRF) as a conduit for the collicular saccade signal. *Front. Neuroanat.*, **11**, 36.

Wang, X.X., Jin, Y., Sun, H., Ma, C., Zhang, J., Wang, M. & Chen, L. (2016) Characterization of rebound depolarization in neurons of the rat medial geniculate body in vitro. *Neurosci. Bull.*, **32**, 16-26.

Wasicky, R., Horn, A.K.E. & Büttner-Ennever, J.A. (2004) Twitch and non-twitch motoneuron subgroups of the medial rectus muscle in the oculomotor nucleus of monkeys receive different afferent projections. *J. Comp. Neurol.*, **479**, 117-129.

Watanabe, M. & Munoz, D.P. (2011) Probing basal ganglia functions by saccade eye movements. *Eur. J. Neurosci.*, **33**, 2070-2090.

Weiser, M., Vega-Saenz de Miera, E., Kentros, C., Moreno, H., Franzen, L., Hillman, D., Baker, H. & Rudy, B. (1994) Differential expression of Shaw-related K^+ channels in the rat central nervous system. *J. Neurosci.*, **14**, 949-972.

Weiss, N. & Zamponi, G.W. (2013) Control of low-threshold exocytosis by T-type calcium channels. *Biochim. Biophys. Acta.*, **1828**, 1579-1586.

Wenning, G.K., Jellinger, K. & Litvan, I. (1997) Supranuclear gaze palsy and eyelid apraxia in postencephalictic parkinsonism. *J. Neural. Transm.*, **104**, 845-865.

Wentzel, P.R., Dezeeuw, C.I., Holstege, J.C. & Gerrits, N.M. (1993) Colocalization of GABA and glycine in the rabbit oculomotor nucleus. *Neurosci. Lett.*, **164**, 25-29.

Wingert, J.C. & Sorg, B.A. (2021) Impact of perineuronal nets on electrophysiology of parvalbumin interneurons, principal neurons, and brain oscillations: a review. *Front. Synaptic Neurosci.*, **13**, 673210.

Wolfart, J., Neuhoff, H., Franz, O. & Roeper, J. (2001) Differential expression of the small-conductance, calcium-activated potassium channel SK3 is critical for pacemaker control in dopaminergic midbrain neurons. *J. Neurosci.*, **21**, 3443-3456.

Wong, A. (2007) An update on opsoclonus. *Curr. Opin. Neurol.*, **20**, 25-31.

Wong, A.M.F., Musallam, S., Tomlinson, R.D., Shannon, P. & Sharpe, J.A. (2001) Opsoclonus in three dimensions: oculographic, neuropathologic and modelling correlates. *J. Neurol. Sci.*, **189**, 71-81.

Yamada, J., Ohgomori, T. & Jinno, S. (2015) Perineuronal nets affect parvalbumin expression in GABAergic neurons of the mouse hippocampus. *Eur. J. Neurosci.*, **41**, 368-378.

Zagha, E., Lang, E.J. & Rudy, B. (2008) Kv3.3 channels at the Purkinje cell soma are necessary for generation of the classical complex spike waveform. *J. Neurosci.*, **28**, 1291-1300.

Zeeh, C., Hess, B.J. & Horn, A.K.E. (2013) Calretinin inputs are confined to motoneurons for upward eye movements in monkey. *J. Comp. Neurol.*, **521**, 3154-3166.

Zeeh, C., Mayadali, Ü.S. & Horn, A.K.E. (2021) Histochemical characterization of the vestibular Y-Group in monkey. *Cerebellum*. **20**, 701–716.

Zhou, Y., Xue, S. & Yang, J.J. (2013) Calciomics: integrative studies of Ca^{2+}-binding proteins and their interactomes in biological systems. *Metallomics*, **5**, 29-42.

Appendices

7. List of publications (In chronological order)

1- **Mayadali ÜS**, Lienbacher K, Mustari M, Strupp M, Horn AKE. 2019. Potassium channels in omnipause neurons. Prog Brain Res. 2019; 249:117-123. doi: 10.1016/bs.pbr.2019.04.017. Epub 2019 Jun 7. PMID: 31325972.

2- Zeeh C, **Mayadali ÜS**, Horn AKE. 2020. Histochemical characterization of the vestibular y-group in monkey. Cerebellum 20, 701–716 (2021). doi:10.1007/s12311-020-01200-z

3- **Mayadali ÜS**, Fleuriet J, Mustari M, Straka H, Horn AKE. Transmitter and ion channel profiles of neurons in the primate abducens and trochlear nuclei. 2021. Brain Struct Funct. 2021 Sep; 226(7):2125-2151. doi: 10.1007/s00429-021-02315-7. Epub 2021 Jun 28.

4- **Mayadali ÜS**, Lienbacher K, Shaikh AG, Horn AKE. Saccadic premotor burst neurons and histochemical correlates of their firing patterns in rhesus monkey. 2022. J. Neurol. Sci. Epub 2022 Jun 20 doi: 10.1016/j.jns.2022.120328

8. List of contributions (In order of appearance)

Paper 1: Potassium channels in omnipause neurons

Mayadali ÜS, Lienbacher K, Mustari M, Strupp M, Horn AKE. 2019

Prog Brain Res. 2019; 249:117-123. doi: 10.1016/bs.pbr.2019.04.017

My Contribution:

- Immunolabelling of all sections
- Acquisition, analysis and interpretation of data
- Preparation of all figures and tables
- Writing and revising, together with all other authors
- Conception of the work together with AKE Horn

Contribution of Lienbacher K, Mustari M, Strupp M, Horn AKE:

- Surgical procedures, fixation and conservation of monkey tissue (M Mustari)
- Acquisition of brainstem tissue (AKE Horn and K Lienbacher)
- Revision (All authors)

Paper 2: Transmitter and ion channel profiles of neurons in the primate abducens and trochlear nuclei

Mayadali ÜS, Fleuriet J, Mustari M, Straka H, Horn AKE. 2021

Brain Struct Funct. 2021 Sep; 226(7):2125-2151. doi: 10.1007/s00429-021-02315-7

My contribution:

- Immunolabelling of all sections
- Acquisition, analysis and interpretation of data
- Acquisition of fluorescent and confocal images
- Quantification of transmitter inputs
- Statistical analysis
- Preparation of all figures and tables except Figure 10.
- Writing and revising, together with all other authors
- Conception of the work together with AKE Horn

Contribution of Mustari M, Straka H, Horn AKE:

- Surgical procedures including tracer injection, fixation and conservation of monkey tissue (Fleuriet J and M Mustari)
- Acquisition and preparation of brainstem tissue (ÜS Mayadali and AKE Horn)
- Preparation of overview illustration (Figure 10; AKE Horn)
- Revision (All authors)

Paper 3: Saccadic premotor burst neurons and histochemical correlates of their firing patterns in rhesus monkey

Mayadali ÜS, Lienbacher K, Shaikh AG, Horn AKE. 2022

J. Neurol. Sci. 2022 doi: 10.1016/j.jns.2022.120328

My contribution:

- Immunolabelling of all sections
- Acquisition, analysis and interpretation of data
- Acquisition of fluorescent and confocal images
- Quantification
- Preparation of all figures and tables except the summary figure (Fig. 7).
- Writing and revising, together with all other authors
- Conception of the work together with AG Shaikh and AKE Horn

Contribution of Mustari M, Straka H, Horn AKE:

- Acquisition and preparation of brainstem tissue (Lienbacher K and AKE Horn)
- Preparation of the summary figure (Fig. 7; AKE Horn)
- Revision (All authors)

Paper 4: Histochemical characterization of the vestibular y-group in monkey

Zeeh C, **Mayadali ÜS**, Horn AKE. 2021

Cerebellum 20, 701–716 (2021). https://doi.org/10.1007/s12311-020-01200-z

My contribution (as shared first author):

- Immunolabelling of most sections
- Acquisition of immunohistochemistry data
- Acquisition of fluorescent and confocal images
- Writing and revising, together with all other authors

Contribution of Zeeh C, Horn AKE:

- Preparation of illustrations related to anatomy and tracer injection sites (AKE Horn)
- Acquisition of brainstem tissue (AKE Horn)
- Statistical analysis (C Zeeh)
- Preparation of Figures (C Zeeh and AKE Horn)
- Writing and revision (All authors)
- Conception of the work (AKE Horn and C Zeeh)

Date, place: 4.7.22

Signatures of Ümit S. Mayadali: Dr. Christina. Zeeh: Prof. Dr. Anja Horn-Bochtler (Supervisor):

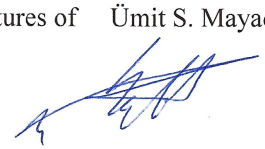
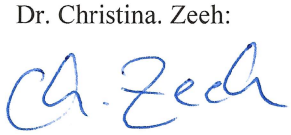
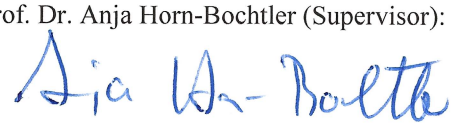

9. Acknowledgements

Firstly, I would like to thank Prof. Dr. Anja Horn-Bochtler for the opportunity she provided me to do my PhD studies in her laboratory. She not only gave endless hours of her time to educate me, but also supported me in even non-academic concerns. It was a great comfort to know that her support, guidance and friendship were within reach at all times. In a similar way, I would like to thank Ahmed Messoudi MPh for his patience and management, whenever I got to play the 'mad scientist'. His advice, support and friendship added much value to my time as a PhD student. I cannot thank enough Christine Unger for her excellent technical assistance and teaching, Karoline, Miriam and Christina for their support and friendship, and finally Prof. Dr. med. Jens Waschke for his continuous support throughout my studies. It has been a pleasure and a great learning experience to have worked with you all.

Next, I would like to thank the GSN team for their incredible support and understanding. Without you, my journey might have been much more difficult, and maybe even impossible. On the way to becoming a scientist, the value and care you have put on us, as PhD students, helped me a lot personally in staying focused on my goals.

Lastly, I would like to thank my family and friends, without whom this work would not come to fruition. They have been there for me in the craziest of situations and kept on believing in me, which makes me thankful and proud to be in their lives.